LBL--22991

DE87 011216

Pulsed Zero Field NMR of Solids and Liquid Crystals

Ann Montgomery Thayer

Lawrence Berkeley Laboratory
University of California
Berkeley, California 94720

February 1987

This work was supported by the Director, Office of Energy Research, Office of Basic Energy Sciences, Materials Sciences Division of the U.S. Department of Energy under Contract No. DE-AC03-76SF00098.

Pulsed Zero Field NMR of Solids and Liquid Crystals

Ann M. Thayer

Abstract

This work describes the development and applications to solids and liquid crystals of zero field nuclear magnetic resonance (NMR) experiments with pulsed dc magnetic fields. Zero field NMR experiments are one approach for obtaining high resolution spectra of amorphous and polycrystalline materials which normally (in high field) display broad featureless spectra. The behavior of the spin system can be coherently manipulated and probed in zero field with dc magnetic field pulses which are employed in a similar manner to radiofrequency pulses in high field NMR experiments.

In Chapter I, the fundamental nuclear spin interactions and formalism used throughout are introduced. The field cycling scheme is explained theoretically and practically in Chapter II, including calculations of the signal function for a few illustrative experimental examples. Technical details are relegated to the appendix. Chapter III introduces how experimental dc pulse sequences can be exploited to improve pulsed field homogeneity with composite pulses. Such sequences are also used for the detection of NMR and NQR spectra with increased sensitivity via level crossings, for isotope selective pulses, and for two dimensional extensions of the experiment. Theoretical considerations of the initial zero field state after demagnetization are also included.

The study of liquid crystalline systems by zero field NMR methods

is the topic of Chapter IV. Nematic phases are studied in order to observe the effects of the removal of an applied magnetic field on sample alignment and molecular order parameters. In nematic phases with positive and negative magnetic susceptibility anisotropies, a comparison between the forms of the spin interactions in high and low fields is made. High resolution zero field NMR spectra of unaligned smectic samples are also obtained and reflect the symmetry of the liquid crystalline environment. These experiments are a sensitive measure of the motionally induced asymmetry in biaxial phases. Homonuclear and heteronuclear solute spin systems are compared in the nematic and smectic phases. In Chapter V, nonaxially symmetric dipolar couplings are reported for several systems. The effects of residual fields in the presence of a non-zero asymmetry parameter are discussed theoretically and presented experimentally. Computer programs for simulations of these and other experimental results are found in Chapter VI.

To my family

ACKNOWLEDGEMENTS

It has been my pleasure to be a graduate student in the research group of Professor Alex Pines. Alex's enthusiasm, creativity and sense of humor made his group an exciting place to work and I thank him for making me part of it. One must also acknowledge the members of the group whose contributions were essential in maintaining its life. In particular, I would like to thank Jean Baum, Tony Bielecki, Herman Cho, Tom Jarvie and Chuck Connor for their friendship and willingness to lend a hand or partake in a scientific discussion. In addition, much of the work included in this thesis would not have been possible without the collaborative efforts of two people: Metka Luzar, with her patience in teaching me about liquid crystals, and John Millar, with his help, support and guidance in teaching me about NMR in general.

TABLE OF CONTENTS

I. INTRODUCTION....1

A. Introduction....1

B. The Density Matrix....2

C. Nuclear Spin Hamiltonians....4

1. Zeeman Interaction....5

2. Chemical Shift Interaction....6

3. Radiofrequency Interaction....6

4. Quadrupolar Hamiltonian....7

5. Dipolar Hamiltonian....9

6. Indirect Coupling....11

D. Rotations and Spherical Tensors....12

1. Rotations....12

2. Spherical Tensors....15

E. References....18

II. EXPERIMENTS IN ZERO FIELD....19

A. Motivation....19

B. Field Cycling Schemes....23

1. The Initial State....25

2. Demagnetization....27

a. Spin Temperature....28

b. Adiabatic Demagnetization....30

3. Evolution in Zero Field....31

4. Remagnetization and High Field Detection....32

5. Field Cycling with Demagnetization to Zero Field....33

a. Demagnetization to Zero Field....33

b. Initiating Evolution with Pulsed DC Magnetic Fields....36
C. Calculation of the Signal....37
1. General Approach....37
2. Two Homonuclear Spin I=1/2 Nuclei (I-I)....42
3. Two Heteronucler Spin I=1/2 Nuclei (I-S)....47
4. Single Spin I=1 Quadrupolar Nucleus....51
D. Appendix: Technical and Experimental Details....59
1. High Field Magnet....59
2. Sample Shuttling....63
a. Container....63
b. Shuttle System....63
3. Zero and Intermediate Field Coils....64
a. Zero Field Coil....64
b. Intermediate Field Coil....67
4. The Basic Field Cycle....68
5. Pulsed DC Magnetic Fields....70
6. High Field Detection....74
7. NMR Spectrometer....78
8. Variations in the Experiment....80
a. Direct Observation in Zero Field....80
b. Removal of the Polarizing Field....81
c. Variable Temperature Zero Field Experiments....81
E. References....84
III. PULSED ZERO FIELD NMR and NQR....88
A. Introduction....88
B. Pulsed DC Fields in Zero Field....89

1. Effects of Single Pulses.....90

2. Field Homogeneity.....102

3. Composite Pulses.....110

C. Field Cycling with Pulsed DC Fields.....120

1. Initial Conditions and Demagnetization.....120

a. Coupled Systems.....120

b. Isolated Systems.....121

2. Zero Field NMR and NQR with Pulsed Fields.....129

D. Indirect Detection and Selective Pulsing.....142

1. Introduction to Level Crossing and Selective Pulse Experiments.....143

a. Sensitivity Enhancement Via Level Crossings.....143

b. Spin Selective DC Pulses.....149

2. Experimental Results.....151

3. Isotope Selectivity with Composite Pulses.....158

E. Two Dimensional Zero Field Experiments.....163

1. One Dimensional Zero Field NQR Spectra.....164

2. Two Dimensional Zero Field Experiment.....165

3. Experimental Results.....169

F. References.....172

IV. ZERO FIELD NMR OF LIQUID CRYSTALS.....175

A. Introduction.....175

1. Liquid Crystalline Phases.....175

a. Nematic.....176

b. Cholester c.....178

c. Smectic.....178

2. Magnetic Field Dependent Behavior.....183

3. NMR of Liquid Crystals.....188

a. Order Parameters.....188

b. Nuclear Spin Interactions in Liquid Crystals.....190

B. Nematic Phases in Zero Field Experiments.....195

1. Observations of the Alignment in Zero Field.....195

a. Spin Hamiltonian in Zero Field.....202

2. Demagnetization and Other Pulsed Experiments.....208

3. Positive and Negative Magnetic Susceptibility Anisotropies.....216

a. Spin Hamiltonian in Zero Field.....222

b. Spin Hamiltonian in High Field.....227

4. Summary.....228

C. Smectic Phases in Zero Field Experiments.....230

1. Introduction.....230

2. High Field and Zero Field Spectra.....231

3. Expressions for the Hamiltonian.....241

4. Summary.....248

D. Heteronuclear Spin Systems in Liquid Crystals.....249

1. High Field and Zero Field Hamiltonians.....250

2. Zero Field Spectra.....256

E. Appendix: Liquid Crystal Samples and Experimental Details.....263

1. Experimental Aspects.....263

a. Sample Preparation.....263

b. Field Cycling.....264

c. Experiments to detect disordering.....265

d. Relaxation Times....265

2. Samples....268

a. Solutes....268

b. Liquid Crystals....268

F. References....272

V. NONAXIALLY SYMMETRIC DIPOLAR COUPLINGS....276

A. Introduction....276

B. Librational Motions in a Polycrystalline Hydrate....276

1. Molecular Motions and Tensor Averaging....276

a. Dipolar tensor....276

b. Quadrupolar tensor....280

2. Zero Field Experiments....280

a. Proton zero field spectra....280

b. Deuterium spectrum....285

3. Discussion....287

C. Proton Jumps in a Carboxylic Acid Dimer....288

1. Introduction....288

2. Motionally Averaged Dipolar Tensor....288

3. Zero Field Spectrum....290

D. Quenching of Residual Fields by Nonaxially Symmetric Dipolar Couplings....291

1. Introduction....291

2. Zero Field NMR Theory with Residual Field Effects....292

a. The Hamiltonian....292

b. Perturbation by Residual Fields....292

c. Numerical Simulations....296

3. Experimental Results....299

4. Conclusions.....301

E. References.....304

IV. COMPUTER PROGRAMS.....306

A. INHOM.....308

B. PLTSIM.....312

C. DEMAG.....317

D. QUAD.....325

E. RESID.....331

I. INTRODUCTION

A. Introduction

Nuclear Magnetic Resonance (NMR) involves the interaction of nuclear spins with static and time dependent magnetic fields. It can be used to obtain information on chemical identity, structure and dynamics. This information is contained in the nuclear spin Hamiltonians which may be probed as perturbations in the presence of an applied static magnetic field or, as will be discussed in this thesis, in the absence of such a field. In this first chapter, the formalism and basic interactions are introduced. Later chapters describe the theory and implementation of zero field NMR techniques and their applications to polycrystalline solids and liquid crystalline mesophases. In the experiments presented, the similarity between the uses of pulsed dc magnetic fields in zero field and the high field radiofrequency pulses of "normal" NMR methods is considered.

B. The Density Matrix

A pure quantum mechanical state can be represented by a single ket, $|\psi\rangle$, which when expanded in a complete orthonormal basis set, $|u_n\rangle$, is written

$$|\psi(t)\rangle = \sum_n c_n(t)|u_n\rangle \qquad (I.1)$$

The coefficients, c_n, may be time dependent and often contain arbitrary phase factors. In NMR, one is generally concerned with measuring the

average expectation value for an ensemble of identical systems, rather than observing a single state. In such cases, it is convenient to employ the density matrix.[1]

The elements of the density matrix, ρ, are defined in the expression for the ensemble averaged expectation value of an operator, O, as

$$\overline{\langle O \rangle} = \sum_n \sum_m \overline{c_m c_n^*} \langle u_n | O | u_m \rangle$$

$$= \sum_n \sum_m \rho_{mn} \langle u_n | O | u_m \rangle \qquad \text{(I.2)}$$

The quantities $c_m c_n^*$ can be thought of as the matrix elements of the Hermitian operator, ρ, where

$$\overline{c_m c_n^*} = \langle u_m | \rho | u_n \rangle \qquad \text{(I.3)}$$

From Equations (I.2) and (I.3), it is evident that the expectation value of any operator is quite easily calculated from

$$\overline{\langle O \rangle} = \mathrm{Tr}\{\rho O\} = \mathrm{Tr}\{O\rho\} \qquad \text{(I.4)}$$

The diagonal elements of the density matrix, ρ_{nn}, correspond to the ensemble averaged populations of the states u_n and the elements ρ_{nm} correspond to coherences between states u_n and u_m. The essence of the random phase approximation[2] is that the off-diagonal elements are equal to zero at thermal equilibrium. The diagonal elements, or populations, are expressed in terms of the Boltzmann distribution

$$\rho_{nn} = \frac{1}{Z} \exp(iE_n/kT) \qquad \text{(I.5)}$$

in which the partition function $Z=\Sigma_n \exp(iE_n/kT)$. Writing Equation (I.5)

in terms of the Hamiltonian of the system yields an expression for the density operator

$$\rho = \frac{1}{Z} \exp(iH/kT) \qquad (I.6)$$

The Hamiltonian for a nuclear spin system at thermal equilibrium in a large applied magnetic field is dominated by the Zeeman Hamiltonian ($H_Z=-\omega_O I_Z$ where $\omega_O=\gamma B_O$) since this interaction is orders of magnitude larger than the internal spin interactions. Expanding the exponential in Equation (I.6) and truncating to the first two terms (since $kT>>H_Z$ in the high temperature limit[3]), the density operator becomes

$$\rho = \frac{1}{Z}(1 - \frac{H}{kT}) = \frac{1}{Z}(1 + \frac{\omega_O I_Z}{kT}) \qquad (I.7)$$

In order to interpret and predict the behavior of an ensemble of nuclear spins with time, the evolution of the density operator must be understood. The evolution of the density operator is given by the Liouville-Von Neumann equation[4]

$$\frac{d\rho}{dt} = i[\rho,H] \qquad (I.8)$$

For a time independent Hamiltonian, H, the solution of Equation (I.8) is

$$\rho(t) = \exp(-iHt)\rho(0)\exp(iHt) \qquad (I.9)$$

in which exp(-iHt) is termed the propagator of the system. The Hamiltonian, H, appearing in the exponential terms can include the effects of local spin interactions or the transformation of the density matrix by application of a pulsed field. The first term of the density operator in Equation (I.7) is unchanged by the unitary transformation of Equation (I.9) and the reduced density operator is then defined as

$$\rho = \frac{\omega_o}{2kT} I_z = \beta I_z \qquad (I.10)$$

representing the high field equilibrium state of the system.

C. Nuclear Spin Hamiltonians

In this section, the nuclear spin Hamiltonians are presented and discussed. Since most of the experiments to be described occur in the absence of an applied magnetic field, the usual rotating frame transformation[3,5] is not used. Instead, general forms of the Hamiltonians are presented and specific frames of reference are indicated for individual examples. The secular or truncated[6,7] form of the Hamiltonians in large magnetic fields (i.e. that part which commutes with I_z) is presented for comparison in some instances. The actual mechanics of the truncation are covered in many texts which can be consulted for reference[3,6-8].

The Hamiltonians can be written as a product of a second rank (3x3) Cartesian tensor and two vectors,[7]

$$H = \mathbf{X} \cdot \underline{\mathbf{A}} \cdot \mathbf{Y} = \sum_{i,j}^{x,y,z} A_{ij} X_i Y_j \qquad (I.11)$$

The tensor, $\underline{\mathbf{A}}$, describes the coupling between the vector components, **X** and **Y**, which can correspond to spin vectors of the same or different nuclei, or a magnetic field vector. The matrix representation of the Cartesian tensor depends upon the choice of reference frame. Transformations between different frames is discussed in a later section. The principal axis system (PAS) of $\underline{\mathbf{A}}$ is that which renders **A** diagonal.

1. Zeeman Interaction

The basis of nuclear magnetic resonance lies in the intrinsic spin angular momentum, I, of most nuclear species. The spin angular momentum is proportional to the magnetic moment, μ, which interacts with an applied magnetic field, B. The interaction is expressed as

$$H_Z = - \mu \cdot B = - \gamma_I (h/2\pi) B_o I_z \qquad (I.12)$$

where the field, B_o, is chosen as the laboratory frame z axis and I_z is the component of spin angular momentum in this direction. The gyromagnetic ratio, γ_I, is a constant for a particular nuclear species and plays an important role in magnetic resonance. For example, the above interaction may be expressed in terms of the resonance frequency, $\omega_o = \gamma_I B_o$, of a nucleus in an applied field

$$H_Z = - \omega_o I_z \qquad (I.13)$$

in angular frequency units of radians/sec. This is by far the largest interaction as it is on the order of megahertz ($\nu = \omega/2\pi$). For a given field, this frequency ω_o is characteristic of a nuclear spin due to its dependence on γ_I. Therefore, in an applied field, one gains a handle on different nuclei allowing them to be distinguisned and manipulated on the basis of resonance frequency. While this may seem a trivial fact for most students of NMR, this property is later shown to be an important experimental factor.

The eigenstates of the Zeeman Hamiltonian are the usual angular momentum states, $|m\rangle$, upon which the angular momentum operators act

according to

$$I_z|m\rangle = m|m\rangle$$
$$I^2|m\rangle = I(I+1)|m\rangle \qquad (I.14)$$

and defining $I_+ = I_x+iI_y$ and $I_- = I_x-iI_y$ as the raising and lowering operators, respectively

$$I_+|m\rangle = [I(I+1)-m(m+1)]^{1/2}|m+1\rangle$$
$$I_-|m\rangle = [I(I+1)-m(m-1)]^{1/2}|m-1\rangle \qquad (I.15)$$

where m=-I, -I+1,...,I-1, I for the (2I+1) eigenstates of a single nucleus, spin I.

2. Chemical Shift Interaction

In the presence of a magnetic field, a nucleus is shielded by surrounding electrons. The chemical shift is a measure of the degree of this shielding effect and takes the form

$$H_{CS} = -\gamma_I \mathbf{I}\cdot\underline{\sigma}\cdot\mathbf{B} \qquad (I.16)$$

and is proportional to the applied field. In the absence of a field, the chemical shift vanishes. The chemical shift tensor is a characteristic of different chemical sites and is therefore frequently used for their identification.

3. Radiofrequency Interaction

The interaction of the nuclear spins with an applied radio-frequency (rf) field can be described by the Hamiltonian

$$H_{rf} = - \gamma_I B_1 I_x 2\cos[\omega t + \phi(t)] \qquad (I.17)$$

in which the irradiation is applied in a direction perpendicular (x) to the static field (z). The applied field is characterized by an amplitude $\omega_1 = \gamma_I B_1$, a frequency ω of the irradiation and a phase ϕ. These experimental variables provide for a complex and varied approach to the manipulation of nuclear spins. The treatment of a pulsed rf or dc field on the density operator is discussed in later sections.

4. Quadrupolar Hamiltonian

Certain nuclear spin interactions exist even in the absence of an applied magnetic field and it is these which are of interest in zero field NMR and NQR experiments. One is the quadrupolar interaction[8] which, in analogy to the chemical shift in high field, acts as a site specific chemical label. For nuclei with spin $I \geq 1$, the nucleus has a nonspherical distribution of electric charge, i.e. a quadrupole moment, eQ. This quadrupole moment is a property of a particular nuclear species and interacts with electric field gradients arising in the local environment of the nucleus (e.g. bonding, crystal structure, etc.). The coupling of the nucleus and electric fields for a single spin is given by

$$H_Q = - \frac{eQ}{2I(2I-1)(h/2\pi)} \; \mathbf{I}_1 \cdot \underline{\mathbf{V}} \cdot \mathbf{I}_1 \qquad (I.18)$$

where $\underline{\mathbf{V}}$ is the electric field gradient (EFG) tensor. As stated previously, in the principal axis frame of the interaction the tensor is diagonal with three components V_{zz}, V_{yy} and V_{xx}. These are defined such that

$$|V_{zz}| >> |V_{yy}| >> |V_{xx}|$$

and

$$V_{zz} + V_{yy} + V_{xx} = 0 \qquad (I.19)$$

the latter in accordance with the Laplace's Equation. The largest component of the electric field gradient is often defined as $V_{zz}=eq$, and the asymmetry parameter η, which describes the deviation from axial symmetry of the electric field gradient, is defined by

$$\eta = \frac{V_{yy} - V_{xx}}{V_{zz}} \leq 1 \qquad (I.20)$$

The Hamiltonian written in the principal axis frame of the interaction, in terms of angular momentum operators, becomes

$$H_Q = - \frac{e^2qQ}{4I(2I-1)(h/2\pi)} [3I_z^2 - I^2 + \eta(I_x^2 - I_y^2)] \qquad (I.21)$$

Note that in the principal axis frame there is no angular dependence.

Two characteristic features of this interaction are the value of e^2qQ/h, the quadrupole coupling constant, and the asymmetry parameter, η, which are very sensitive measures of different sites in a molecule, motions or bonding. Molecular motions produce an averaging effect of the quadrupolar interaction making it a sensitive measure of these effects. The quadrupolar interaction can be quite large (kilohertz to many megahertz) but, in the cases relevant to this work, is often on the order of 100-200 kHz. In high field, an interaction of this magnitude would be truncated with respect to the applied field and the secular form is

$$H_Q^o = - \frac{e^2qQ}{8I(2I-1)(h/2\pi)} [(3\cos^2\beta-1) + n\sin^2\beta\cos 2\alpha](3I_z^2 - I^2) \quad (I.22)$$

The orientation dependence arises from the relation of the principal axis frame to the laboratory/field frame. For a powder distribution of crystallites, the angular dependence differs for each orientation and results in a broad range of quadrupolar frequencies and hence a broad spectrum.

5. Dipolar Hamiltonian

Another such field independent interaction is the direct, through space coupling of nuclear magnetic moments as described by the dipolar Hamiltonian.[8] The Hamiltonian may be written as a sum over the couplings of many spins, or for just two spins as

$$H_D = - \mathbf{I}_1 \cdot \underline{\mathbf{D}} \cdot \mathbf{I}_2$$

$$H_D = - \frac{\gamma_1\gamma_2 h}{2\pi r_{12}^3} \left[\frac{3(\mathbf{I}_1\cdot\mathbf{r})(\mathbf{I}_2\cdot\mathbf{r})}{r_{12}^2} - \mathbf{I}_1 \cdot \mathbf{I}_2 \right] \quad (I.23)$$

where r_{12} is the internuclear distance between nuclei 1 and 2 and $\mathbf{r}$ is the unit vector. The dipolar interaction is a traceless, second rank tensor and is generally considered to have axial symmetry. The dipolar Hamiltonian is similar in form to the quadrupolar Hamiltonian (n=0) with products of two spin, rather than single spin, operators. The Hamiltonian may be expanded into a sum of six terms

$$H_D = -\frac{\gamma_1\gamma_2 h}{2\pi r_{12}^3}[A + B + C + D + E + F] \qquad (I.24)$$

in which

$$\begin{aligned} A &= (3\cos^2\beta-1)I_{z1}I_{z2} \\ B &= \tfrac{1}{2}(3\cos^2\beta-1)(I_{z1}I_{z2} - I_1\cdot I_2) \\ C &= \tfrac{3}{2}\sin\beta\cos\beta\exp(-i\alpha)(I_{z1}I_{+2} + I_{+1}I_{z2}) \\ D &= C^* = \tfrac{3}{2}\sin\beta\cos\beta\exp(i\alpha)(I_{z1}I_{-2} + I_{-1}I_{z2}) \\ E &= \tfrac{3}{4}\sin^2\beta\exp(-2i\alpha)I_{+1}I_{+2} \\ F &= E^* = \tfrac{3}{4}\sin^2\beta\exp(2i\alpha)I_{-1}I_{-2} \end{aligned} \qquad (I.25)$$

expressed in an arbitrary frame. The angles, α and β, relate this frame to the principal axis frame with the PAS z axis generally chosen to be the internuclear vector. When the reference frame is determined by an applied field (z axis), the Hamiltonian reduces to the secular terms A and B

$$\begin{aligned} H_D^o &= -\frac{\gamma_1\gamma_2 h}{4\pi r_{12}^3}[3I_{z1}I_{z2} - I_1\cdot I_2](3\cos^2\beta-1) \\ H_D^o &= -\frac{\gamma_1\gamma_2 h}{4\pi r_{12}^3}[2I_{z1}I_{z2} - 1/2(I_{+1}I_{-2} + I_{-1}I_{+2})](3\cos^2\beta-1) \end{aligned} \qquad (I.26)$$

As in the case of the quadrupolar interaction, the angular dependence on β (relating the orientation of the internuclear vector and the field direction) produces a broad range of spectral frequencies for polycrystalline samples. If structure in a spectrum due to dipolar couplings can be deciphered, then the geometry of the spins can be

determined from the r dependence of the interaction.

For a heteronuclear pair of spins, the dipolar coupling is written in the same form as Equation (I.23) replacing the vector operator of the second spin I_2 by S such that

$$H_D = - \mathbf{I} \cdot \underline{\mathbf{D}} \cdot \mathbf{S} \qquad \text{(I.27)}$$

where S is generally used to denote a rare spin species and I an abundant one. The Hamiltonian can be expanded in the same manner as Equations (I.24)-(I.25). In contrast, the I_+I_- "flip-flop" term in Equation (I.26), describing a simultaneous $\Delta m=1$ flip of one spin and a $\Delta m=-1$ flip of the other, is no longer energy conserving for a heteronuclear spin pair in high field due to the different I and S resonance frequencies. The secular form of the heteronuclear dipolar coupling is then

$$H_D^o = - \frac{\gamma_I \gamma_S h}{4\pi r_{IS}^3} [2I_zS_z](3\cos^2\beta - 1) \qquad \text{(I.28)}$$

In the absence of a field, when $(\omega_{oS} - \omega_{oI}) \to 0$, the form of the Hamiltonian changes as will be shown in later discussions.

6. Indirect Coupling

The indirect spin-spin coupling, or J-coupling, is an interaction which is mediated by the electrons of a molecule. The coupling constant, J, is generally considered isotropic (although in some cases anisotropic components which have the same form as the dipolar coupling contribute), and the Hamiltonian may be written for two spins as

$$H_J = - \mathbf{I}_1 \cdot \underline{J} \cdot \mathbf{I}_2 = - J_{12} \mathbf{I}_1 \cdot \mathbf{I}_2 \qquad (I.29)$$

$$H_J^o = - J_{12}[I_{z1}I_{z2} + \tfrac{1}{2}(I_{+1}I_{-2} + I_{-1}I_{+2})]$$

If the chemical shift difference between spins 1 and 2 is large compared to J, the secular term is no longer given by Equation (I.29) but rather

$$H_J^o = - J_{12} I_{z1} I_{z2} \qquad (I.30)$$

For heteronuclear spins, the Hamiltonian has the same form

$$H_J = - J_{IS} \mathbf{I} \cdot \mathbf{S} \qquad (I.31)$$

except that this always reduces in high field to the secular form

$$H_J^o = - J_{IS} I_z S_z \qquad (I.32)$$

as the I_+S_- and I_-S_+ terms are not energy conserving.

D. Rotations and Spherical Tensors

1. Rotations

Rotations include the effects of rf pulses (rotations on the spin degrees of freedom), averaging of tensor interactions (rotations relating spin and/or spatial degrees of freedom), and the representation of tensors in different coordinate frames. A vector, **X**, or tensor, **T**, in a coordinate system (x,y,z) can be expressed in another coordinate system (x',y',z') through the use of a rotation operator, R, where

$$\mathbf{X}' = \mathbf{R}\,\mathbf{X}$$
$$\mathbf{T}' = \mathbf{R}\,\mathbf{T}\,\mathbf{R}^{-1} \qquad \text{(I.33)}$$

The rotation operator, R, is defined as[9]

$$R(\alpha\beta\gamma) = R(\Omega) = R_{z''}(\gamma)R_{y'}(\beta)R_z(\alpha) \qquad \text{(I.34)}$$

and is composed of three successive rotation operators, or in matrix form, three rotation matrices. The $R(\alpha\beta\gamma)$ term describes the rotation in Cartesian space by the angles α, β, γ, commonly referred to as the Euler angles. These angles relate the two coordinate systems as illustrated in Figure I.1.[10] Equation (I.34) describes the rotation by the angle α ($0 \leq \alpha \leq 2\pi$) about the original z axis of the system, followed by β ($0 \leq \beta \leq \pi$) about the new y' axis and lastly, by γ ($0 \leq \gamma \leq 2\pi$) about the final z'' axis. These rotations may also take place about a set of fixed axes (x,y,z) for which R is redefined as

$$R(\alpha\beta\gamma) = R_z(\alpha)R_y(\beta)R_z(\gamma) \qquad \text{(I.35)}$$

The rotation operators can be expressed in terms of the angular momentum operators[9] and Equation (I.35) becomes

$$R(\alpha\beta\gamma) = \exp(-i\alpha I_z)\exp(-i\beta I_y)\exp(-i\gamma I_z) \qquad \text{(I.36)}$$

The effects of rotations on spherical tensors is covered in the following section.

A pulsed radiofrequency or dc magnetic field, B_1, acts as a rotation on a spin system if the pulse is strong, so that the Zeeman

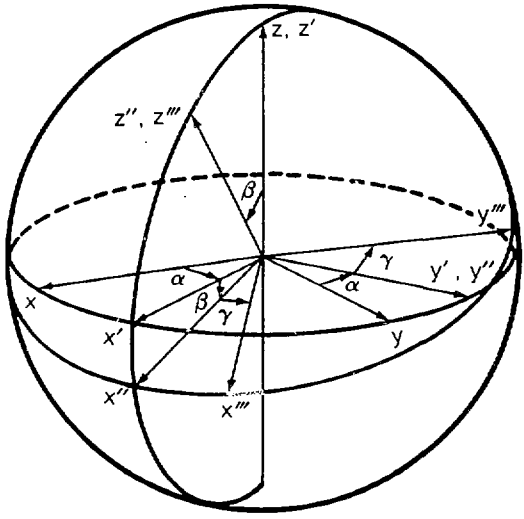

XBL 8610-10174

Figure I.1: The relation of coordinate frames by the Euler angles (α,β,γ) in which the frame of reference moves with the rotated body (as defined in Reference 10). Rotation about the z axis by the angle α ($0 \leq \alpha \leq 2\pi$) takes the axes from the original frame (x,y,z) to the frame labelled (x',y',z'). In this frame, rotation about the y' axis by the angle β ($0 \leq \beta \leq \pi$) results in the position labelled by (x'',y'',z''). Rotation into the final frame (x''',y''',z''') occurs with a rotation by the angle γ ($0 \leq \gamma \leq 2\pi$) about the z'' axis. When there is cylindrical symmetry about the z'' axis, the rotation by the angle γ is no longer necessary to make the frames coincident. In such cases the angles α and β can be related to the more common polar coordinates, ϕ and θ, of the z'' axis in the original frame. Rotations can also be conducted about the original fixed axes (x,y,z) as mentioned in the text.

interaction with the applied field dominates and internal interactions can be neglected. The Hamiltonian for a field in the x direction (in the rotating frame for an rf field[3], or in the laboratory frame for a dc field) is $H = \gamma_I B_1 I_x$ and the propagator in Equation (I.9) becomes

$$\rho(t) = \exp(-i\gamma B_1 I_x t)\rho(0)\exp(i\gamma B_1 I_x t) \qquad (I.37)$$

This is readily recognizable as a rotation operator with a pulse angle, $\theta=\gamma B_1 t$. As an example, consider a pulse applied to the initial state of a spin system in a large field where $\rho(0) \propto I_z$,

$$\begin{aligned}\rho(t) &= \exp(-i\theta I_x) I_z \exp(i\theta I_x) \\ &= I_z\cos\theta - I_y\sin\theta\end{aligned} \qquad (I.38)$$

which corresponds to the rotation of a vector, $(0,0,I_z)$. The rf pulse thereby produces a transverse component of magnetization which may be detected by the voltage it induces in a coil of a tuned circuit.

2. Spherical Tensors

Spherical tensor notation[7,9-11] is introduced in the following section as an alternative representation of the Hamiltonians. This representation is convenient when considering the effect of transformations of tensors under rotations. The elements of a second rank Cartesian tensor, T_{ij} (i,j = x,y,z), may be combined to form irreducible tensors of

$$\text{zero rank:} \quad T_0 = 1/3\mathrm{Tr}\{T_{ij}\} = 1/3\Sigma T_{ii}$$

$$\text{first rank:} \quad T_1 = 1/2(T_{ij}-T_{ji}) \qquad (I.39)$$

second rank: $T_2 = 1/2(T_{ij}+T_{ji})-1/3Tr\{T_{ij}\}$

The irreducible tensor T_l of rank l has 2l+1 components T_{lm} and can be represented in a new frame by

$$T'_{lm} = R(\alpha\beta\gamma)T_{lm}R^{-1}(\alpha\beta\gamma) = \sum_{m'=-l}^{l} T_{lm'}D^{l}_{m',m}(\alpha\beta\gamma) \qquad (I.40)$$

where $R(\alpha\beta\gamma)$ is the rotation operator defined in the previous section. The rotation operation does not alter the rank of the tensor, nor does it change the measured observables associated with the tensor if only a change of coordinate frame is made. The $D^{l}_{m',m}$ terms are the elements of the Wigner rotation matrices

$$D^{l}_{m',m}(\alpha\beta\gamma) = \langle lm'|\exp(-i\alpha I_z)\exp(-i\beta I_y)\exp(-i\gamma I_z)|lm\rangle$$
$$= \exp(-im'\alpha)\, d^{l}_{m',m}(\beta)\, \exp(-im\gamma) \qquad (I.41)$$

The $D^{l}_{m',m}$ elements are tabulated in many books as are descriptions of their symmetry and orthogonality properties.[7,9,10]

The Hamiltonians are conveniently expressed as a product of tensors which is written as

$$\mathbf{A}_l \cdot \mathbf{T}_l = \sum_{m=-l}^{l} (-1)^m A_{lm}T_{l-m} = \sum_{m=-l}^{l} (-1)^m A_{l-m}T_{lm} \qquad (I.42)$$

For example, using Equation (I.11) from Section C.1, the expression for the NMR Hamiltonian in Cartesian tensor and vector notation

$$H = \mathbf{X}\cdot\underline{\mathbf{A}}\cdot\mathbf{Y} = \Sigma_{ij}A_{ij}X_iY_j$$

can now be written in spherical tensor notation as

$$H = \sum_{l=0}^{2} \sum_{m=-l}^{l} (-1)^m A_{lm} T_{l-m} \qquad \text{(I.43)}$$

where the dyadic product of spin vectors forms the tensor **T** and the tensor **A** describes the spatial terms. The NMR interactions are composed of tensors of rank 0,1,2, thus the limits of the index l are determined in Equation (I.43). The truncation of the Hamiltonians is easily seen from the commutation properties of the spherical tensors[12]

$$[I_z , T_{lm}] = mT_{lm} \qquad \text{(I.44)}$$

thus only those elements with m=0 commute with the high field state.

The tensor elements, T_{lm}, are given by[6,7]

$$\begin{aligned}
T_{00} &= -\frac{1}{\sqrt{3}} [T_{xx} + T_{yy} + T_{zz}] \\
T_{10} &= -\frac{i}{\sqrt{2}} [T_{xy} - T_{yx}] \\
T_{1\pm1} &= -\frac{1}{2} [T_{zx} - T_{xz} \pm i(T_{zy} - T_{yz})] \\
T_{20} &= \frac{1}{\sqrt{6}} [3T_{zz} - (T_{xx} + T_{yy} + T_{zz})] \\
T_{2\pm1} &= \mp \frac{1}{2} [T_{xz} + T_{zx} \pm i(T_{yz} + T_{zy})] \\
T_{2\pm2} &= \frac{1}{2} [T_{xx} - T_{yy} \pm i(T_{xy} + T_{yx})]
\end{aligned} \qquad \text{(I.45)}$$

in terms of their Cartesian components.

E. References

1. U. Fano, Rev. Mod. Phys. **29**, 74 (1957).
   D. Ter Haar, Rep. Prog. in Phys. **24**, 304 (1961).

2. A. Abragam and M. Goldman, Nuclear Magnetism: Order and Disorder (Clarendon, Oxford, 1982).

3. C.P. Slichter, Principles of Magnetic Resonance (Springer-Verlag, Berlin, 1978).

4. J. von Neumann, Mathematical Foundations of Quantum Mechanics (Princeton University, Princeton, 1955).

5. I.I. Rabi, N.F. Ramsey and J. Schwinger, Rev. Mod. Phys. **26**, 169 (1954).

6. U. Haeberlen, High Resolution NMR in Solids: Selective Averaging in Adv. Magn. Reson., Supplement 1, (Academic, New York, 1976).

7. M. Mehring, Principles of High Resolution NMR in Solids (Springer Verlag, Berlin, 1983).

8. A. Abragam, Principles of Nuclear Magnetism (Oxford University, Oxford, 1963).

9. M.E. Rose, Elementary Theory of Angular Momentum (J. Wiley, New York, 1967).

10. A.R. Edmonds, Angular Momentum in Quantum Mechanics (Princeton University, Princeton, 1974).

11. B.L. Silver, Irreducible Tensor Methods (Academic, New York, 1976).

12. G. Racah, Phys. Rev. **61**, 186 (1942).

II. EXPERIMENTS IN ZERO FIELD

A. Motivation

It is customary in the NMR experiment to observe the nuclear spin interactions as a perturbation on the much larger Zeeman interaction of the nuclear moments in a large magnetic field. The magnetic field makes two very important contributions; firstly, it produces an observable magnetization or polarization of the nuclear spins proportional to the field strength and secondly, it provides for increased sensitivity in detection due to the dependence of the induced signal voltage on resonance frequency. Thus experimentalists often strive for higher and higher fields for sensitivity enhancement and the increased resolution of the field proportional chemical shifts. This is understandable when studying liquid samples, as the anisotropic components of the nuclear spin interactions are averaged away, but complications arise when applying the same principles to polycrystalline solids or amorphous materials.

The resulting problems are directly attributable to the angular terms arising in the secular forms of the Hamiltonians in a magnetic field. For a given molecular orientation in an applied field, the observed frequency is shifted from its unperturbed value by an amount related to the angular term and the size of the interaction. In liquids, this angular dependence is averaged to zero due to the fast, random isotropic motions of the molecules. When a static distribution of all possible orientations is present, as in a polycrystalline powder, the resulting spectrum is a superposition of spectra from the individual

crystallites. The result is a broad powder spectrum[1] covering a range of frequencies.

For a small number of spins, the powder spectrum retains enough distinctive structure, as shown in Figure II.1, to determine internuclear distances, or quadrupolar coupling constants and asymmetry parameters. As the number of spins increases, so does the complexity of the spectrum making fine structure in the spectrum difficult to interpret. Geometrical information concerning a number of dipolar coupled spins becomes intractable, and equally difficult is the distinction of similar yet inequivalent quadrupolar sites with small asymmetry parameters. Similarly, dynamical effects often produce only subtle changes in a powder spectrum which may not be pronounced enough to interpret. Much experimental time is devoted to unravelling complex spectra and developing approaches to obtain high resolution spectra in solids.[2,3] Often this involves selectively averaging or removing the effects of the orientation dependent interactions while, unfortunately, simultaneously ridding the spectrum of some of its most valuable information. The orientational broadening is avoidable through the use of oriented samples such as single crystals or liquid crystals; although to gain a complete analysis from a single crystal study, the system must be measured as a function of many orientations[3] and the data must then be disentangled.

Ideally, one would like to remove the anisotropy of the interactions in high field while maintaining the information content. Consider then, that the only difference between the crystallites in a powder sample is their orientation dependence with respect to a field direction; in the absence of a field, with no preferential direction in

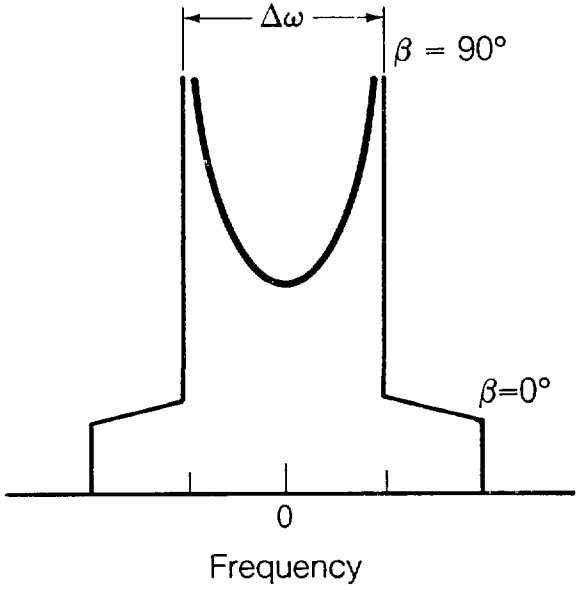

XBL 8610-10169

Figure II.1: Theoretical powder pattern representative of either two dipolar coupled spin I=1/2 nuclei or a single spin I=1 quadrupolar nucleus with η=0. The distribution in frequency is a function of the angle, β, which relates the z axis of the principal axis system (PAS) of the spin interaction to the field direction. In the former, the separation in the singularities is given by the dipolar coupling $\Delta\omega=3\gamma^2h/4\pi r^3$ (tens of kHz) from which the internuclear distance can be calculated. For a spin I=1, with η=0, the powder spectrum has the same characteristic shape with the separation equal to $\Delta\omega=2\pi\cdot(3e^2qQ/4h)$ (tens to hundreds of kHz).

space, every orientation is identical. Thus the energies corresponding to the untruncated zero field Hamiltonian are finite in number and should yield discrete, well-resolved spectral lines. Although the Zeeman, chemical shift and radiofrequency interactions will have vanished, the information rich dipolar and quadrupolar interactions remain. The frequencies corresponding to the dipolar and quadrupolar Hamiltonians can be extremely low on an NMR scale (<200 kHz) and therefore direct detection in zero field is difficult. The conflicting desires to use high field sensitivity and zero field resolution are overcome by using field cycling techniques. Field cycling methods employ an applied field in the preparation and detection periods of the experiment, with the field removed during the evolution period of the spins under the zero field Hamiltonian.

Zero field and field cycling techniques have existed for many years as there has long been interest in the behavior of spin systems in low and zero fields,[4,5] either for measuring relaxation[6] and demagnetization effects,[7-9] or for measuring quadrupolar frequencies.[10,11] There are several review articles and texts[5,9-11] which cover the field in depth and only a brief discussion of a few related experiments follows. The most common experiment is pure Nuclear Quadrupole Resonance (NQR)[10,11] in which the isotopic abundance and differences in quadrupolar energy levels in zero field are large enough (>few MHz) so that the population differences produce an observable polarization. The NQR resonances are detected directly in zero field after perturbing the system with either an rf pulse and Fourier transforming a time domain signal, or with continuous irradiation and detection of the frequency domain signal.[11] Quadrupolar nuclei with small quadrupolar coupling

constants are unaccessible by such experiments. In these cases, field cycling techniques and double resonance NQR methods utilizing sensitivity enhancement via level crossings are employed.[12-14] Most NQR experiments are frequency domain experiments which means that the system is irradiated in zero field. Often this leads to power broadening of the resonance lines,[13] and in double resonance experiments, the undesirable absorption of energy by a second spin species.[13] The experiment to be described in the following sections is a time domain Fourier transform adaptation of previous methods of field cycling developed by Ramsey and Pound,[15] Hahn,[4,16] Redfield[17] and others.[18]

B. Field Cycling Schemes

The field cycle is used to prepare the initial state, induce evolution in zero field, and detect the signal. The basic concept behind the ideal time domain sequence, as depicted in Figure II.2, is as follows. If the sample is prepared in an equilibrium high field state, a magnetization, M_z, proportional to the field, B_z, develops. Sudden removal (in the quantum mechanical sense) of the field leaves the system in a nonequilibrium state and evolution for a given time, t_1, occurs under the zero field Hamiltonian. Terminating the evolution by reapplying the field traps a component of the magnetization[9], and the signal is then detected in high field for that value of t_1. As in a two dimensional experiment,[19] the evolution in zero field is monitored at a later time in successive field cycles as a function of the incremented time, t_1. Fourier transforming this signal produces the frequency domain spectrum. Practically, it is difficult to quickly remove a field

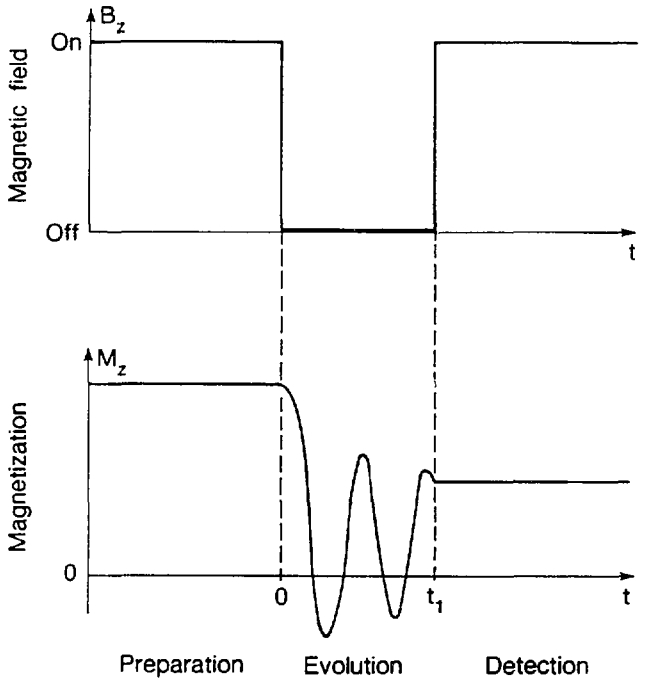

XBL 854-10156

Figure II.2: Idealized version of the field cycle to zero field. At top, the field, B_z, as a function of time and below the magnetization, M_z, as a function of time are illustrated. In the preparation stage, a magnetization M_z, proportional to B_z, develops. Sudden removal of the field to zero at time t_1=0 causes the magnetization to oscillate in the presence of the dipolar or quadrupolar local fields. Evolution in zero field continues for a time, t_1, until it is halted by rapidly reapplying the z field. This traps a component of the magnetization which is then detected in the presence of B_z. Sampling the magnetization, point by point, as a function of t_1 indirectly maps out the oscillations in zero field.

of the magnitude desired for preparation and detection, therefore a stepwise field cycle is used. The experimental field cycle is illustrated schematically in Figure II.3, and is explained step by step in the following sections. A variation of this field cycle using pulsed dc magnetic fields, as an alternative means of inducing evolution in zero field, is also presented. Applications and variations of the experiment are explored in later chapters.

1. The Initial State

Any experiment must begin with an observable, and in NMR it is the behavior of the magnetization of the spin system which is usually examined. In an applied field, the equilibrium state of the system is described by the Zeeman interaction which means that for a spin I there are 2I+1 energy levels separated in energy by $\Delta E=\gamma h B_o/2\pi$. For N spins, an unequal population of the energy levels, as given by the Boltzmann distribution gives rise to a net macroscopic magnetization in the field direction proportional[8] to

$$M_o = \frac{N\gamma h}{2\pi} \frac{\sum_m m\exp(\gamma hmB_o/2\pi kT)}{\sum_m \exp(\gamma hmB_o/2\pi kT)} \qquad (II.1)$$

where m = -I to I. The Boltzmann distribution can also be expanded in the high temperature limit,[8] Equation (II.1) takes the form

$$M_o = \frac{N\gamma^2 h^2 I(I+1)}{12\pi^2 kT} B_o = \chi_o B_o \qquad (II.2)$$

where χ_o, the bulk susceptibility of the system, is proportional to 1/T by the Curie Law. The magnitude of the magnetization is proportional to

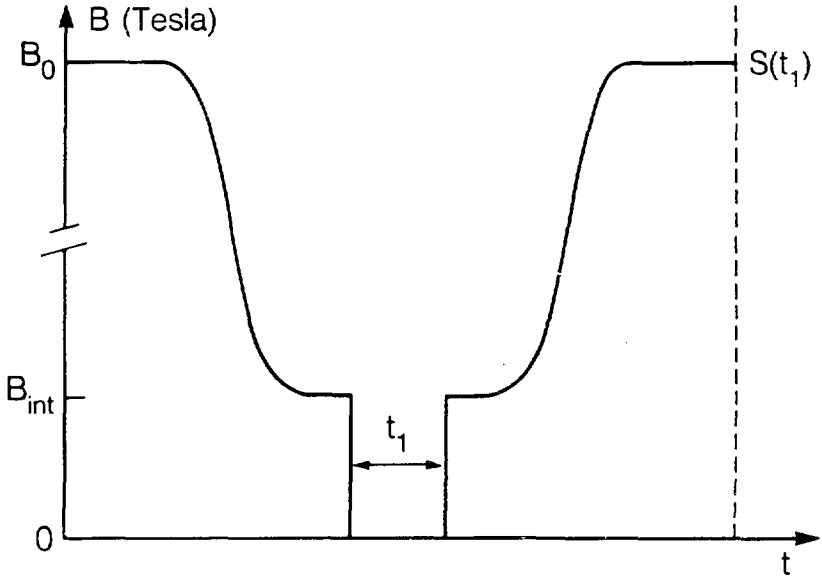

XBL 863-11046

Figure II.3: Schematic representation of the experimental field cycle. The sample originates in a large applied field magnetic field, B_o, during which time an equilibrium magnetization is produced. The field is then adiabatically reduced by removal of the sample to a field level $B_{int} > B_{loc}$. Two magnet coils are used to produce the zero field region and provide a sudden transition in the field which leaves the sample in zero field and initiates evolution for t_1. Reapplying the field, terminates evolution and preserves the z component of magnetization. The sample is adiabatically remagnetized to B_o and the signal is detected by standard NMR methods. Sampling the signal as a function of t_1 produces $S(t_1)$, the time domain signal, which when Fourier transformed yields the zero field frequency domain spectrum.

the inverse temperature, the number of spins, N, the isotopic abundance of the resonant nucleus and the gyromagnetic ratio, γ, which determines the energy level separation for a given field. Examples of these factors have been tabulated for a few nuclei of interest.[20]

The net magnetization in the field direction, M_z, approaches its equilibrium value, M_o, roughly exponentially from a unmagnetized state with a time constant, T_1, known as the spin lattice relaxation time.[21] When allowed to equilibrate and develop a net magnetization, the high field state of a system of many spins, N, is described by the density operator at time t=0,

$$\rho_L(0) \quad \alpha \; I_{z,L} = \sum_{i=1}^{N} I_{zi,L} \qquad \text{(II.3)}$$

where the subscript, L, indicates that this operator is expressed in the laboratory frame with the z axis defined by the field direction. (Operators in the zero field representation will not have subscripts in order to simplify the notation). The initial density operator contains only spin angular momentum terms and is independent of molecular orientation. The eigenstates of the system correspond to the eigenbasis of the high field Hamiltonian. Since the magnetization is proportional to the field strength, the initial preparation stage of the experiment occurs in a field of approximately 4 Tesla.

2. Demagnetization

The next stage of the field cycle is demagnetization to an intermediate field level, B_{int}, as shown in Figure II.3. The notation B_{int} and B_i will be used interchangeably for the intermediate field

level. The demagnetization is accomplished by mechanically moving the sample out of the center of the large magnetic field through the fringe field of the magnet. The fringe field is aligned in the same direction as the main field over the entire transit, thus the shuttling process is simply adiabatic demagnetization in the laboratory frame (ADLF).[9] This process is described by defining two concepts, spin temperature and adiabatic demagnetization.

a. Spin Temperature. The idea of spin temperature originates in a discussion[8,9] of the thermodynamic properties of nuclear spin systems. A macroscopic quantity such as temperature becomes useful in describing the establishment of equilibrium states, cross-relaxation effects and adiabatic demagnetization. A system can be considered to contain at least two reservoirs, namely the spins and the lattice, each with its own thermodynamic properties such as heat capacity and temperature. The lattice is composed of the quasi-continuous distribution of energy levels corresponding to the other degrees of freedom of the system, such as vibrational or phonon modes in the solid. Therefore, the lattice has a much greater heat capacity than the nuclear spin reservoir, and generally is considered to be in a state of thermal equilibrium. The lattice and spins exchange energy through spin-lattice relaxation mechanisms, and the time constant which describes the rate at which the spins come into thermal equilibrium with the lattice is known as T_1. At equilibrium, the lattice has a temperature, T_L.

A temperature, T_S, different from T_L, may be defined for the nuclear spin system if a few conditions exist.[9] If the spin-spin couplings are greater than the coupling to the lattice, then the spin system may be considered isolated from the lattice with its own

temperature. This is often the case in solids with abundant magnetic nuclei, such as protons, among which the dipolar couplings are strong. These couplings rapidly bring the spin system into a state of internal equilibrium with the ratio of the populations of any two of its energy levels is given by the Boltzmann term,[9]

$$\frac{p_m}{p_{m-1}} = \exp\left(\frac{-\gamma h B_o}{kT_s}\right) \qquad \text{(II.4)}$$

with a corresponding spin temperature, T_s, for a two level system. The equilibrium is reached rapidly through the "flip-flop" terms of the secular dipolar Hamiltonian in a time roughly on the order of T_2. This is an energy conserving process for spin I=1/2 nuclei with their equidistant energy levels in an applied field. After a time comparable to the spin-lattice relaxation time, T_1, the spin system will come into thermal equilibrium with the lattice such that $T_s=T_L$. This corresponds to the establishment of a new Boltzmann distribution at the temperature, T_L. If the system is to remain isolated such that $T_s \neq T_L$, then the condition of $T_2 \ll T_1$ must exist and is generally the case in solids.

Some states are not describable by a spin temperature.[9] For example, since a spin temperature is defined by the populations of states, the density operator must be proportional to the diagonal form of the Hamiltonian. Anything which alters this, such as a sudden change in field or an rf pulse, produces off-diagonal elements of the density matrix corresponding to coherences. These coherences, according to the random phase approximation,[22] decay with a time constant T_2. Thus a minimum time T_2 must pass before one can reasonably talk about the establishment of a new spin temperature.

b. Adiabatic Demagnetization. The demagnetization step can be defined as adiabatic if a few conditions are met.[21] An adiabatic process is reversible and occurs with constant entropy, therefore no heat flows in or out of the system. For a nuclear spin system, this indicates that the change in field must be fast compared to T_1 as otherwise energy is exchanged with the lattice thereby producing new Boltzmann populations. Additionally, after each small decrease in the field, a new state of internal equilibrium must be reached. For a system of spin I=1/2 nuclei, this equilibrium is established through the flip-flop terms of the dipolar coupling which conserve the populations of the energy levels. This requires that the change must be slow on a timescale compared to the precession period of the nuclei in the local fields ($t<1/\gamma B_{loc}$) which is generally on the order of tenths of milliseconds and roughly proportional to T_2.[8,21] In solids, a rate of demagnetization can usually be chosen which meets these requirements since $T_2<<T_1$ thereby making the system always describable by a spin temperature.

Since the changes are made adiabatically, fast compared to T_1 (the time required to establish a new equilibrium M_o) and the flip-flop terms conserve M_o, the magnetization remains constant with decreasing field and the spin temperature must therefore decrease. This can be seen by rewriting the Curie Law (Equation II.2) in the high temperature limit as,

$$M_o = \frac{C\,B}{T_s} \qquad \text{(II.5)}$$

where C is the Curie constant containing several nuclear constants and T_s is the spin temperature of the system. The final spin temperature is approximated[13] by

$$T_s \approx T_i\left(\frac{B_f}{B_i}\right) \qquad \text{(II.6)}$$

for B_f greater than the local fields and where, i, corresponds to the initial values and, f, the final.

The adiabatic changes in the state of the system and reestablishment of equilibrium with each field step means that the density operator is always proportional to the instantaneous Hamiltonian.[8] Therefore, if the demagnetization proceeds to an intermediate field level, B_i (where $B_i >> B_{loc}$), the state of the system is still described by the high field Zeeman Hamiltonian as given by Equation (II.3) and retains the polarization of the high field state. If the field is allowed to reach a level where $B_i < B_{loc}$, it no longer is easy to describe the system as being in a purely high field or zero field state unless $B_i \approx 0$.

3. Evolution in Zero Field

The spin system, demagnetized to an intermediate field, B_i, chosen such that the Zeeman interaction in this field dominates over any local spin interactions, is in a state proportional to the Zeeman Hamiltonian. The system remains in the eigenstates quantized with respect to the field direction and retains the full high field magnetization, M_z if no relaxation occurs. Two electromagnetic coils of manageable (i.e. switchable) field strengths are used to maintain this state and provide the transition to zero field (see Appendix A). Evolution under the zero field Hamiltonian can be initiated with the sudden removal of B_i as illustrated in Figure II.3 by the sharp transition in field. Sudden is defined in the quantum mechanical sense,[23] whereby the change in the

Hamiltonian (i.e. field) is too rapid for the system to follow, in contrast to the adiabatic transitions described earlier. The state of the system is unable to change instantaneously, thus the density operator immediately before and after the transition in field is proportional to $I_{z,L}$.

Once the field is removed, the system is in zero field. With the discontinuous change in the field, there has also been a discontinuous change in the Hamiltonian describing the spin system. The high field and zero field Hamiltonians do not commute. In fact, the zero field Hamiltonian is now in an untruncated form and is best represented in a molecular based frame of reference. Because the system is not in the eigenstates of the zero field Hamiltonian, evolution occurs at frequencies corresponding to the local interactions. Evolution continues for a time, t_1, and is described by the time evolution of the density operator (See Section I.1). Evolution is terminated after the t_1 interval by the sudden reapplication of the intermediate field in the laboratory z direction (with $\tau_s << T_2$, to avoid the decay of the evolved state). This traps components of the magnetization in the field direction (i.e. those proportional to $I_{z,L}$) while transverse components, (i.e. those perpendicular to the longitudinal field direction) decay.[9]

4. Remagnetization and High Field Detection

The last step of the field cycle illustrated in Figure II.3 is the detection of the evolution of the nuclear spin system in zero field. After terminating evolution and preserving the laboratory frame z component of the zero field state, the sample is adiabatically remagnetized. As in the case of the demagnetization, the state of the

system is conserved while increasing the field under the same adiabatic constraints. Upon return to the high field, the magnitude of the z component is detected (see Appendix A). The measured signal is a single data point in the period of the zero field oscillations for a given value of t_1. After waiting a delay to allow for relaxation of the nuclear spins, the field cycle is repeated for the next value of t_1. The detected signal, $S(t_1)$, is modulated as a function of t_1 at the frequencies corresponding to the zero field interactions. Fourier transforming this time domain signal produces the frequency domain spectrum.

5. Field Cycling with Demagnetization to Zero Field

Other approaches to field cycling are possible and one which is frequently used involves complete demagnetization to zero field.[12-14] Once demagnetized, the spin system can be probed with rf pulses[24] or continuous rf irradiation as is common in frequency domain experiments,[12-14] or, as developed in the time domain experiments described in Chapter III,[25,26] with pulsed dc magnetic fields. A schematic representation of two such time domain field cycles are illustrated in Figure II.4. In the following sections, the features of these field cycles which differ from the one described previously are discussed.

a. Demagnetization to Zero Field. Many years ago in an experiment conducted by Pound[27] it was found that after adiabatically demagnetizing a system to zero field, such that when $B_0=0$ so does $M_0=0$, the full magnetization was recovered with reapplication of the field. Remagnetization occurred in a time much less than T_1 which indicated that, by

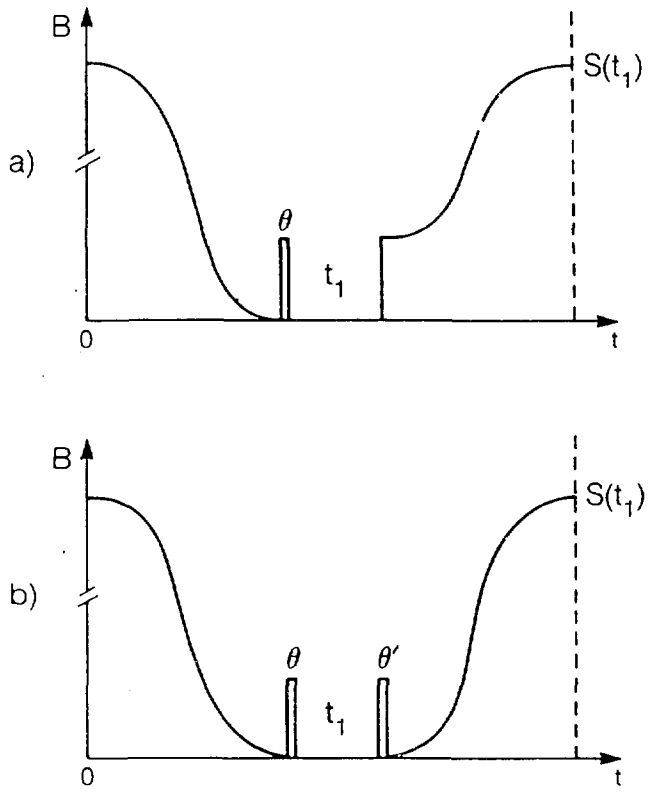

XBL 853-8828

Figure II ": Field cycles utilizing demagnetization to zero field and pulsed dc magnetic fields. The sample is demagnetized to an intermediate field level then to zero field in two steps. In both (a) and (b), the equilibrium state of the spin system is caused to evolve for t_1 by applying a pulsed dc magnetic field. Evolution can be stopped by either, (a) suddenly applying a field in the z direction thereby trapping a component of magnetization before remagnetization and detection, or (b) applying a second dc pulsed field, remagnetizing the sample from zero field and detecting the signal as a function of t_1.

some means, the order of the spin system, once corresponding to a magnetization, was preserved even in the absence of a field. A demagnetized state is therefore intrinsically different than an unmagnetized state. The order is maintained by the nuclear moments aligning with the local fields. Due to the random distribution of local fields, there is no net magnetization. The order in the local fields decays with a time constant different than T_1 and characteristic of the type of order present (e.g. T_{1D} for dipolar order, T_{1Q} for quadrupolar order).

A remaining question is: What is the nature of the demagnetized state and how might it be described? Previously it was stated that during demagnetization the density operator is always proportional to the instantaneous Hamiltonian. This is true for large numbers of coupled spins which are describable by a spin temperature. The transition by adiabatic demagnetization from high to zero field consists of the Hamiltonian, and the eigenstates, going smoothly over to that which describes the system in zero field.[9] The density operator is then proportional to an equilibrium condition in zero field such that

$$[\rho, H_{ZF}] = 0 \qquad \text{(II.7)}$$

For example, as the Zeeman order is transferred to dipolar order, the Hamiltonian of the system changes from being proportional to H_Z to proportional to H_D (which is also H_{ZF}).

For isolated spins or spin I=1 systems, the demagnetization can not be described by the spin temperature approximation.[8,9] In such cases, it is more difficult to simply describe the initial condition in zero field. Equally as difficult is a simple description of the initial state in those instances where spin systems, isolated in high field,

come into contact via the equalization of their energy levels as a consequence of demagnetization. These circumstances and their bearing on the zero field experiment are discussed in more detail in Chapter III.

b. Initiating Evolution with Pulsed DC Magnetic Fields. Without explicitly specifying the form of the initial zero field state, it can be safely assumed that after demagnetization the spin system is in an equilibrium (non-evolving) state in zero field[9] and evolution must be initiated. Previously, this was accomplished by a sudden change in the Hamiltonian. Since the system is already in a state related to the zero field Hamiltonian, instead of a change in the Hamiltonian, a pulsed field can be used to bring about a change in the state of the system. Two such schemes are illustrated in Figure II.4 using pulsed dc magnetic fields. As described in section I.D.7, if $B_i >> B_{loc}$, the pulsed field acts as a rotation (θ) on the density operator causing part, but not all, of the original diagonal elements to be rotated into off-diagonal elements. These off-diagonal elements correspond to coherences between zero field eigenstates and thus the system, no longer in an equilibrium state, begins to evolve under the zero field Hamiltonian.

Evolution continues for t_1 in a manner identical to that described before and can be terminated in two ways. In Figure II.4a, a field is reapplied suddenly in the laboratory z direction to trap those components proportional to $I_{z,L}$. This state is then remagnetized and detected as before measuring the change in $I_{z,L}$ with time. An alternative method in Figure II.4b is to apply a second pulse (θ') which rotates the off-diagonal elements of the density matrix back into diagonal population differences. Remagnetization of this state

preserves the populations and transforms it back into high field for detection in much the reverse of the demagnetization step.

The Zeeman interaction with the pulsed field should dominate over local interactions so that the pulses act like rotations and no evolution occurs during their application. For quadrupolar nuclei with large quadrupole coupling constants and low gyromagnetic ratios, a field on the order of several hundred Gauss to a kGauss is then required. This is much more easily produced as a short intense pulse than for the longer time required of the intermediate field in the sudden transition field cycle. Thus pulsed field cycles have some distinct practical advantages. Additionally, the second field cycle of Figure II.4 allows pulses to be used selectively in exciting different nuclei and the exploitation of the naturally occurring level crossings in the demagnetization step.

C. Calculation of the Signal

1. General Approach

In this section, an approach to calculating the analytical form of the zero field signal is presented for the field cycle shown in Figure II.3. These calculations are based almost entirely on the principles introduced in Chapter I for the density operator and transformations between reference frames. The signal after the zero field t_1 period is calculated as the expectation value of the detected high field operator. This operator is generally $I_{z,L}$, such that the normalized signal is given by Equation I.4

$$S(t_1) = Tr\{\rho(t_1)I_{z,L}\} \qquad (II.8)$$

in which $\rho_L(t_1)$ is the time evolved state of the initial density operator under the zero field Hamiltonian, H_{ZF}. As given by Equation (I.9), the time evolution is written in the zero field frame as

$$\rho(t_1) = \exp(-iH_{ZF}t_1)\rho(0)\exp(iH_{ZF}t_1) \qquad (II.9)$$

in which $\rho(0)$ is the initial density operator prepared in high field and through demagnetization. One characteristic of the field cycle with a sudden transition to zero field (Figure II.3) is that the prepared and detected operators are identical. The initial state has thus far always been expressed in the laboratory frame as

$$\rho_L(0) = I_{z,L} \qquad (II.10)$$

and Equation (II.8) would then represent the correlation function of $I_{z,L}$ with its time evolved counterpart.

For convenience in the calculation of the propagator, the zero field Hamiltonian is best expressed in its eigenbasis referenced to a frame descriptive of the zero field state. This frame is most often chosen to be some molecular based frame in which the Hamiltonian is identical (homogeneous) for all orientations. When working in a zero field/molecular frame, the properties of rotation operators must be used to express the laboratory based operators in the zero field frame. The normalized signal function, reexpressed by substituting Equation (II.9) into Equation (II.8) and including the proper transformations into the zero field frame, is

$$S_{\Omega}(t_1) = Tr\{\exp(-iH_{ZF}t_1)R\rho_L(0)R^{-1}\exp(iH_{ZF}t_1)RI_{z,L}R^{-1}\} \qquad (II.11)$$

The subscript, Ω, indicates that this expression contains an angular dependence relating the laboratory frame to the crystallite molecular frames by the rotation elements, $R(\Omega)=R(\alpha\beta\gamma)$. The angular terms differ for each orientation and since there is a random distribution of orientations of crystallites in a polycrystalline sample, each equally probable, the signal must be integrated over all possible orientations to yield a powder average where

$$S(t_1) = \int_{\Omega} S_{\Omega}(t_1)P(\Omega)d\Omega \qquad (II.12)$$

and for an isotropic distribution $P(\Omega)d\Omega = \sin\beta d\beta d\alpha d\gamma$ over the limits of the Euler angles.[3]

A few important points can be illustrated by discussing the relationship between laboratory and zero field/molecular frames. For the sudden transition field cycle, immediately before and after the removal of the field, $\rho_L(0)=I_{z,L}$. It was stated previously that this corresponds to a non-equilibrium (evolving) state under the zero field Hamiltonian and is easily demonstrated by expressing the density operator in the zero field frame through

$$\rho(0) = R(\alpha\beta\gamma)\rho_L(0)R^{-1}(\alpha\beta\gamma)$$

$$= I_z\cos\beta + I_y\sin\beta\sin\alpha + I_x\sin\beta\cos\alpha \qquad (II.13)$$

where the angular momentum operators in the final line are in the molecular/zero field frame. Note that there is no dependence on the

angle, Y, which may be attributed to the axial symmetry of the initial condition. The matrix representation in the zero field basis of Equation (II.13) contains off-diagonal terms corresponding to coherences which describe the evolution of the system. Thus Equation (II.13) does not represent an equilibrium state of the zero field Hamiltonian, which is to say

$$[\rho(0), H_{ZF}] \neq 0 \qquad \text{(II.14)}$$

indicating from the Liouville-von Neumann equation that evolution occurs since

$$\frac{d\rho}{dt} \neq 0 \qquad \text{(II.15)}$$

Equations (II.14) and (II.15) are a concise general statement about the conditons required for evolution in zero field.

The general approach to calculating the zero field signal can be stated in a few words. First, choose a convenient basis set in which the zero field Hamiltonian is diagonal and calculate the eigenvalues (or as is more often the case, diagonalize H_{ZF} to find the eigenbasis and eigenvalues). The eigenstates and eigenvalues in a molecular based/zero field frame should contain no dependence on crystallite orientation. The initial condition, if proportional to a lab based operator, must be expressed in the zero field frame. For initial and detected operators equal to $I_{z,L}$, substituting Equation (II.13) into Equation (II.11) yields

$$S_z(t_1) = \mathrm{Tr}\{\exp(-iH_{ZF}t_1)(I_z\cos\beta + I_y\sin\beta\sin\alpha + I_x\sin\beta\cos\alpha)$$
$$\times \exp(iH_{ZF}t_1)(I_z\cos\beta + I_y\sin\beta\sin\alpha + I_x\sin\beta\cos\alpha)\} \qquad \text{(II.16a)}$$

and defining the time evolved operator $I_n(t_1)=\exp(-iH_{ZF}t_1)I_n\exp(iH_{ZF}t_1)$.

$$S_{\Omega}(t_1) = Tr\{(I_z(t_1)\cos\beta + I_y(t_1)\sin\beta\sin\alpha + I_x(t_1)\sin\beta\cos\alpha)$$
$$x\ (I_z\cos\beta + I_y\sin\beta\sin\alpha + I_x\sin\beta\cos\alpha)\} \qquad (II.16b)$$

The explicit form of $I_n(t_1)$ consists of terms which are products of spin operators and frequency containing terms.[28] Only certain combinations of operators will survive the trace operation since

$$Tr\{I_jI_k\} = \delta_{jk}$$
$$Tr\{I_jI_kI_l\} = 0 \qquad (II.17)$$

Taking the trace and powder average yields

$$S(t_1) = \frac{1}{3}\sum_{jk}(|I_{xjk}|^2 + |I_{yjk}|^2 + |I_{zjk}|^2)\cos\omega_{jk}t_1 \qquad (II.18)$$

where, for example, I_{xjk} is the (jk)th matrix element of I_x, the molecular frame operator, and $\omega_{jk} = E_j - E_k/(h/2\pi)$, the frequencies of the zero field Hamiltonian. Positive and negative frequencies are indistinguishable and therefore the spectrum is symmetric around zero. Fourier transforming $S(t_1)$ yields the frequency domain spectrum.

In spite of the fact that the detected operator was chosen to be $I_{z,L}$, the calculation discussed thus far can easily incorporate different initial conditions or detected operators or both. One must be consistent in expressing the operators or propagators in a common basis set or frame. Often careful selection, via symmetry arguments, leads to a choice of molecular frame which simplifies the calculation. In later chapters, more explicit calculations including features such as dc pulses, different initial and detected conditions, and transformations between molecular and liquid crystalline frames are covered. Having

demonstrated the general approach, a few specific examples of simple spin systems follow.

2. Two Homonuclear Spin I=1/2 Nuclei (I-I)

For two dipolar coupled spin I=1/2 nuclei, such as the two protons in a water molecule, the initial density operator is

$$\rho_L(0) = I_{z,L} = I_{z1,L} + I_{z2,L} \qquad \text{(II.19)}$$

The protons are assumed to be identical with respect to exchange, consequently, the constants preceding the operators have been dropped to facilitate the following calculations. In zero field, the Hamiltonian is the full untruncated form of the dipolar coupling as given by Equation (I.24) and will be expressed in a molecular based frame. If the z axis of this frame is chosen to be the internuclear vector (which is also the z axis of the PAS), the angle ß equals zero and the Hamiltonian reduces to the axially symmetric form

$$H_D = \frac{-\gamma^2 h}{2\pi r^3}\left[3I_{z1}I_{z2} - I_1 \cdot I_2\right] \qquad \text{(II.20)}$$

Written in the zero field basis set, the eigenstates are given by

$$\begin{aligned} |1\rangle &= 2^{-1/2}(|\alpha\alpha\rangle + |\beta\beta\rangle) \\ |2\rangle &= -i(2^{-1/2})(|\alpha\alpha\rangle - |\beta\beta\rangle) \\ |3\rangle &= 2^{-1/2}(|\alpha\beta\rangle + |\beta\alpha\rangle) \end{aligned} \qquad \text{(II.21)}$$

and

$$|4\rangle = 2^{-1/2}(|\alpha\beta\rangle - |\beta\alpha\rangle)$$

where α is defined as m=1/2 and ß is m=-1/2 (from $\langle I_z\rangle$ in the zero field frame for the state $|I_1 I_2\rangle$). The first three states are commonly

referred to as the triplet manifold and the latter as the singlet state. The eigenvalues corresponding to these states are

$$E_1 = E_2 = -\frac{\omega_D}{2}$$
$$E_3 = \omega_D \qquad \text{(II.22)}$$
$$E_4 = 0$$

with $\omega_D = \gamma^2 h/2\pi r^3$ and contain no orientation dependence, unlike the dipolar energies in high field. The energy levels and allowed transitions are illustrated in Figure II.5. The angular momentum operators do not couple the singlet and triplet manifolds, and the allowed transitions occurring only among the triplet energy levels are

$$\omega_{12} = 0$$
$$\omega_{13} = \omega_{23} = \frac{3}{2}\omega_D \qquad \text{(II.23)}$$

The signal, calculated as for the sudden transition field cycle, is given by Equation (II.16). The matrix representations of the operators in the zero field basis[28] are left as an exercise, as is solving for the trace of their products. Calculating the trace yields

$$S_\Omega(t_1) = \cos^2\beta\cos\omega_{12}t_1 + \sin^2\beta\sin^2\alpha\cos\omega_{23}t_1$$
$$\sin^2\beta\cos^2\alpha\cos\omega_{13}t_1 \qquad \text{(II.24)}$$

Note that only the intensities of the transitions are affected by the angular terms and not the frequencies which correspond to those above. This indicates that each relative orientation of the initial state and a molecular frame, as described by a pair of values of the angles α and β,

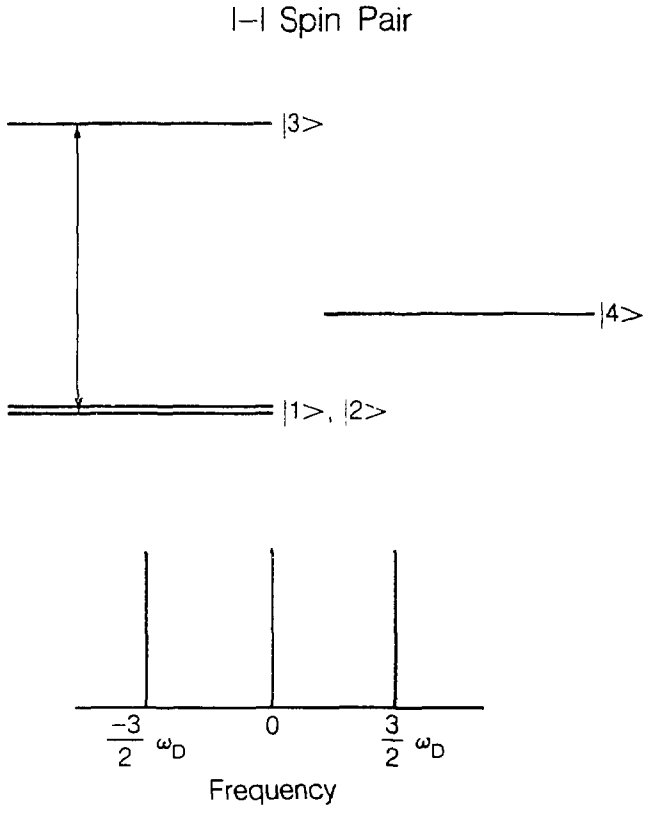

Figure II.5: Energy levels and allowed transitions for two identical dipolar coupled spin I=1/2 nuclei. The eigenstates and energies are given in the text. Allowed transitions occurring between the triplet energy levels are $\omega_{13}=\omega_{23}$ and ω_{12}. The resulting spectrum consists of three peaks of equal intensity at $\pm 3\omega_D/2$ ($\omega_D=\gamma^2\hbar/2\pi r^3$, the dipolar coupling) and zero frequency. The internuclear distance can be calculated from the separation in peaks.

contributes differently to the intensity of the zero field signal but not to the frequency. This is in direct contrast to the high field case in which the frequencies depend upon the values of the angular terms (Equation I.26). Integrating over the powder to include contributions from all crystallites and combining terms, the normalized signal is

$$S(t_1) = \frac{1}{3} [\ 1 + 2\cos(\frac{3}{2}\omega_D t_1)\ ] \qquad (II.25)$$

where $S(t_1)=1$ at $t_1=0$. The spectrum for two identical dipolar coupled spin I=1/2 nuclei is a triplet of three lines of equal intensity; one at zero frequency and two at $\pm 3\omega_D/2$, as illustrated in Figure II.5. An example of an experimental spectrum is shown in Figure II.6 for the protons of the water molecules in an inorganic hydrate, $Ba(ClO_3)_2 \cdot H_2O$. The spectrum appears as predicted by Equation (II.25) and from the frequency separation, the internuclear distance can be calculated.[29]

Calculations and experiments such as these can easily be extended to larger spin systems allowing one to determine the geometry of a group of spins from the characteristic pattern of dipolar couplings in the zero field NMR spectrum. This area is not covered specifically in this thesis but has been dealt with extensively in other work.[28,30] The experiment has been successfully applied in determining internuclear distances in other inorganic hydrates,[30] and in determining structures of four spin systems[28,31] in good agreement with crystallographic data. The more complex systems are not deciphered by direct calculation but rather interpretation is aided by computer simulations. An additional experiment should also be mentioned in which, instead of detecting only the magnitude of the signal in high field, the full high field evolution

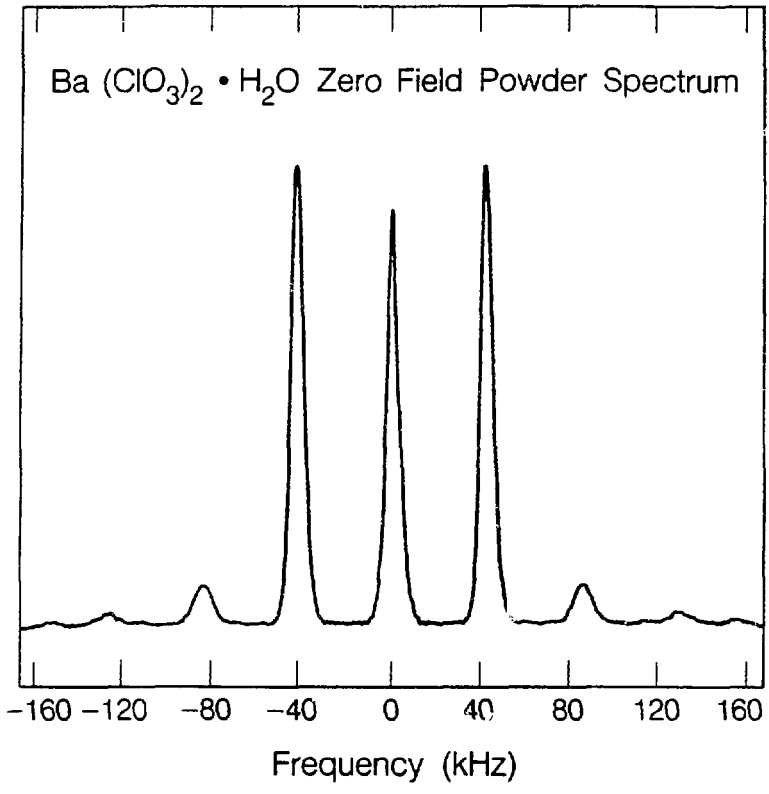

XBL 8610-10168

Figure II.6: Experimental proton zero field spectrum of polycrystalline $Ba(ClO_3)\cdot H_2O$. Three lines of nearly equal intensity are observed at approximately ±40 kHz and zero frequency. The distortion in the intensity of the center line may be attributed to experimental factors. The lines appearing at two and three times the dipolar frequencies are not completely understood but may possibly be attributed to couplings between more than two spins or other types of order present in the demagnetized state.

is allowed to occur for a time, t_2. Fourier transforming with respect to both the zero field t_1 domain and the high field t_2 domain produces a two-dimensional spectrum showing correlations between the high field and zero field signals.[28] The time domain zero field NMR experiment is the only technique generally applicable for the observation of dipolar frequencies in zero field.

3. Two Heteronuclear Spin I=1/2 Nuclei (I-S)

Generally nuclear spins with different gyromagnetic ratios are differentiated on the basis of resonance frequency. In contrast, the sudden transition in field or dc pulses in the zero field NMR experiment excites the evolution of all spin species present since resonance frequency no longer has a bearing. The following discussion focuses on the simplest example of an isolated I-S dipolar coupled pair of spins. The initial state prepared in high field and preserved through demagnetization is presumed proportional to the Zeeman Hamiltonian for each nucleus. The polarization produced in high field must be considered independently for each nucleus such that

$$\rho_L(0) = aI_{z,L} + bS_{z,L} \qquad \text{(II.26)}$$

in which a and b are constants describing the relative polarizations of I and S spins. These constants depend upon the gyromagnetic ratios, γ_I and γ_S, and are therefore unequal for the two spin types (see Equation I.10).

In zero field, chemical shift and resonance frequency differences vanish and the acting Hamiltonian is the mutual dipolar coupling (and probably J coupling) of the two spins. The result is that the hetero-

nuclear spin Hamiltonian is indistinguishable with respect to exchange. The form of the zero field Hamiltonian now includes all additional terms, such as the flip-flop term, as these become energy conserving. The Hamiltonian, written in the molecular/zero field frame with the z axis along the internuclear vector becomes

$$H_D = -\frac{\gamma_I \gamma_S h}{2\pi r^3}\,[3I_z S_z - \mathbf{I}\cdot\mathbf{S}] \qquad \text{(II.27)}$$

in direct contrast to the high field case, but in analogy to the homonuclear case (Section I.C.5). The eigenstates and energies are illustrated in Figure II.7 and are identical in form to the homonuclear case given in Equation (II.21) except that the states here refer to $|IS\rangle$ spin combinations. The energies corresponding to these states are

$$\begin{aligned} E_1 &= E_2 = -\frac{\omega_D}{2} \\ E_3 &= \omega_D \\ E_4 &= 0 \end{aligned} \qquad \text{(II.28)}$$

where $\omega_D = \gamma_I \gamma_S h/2\pi r^3$ and depends upon the product of the gyromagnetic ratios of the I and S spins. Unlike the homonuclear case, matrix elements now connect transitions between the singlet and triplet manifolds with the frequencies given by

$$\begin{aligned} \omega_{12} &= 0 \\ \omega_{13} &= \omega_{23} = \frac{3}{2}\,\omega_D \\ \omega_{14} &= \omega_{24} = \frac{1}{2}\,\omega_D \\ \omega_{34} &= \omega_D \end{aligned} \qquad \text{(II.29)}$$

This effect can be attributed to the differences in magnetogyric ratios

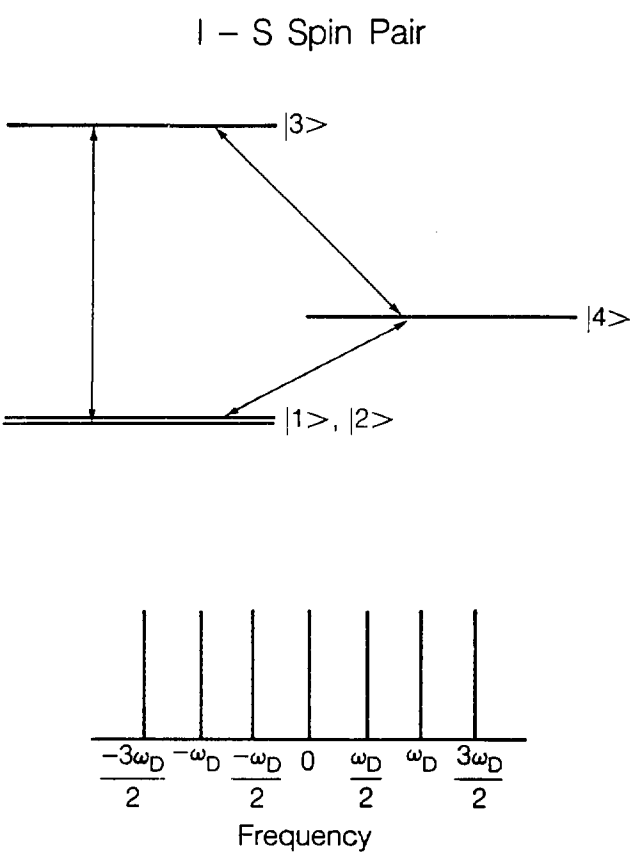

Figure II.7: Energy levels and allowed transitions for two heteronuclear dipolar coupled nuclei (I-S). Energies and eigenstates are given in the text. Transitions are allowed between the triplet and singlet energy levels for certain initial conditions in the heteronuclear spin system. Peak positions in the spectrum occur at multiples of the dipolar coupling frequency ($\omega_D = \gamma_I \gamma_S h/2\pi r^3$) with the intensities dependent on the initial polarization of the I and S spins.

which result in unequal initial populations of the I and S spin states as shown later in this section.

The signal can be calculated as before using Equations (II.10) and (II.11) with the detected operator corresponding to either the I or S spins. Since the former has the larger gyromagnetic ratio and higher natural abundance, sensitivity is expected to be higher. Calculating the signal for the sudden transition field cycle with the detection of $I_{z,L}$ is carried out by solving

$$S_{\Omega}(t_1) = Tr\{RI_{z,L}R^{-1}\exp(-iH_D t_1)R(aI_{z,L}+bS_{z,L})R^{-1}\exp(iH_D t_1)\} \quad (II.30)$$

and taking the trace, $S_{\Omega}(t_1)$ equals

$$S_{\Omega}(t_1) = 2(a+b)\cos^2\beta + 2(a+b)\sin^2\beta\cos(\tfrac{3}{2}\omega_D t_1) + 2(a-b)\cos^2\beta\cos(\omega_D t_1) + 2(a-b)\sin^2\beta\cos(\tfrac{1}{2}\omega_D t_1) \quad (II.31)$$

Averaging over the powder distribution yields for the normalized signal

$$S(t_1) = \frac{1}{6a}\{(a+b) + 2(a-b)\cos(\tfrac{1}{2}\omega_D t_1) + (a-b)\cos(\omega_D t_1) + 2(a+b)\cos(\tfrac{3}{2}\omega_D t_1)\} \quad (II.32)$$

The intensities of the lines in the spectrum depend upon a and b, the relative polarizations. The positions of the predicted transitions are shown in Figure II.7.

Since the nuclei can be manipulated independently with rf pulses in high field to change the relative values of a and b, the appearance of the zero field spectrum can be altered. For the usual equilibrium state with a=1, b=0.25 and lines appear at all four frequencies. By applying pulses which equalize the populations, the signal reduces to

$$S(t_1) = \frac{1}{6}\{\ 2 + 4\cos(\frac{3}{2}\omega_D t_1)\ \} \qquad \text{(II.33)}$$

which is identical to the homonuclear case. This is reasonable since the initial density operator for an I-S pair will be indistinguishable with respect to exchange when a=b as for the homonuclear case. The singlet to triplet transitions (ω_{34}, $\omega_{14}=\omega_{24}$) no longer occur and are directly attributable to the differences in populations. Experiments illustrating the selection of spectral transitions through the altering of a and b have been presented elsewhere.[32] Spectra characteristic of more complicated heteronuclear spin systems such as CH, CH_2 and CH_3 have also been discussed theoretically.[28,30] Additionally, heteronuclear J couplings have also been observed.[32] In later chapters, specific cases of heteronuclear spin systems (^1H,^2H), (^1H,^{14}N) and (^1H,^{13}C) are explored. Although, in general, for an arbitrary dc pulse angle all spins are excited in zero field, this is not rigorously correct. Some of the experiments to be presented involve the selectivity of spin species in zero field with pulsed dc fields and the behavior of heteronuclear spin systems in liquid crystals.

4. Single Spin I=1 Quadrupolar Nucleus

The final case is the quadrupolar spin I=1. Interest in nuclei such as deuterium frequently arises due to the ease of its substitution for protons, and its sensitivity as a chemical and structural probe. The signal for a spin I=1 nucleus in the sudden transition field cycle of Figure II.3 is calculated from Equation (II.11)

$$S_{\Omega}(t_1) = Tr\{RI_{z,L}R^{-1}\exp(-iH_Qt_1)RI_{z,L}R^{-1}\exp(iH_Qt_1)\} \qquad (II.34)$$

in much the same manner as before and evolution occurs under the full untruncated quadrupolar Hamiltonian (Equation (I.21)). The eigenstates in the zero field basis set, shown in Figure II.8, are

$$\begin{aligned} |1\rangle &= 2^{-1/2}(|+1\rangle + |-1\rangle) \\ |2\rangle &= -i2^{-1/2}(|+1\rangle - |-1\rangle) \\ |3\rangle &= |0\rangle \end{aligned} \qquad (II.35)$$

and

and are very similar to the triplet manifold of the two dipolar coupled spin I=1/2 nuclei when η=0. In contrast, the quadrupolar interaction is generally not axially symmetric ($\eta \neq 0$) and the lowest energy levels are no longer degenerate. The similarity of these Hamiltonians is discussed later in Chapter V.

The energies depend upon the quadrupole coupling constant e^2qQ/h and the asymmetry parameter, η,

$$\begin{aligned} E_1 &= -K(1+\eta) \\ E_2 &= -K(1-\eta) \\ E_3 &= 2K \end{aligned} \qquad (II.36)$$

in which $K=2\pi\cdot(e^2qQ)/4h$ for I=1. The signal function, integrated over all orientations in a powder becomes

$$S(t_1) = \frac{1}{3}\{\cos(2\eta)Kt_1 + \cos(3-\eta)Kt_1 + \cos(3+\eta)Kt_1\} \qquad (II.37)$$

and the spectrum consists of six lines of equal intensity as illustrated in Figure II.8 at ± the frequencies (in kHz)

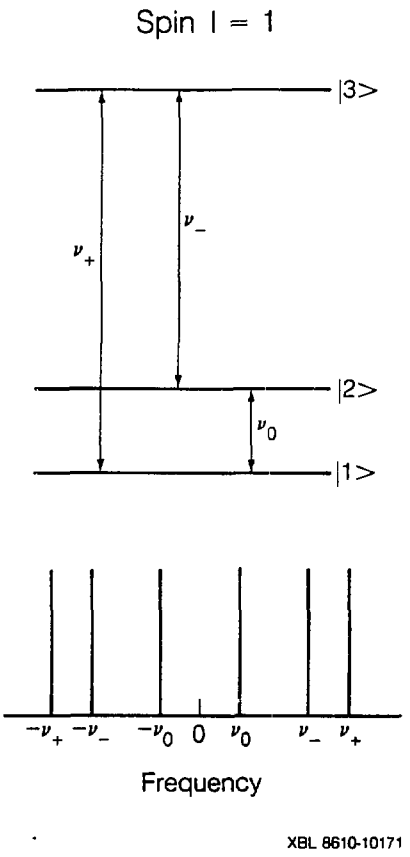

Figure II.8: Energy levels and allowed transitions for a single spin I=1 quadrupolar nucleus with $\eta \neq 0$. The energies and eigenstates are described in the text. Transitions occur between all three levels at frequencies corresponding to ν_+, ν_- and $\nu_0 = \nu_+ - \nu_-$. When $\eta = 0$, the lowest two energy levels are degenerate and the system reduces to three lines; one at zero frequency and two at $\pm(3e^2qQ/4h)$. This spin I=1 case is very similar to the triplet manifold of two dipolar coupled spin I=1/2 nuclei.

$$\nu_+ = (3+\eta)K$$
$$\nu_- = (3-\eta)K \qquad \text{(II.38a)}$$

and the difference frequency

$$\nu_o = 2\eta K = \nu_+ - \nu_- \qquad \text{(II.38b)}$$

From the high frequency lines one may determine K and η, which characterize a quadrupolar site. When two inequivalent sites are present, the spectrum will consist of two sets of overlapping lines and only through the difference frequencies can the separate lines be assigned to calculate the quadrupolar parameters for a given site. When η=0, the two lowest energy levels are degenerate and the spectrum reduces to three lines of equal intensity (not unlike the I-I case, Section C.2).

An example is shown in Figure II.9 for perdeuterated diethylterephthalate. In Figure II.9a, the high field powder spectrum consists of three overlapping powder patterns corresponding to the methyl, methylene and aromatic sites. In the zero field NQR spectrum of Figure II.9b, four distinct regions are observed corresponding to the low frequency ν_o lines, methyl, methylene and aromatic sites in increasing order of frequency. Note that unlike the high field spectrum, the signal intensity is concentrated in a few sharp lines rather than distributed across a broad frequency range. Five distinct sites on the molecule are resolved with e^2qQ/h and η values presented in the following Table.

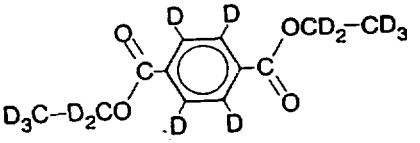

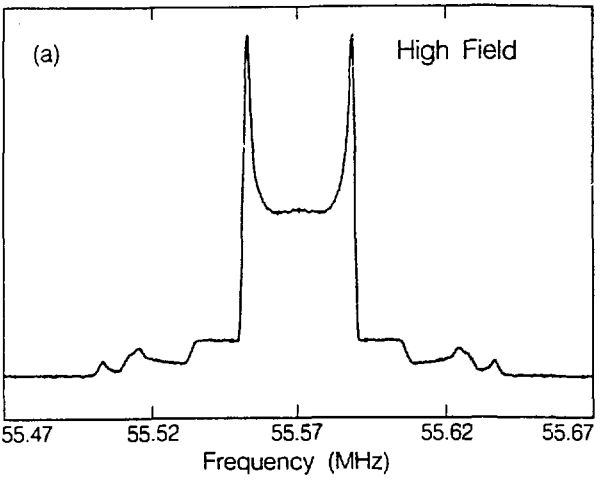

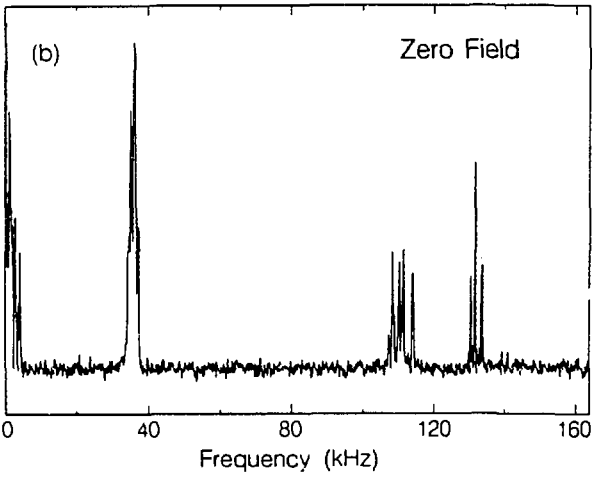

XBL 863-11045

Figure II.9: a). Deuterium high field NMR spectrum of polycrystalline perdeuterated diethylterephthalate. From the overlapping powder lineshapes, three separate quadrupolar sites can be discerned corresponding to the methyl, methylene and aromatic sites on the molecule (although only the singularities are evident for the latter two). b). Zero field deuterium NQR spectrum of the same polycrystalline sample showing only the positive frequencies. Four distinct regions with well-resolved peaks are evident and correspond to the aromatic, methylene, methyl and ν_Q lines in order of decreasing frequency. Quadrupolar coupling constants and small asymmetry parameters can be assigned to five inequivalent sites on the molecule (as given in Table II.1 in the text).

Table 1: Diethylterephthalate ^2H Quadrupole Coupling Parameters

Site	e^2qQ/h (kHz)	n
methyl	48.9	0
methylene	149.53	0.042
	152.76	0.049
aromatic	178.33	0.015
	180.53	0.022

These sites could not be determined from the powder spectrum but can from the well-resolved zero field spectrum. The differentiation of such similar sites is unusual as the differences in quadrupole coupling constants is small and the very small asymmetry parameters are often difficult to measure even in the high field powder spectrum of only one site.

Although expected to be a very small effect, dipole-dipole couplings between deuterons have been detected.[33,34] In the zero field deuterium NQR spectrum, this manifests itself as extra lines and/or structure in the CD_2 region of the spectrum and the corresponding ν_0 lines. Since these couplings depend on many features such as the internuclear distance, relative tensor orientations and bond angle, through computer simulation of the zero field spectrum estimates of the EFG tensor orientations can be determined without requiring the use of a single crystal.[34] More extensive examples and details of quadrupolar spectra are also presented elsewhere,[30,34,54] including the observation of half-integer quadrupolar nuclei. Quadrupolar nuclei which have been studied by zero field NQR methods include 2-Hydrogen, 14-Nitrogen, 27-Aluminum[35] and 7-Lithium[36]. Some extensions of these experiments for

increased sensitivity and selectivity as applied to the observation of ^{2}H and ^{14}N are discussed in the following chapter.

D. Appendix: Technical and Experimental Details

This appendix includes brief descriptions of the experimental design, apparatus and implementation of the field cycling techniques presented in the first part of this chapter. This reflects only one possible method of field cycling, examples of other approaches and equipment can be found in a review articles by Noack[5], and in the series Advances In NQR, and others.[10-13] In practice, the steps of the field cycle involve the simultaneous timing and functioning of many separate pieces of apparatus as illustrated in Figure II.10. In Figure II.10a, the placement of the probe, shuttling system and low field coils relative to the superconducting magnet are shown. Each of these components is described separately in the sections below and after which an outline of the overall field cycle is given.

1. High Field Magnet

The polarization of the sample occurs in a 4.2 Tesla persistant superconducting magnet of reasonable homogeneity with three superconducting shims. The fringe field of the magnet is roughly cylindrically symmetrical and drops off approximately exponentially as shown in Figure II.11. At a distance of ~45 cm below the base of the magnet, the fringe field reaches a value of 100 Gauss. It is in this region that the electromagnetic coils are positioned. The room temperature bore of the superconducting magnet is 89 mm in diameter (without room temperature shim coils) and generally allows ample room to house a room temperature probe and shuttling system.

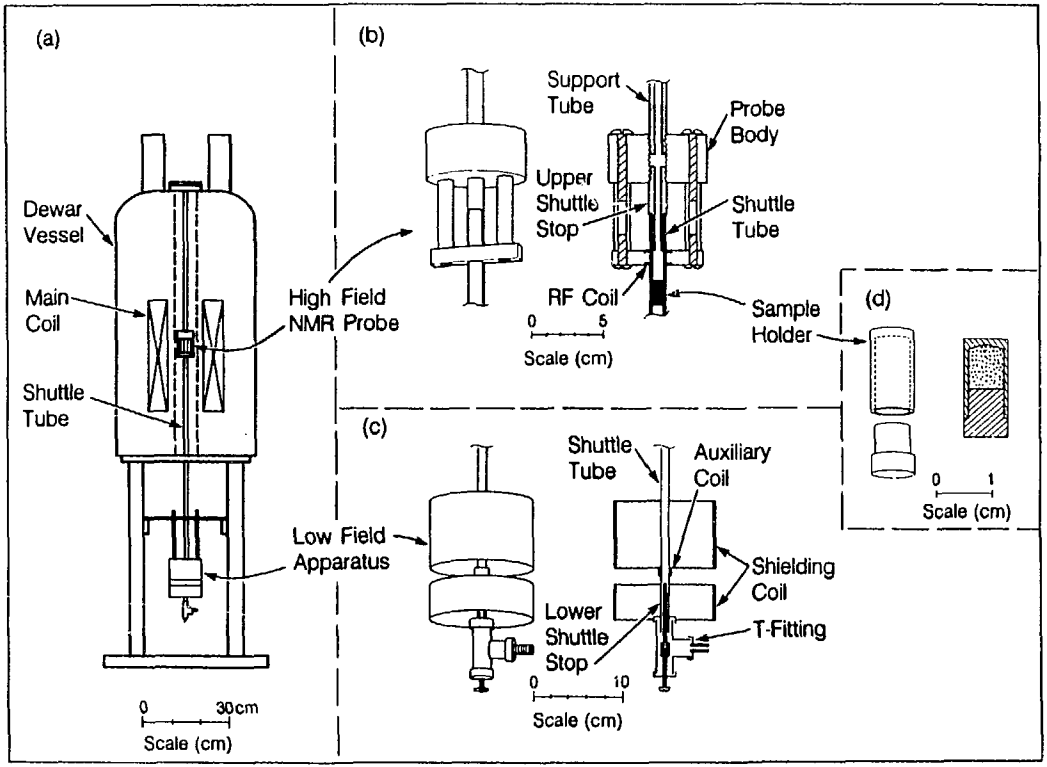

XBL 854-10152

Figure II.10: Schematic of the different components of the field cycling apparatus. In (a), an overview of the entire system showing the placement of the rf probe, shuttling system and low field coils relative to the high field magnet is illustrated. Expanded views of each of these regions are shown in (b)-(d) and are described in separate sections in the text.

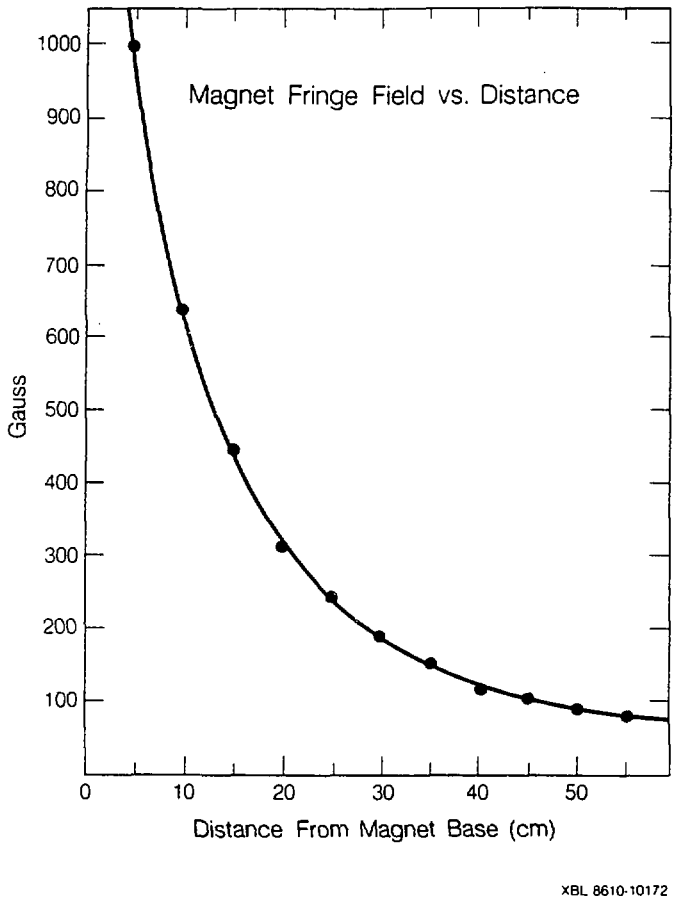

Figure II.11: Magnetic field B_0 vs. distance. The fringe field was measured axially below the magnet. The distance scale corresponds to zero being at the base of the magnet dewar, roughly equal to the lower opening of the bore. The high field center of the magnet is ~35 cm above this where the field reaches a maximum value of ~42 kGauss.

2. Sample Shuttling

a. Container. The sample is packed into a cylindrical nylon or Kel-F shuttle (Figure II.10b) with a tight fitting cap sealing either by a pressure tight fit or an O-ring. The typical sample volume is approximately 0.20 cm^3 although smaller volumes are often used for better zero field or dc pulsed field homogeneity, or when limited amounts of sample are available.

It was discovered empirically that liquid crystal samples are most easily prepared directly in the shuttle to avoid evaporation of the solute. For liquid crystal samples which contained CH_2Cl_2, a specially inert O-ring is required as the usual Viton or Buna varieties absorb the solute. The most successful O-rings found are Kalrez, manufactured by Dupont Co. (Finishes and Fabricated Product Dept., Tralee Park, Wilmington , DE. 19898; size 1/8 x 1/4 x 1/16 inches). The translucent material of the shuttle allows for the determination of the clearing points upon heating. Often an excess of material is added and discarded upon sealing the shuttle to insure the absence of bubbles in the samples. The shuttles very seldom leak and samples remain intact for many months.

b. Shuttle System. The sample shuttles fit closely into a standard walled 10 mm o.d. (~8 mm i.d.) glass tube (Figure II.10). Transporting the shuttles at room temperature is easily accomplished using air, nitrogen and/or vacuum. Gas can be applied to both ends of the shuttle tube or, switching between air for the upward shuttle and vacuum for the downward one, only on the lower end. Switching between the upward and downward transits is conducted with a logic controlled circuit[37] switching ~60 V and driving a commercially available three-way

solenoid valve. (Most reproducible switching results when using a dc activated valve.) The sample travels a distance of approximately 75 cm between the high field rf helmholtz coil and the zero field switching coils. Transit one way takes approximately 200 msec using a gas pressure of 5 psi. The movement of the sample must meet at least two criteria for a successful experiment; one, the time to travel to zero field (including the switching of the coils, ~5-50 msec) must be shorter than T_1 to maintain the polarization, and two, the change in the field with time must meet the conditions for adiabatic demagnetization. Short relaxation times are the more serious problem as these are not under the experimentalist's control (at a given temperature) whereas regulating the shuttling speed more easily controls the demagnetization. Relaxation times are generally field dependent[21] which adds an additional level of complication in deciding which samples will work. The sample is positioned and stopped at either end of its trip by plastic stops which also help to support the shuttle tube. The shuttling procedure is reasonably reproducible in terms of time and impact. Irregularities in the shuttling introduce noise in the t_1 domain of the experiment.[38]

3. Zero and Intermediate Field Coils

Specific design features of the coils and electronics are described elsewhere[37,39], and only a brief description is given here. Two requirements exist for the switching electromagnets. The first is that a homogeneous region of zero field is produced over the sample, and the second is that the change in the intermediate field occurs on the order of a microsecond. The homogeneity of the field scales with the volume of the coil, as does its inductance. Unfortunately though, the

rise time, τ, of the turn on of the coil is directly proportional to the inductance and inversely proportional to the series resistance ($\tau=L/R$). Additionally, the available current for producing the field in the coil is inversely related to this resistance. Thus, although theoretically the shut off of the field and the zero field region could be controlled with one coil, conflicting requirements of homogeneity and speed make two more practical. As shown in Figure II.10a and 10c, the region under the magnet is occupied by two coils labelled the auxiliary coil and the shielding coil used to perform the field step in the experimental sequence. These are also referred to as the B_1 and B_2 coils, respectively, in Figure II.12 where the profiles of the fields from the coils during the field cycle are shown.

a. Zero Field Coil. The larger, more homogeneous coil B_1 cancels the field over the volume of the sample. The cylindrical coil is wound in two sections (as shown in Figure II.10c) to produce a gradient designed to match the gradient of the fringe field, B_f, around 100 G.[39] To first order in the field gradients, this effectively matches and cancels the field. The B_1 coil, due to its size, has a much slower switching time on the order of a few milliseconds to a few tens of milliseconds depending on the inductance placed in series with the coil. The coil operates with a logic controlled feedback network to produce a regulated current of ~7-10 amps with a voltage of 20-30 volts.[39]

The coil is aligned and shimmed using a Hall effect Gaussmeter (F.W. Bell, Inc., Model 811A). Routinely fields of <0.1 G and generally as low as 0.025 G or better are obtained by careful shimming. To cancel inhomogeneities in the zero field region or misalignment of the coil, a set of three static orthogonal shim coils (one gradient z, two trans-

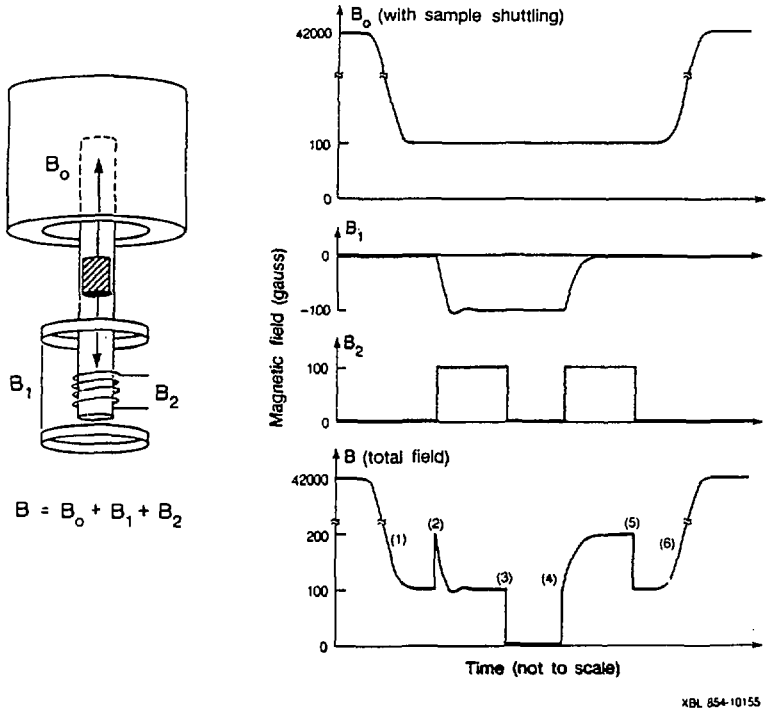

Figure II.12: Schematic of the coil apparatus and graphs of field vs. time for the switching electromagnetic coils. The field, Bo, corresponds to the high field magnet used to polarize and detect the nuclear spins. The coils B_1 and B_2 correspond to the zero field (or shielding) coil and the intermediate field (or auxiliary) coil, respectively. At right, the field profiles of the different coils are illustrated. At top, the fringe field of the B_0 coil experienced by the sample when shuttled to the low field region. The next two graphs represent the switching of the homogeneous zero field coil, B_1, and the rapid switching intermediate field coil, B_2. When combined into the field cycle, the field profile appears as shown at bottom. The steps 1-6 are described in the text (Section D.4).

verse) are mounted on the coil. These operate with a power supply producing in the

x or y directions:	0.8 G/amp (1 amp full)
z direction:	0.4 G/cm per amp (4 amps full)

over a volume of approximately a 1 cm^3. For solids, the homogeneity limitations are not as stringent as those for liquids or liquid crystals in which the natural linewidths are very narrow and the couplings relatively small.

b. Intermediate Field Coil. While the slower, more homogeneous bucking coil is turning on, the sample must remain polarized before the sudden transition in field. This is accomplished with the second intermediate or auxiliary field coil, B_2, producing a field, B_i, which reinforces the fringe field, B_f, of the magnet. The B_2 coil is on when the sample reaches the low field region and the nuclear spins see a field of B_i+B_f. After the bucking coil has turned on completely to cancel B_f, the sample remains in a field $B_i \gg B_{loc}$. The field, B_i, must be greater than the local fields in order to maintain and detect high field states. If $B_i < B_{loc}$, the spin system may disorder to some extent depending on the relative sizes of the fields and result in a loss or distortion in signal. It is the sudden switching off of this field which initiates the zero field period. Since this coil need not produce as homogeneous a field and must be switched rapidly, it is much smaller in size. In fact, the intermediate field coil is usually wound directly on the glass shuttle tube and a typical coil consists of ~20 turns of 28 AWG wire with a length of ~1 cm and an i.d. of 1 cm.

For the transition to be sudden requires that the switching time

$\tau_s << 1/\omega_{max}$, where ω_{max} is the maximum frequency in the zero field spectrum. This generally dictates that τ_s is on the order of 1 μsec which is obtainable using a small inductor and large series resistance such that $L/R=\tau_s$ is small. The series resistance limits the current to the coil and therefore the maximum field, but working with R=5-25 Ω and a coil of the size described, fields of ~400-100 G can be produced and switched in a few hundred nanoseconds. For proton dipolar coupled systems in solids, 100 G is usually a more than adequate field strength and for samples such as liquid crystals the field can be much lower. For quadrupolar nuclei or nuclei with low gyromagnetic ratios, fields of 300-400 G are beginning to only marginally meet the required magnitudes.

The field is governed by a logic controlled high power current pulser for which there are limitations in the accessible power and electronics to switch and produce high fields.[39] The power supplies used are generally not regulated as the field level, if greater than B_{loc}, need not be absolutely constant. In fact, there is often a noticeable droop of ~5-10% in the output voltage with pulses longer than a few milliseconds. The pulsers generally operate at 180 V switching between 7-30 amps. Excessive duty cycles which result in resistive heating can damage the coils and/or pulsers and must be avoided. The intermediate field coil is required to be on for both the turn on and off of the B_1 coil which requires that a fairly large field is produced for a few to several tens of milliseconds.

4. The Basic Field Cycle

A composite of the field switching is illustrated in the last diagram of Figure II.12 in which the numbers refer to the steps of the

basic field cycle as follows:

1. The samples originates in the high field magnet for a time greater than T_1 to polarize the nuclear spins. Downward gas pressure (from the top) or vacuum (from the bottom) is applied to move the sample from high field through the fringe field to the intermediate field level (~100-200 msec).

2. Both the B_1 and B_2 coils are turned on. B_2 turns on quickly (few tenths of μsec) producing a field, B_i, at least as large as the local fields and in the same direction as the fringe field. The B_2 field maintains the spin magnetization, while simultaneously, the slower B_1 coil (tens of msec) turns on to its regulated level cancelling the fringe field.

3. After B_1 is completely on (field level = B_i), the B_2 coil is turned off rapidly. As the sample is now in zero field, evolution of the spin system is allowed to proceed for a time t_1.

4. The evolution is terminated by rapidly reapplying B_2.

5. The B_1 coil is turned off producing a field B_i+B_f, then B_2 is shut off.

6. The sample is adiabatically remagnetized to high field by applying upward air pressure. The shuttle back to high field may occur anytime after step 4 as there is no neccessity in waiting for the coils to switch off as the sample can just as easily be remagnetized from any field level as from B_f. The signal is detected using one of the rf pulse schemes described in Section 5 of this appendix and recorded.

The cycle is then repeated beginning with step 1 and incrementing the time period t_1 for a second point in the time domain signal.

5. Pulsed DC Magnetic Fields

The use of pulsed dc magnetic fields avoids many of the problems associated with controlling large fields for relatively long periods of time. A brief, intense dc pulsed field can be much larger in amplitude and can be produced using a larger current. In addition, a certain amount of flexibility is added to the experiment in the choice of pulse direction, amplitude (B_i) and duration (τ), i.e. pulse angle $\theta=\gamma B_i \tau$. The same pulsers and coils described earlier can be used for the pulsed experiments. To produce the field cycle of Figure II.4b the sequence of the basic field cycle is slightly altered. After completing step 1, removing the sample to the fringe field, steps 2-5 are replaced by:

2. The bucking coil, B_1, is turned on slowly to adiabatically demagnetize the sample to zero field. The rise and fall times of this coil may be tailored to meet adiabatic constraints through the series inductance used.

3. The B_2 coil is turned on for a brief dc pulse (few μsec) of the desired features mentioned above. The zero field period lasts for t_1.

4. A second dc pulse is applied at the end of the t_1 period.

5. The B_1 coil is then turned off, adiabatically remagnetizing the sample to B_f.

Step 7 occurs as before. With added pulsers, coils and alternative sequences of events, more complicated dc pulsed field schemes can be imagined

The rise and fall times of the dc pulsed fields should also be sudden as described previously. For many experiments using dc pulses in zero field, a compromise between field strength (related to current and

resistance), coil homogeneity (related to coil size and inductance) and rise times (related to inductance and resistance) is met to obtain the correct behavior. Homogeneity plays an important role in the dc pulsed field experiments since, in order for the pulse to act as a uniform rotation over the entire sample, the pulsed field must be reasonably homogeneous over the sample volume. This is often accomplished by using larger coils (longer solenoids or helmholtz's) to increase homogeneity. The increased inductance requires a larger series resistance for a rapid rise time. This resistance of course decreases the available current and field but, for homonuclear proton dipolar coupled or liquid crystal samples, quite useable fields are produced. To avoid droop of the dc pulses over long sequences, regulated power supplies are used for increased stability of the pulse amplitudes.

To obtain a desired pulse angle, either the length of the pulse or its amplitude can be altered. For large fields, the available 0.1 μsec setability in length corresponds to a large change in rotation angle. Fine tuning of the pulses is instead easily accomplished through altering the voltage level. If the power supply does not have a variable output, a variac can be inserted between the ac source and the supply to adjust the output voltage of the power supply. This allows one to establish a given pulse angle accurately, but may not allow simultaneous setting of many different pulse angles.

To change the "phase" of the pulsed field (e.g. to give an x or y pulse), as is required in some experiments, coils must be placed in different directions in space as dc fields have no variable phase as do rf fields. The design of a set of three orthogonal coils is shown in Figure II.13. The form for supporting the wires was machined from 1"

Inserted to preserve pagination

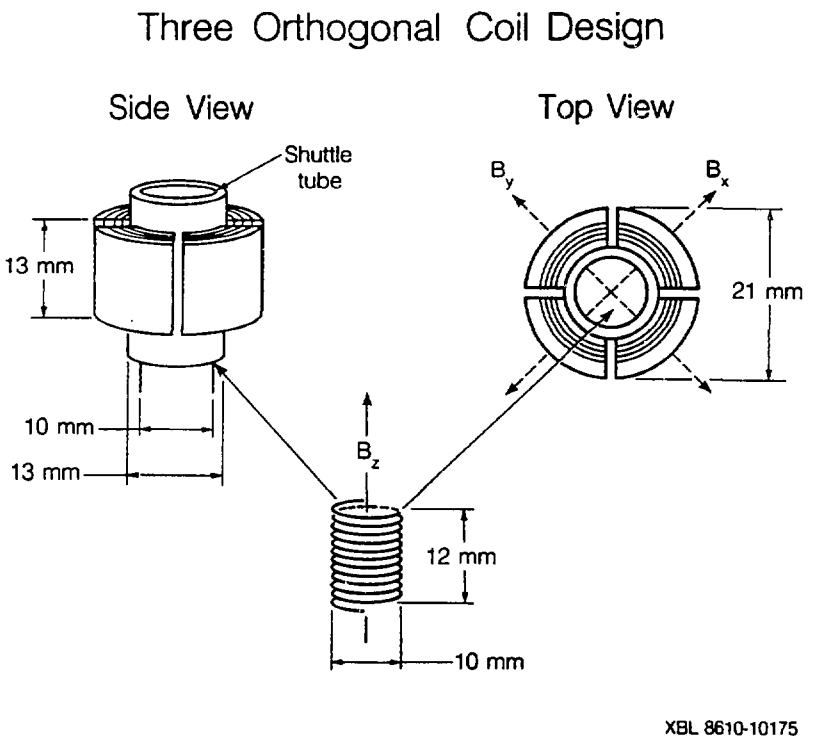

Figure II.13: Design for three orthogonal intermediate field coils. A nylon form is machined to hold two transverse saddle shaped coils on the four sections and an internal solenoid coil. The solenoid produces a field colinear to the main field of the magnet. The solenoid and coil form fit snugly about the 10 mm shuttle tube. The characteristics of these coils are described in the text.

nylon. The two helmholtz coils are 13 mm long by 13 mm in diameter at the center. They consist of 20 turns (10 on each side) of 28 AWG wire spaced radially from the center of the coil form. The angle of the helmholtz was chosen to be the maximum possible (90^{o}) to increase field homogeneity[40] yet avoid overlap and coupling of the coils. The center solenoid is 10 mm i.d. by 12 mm in length. These coils have reasonable homogeneity over the usual sample volume of 0.2 cm^3 (r=0.3 cm, h=0.7 cm) and even better over a 0.1 cm^3 volume (r=0.25 cm, h=0.5 cm) which was often used for liquid crystal samples. The fields produced with these coils using 180 V, 25 Ω in series (~7 amps) were ~40 G. The rise and fall times were ~0.2-0.4 μsec from the beginning of the pulse. (Note that the pulsers have a "deadtime" of ~0.5 μsec before a pulse is produced.) The individual helmholtz coils were found to behave essentially identically. The pulses could be timed and applied immediately after one another with no overlap. To produce six phases of pulsed fields in the three orthogonal coils, six directions of current must be controlled. A bidirectional current pulser was designed to switch between two directions of current in a single coil and a circuit diagram and description can be found in reference 37.

6. High Field Detection

To measure the magnitude of the signal in high field, a component of transverse magnetization which is detectable by standard NMR means must be created. To do this, an rf pulse or series of pulses is applied. Four examples of detection sequences are given in Figure II.14. In the first, a 90^{o} pulse is applied to the spin system and the signal is detected. Generally only the magnitude of this signal is of

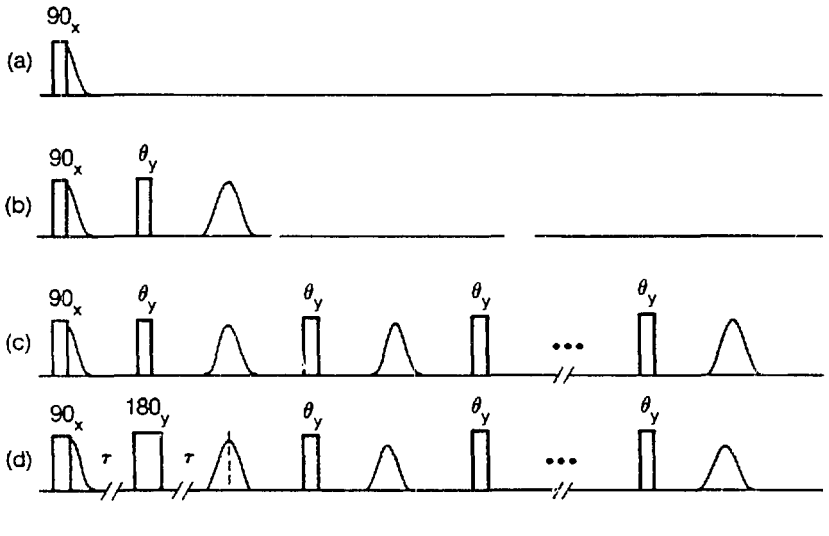

Figure II.14: High field detection sequences. a). A 90°_{x} pulse is applied and the transverse component of magnetization is detected. Often only the magnitude of the signal is required, thus only the first point of the free induction decay (FID) is sampled. b). Solid echo sequence used to avoid probe and receiver recovery by echoing the signal at a later time. In solids, θ_y generally equals 90° and the height of the echoed signal is detected. The full FID signal can be detected in (a) and (b). A pulsed spin-locking or multiple echo sequence, (c) and (d), may be used to prolong the decay of the magnetization and allow for repeated sampling of the signal. The θ_y pulses are generally $<90^{\circ}$ often obtaining maximum signal with $\theta_y=45^{\circ}$. The echo amplitudes are averaged as a single t_1 data point for increased signal-to-noise. The difference between (c) and (d) is in the first echo pulse and delay. The sequence in (c) is generally used for a single component system. The sequence in (d) uses a Hahn echo to separate out the long and short lived signals on the basis of T_2.

interest (see Section B.4) and thus only the first point is recorded. For solids, the use of a solid echo[41] as shown in Figure II.14b aids in detecting the quickly decaying (because of short T_2) signal. This avoids losing the signal, while the probe and receiver electronics are recovering, by echoing it at a later time.

Since one is generally interested only in the magnitude of the signal, there is no need to allow evolution of the signal during the high field time t_2. To increase signal-to-noise, a "pulsed spin-locking" or multiple echo train may be used to extend the decay of the magnetization.[42] This type of pulse sequence is illustrated in Figure II.14c where the echo amplitudes are detected between pulses. Thus one repeatedly samples the signal with its decay governed by a time constant approaching $T_{1\rho}$ rather than T_2. The averaged data recorded as a single t_1 point in the zero field time domain signal. Sample heating is not found to be a problem with these detection sequences as the duty cycle is low.

When wishing to observe only the solute signal in liquid crystal samples, the signal from the liquid crystal solvent must be removed. This is possible due to the very different T_2 relaxation times of the two components. A similar multiple echo sequence, shown in Figure II.14d, is used. In the initial stages, a 90°_x pulse is applied. This produces transverse components of the liquid crystal and solute magnetizations which decay with time constants, $T_{2,lq}$ and $T_{2,s}$, respectively. Since in general $T_{2,lq} \ll T_{2,s}$, waiting a time $\tau \gg T_{2,lq}$ results in the liquid crystal signal decaying to zero. By applying a 180° pulse (Hahn Echo[43]), the solute signal alone refocuses at 2τ and is repeatedly echoed and sampled.

For stability in the experiment, the first pulse of any of the sequences is cycled between the phases x and $\bar{x}$. This inverts the sign of the signal while spectrometer artifacts and dc drift are unaffected. Subtraction of the phase cycled signals should rid the time domain signals of these instabilities. This is an important feature as the experiment can require many hours of signal averaging, especially in those samples with long relaxation times. Drift can occur over time in the rf electronics, amplifier output, or in such areas as the probe tuning (due to mechanical shock), and temperature fluctuations (liquid crystals are especially sensitive). A discussion of the probe electronics can be found in reference 54.

One field cycle produces a single t_1 data point in the time domain cycle. The field cycle is repeated after waiting a few times T_1 to allow for relaxation of the nuclear spins and is repeated for a new value of t_1. The increment in time, Δt_1, is directly related to the range of spectral frequencies as $1/\Delta t_1$=full bandwidth (kHz). According to the Nyquist theorem[44], a signal must be sampled at least two times a period to avoid "folding in" or aliasing of the signal to lower frequency. For example, if the highest frequency in the spectrum is 100 kHz, the signal must be sampled at least with Δt_1=5 μsec as this gives a bandwidth of ±100 kHz. (Recall that the zero field spectra are symmetric around zero frequency).

The high field detection sequences should be optimized to excite as much of the signal as possible. Due to the broad lines of many powders or quadrupolar nuclei this is often difficult. Thus the high field part of the experiment includes many of the rigors of any typical NMR experiment in solids.[44] Additionally, if one desires to detect the

evolution of the sample under the high field Hamiltonian in t_2, there are a wide variety of pulse sequences other than those presented here which can be applied to correlate specific high field information with the zero field spectrum.[2]

7. NMR Spectrometer

A solid state NMR spectrometer has been modified for the field cycling experiments and required no alterations from the basic NMR instrument except for the addition of the coils, shuttling system and coil electronics which are all external to the basic spectrometer electronics. Additionally, the computer capabilities to control the various aspects of the experiments must be available. The spectrometer is a homebuilt instrument based on a 4.2 Tesla magnet and operating at a frequency of 185.03 MHz for protons. A complete description of this spectrometer is given elsewhere[45] and only those aspects which have been altered or adapted are discussed. The data collection and manipulation is controlled by software written specifically for the spectrometer systems in this laboratory[46] and works in conjunction with the pulse programmer unit. The pulse sequences and timing of the zero field and high field instrumentation is controlled by a homebuilt pulse programmer based on its own independent microprocessor and microcode.[47] This unit generates the timing and gate words controlling the sequence of experimental events. Timing is based on a 10 MHz clock therefore the smallest timing increment is 100 nsec. There are ~16 independent logic output gates divided among the tasks as follows: four rf gates, five dc pulsed field controls, one zero field coil logic control line, one shuttling trigger, one temperature controller blank, one deblanking of

the receiver pulse, one data sampling trigger and one scope trigger. The basic limitations of this pulse programmer unit arises when attempting to output many short timing words which causes the unit to "clock-out" its memory. These difficulties often arise with complicated rf or zero field pulse sequences and caution should be exercised as the resultant behavior is not to be trusted. For the basic field cycle, delays for shuttling and coil turn on are often long enough to avoid clocking out of the memory.

Two alterations have been made to the pulse programmer for use on this particular spectrometer. The pulse programmer contains two types of memory units; a RAM and a FIFO. The RAM is generally used for long repetitive sequences such as the pulsed spin-locking and signal detection. In order to facilitate the operation of more complex sequences, the RAM has been "split". Splitting the RAM memory merely allows the one physical memory unit to be accessed at independent starting locations allowing it to act as two RAM memories each half the size. But, since there is only the one RAM memory present, all RAM output statements should begin with 01. To access the split RAM, the "flag" statements in the FIFO which call the RAM into action should be either PA 01 00 or PA 03 00. The former executes the statements in the first 128 steps, and the latter in the following 128 steps. Note that the RAM is loaded sequentially and that the first half must be filled (even with dummy statements that are never executed) in order that the second half begins being loaded at the proper memory location. The split in the RAM need not be 50:50 as was chosen here and can be divided differently with the proper hardware changes. Of course, the full 256 steps of the total RAM memory can be accessed for a single execution by

calling the RAM from the FIFO with only the PA 01 00 statement. The second change consists in the size of the FIFO memory. The basic pulse programmer design[47] incorporates FIFO memories which can hold 16 executable steps. These chips (Fairchild 9403's) were replaced with Fairchild 9423 memory chips which hold 64 steps. Hopefully this will aid in execution and timing problems. Unfortunately, precise information on the loading and emptying times of this FIFO memories is not available but can easily be found experimentally.

8. Variations in the Experiment

Alternatives to sample shuttling, field control and field pulsing are all possible. In the following sections, a few alternative approaches to the zero field experiment are very briefly discussed. These changes may or may not be technically more difficult, but for one reason or another have features which make them attractive.

a. Direct Observation in Zero Field. Extremely high sensitivity detectors would be required to directly observe the oscillating magnetization in zero field. Recently in experiments by other groups, such a device has been used to detect spin noise[48], quadrupolar signals[49] and other low frequency signals[50]. These devices, known as superconducting quantum interference devices (SQUIDs), are flux to voltage transducers and can be frequency independent.[51] Experiments with direct detection would be extremely advantageous as the two dimensional point-by-point field cycle would be reduced to a one dimensional experiment with a great reduction in time. The high sensitivity might be expected to allow for the detection of very small amplitude signals such as those due to the polarization produced in small dipolar or quadrupolar local

fields. If possible, this reduces the necessity of using a large polarizing field. Experiments along these lines are being developed and are discussed elsewhere in more detail.[37,39]

b. Removal of the Polarizing Field. Another experimental approach is to cycle the field by removing the polarizing field through switching the high field coil. Switchable coils with reasonably large fields (up to 1.5 Tesla) are often used in field dependent relaxation studies[5,52] and can be switched on a timescale of a few milliseconds.[5] Although the switch off is not sudden, it is more rapid than mechanical shuttling. Combined with an intermediate field coil to maintain the polarization, the range of samples could be greatly extended to those with short relaxation times for which M_0 would not survive the field cycle. Some of the high field sensitivity would be sacrificed for the ability to switch the field in using a lower field level . In addition, homogeneity and reproducibility of the field level might not be as stable as with a persistent field.

c. Variable Temperature Zero Field Experiments. The integration of a variable temperature field cycling system has numerous applications to zero field NMR experiments. Low temperature field cycling apparatus are in use for many zero field NQR experiments[13] generally operating at 77 K to insure the long relaxation time required for the frequency domain field cycle. Many of the low temperature systems in use involve either the transport of an entire sample cryostat[13] or the mechanical transport of the sample.[53] Many such apparatus are designed around electromagnets whereas here, the system would have to be incorporated into a superconducting solenoid system.

The ability to control the temperature provides a means of

effecting the relaxation times of different samples making their observation possible. Even more interesting is the prospect of measuring the dynamics of molecular systems. The zero field NMR and NQR spectra of solids have narrow lines, unlike powder spectra in large magnetic fields. The changes due to motional averaging should then be more easily observed in the changes in frequencies and lineshapes in the zero field spectra.[55] Observing the spectra as a function of temperature should lead to a great deal of information on the molecular dynamics.

Previously, a design for a low temperature shuttling system was presented.[54] This design was a direct adaptation of the existing zero field set up, since the gas transporting the sample was simply temperature regulated, and the shuttling tube was replaced by a dewared glass tube. This design posed many problems as the temperature control and the shuttling gas were one and the same. Often to control the temperature accurately required that a lower gas pressure be used. This of course detrimentally affected the shuttling of the sample. Special low temperature valves were also required to switch the gas. The rf probe was designed with the helmholtz rf and intermediate field coils outside of the dewar which lead to problems with signal-to-noise and probe arcing.

A new design was developed during the course of this work which hopefully improves upon many of these problems. It was decided that the most efficient way in which to move the sample and control the temperature was to do these independently. Therefore a piston with a stroke length of ~60 cm (ajustable to ~±5 cm) was designed to move the sample in approximately 300-500 msec. The piston operates using room temperature compressed air at pressures from 20-50 psi. The high pressure gas

is controlled by the switching of electronically controlled solenoid valves. The sample is fixed on the end of a rigid fiberglass rod of 3/16" diameter. A glass dewar, supported by mounting to the probe, encloses a region between the rf coil and the zero field coils in which the sample travels. The temperature controlled nitrogen gas impinges on the sample from the lower end making either high or low temperature regulation possible. With this arrangement the temperature can be more easily controlled and is independent of the movement of the sample. The rf coil and intermediate field coils are housed inside the dewar system allowing for increased signal-to-noise, lower rf power requirements and larger pulsed dc fields. Leads from the coils pass through the dewar allowing all rf and zero field electronics to remain at room temperature. The ideal combination for a variable temperature experiment which can be invisioned consists of a switchable high field coil or a zero field detector and a temperature controlled sample region. This requires no movement of the sample and can be designed for temperature regulation of a limited sample region.

E. References

1. (a) G.E. Pake, J. Chem. Phys. **16**, 327 (1948).
   (b) N. Bloembergen and J.A. Rowland, Acta. Met. **1**, 732 (1953).

2. M. Mehring, Principles of High Resolution NMR in Solids, 2nd edition (Springer-Verlag, Berlin, 1983).

3. U. Haeberlen, High Resolution NMR in Solids: Selective Averaging in Adv. Magn. Reson., Suppl. 1 (Academic, New York, 1976).

4. R.L. Strombotne and E.L. Hahn, Phys. Rev. A**133**, 1616 (1964).

5. F. Noack, Prog. in NMR Spectr. **18**, 171 (1986) and references therein.

6. M. Stohrer and F. Noack, J. Chem. Phys. **67**, 3729 (1977).

7. A. Abragam and W.G. Proctor, Phys. Rev. **109**, 1441 (1958).

8. A. Abragam, Principles of Nuclear Magnetism (Oxford University, Oxford, 1963).

9. M. Goldman, Spin Temperature and Nuclear Magnetic Resonance in Solids (Clarendon, Oxford, 1970).

10. M.H. Cohen and F. Reif, Solid State Phys. **5**, 321, (1957).

11. T.P. Das and E.L. Hahn, Solid State Phys., Suppl. 1 (1958).

12. R. Blinc, Adv. Nuc. Quad. Reson. **2**, 71 (1975). (review article)

13. D.T. Edmonds, Phys. Rep. **29**, 233 (1977). (review article)

14. D.T. Edmonds, Int. Rev. Phys. Chem. **2**, 103 (1982). (review article)

15. N.F. Ramsey and R.V. Pound, Phys. Rev. **81**, 278 (1951).

16. (a) R.E. Slusher and E.L. Hahn, Phys. Rev. **166**, 332 (1968).
    (b) J. Koo and Y.N. Hsieh, Chem. Phys. Lett. **9**, 238 (1971).
    (c) Y. Hsieh, J.C. Koo and E.L. Hahn, Chem. Phys. Lett. **13**, 563 (1972)

17. A.G. Redfield, Phys. Rev. **130**, 589 (1963).

18. (a) A.G. Anderson, Phys. Rev. **115**, 863 (1959).
    (b) A.G. Anderson, Phys. Rev. **125**, 1517 (1962).
    (c) R. Blinc et al., J. Chem. Phys. **57**, 5087 (1972).
    (d) L.S. Batchelder, J. Clymer and J.L. Ragle, J. Chem. Phys. **74**, 4791 (1981).
    (e) T.L. Brown et al., J. Amer. Chem. Soc. **104**, 1172 (1982).

19. (a) J. Jeener, Ampere International Summer School, Basko Polje, Yugoslavia (1971).
(b) W.P. Aue, E. Bartholdi and R.R. Ernst, J. Chem. Phys. **64**, 2229 (1976).

20. T.M. Duncan and C. Dybowski, Surface Sci. Rep. **1**, 157 (1981).

21. C.P. Slichter, Principles of Magnetic Resonance, 2nd edition (Springer-Verlag, Berlin, 1980).

22. A. Abragam and M. Goldman, Nuclear Magnetism: Order and Disorder (Clarendon, Oxford, 1982).

23. L.I. Schiff, Quantum Mechanics, 3rd edition (McGraw, New York, 1968).

24. R. Kreis, D. Suter and R.R. Ernst, Chem. Phys. Lett. **123**, 154 (1986).

25. J.M. Millar, A.M. Thayer, A. Bielecki, D.B. Zax and A. Pines, J. Chem. Phys. **83**, 934 (1985).

26. R. Kreis, D. Suter and R.R. Ernst, Chem. Phys. Lett. **118**, 120 (1985).

27. R.V. Pound, Phys. Rev. **81**, 156 (1951).

28. D.B. Zax, A. Bielecki, K.W. Zilm, A. Pines and D.P. Weitekamp, J. Chem. Phys. **83**, 4877 (1985).

29. D.P. Weitekamp, A. Bielecki, D. Zax, K. Zilm and A. Pines, Phys. Rev. Lett. **50**, 1807 (1983).

30. D.B. Zax, Ph.D. Thesis, University of California, Berkeley, (1985).

31. D.B. Zax, A. Bielecki, M.A. Kulzick, E.L. Mutterties and A. Pines, J. Phys. Chem. **90**, 1065 (1986).

32. D.B. Zax, A. Bielecki, K.W. Zilm and A. Pines, Chem. Phys. Lett. **106**, 550 (1984).

33. (a) D.T. Edmonds, M.J. Hunt and A.L. MacKay, J. Magn. Reson. **11**, 77 (1973).
(b) D.T. Edmonds, M.J. Hunt and A.L. MacKay, J. Magn. Reson. **20**, 505, (1975).

34. J.M. Millar, A.M. Thayer, H. Zimmermann and A. Pines. J. Magn. Reson, **69**, 243 (1986).

35. D.B. Zax, A. Bielecki, A. Pines and S.W. Sinton, Nature **312**, 351 (1984).

36. A. Bielecki, J.B. Murdoch, D.P. Weitekamp, D.B. Zax, K.W. Zilm , H.

Zimmermann and A. Pines, J. Chem. Phys. **80**, 2232 (1984).

37. A. Bielecki, Ph.D. Thesis, University of California, Berkeley, (1986).

38. D.P. Weitekamp, Adv. Magn. Reson., **11** (Academic, New York, 1983).

39. A. Bielecki, D.B. Zax, K.W. Zilm and A. Pines, Rev. Sci. Instrum. **57**, 393 (1986).

40. D.I. Hoult and R.E. Richards, J. Magn. Reson. **24**, 71 (1976).

41. (a) J.H. Davis, K.R. Jeffrey, M. Bloom, M.J. Valic and T.P. Higgs, Chem. Phys. Lett. **43**, 390 (1976).
(b) R. Blinc, V. Rutar, J. Seliger, J. Slak and V. Smoles, Chem. Phys. Lett. **48**, 576 (1977).

42. (a) E.D. Ostroff and J.S. Waugh, Phys. Rev. Lett. **16**, 1097 (1966).
(b) W.K. Rhim, D.P. Burum and D.D. Elleman, Phys. Rev. Lett. **37**, 1764 (1976).
(c) D. Suwelack and J.S. Waugh, Phys. Rev. B**22**, 5110 (1980).
(d) M. Matti Maricq, Phys. Rev. B**25**, 6622 (1982).

43. E.L. Hahn, Phys. Rev. **80**, 580 (1950).

44. E. Fukushima and S. Roeder, Experimental Pulse NMR (Addison-Wesley, Reading, 1981).

45. S.W. Sinton, Ph.D. Thesis, University of California, Berkeley, (1981).

46. S. Sinton, J.R. Garbow, J.L. Ackerman, G. Drobny, D.J. Ruben and A. Pines, LBL Publication 3033.

47. G.P. Drobny, Ph.D. Thesis, University of California, Berkeley, (1982).

48. T. Sleator, E.L. Hahn, C. Hilbert and J. Clarke, Phys. Rev. Lett. **55**, 1742 (1985).

49. C. Hilbert, J. Clarke, T. Sleator and E.L. Hahn, Appl. Phys. Lett. **47**, 637 (1985).

50. L.J. Friedman, A.K.M. Wennberg, S.N. Ytterboe and H.M. Bozler, Rev. Sci. Instrum. **57**, 410 (1986).

51. (a) B.D. Josephson, Phys. Lett. **1**, 251 (1962).
(b) R.C. Jaklevic, J. Lambe, A.H. Silver and J.E. Mercereau, Phys. Rev. Lett. **12**, 159 (1964) and **12**, 274 (1964).

52. R.D. Brown and S.H. Koenig, IBM Research Rep. RC6712 (#28906) 8/71.

53. (a) G.P. Jones, J.T. Daycock and T.T. Roberts, J. Sci. Instrum. (J.

Phys. E.) 2, 630 (1969).
(b) Y. Hsieh, P.S. Ireland and T.L. Brown, J. Magn. Reson. 21, 445 (1976).

54. J.M. Millar, Ph.D. Thesis, University of California, Berkeley, (1986).

55. P. Jonsen, M. Luzar, A. Pines and M. Mehring, J. Chem. Phys. 85, 4873 (1986).

III. PULSED ZERO FIELD NMR AND NQR

A. Introduction

In the previous chapter, the basic outline of time domain field cycling methods was presented. These approaches, although extremely useful for observing simple dipolar coupled or quadrupolar spin systems, are not at all selective in either the excitation of the nuclear spins or in determining the subsequent course of evolution of the spin system, since a sudden transition in field or an arbitrarily chosen pulsed field simultaneously excites all nuclear species in zero field. It is desirable to gain a degree of control over these aspects of the experiment and, in analogy with high field NMR with radiofrequency (rf) pulses, pulsed dc fields applied in zero field are one such approach.

DC pulses can be used in field cycles with demagnetization to an intermediate field (i.e. after the sudden removal of the field) or after demagnetization to zero field. Incorporating pulsed fields into the latter has technical advantages already enumerated in the preceding chapter. An additional advantage of the pulsed fields is the experimental flexibility allowed in their duration, magnitude and direction. With these variable parameters, the uses of pulsed fields can go much beyond simple pulsing to initiate evolution into the realm of coherently manipulating the nuclear spin system in zero field. Numerous reasons for applying pulses in zero field are imaginable. Many of these are identical to the uses of rf pulses in high field experiments[1]; among them, to alter the state of the magnetization before evolution and observe its behavior, to select spectral transitions, as

mixing pulses in two dimensional correlation experiments, decoupling of heteronuclear spin systems, refocussing pulses, composite pulses and isotope selectivity.

In this and following chapters, experiments on polycrystalline solids which explore the use of pulsed dc fields in zero field are presented. In the first section, the basic behavior of nuclear spins under such fields is discussed. From this foundation, the uses of pulses in observing zero field NMR and NQR spectra, in two dimensional pulsed correlation experiments, for increasing pulsed field homogeneity and for isotope selectivity are examined. Pulsed fields are also combined with sensitivity enhancement via level crossings for the detection of quadrupolar nuclei.

B. Pulsed DC Fields in Zero Field

Before incorporating dc field pulses into the field cycling schemes of zero field NMR and NQR, an introduction to the characteristics of the pulsed fields and to the behavior of the spin system is given. Much of what is described is analogous to the application of rf pulses in the typical high field NMR experiment and may not seem surprising. Often though, the differences which arise between working in high and zero field or with rf vs. dc pulses require creative approaches to succesfully manipulate the nuclear spins. Stepped dc fields, those turned on continuously to a fixed level, have been frequently used in many experiments to study the relaxation behavior in low field or to test the predictions of spin temperature theories.[2,3] While the applications of brief dc field pulses are

relatively unexplored.[4,5]

1. Effects of Single Pulses

A pulsed field acts as a rotation on the nuclear spin system as first described in Chapter I.D. For an effective pulse, this requires that the field, B_i, of the pulse is much larger than the local fields of the dipolar or quadrupolar spin interactions. When working in the limit of the Zeeman interaction of the spins with B_i being greater than the local fields, the dc pulse is formally described as

$$\rho_L(\tau) = \exp(-iH_{dc}\tau)\rho_L(0)\exp(iH_{dc}\tau) \qquad \text{(III.1)}$$

acting on the state of the spin system as described by the operator ρ expressed in the laboratory frame. The operator for the pulsed field is given by

$$H_{dc} = \gamma_I B_i I_{n,L} \qquad \text{(III.2)}$$

where n=x,y or z, corresponds to the direction in the laboratory frame of the pulsed field. A pulse angle, θ, is defined by

$$\theta = \gamma B_i \tau \qquad \text{(III.3)}$$

and thus Equation (III.1) becomes

$$\rho_L(\theta) = \exp(-i\theta I_{n,L})\rho_L(0)\exp(i\theta I_{n,L}) \qquad \text{(III.4)}$$

For example, if a sample is demagnetized to an intermediate field level, B_i, applied in the laboratory z direction and then suddenly demagnetized as illustrated in Figure III.1, the initial condition for all crystallite orientations in zero field is given by $I_{z,L}$. Applying a

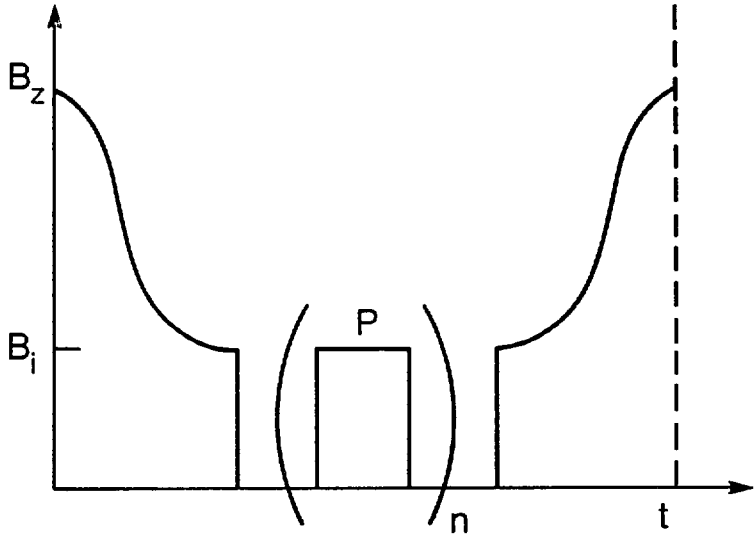

XBL 866-11176

Figure III.1: Field cycle employing pulsed dc magnetic fields after a sudden transition in the intermediate field. Demagnetization from a large field, B_z, to an intermediate z field, B_i ($>B_{loc}$), results in a zero field state proportional to $I_{z,L}$ immediately after the sudden transition in field. A single dc field pulse, P, or several pulses repeated n times can be applied in any direction in space immediately after the removal of the field. The effect of the coherent manipulation of the magnetization in zero field can be monitored by reapplying the field in the z direction, and remagnetizing to B_z where the magnetization is sampled. Field cycling and pulsed dc field times are not drawn to scale and no evolution of the spin system is allowed before or after the pulse.

pulsed field, P, in the laboratory z direction causes no change in the initial state since a torque is not applied by the field to the initial magnetization. This can be shown by solving Equation (III.4) to find that $\rho_L(\tau)=\rho_L(0)$. If, though, the field is applied in either the laboratory x or y directions, the result is to rotate the magnetization such that

$$\rho_L(\theta) = \exp(-i\theta I_{x,L})I_{z,L}\exp(i\theta I_{x,L})$$

$$= -I_{y,L}\sin\theta + I_{z,L}\cos\theta \qquad \text{(III.5)}$$

producing components proportional to I_y and I_z. If the intermediate z field is suddenly reapplied immediately after the pulse, the z component of magnetization is trapped and can be detected in high field. Measuring the amplitude of the magnetization results in an oscillating function, $S(\tau)$, proportional to $\cos\theta$ as can be calculated from

$$S(\tau) = Tr\{\rho(0)\rho(\tau)\} = Tr\{I_{z,L}\rho_L(\tau)\} \qquad \text{(III.6)}$$

$S(\tau)$ represents the projection of the final state on the initial state which, in this case, can be considered the scalar product of two magnetization vectors. The theoretical curve and an experimentally obtained example are shown in Figure III.2. The pronounced decay of the signal with time is not predicted and may be attributed to several factors which are discussed later.

The above situation is identical to that in high field where rf pulses cause the nutation of the magnetization, $I_{z,L}$. Unlike high field NMR where the frequency of the irradiation (γB_o) affects only one nuclear species, in zero field all nuclear spin species are

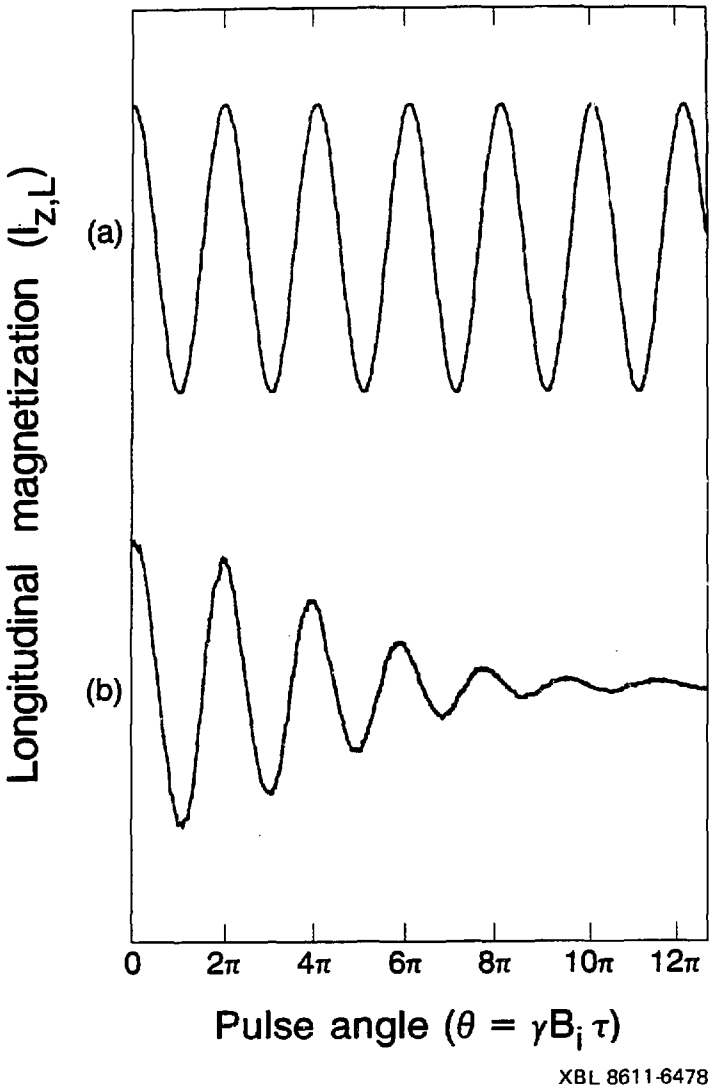

XBL 8611-6478

Figure III.2: Theoretical and experimental curves of the longitudinal magnetization vs. single pulse applied in zero field. The pulsed field is applied in a direction transverse to an initial state proportional to $I_{z,L}$, which is also the detected component (see Figure 1). The signal oscillates according to $|I_z|\cos\theta$ as shown in (a) for ideal pulse conditions in the absence of relaxation. In (b), an experimental curve of the signal from a sample of CH_2Cl_2 in a nematic liquid crystal shows the same general behavior, but decays due to field inhomogeneity and other effects.

simultaneously irradiated by a dc field and the effective pulse angle ($\theta=\gamma B_i \tau$) varies with γ. DC fields are used since the resonance frequency is zero for all nuclei. As for an rf pulse, a dc pulse will still excite over a range of frequency given by $\sin\omega\tau/\omega\tau$. In Figure III.2 the behavior of one spin species (here, ^1H) is shown as only this nucleus is detected in high field.

If the sample is instead demagnetized completely to zero field, the situation is different as the pulses are now applied to an equilibrium zero field state for which

$$[\rho(0),H_{ZF}] = 0 \qquad \text{(III.7)}$$

in which ρ is proportional to the components of a second rank tensor. The effect of a single dc pulse on such a system can also be observed. The pulse, referenced to a laboratory based frame, must be reexpressed in the molecular/zero field frame of ρ and Equation (III.4) becomes

$$\rho_\Omega(\theta) = R\exp(-i\theta I_{n,L})R^{-1}\rho(0)R\exp(i\theta I_{n,L})R^{-1} \qquad \text{(III.8)}$$

where $R=R(\alpha\beta\gamma)$, the rotation operator. As a simple test of these ideas, consider the following experiment illustrated in Figure III.3. The sample, initially in high field, is shuttled down to zero field where it is subjected to a single dc pulse of varying length, then shuttled back to high field where its proton pulsed spin locking signal is recorded. The high field signal for a pulse of length τ using Equation (III.6) is

$$S_\Omega(\tau) = Tr[\rho(0)R\exp(-iH_{dc}\tau)R^{-1}\rho(0)R\exp(iH_{dc}\tau)R^{-1}] \qquad \text{(III.9)}$$

Because of the powder distribution of crystallites, $R(\alpha\beta\gamma)$ differs for

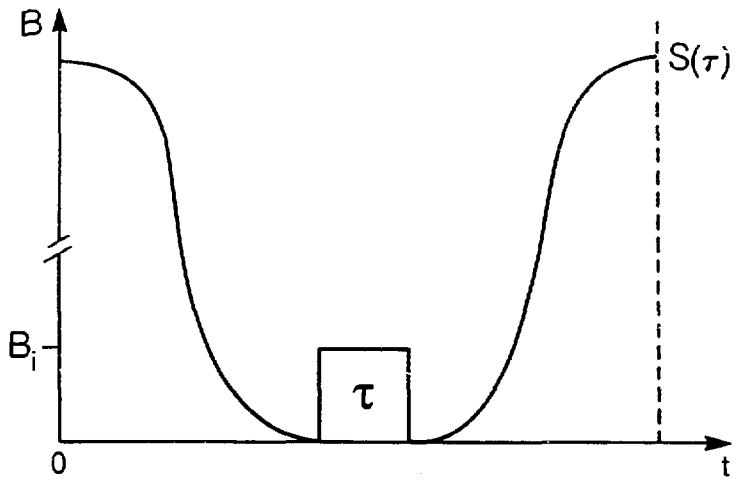

Figure III.3: Field cycle for the application of a single dc magnetic field pulse after demagnetization to zero field. The sample is shuttled adiabatically from the large magnetic field to zero field. The pulsed field is applied for a time τ (few μsec) with a corresponding pulse angle given by $\theta = \gamma B_1 \tau$. The direction, duration and amplitude of the pulse is variable. After remagnetization, the signal is detected as a function of τ.

each orientation as does the orientation of the rotation axis in the crystallite molecular frame. The pulses correspond to rotations by the angle $\theta=\gamma B\tau$ about an axis oriented at some values of α and β in the molecular frame. The expression for the signal is the correlation function of the initial zero field state and its rotated counterpart. Simulations in Figure III.4 illustrate the effects of a pulse applied in the laboratory z direction on different crystallite orientations. The periodicity of the signal can be found by solving Equation (III.9) for a given orientation.

For a powder sample, Equation (III.9) must be averaged over all possible orientations, i.e. over all α, β and γ. Figure III.5a shows that the average behavior over a powder is periodic as a function of τ and that the signal magnitude for $\theta=2\pi$ is nearly equal to that for $\theta=0$. This experimental result is for the protons in polycrystalline $Ba(ClO_3)_2\cdot H_2O$, a dipolar system consisting of strongly coupled pairs of protons within the water molecules, and similar behavior has been observed in other systems. Assuming that a single spin temperature describes the demagnetized state[3] as discussed in Chapter II,

$$\rho(0) = H_D \qquad \text{(III.10)}$$

for the pairs of protons. Performing the integration over the powder distribution, the signal function calculated by substituting Equation (III.10) into Equation (III.9) is

$$S(\tau) = 1/5[1 + 2\cos(\gamma_I B_{dc}\tau) + 2\cos 2(\gamma_I B_{dc}\tau)]S(\tau=0) \qquad \text{(III.11)}$$

This agrees with the experimental results showing local maxima at $n\pi$ as illustrated in Figure III.5b, but predicts no signal decay.

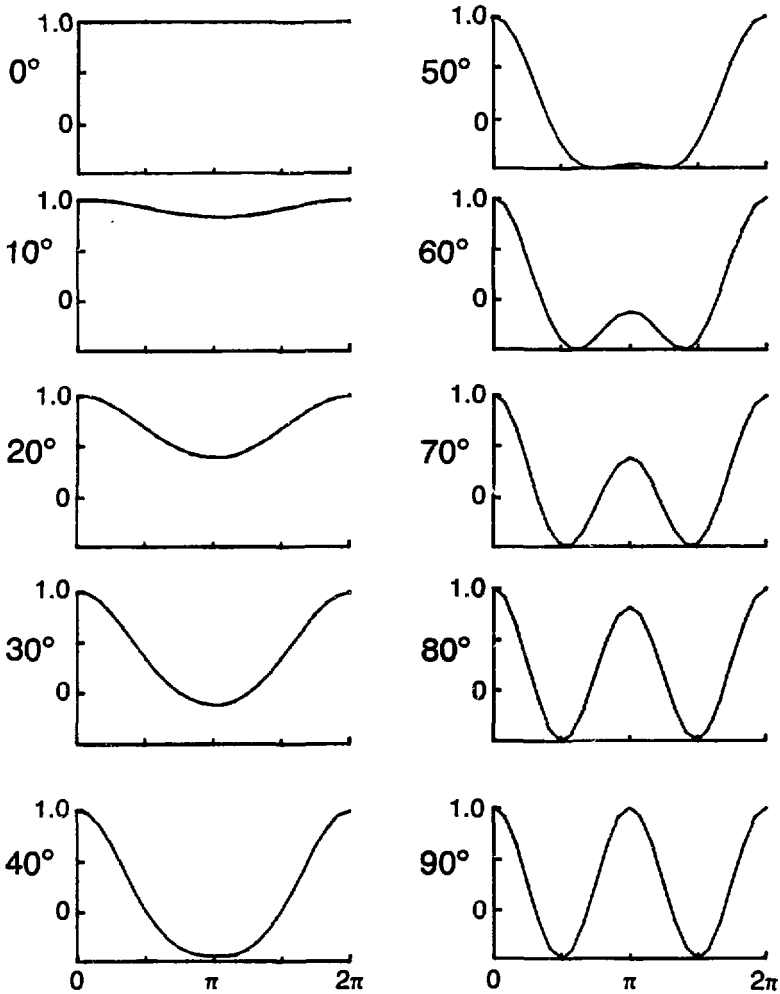

XBL 8611-6474

Figure III.4: Simulations of the signal amplitude as a function of dc pulse angle in the field cycle of Figure III.3, for different crystallite orientations. The initial condition is assumed to be equal to H_D. Because of the axial symmetry of the initial condition only the angle β, between the z axis of the PAS/molecular frame and the direction of the pulsed field (laboratory z axis), is necessary. For the orientation shown at top left, where the pulsed field is along the direction of the local field ($\beta=0$), no change is seen to occur. For orientations close to $\beta=45^{\circ}$, the signal goes through a single period over the range $0-2\pi$ whereas for the orientation perpendicular to the field direction, $\beta=90^{\circ}$, the signal goes through two periods in 2π. Note that for all crystallite orientations shown the signal returns to its initial value with a 2π dc pulse.

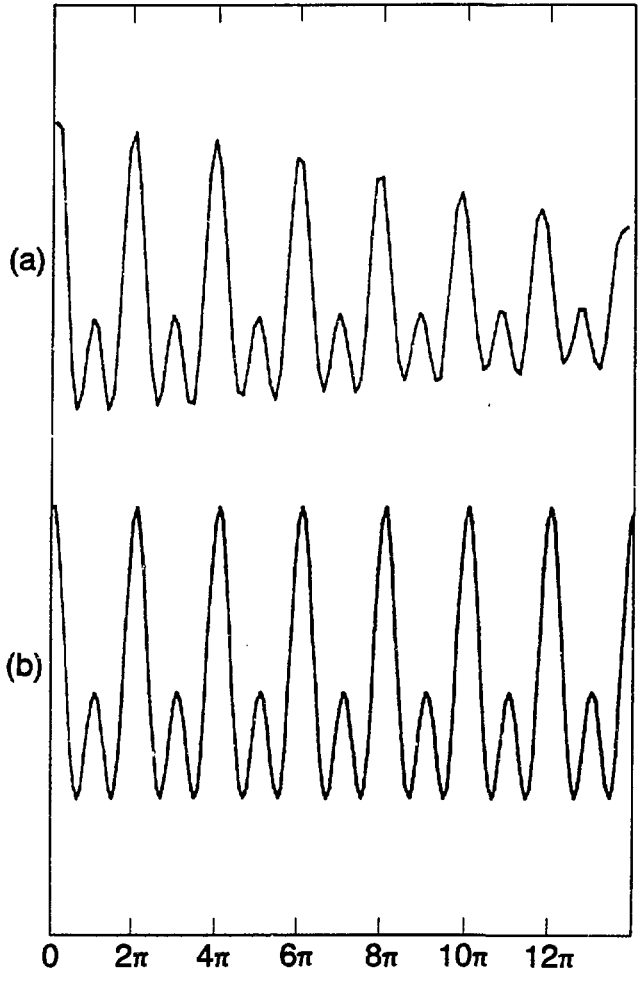

XBL 8611-6475

Figure III.5: Signal as a function of a single dc field pulse applied in the laboratory z direction after demagnetization to zero field (Figure III.3). The pulse angle is given by $\theta = \gamma_H B_i \tau$ where τ is on the order of a few microseconds, and $B_i >> B_{loc}$. The magnitude of the proton magnetization from a sample of $Ba(ClO_3)_2 \cdot H_2O$ is detected and shown in (a). For comparison, the theoretically predicted signal function (Equation III.9) is plotted in (b) for an initial condition equal to H_D. The detected signal shows the predicted periodicity and after a $nx2\pi$ pulse, the magnetization is nearly equal to its initial value. The damping effect may be attributed to imperfections in the pulsed field homogeneity and amplitude.

Experimental curves such as those shown in Figures III.2 and 5 are used as a means of calibrating the pulsed field.

A component of the dipolar ordered state in zero field is not effected by the pulse as seen by the constant term in Equation (III.11). This corresponds to a projection along the field direction of a component of the zero field state from each orientation. The actual direction of the applied field in the laboratory frame does not affect the behavior of the spin system as a whole when $\rho(0)\alpha H_{ZF}$. This is due the isotropy of space and a random distribution of all crystallite orientations. The direction of the pulsed field has some significance when the initial condition or detected operator still bears a "direction", that is to say, it is proportional to a laboratory based operator.

2. Field Homogeneity

The decay of the experimental signals can be partly explained by the inhomogeneity of the pulsed fields together with evolution and relaxation which occurs during the dc pulse.[1] Ultimately, even under ideal pulse conditions, the signal loses coherence and decays due to T_1 and T_2 processes. Evidence for evolution under the internal Hamiltonian during the dc pulse has been seen in quadrupolar systems in which the damping effect is more pronounced as the condition $B_i > B_{loc}$ is only marginally met. A formal description of this effect will not be given explicitly although evidence of its presence is seen in some of the experimental results. Certainly, this is not a regime in which one would chose to work and although one remedy is obvious (use larger fields), it is not always obtainable practically.[6]

Inhomogeneous pulsed fields result in a more severe damping of the observed signal and the efficiency of the pulsed field has great bearing on the experiment. Empirically, it was found that changing either the size or form of the coil or sample greatly altered the homogeneity as is expected.[7] Of course, there are drawbacks to larger coils (see Chapter II) and reducing the sample size is not desirable due to the loss in signal. The decay evident in the previous signals and its dependence on experimental parameters can be illustrated by plotting the signal magnitude at specific pulse angles such as 180°, 360°,...,$n\times\pi$ as shown in Figure III.6. A completely undistorted signal (no relaxation, evolution or inhomogeneity during the pulse) would show no change in the level of the signal. For a given dc field strength (~40 G) and a small dipolar coupling (~0.5 G), the decay increases for larger sample volumes, indicating the presence of field inhomogeneity over the sample (Figure III.6a). This can be attributed primarily to field inhomogeneities by measuring the signal from a small sample volume at two different dc field levels (~40 G and ~100 G in Figure III.6b). Comparison of these signals shows that there is no change with a change in field, and one can assume that the lower field is already in the limit, $B_i >> B_{loc}$, as expected since the ratio of the lower field to the dipolar coupling is already ~80:1. Finally, the effect of the relative field strength and dipolar coupling is made by using different samples (Figure III.6c), one with a large dipolar coupling (~10 G), and a second smaller one (~0.5 G) with a pulsed field of ~40 G. The decay is seen to be more pronounced with the larger coupling. (Note that in this latter case both samples are large, thus inhomogeneity is also a factor, although it should be equal for the two samples volumes.) The zero

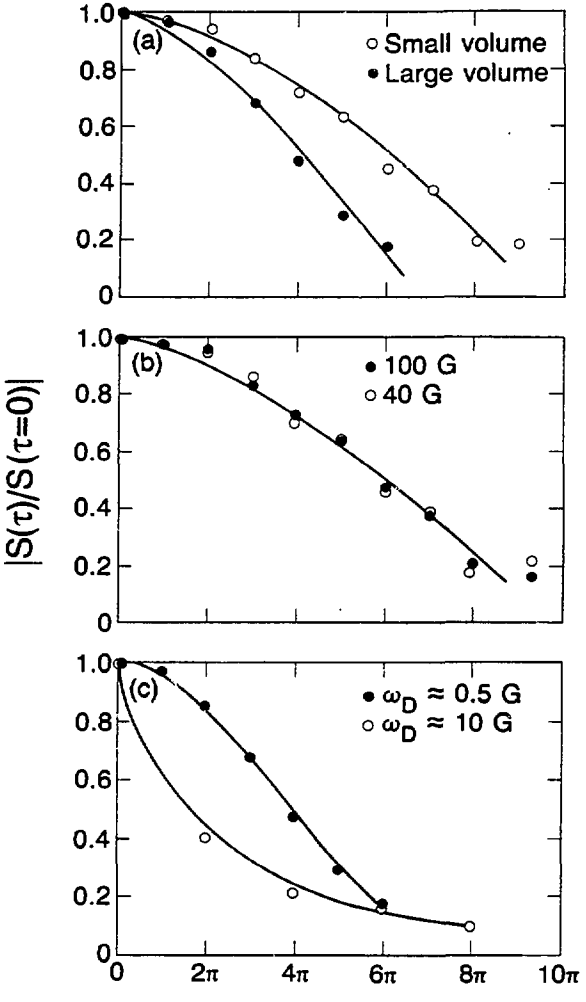

XBL 8611-6455

Figure III.6: Comparison of different experimental factors on the behavior of the signal as a function of a single dc pulse in zero field. An undistorted signal, one that is only affected by relaxation, would be expected to show little decay from the initial value. In (a) with a small dipolar coupling, a change in sample volume shows the effect of decreased field homogeneity over a larger sample. The field is approximately 40 G unless stated otherwise. Increasing the field to ~100G as shown in (b) for the same size dipolar coupling, illustrates that the decay in (a) is not due to evolution under a weak pulse. A weak field will however not act as effectively over large samples with a large dipolar coupling as compared to a small coupling as in (c).

field relaxation times are all substantially longer than the pulse lengths used.

Minor differences in coil designs can be significant in their behavior in pulsed experiments. Two examples are discussed, that of a solenoid and a helmholtz of approximately the same size. Both coils produce fields in the laboratory z direction, but the helmholtz is less efficient as the field per amp produced is smaller. The field from a finite length solenoid (a helmholtz coil is modelled as two solenoids contributing to a field centered between them) is calculated by solving the equation[8]

$$B_z(\text{Tesla}) = \frac{2\pi k' NI}{l}\left[\frac{1/2 - z}{\sqrt{r^2 + (1/2-z)^2}} + \frac{1/2 + z}{\sqrt{r^2 + (1/2+z)^2}}\right] \qquad \text{(III.12)}$$

where $2\pi k' = 6.3\times10^{-7}$ $TA^{-1}m^{-1}$, r equals the coil radius, z the distance from the coil center, l the coil length, I the current and N the number of turns. The calculated profiles of the fields over the length of the two coils are shown in Figure III.7. For the same length coils, the field from the helmholtz does not drop off as rapidly as does the field for the solenoid. As the coils increase in length, the curves are expected to flatten out and the fields become more uniform.[8]

Experimentally, the coils are seen to behave quite differently. In Figure III.8, the signal as a function of pulse angle is shown for the two coils. The helmholtz is more homogeneous as predicted from Figure III.7 and its effect is improved when the sample size is reduced. A computer program, INHOM.FOR, was written to simulate the behavior of the coils. The signal is calculated numerically according to Equations (III.9) and (III.10), and due to the rather complex function of z, as

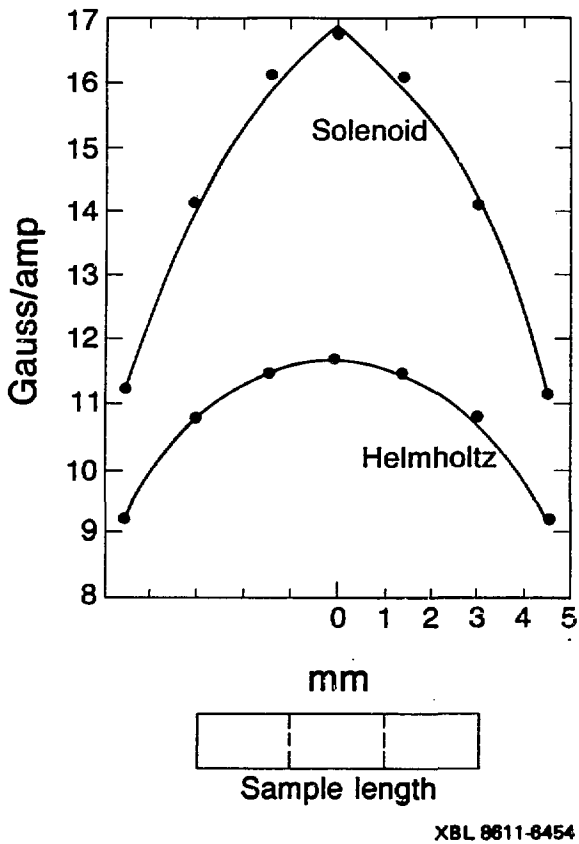

Figure III.7: Calculated profiles of the field produced by a solenoid or helmholtz pulsed dc field coil. Each coil is approximately 1 cm long by 1.2 cm in diameter producing a field in the laboratory z direction. The field is calculated over the length of the coil, and is assumed to be cylindrically symmetric. The field produced by the solenoid, although larger per amp of current, drops off more rapidly over the length of the sample than that of the helmholtz. The dashed lines in the representative sample length indicate the length of a smaller sample often used for improved homogeneity. The predicted field droop over the solenoid is -16% and -8% for the helmholtz.

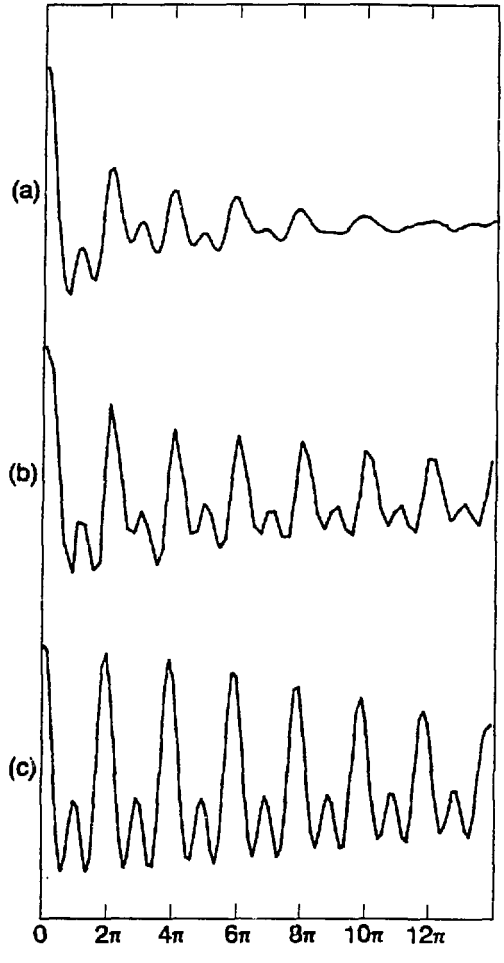

XBL 8611-5476

Figure III.8: Experimental curves of proton signal vs. pulse angle for a single z field pulse in the field cycle of Figure III.3. The sample for all three is $Ba(ClO_3)_2 \cdot H_2O$. A solenoid coil with a field of ~125 G and a large sample results in the curve seen in (a) where there is a pronounced decay of the signal due to pulsed field inhomogeneity. In (b), a field of ~250 G from a helmholtz coil over the same large sample volume shows some improvement. The best behavior is seen in (c) for the helmholtz coil with a small sample and a field of ~155 G. Most direct comparison can be made between (a) and (c) due to the comparable field strengths. Fourier transforming these signals and measuring the line widths predicts a distribution in field of ~20% for the solenoid and ~7% for the helmholtz. Note that due to the much larger field in (b), the 0.1 μsec increment in τ produces a large change in θ as in evidence by the fewer data points and jagged appearance of the signal.

given by Equation (III.12), a linear or quadratic approximation to the field homogeneity over the sample was incorporated. The latter is generally found to more closely model the experimental situation and therefore is used in the simulations. The simulations include only the effect of inhomogeneity, calculated by assuming different pulse angles over different regions of the sample. The sample is also assumed to be centered in the field. Misalignment of the relative positions of the coil and sample will greatly exacerbate any effects.

The resulting simulations shown in Figure III.9 model the experimental results reasonably well. The percent variations in the fields used were obtained by Fourier transforming the experimental signal and assuming that the distribution in B_1 is related to the linewidth. The percent inhomogeneities found by this method are actually very close to those predicted by calculation in Figure III.7 The performance of the helmholtz is slightly better than predicted and the solenoid slightly worse and may be due to exeperimental factors not accounted for in the simulations.

3. Composite Pulses

The design and implementation of radiofrequency pulse sequences is a well explored area in NMR. Pulse sequences which take advantage of the phase, amplitude and duration of the radiofrequency irradiation can be devised to produce a desired response from a nuclear spin system. Composite pulses[9] have been used in NMR for spin decoupling[10], broadband, narrowband and bandpass excitation[11], spatial selectivity[12], multiple quantum excitation[13] and more[14]. Composite pulses generally consist of a sequence of closely spaced pulses whose net effect is the

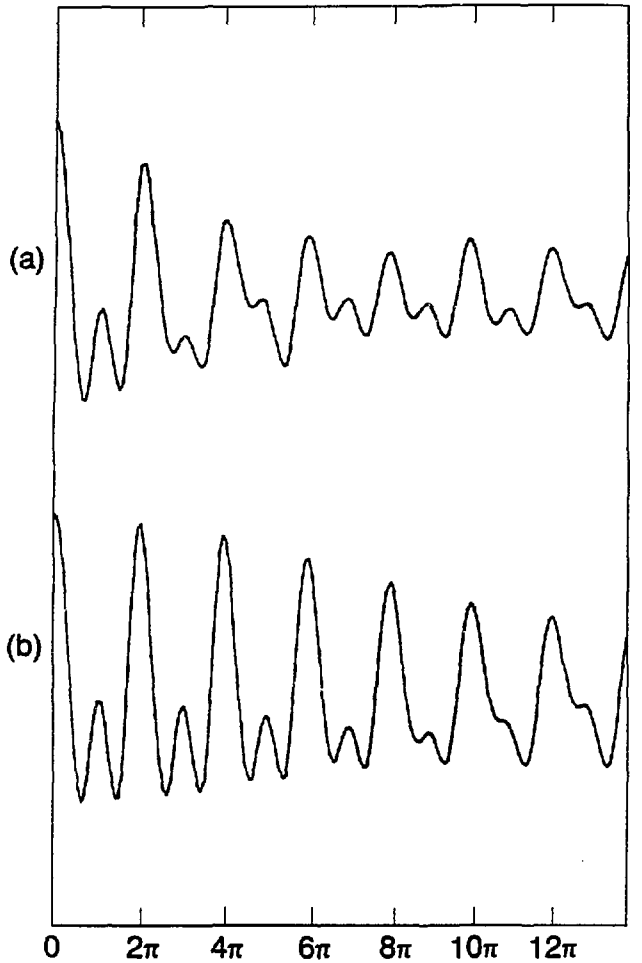

XBL 8611-6477

Figure III.9: Simulations of the behavior of the solenoid and helmholtz coils using the program INHOM.FOR. The contribution of the field inhomogeneity is included by calculating different pulse angles over different portions of the sample. Using a quadratic approximation to the field profile over the sample and percent inhomogeneities predicted from Figure III.8a and 8c, the simulations are shown for the solenoid and helmholtz in (a) and (b), respectively. The theoretical data matches the experimentally obtained data reasonably well, especially in the latter case.

same as that from a single pulse of a given rotation angle. These can be used to correct for resonance offsets and/or pulsed field inhomogeneity which would otherwise distort the desired response from a single pulse. In specific cases, the desired behavior in exciting the nuclear spins can be tailored to be broadband or narrowband in some characteristic of the irradiation (i.e. amplitude, bandwidth, etc). Broadband behavior is required, for example, to overcome the inhomogeneity of the dc pulses. Narrowband excitation is important in the selectivity between spins and isotopes; for example, if one wishes to apply a zero field pulse to carbon-13 spins without affecting protons or deuterium (a feat easily accomplished in high field NMR because of the frequency differences). The ability to use pulses selectively is discussed later in Section D of this chapter.

As in high field NMR, one hopes that the excitation of the nuclear spins is uniform across the sample, that is to say, the spatial inhomogeneity of the field is a minimum. As an alternative to using larger more homogeneous coils, composite pulses can be implemented in the dc pulsed zero field experiment as in high field NMR experiments. In this section, composite π pulses, which are not sensitive to pulsed field inhomgeneity, are produced by applying dc fields in different directions in the laboratory frame. Unlike high field NMR, a pulsed dc field does not have the feature of a variable phase, although the amplitude and duration of the field can be easily altered. Producing the analog of a phase shifted pulse sequence in zero field, requires a cross coil configuration. In this case, a system composed of three orthogonal coils with uniform characteristics such as inductance, homogeneity and field strength was designed. High power current pulsers

which provide for rapid reversal of the direction of current flow were designed to provide the complementary 180^{o} phase shifts to the x, y and z coils. Thus, six basic directions ("phases") and their linear combinations of pulses can be manipulated in the composite pulse sequence. Technical details on the coils and current pulsers appear in Chapter II.

The composite pulse sequence used is a very simple $90_{x}180_{y}90_{x}$ first suggested by Levitt and Freeman for inversion of nuclear spins in the presence of resonance offset and rf inhomogeneity.[11a-c] The combination of these pulses more effectively acts as a 180^{o} pulse while compensating for field inhomogeneities. The behavior of the spin system in zero field is identical to that in high field if the field cycle produces an initial condition proportional to $I_{z,L}$. It is fair to assume for a homonuclear spin system with small dipolar couplings, as will be used, that resonance offset effects are minimal as there are no chemical shifts in zero field, yet the spins must be excited over a range of dipolar or quadrupolar couplings (the zero field analog of resonance offset). One can simply picture the compensation of the on resonance $90_{x}180_{y}90_{x}$ pulse by observing the trajectory of the magnetization as shown in Figure III.10. In addition to the 180^{o} inversion pulse, multiples of 180^{o} also prove useful in the zero field experiment, thus the simple three pulse sequence is extended in the most straightforward manner by concatenating the composite 180's.

A sample of $CH_{2}Cl_{2}$ in a nematic liquid crystal, a system which when demagnetized in the field cycle shown in Figure III.1 has an initial state proportional to $I_{z,L}$ (see Chapter IV). Instead of only a single pulse in zero field, the pulse P in Figure III.1 represents the

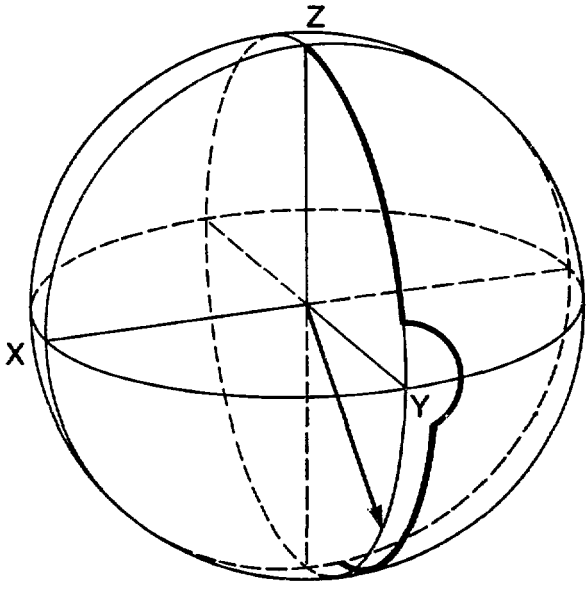

XBL 8611-9255

Figure III.10: Trajectory of a magnetization vector under a single pulse of 180°_{x} and a composite $90^{\circ}_{x}180^{\circ}_{y}80^{\circ}_{x}$ pulse. The final position of the magnetization for a single $(180^{\circ}_{x}+\Delta)$ pulse is shown by the arrow for one value of Δ corresponding to the error in the pulse angle. The trajectory of the tip of the vector under the composite pulse is shown by the bold line. The first nominal 90°_{x} pulse places the magnetization vector somewhere in the zy plane above the xy plane. The nominal 180°_{x} rotates the magnetization about the y axis. The final nominal 90°_{x} pulse places the vector near the -z axis closer than the single 180° pulse. The error in the 90° pulses is compensated for by the 180° pulse where an exact rotation 180° would place the magnetization vector at the -z axis. Other errors in pulse lengths will show similar trajectories corresponding to a distribution of final positions near the -z axis. 360° composite pulses can be produced by applying a second $90^{\circ}_{x}180^{\circ}_{y}90^{\circ}_{x}$ or $90^{\circ}_{x}180^{\circ}_{\bar{y}}90^{\circ}_{x}$ pulse which brings the magnetization up the other side of the sphere toward the +z axis.

application of one or several dc pulses which can be repeated n times. A comparison of single pulses of nominal pulse angles of $nx180^{o}$ and composite pulses are shown in Figure III.11. The single $nx180^{o}$ pulses were extracted from an experimental curve of signal intensity vs. pulse length such as that shown previously in Figure III.2. Single pulses are seen to produce a curve which decays with increasing pulse length. This is the case of a small coupling and small sample (see Figure III.6) and the effect is therefore primarily due to the inhomogeneity.

Using composite pulses, the nx180 and nx360 rotations of the magnetization are seen to show some improvement as the result of compensation. In both the single and composite pulse cases, cummulative errors in the pulses result from long sequences. When larger pulse angles are needed, the efficiency can be improved to some extent by phase cycling the second pulse of the composite sequence. Figure III.11c illustrates this effect by using $(90_x180_y90_x\text{-}90_x180_{\bar{y}}90_x)$ sequences. The compensation is improved on subsequent pulses and can be understood by the fact that the reverse sense of rotation of the 180_y and $180_{\bar{y}}$ pulses corrects for some of the error due to the 180 pulse and returns the magnetization more effectively to the +z axis.

These experiments illustrate simple applications of composite pulses, originally designed for high field radiofrequency irradiation but applied in zero field. Rotations of the magnetization by integer multiples of 180^{o}, and the desire for other large angle rotations arises from the fact that in zero field different nuclear species can be selectively excited with the proper choice of dc pulses. The degree of selectivity or successful excitation of the spins depends upon the uniformity of the pulsed field over the sample. Other uses might be

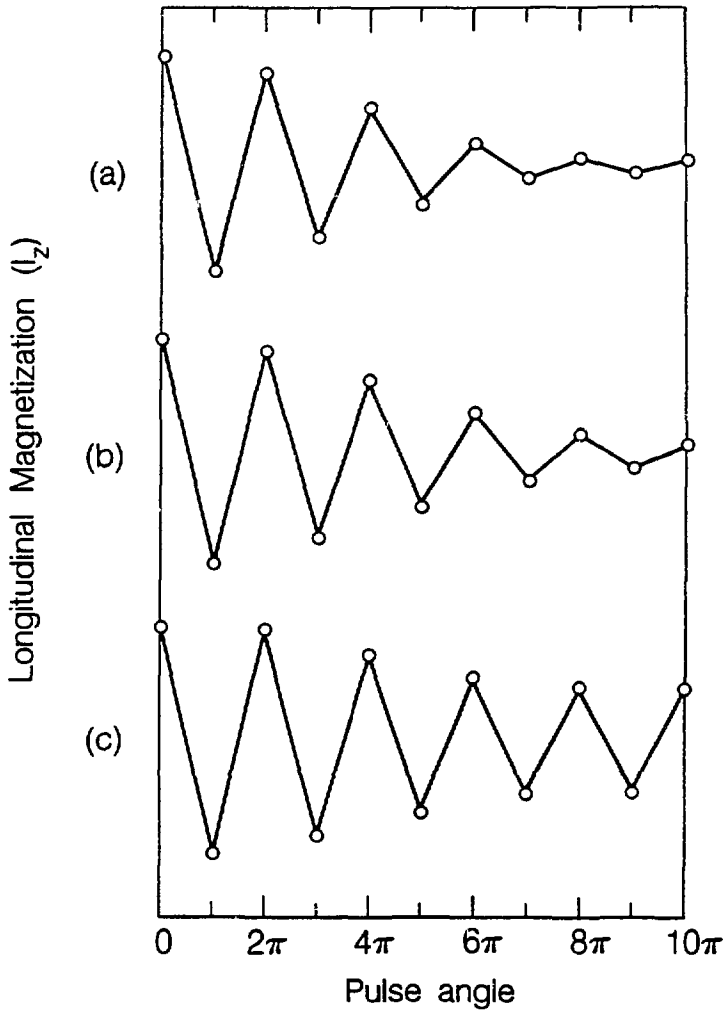

XBL 866-11175

Figure III.11: Experimental comparisons of single and composite dc magnetic field pulses. The sample is CH_2Cl_2 in a nematic liquid crystal which has a proton dipolar coupling of approximately 2 kHz. Pulsed fields used were on the order of 45 G for all directions. In (a), single pulses of $nx180^{\circ}$, chosen from a function of signal intensity vs. pulse length, are shown to cause the magnetization to decay rapidly with increasing pulse length. In (b), using concatenated composite pulses of $90_x180_y90_x$ the behavior is slightly improved. To reduce the cummulative errors in repeated 180° pulses, a phase cycled pulse $90_x180_{\bar{y}}90_x$ was alternated with $90_x180_y90_x$ in (c) yielding an improvement in the longterm behavior.

found in better refocussing pulses to improve zero field homogeneity (as in the echo experiments to be discussed in Chapter IV) and the use of composite pulses in two dimensional zero field experiments. The use of phase shifted pulsed dc fields might be combined with the wealth of composite and spatially selective pulses already designed for rf irradiation.[9,10] More sophisticated dc pulses and pulses sequences which are zero field analogues of rf NMR experiments can easily be imagined.

A number of applications of these ideas are envisaged such as the selective excitation and evolution of protons in the presence of a heteronucleus such as carbon. This would be a zero field analog of observing a high field decoupled spectrum when only one nucleus is excited, and the heteronuclear dipolar or quadrupolar couplings are removed. Possible approaches involve the "quenching" of the coupling by selectively averaging the I_x, I_y and I_z components of spin angular momentum of the heteronucleus. Hopefully higher order terms of the dipolar coupling will also be removed. This is analogous to the naturally occurring quenching of the coupling of spin I=1 nuclei in zero field.[15] With dc pulses, there is the added complication of irradiating one spin species yet leaving the nucleus to be detected remains untouched except for evolution under the desired Hamiltonian. Not all high field pulses sequences are directly transferable to the realm of pulsed dc experiments, due the added terms of the zero field Hamiltonians which must be dealt with (i.e. no high field truncation to assist the experimentalist) and the fact that pulsed fields do not appear as uniform rotation axes in the molecular frame for all orientations in zero field. These complexities make the problem much

more challenging to approach and answers might best be sought via computer simulations as the calculations of the signal under pulsed fields quickly becomes overwhelming.

C. Field Cycling with Pulsed DC Fields

1. Initial Conditions and Demagnetization

The preceding section introduced the behavior of nuclear spins under dc pulses after being demagnetized to low ($\rho(0)\alpha I_{z,L}$) or zero field ($\rho(0)\alpha H_{ZF}$) in field cycles such as those shown in Figures III.1 and III.3. Only in certain cases, used as experimental examples thus far, can the initial state after complete demagnetization to zero field be easily characterized. States which are simply described during demagnetization are those of tightly coupled spin I=1/2 nuclei for which a spin temperature can be defined.[3] Since the development of the spin system in time, its behavior under pulsed fields and the appearance of the spectrum all depend upon the initial zero field state, the dynamics of demagnetization to zero field are discussed in more detail. The comments made are based upon more complete discussions found in several excellent texts on the subject.[3,16,17] Related discussions can also be found in another thesis.[18] At present, considerations are limited primarily to systems of only one spin species. In later sections, particularly Section D.1, a description of level crossings which occur between the energy levels of heteronuclear systems is presented.

a. Coupled systems. When a nuclear spin system is tightly coupled, that is to say mutual spin flips or spin diffusion through the system can rapidly establish an equilibrium state, the system can be

described by a spin temperature[3,16] as described in Chapter II.B.5. An appropriate spin system will be defined by a collection of single spins with equidistant Zeeman energy levels in which the couplings to other nuclei introducing a "width" to the levels. (This is not a rigorous treatment as in reality the spins should be treated collectively and $I_{zi}=m_i$ of individual i spins is not a good quantum number.) The relative width and the separation in energy levels is a measure of the degree of coupling in the system.

Energy and population conserving flip-flop transitions occur between the levels. The establishment of an equilibrium state corresponds to the most probable distribution of the populations among any two energy levels as given by Equation (II.4) and a single spin temperature can be defined if the ratio is independent of m.[3] When an external parameter of the system, such as the field, is changed adiabatically, the populations are conserved and the system reaches a new spin temperature. For a tightly coupled, homonuclear system this process is always reversible when conducted in a time, t, where $T_2 \ll t \ll T_1$. Throughout adiabatic demagnetization to zero field, the density matrix describing the system is always proportional to the instantaneous Hamiltonian. An example would be a dipolar coupled spin system of spin I=1/2 nuclei, such as protons in a solid, in which the Zeeman levels are equidistant and strong dipolar couplings exist. The zero field demagnetized state would then be equal to the dipolar Hamiltonian, H_D, with its corresponding eigenstates and energies.

b. Isolated systems. Isolated spin systems are generally not describable by a spin temperature.[3] Spin systems which are weakly coupled, either due to proximity or low isotopic abundance, can be

considered isolated. Also systems in which the energy levels are unequally spaced, thereby preventing energy conserving transitions involving all pairs of levels, behave as isolated systems. Heteronuclear spin systems, in which the differences in resonance frequencies are greater than the dipolar coupling, are effectively isolated since cross relaxation or transitions between pairs of Zeeman levels are only weakly allowed. Separately, the heteronuclear spin reservoirs may or may not be tightly coupled subsystems in and of themselves, thus allowing independent spin temperatures to be defined for each. For times greater than T_2 of a separate subsystem and less than the time for a mutual spin flip to occur, a separate spin temperature can be ascribed to each. If the cross-relaxation time is greater than T_1, the state of the entire system can be described by a common spin temperature equal only to the lattice temperature.

An example of an isolated spin system is that of a quadrupolar spin I=1 system such as deuterium.[3,16] A spin I=1 system can not be described by a single uniform spin temperature at all times. If the system is allowed to reach equilibrium in a large applied magnetic field, then the populations of the Zeeman energy levels correspond to the most probable distribution of the spins among the levels as given by a Boltzmann distribution. For nonzero quadrupolar coupling constants, the three energy levels correspond to quadrupolar perturbed Zeeman levels and are unequally spaced. Assigning a spin temperature to the spin system imposes a condition on the populations. Only for equally spaced levels (in a spin I=1 system when $e^2qQ/h=0$), a flip-flop exchange of one spin by +1 and another by -1 does not change the populations of the levels and a single uniform spin temperature can be defined. For

unequal levels, a change in the populations of any two levels will alter the relative populations of other pairs of levels, and a single uniform spin temperature can not be assigned. It often becomes useful though to assign a spin temperature for a limited time to a given pair of levels.

There exists no mechanism in isolated systems which will uniformly reestablish equilibrium populations for all levels, as does the flip-flop term of the dipolar Hamiltonian for equidistant levels, and rapidly establish a new spin temperature. A new Boltzmann distribution can be reached, but only in a time greater than T_1, when the spin temperature of the entire system corresponds to the lattice temperature. Since the system cannot be described by a single spin temperature in times less than T_1, a simple description of adiabatic demagnetization does not follow as before. If the field is changed adiabatically, the populations prepared in high field can be expected, according to the adiabatic theorem[16,21], to remain unchanged and transfer smoothly to the zero field eigenstates. The trajectory of the energy levels from high field to zero field must then be determined as accidental degeneracies of the levels can alter the transfer of populations to the zero field states. In high field, $H_Z >> H_{ZF}$, the eigenstates correspond to those of the high field Hamiltonian. Similarly in low fields, $H_Z << H_{ZF}$, the eigenstates approach those of the pure zero field Hamiltonian.

In intermediate field regions, the states are less well defined. The behavior of the eigenstates for a spin I=1 nucleus as a function of field and orientation were calculated using the program DEMAG.FOR. The analytical solution begins by setting up the high field state.

$$H = H_Z + H_Q \qquad \text{(III.13)}$$

The Hamiltonian is most easily expressed in the zero field basis, given in Chapter II.C, as

$$H = H_Q + D_x I_x + D_y I_y + D_z I_z \qquad \text{(III.14a)}$$

or in matrix form as

$$H = \begin{bmatrix} -(1+\eta)K & -iD_z & D_x \\ iD_z & -(1-\eta)K & D_y \\ D_x & D_y & 2K \end{bmatrix} \qquad \text{(III.14b)}$$

where the molecular frame components of the applied field, related by the angles α and β, are given by $D_x = D\sin\beta\cos\alpha$, $D_y = \sin\beta\sin\alpha$, $D_z = D\cos\beta$ with $D = \gamma B$. The eigenstates and eigenvalues can be solved for through diagonalization of Equation (III.14b). There is an orientation dependence and field dependence to the eigenstates and eigenvalues, such that the demagnetization differs for each crystallite orientation. Using analytical expressions for the eigenvalues,[22] the program searches for degeneracies in the eigenvalues which correspond to crossings of the energy levels. If no level crossings are found, the states follow smoothly from high field to zero field with the populations unchanged and ordered the same with respect to energy level. When crossings occur, the correlations between states before and after the crossing are found by solving for the maximum overlap between eigenstates.

It was found that crossings only occur for particular orientations; in fact, those in which the field direction is along one of the principal axes of the quadrupolar tensor. These crossings are illustrated in Figure III.12. The infrequent number of level crossings is convenient as, when levels cross, no rate of demagnetization conforms

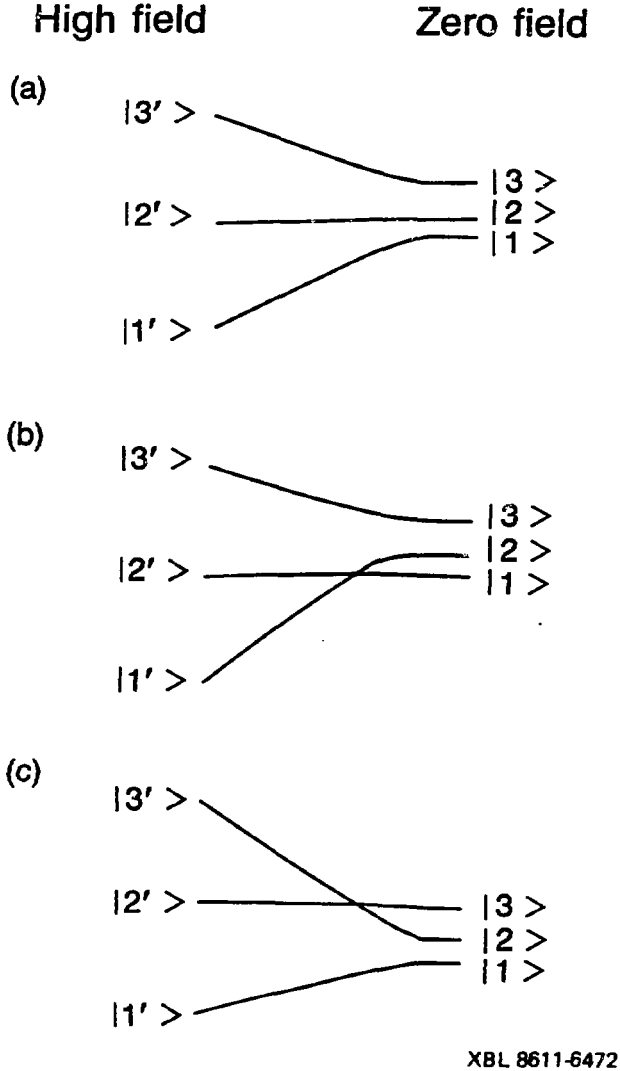
High field
Zero field
(a)
|3′ >
|2′ >
|1′ >
|3 >
|2 >
|1 >
(b)
|3′ >
|2′ >
|1′ >
|3 >
|2 >
|1 >
(c)
|3′ >
|2′ >
|1′ >
|3 >
|2 >
|1 >
XBL 8611-6472

Figure III.12: Illustrations of spin I=1 energy levels as a function of field and the allowed level crossings. (The zero field eigenbasis is given in Chapter II.C.) Level crossings were found to occur only for those orientations where the applied field is along one of the principal axes of the quadrupolar tensor. In (a), the field is along the x axis and no crossings occur. In (b) and (c), the field is along the z and y axes, respectively. Energy level separations in high and zero field are not shown to scale.

to the adiabatic condition when $\Delta E=0$. If the crossings do not occur, or are avoided, adiabatic constraints still hold. The frequent occurrence of avoided crossings is not surprising and a clear discussion of the principles is presented in the book on quantum mechanics by Cohen-Tannoudji et al.[23] The two possible outcomes are shown in Figure III.13 where the levels may either cross or avoid one another. When a coupling or perturbation term is present in the Hamiltonian, an avoided crossing occurs where the unperturbed energies would approach one another and cross. Under the effect of the coupling, the energy levels are mixed, the perturbation becomes more significant close to the crossing region and the states repel one another. Thus over almost the entire powder distribution, the demagnetization is independent of orientation. Only populations survive the demagnetization and the state of the system in zero field, written in the eigenbasis of the zero field quadrupolar Hamiltonian, has the populations corresponding to those prepared in high field such that

$$\rho_{ZF} = \begin{bmatrix} -1 & & \\ & 0 & \\ & & 1 \end{bmatrix} \qquad \text{(III.15a)}$$

where the density operator is related to H_Q[5,18]

$$\rho_{ZF} = \frac{-3}{2}\left(I_z^2 - \frac{2}{3}\right) - \frac{1}{2}\left(I_x^2 - I_y^2\right) \qquad \text{(III.15b)}$$

Unfortunately, approaching the problem by computer simulation requires a knowledge of the values of e^2qQ/h and η, two parameters which are the goal of the measurement, to correctly simulate the frequencies. Of course, the simulations can always be used in retrospect to model the zero field spectrum and is discussed in the following sections.

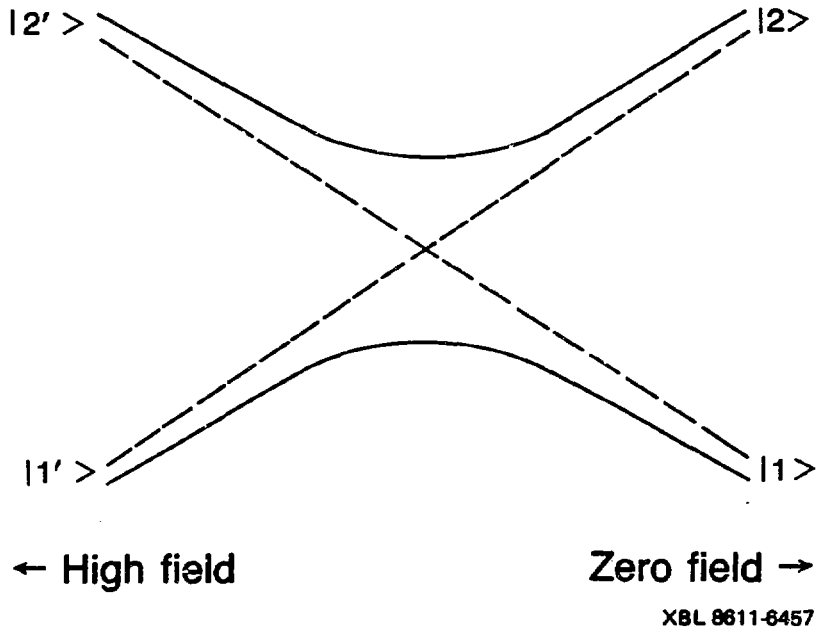

Figure III.13: Illustration of an avoided level crossing. The unperturbed energy levels would follow the dashed lines as the field is reduced through the level crossing region. In the presence of a perturbation or coupling, the energy levels do not cross. The energies of the perturbed levels approach those of the unperturbed asymptotically.

2. Zero Field NMR and NQR with Pulsed Fields

To apply dc magnetic field pulses in obtaining zero field spectra, many schemes are possible. Two simple examples of the field cycles and pulse sequences were shown in Figure II.4. After demagnetization to zero field, the reduced density matrix is diagonal in the zero field basis set and is proportional to second rank tensor interactions. The form of the initial state in zero field depends on the dynamics of the demagnetization and the type of spin system. An initial dc z pulse results in off-diagonal terms which evolve for a time t_1 under the zero field Hamiltonian. Detection of the zero field evolution may be accomplished by application of a suddenly switched field in the same direction as the first pulse and remagnetization to high field where the z component of the magnetization is sampled. This field cycle is illustrated in Figure II.4a and the high field signal is formally given by

$$S_\Omega(t_1) = \mathrm{Tr}\{RI_{z,L}R^{-1}\exp(-iH_{ZF}t_1)R\exp(-i\theta I_{z,L})R^{-1} \rho(0)R\exp(i\theta I_{z,L})R^{-1}\exp(iH_{ZF}t_1)\} \qquad \text{(III.16)}$$

For a homonuclear system of spins I=1, the signal produced in this case is analogous to directly detected magnetization in a pulsed NQR experiment where the signal is sinusoidal and begins with zero intensity.[24] This is due to the orthogonality of second rank (the initial density matrix) and first rank tensors (the detected operator). That is to say, when pulsing an equilibrium zero field state, a magnetization develops in time along the direction of the pulsed field. This

can be seen by calculating the analytic form of Equation (III.16) for $\rho(0)$ equal to Equation (III.15) and is reproduced from reference 18,

$$S(t_1) = \frac{\sqrt{3}}{15}[(2\sin 2\theta + \sin\theta)(\sin\omega_{23}t_1 + \sin\omega_{31}t_1)] \qquad \text{(III.17)}$$
$$+ \frac{1}{15}[(2\sin 2\theta+\sin\theta)(\sin\omega_{23}t_1+2\sin\omega_{12}t_1) + (\sin 2\theta+2\sin\theta)\sin\omega_{31}t_1$$

The intensities as a function of the first pulse θ are given in reference 18 and maximum signal intensity is obtained for θ approximately equal to $\pi/4$. Pulsing in the z direction and detecting in this direction will show a time varying component of magnetization at frequencies corresponding to $\sin(\omega t_1)$, where ω is any of the possible quadrupolar frequencies of the system. Due to the sinusoidal dependence of the signal, at $t_1=0$ no component proportional to $I_{z,L}$ exists and the maximum value for different transitions occurs at different times corresponding to ωt_1.

Alternatively to detect zero field evolution, a second pulse applied after the t_1 period returns a portion of the off-diagonal elements to the diagonal as shown in Figure II.4b. Upon remagnetization these population differences are measurable by standard high field pulse sequences. The signal in high field is given by

$$S_\Omega(t_1) = \mathrm{Tr}\{\rho(0)R\exp(-i\theta' I_{z,L})R^{-1}\exp(-iH_{ZF}t_1)R\exp(-i\theta I_{z,L})R^{-1} \qquad \text{(III.18)}$$
$$\times\ \rho(0)R\exp(i\theta I_{z,L})R^{-1}\exp(iH_{ZF}t_1)R\exp(i\theta' I_{z,L})R^{-1}\}$$

where $\theta'=2\pi-\theta$. The magnetization detected in high field is assumed to be proportional to the remagnetized zero field state. Again, as for other dc pulsed experiments with demagnetization and remagnetization to and from zero field, the signal is calculated by taking the trace with

respect to the initial state in zero field.

This field cycle can be used to detect evolution in zero field under either the quadrupolar or dipolar Hamiltonians for the initial conditions described previously in Section C.1. If the range of couplings is broad and/or extends over many spins, the zero field dipolar spectrum is expected to be structureless.[18,19] Yet when structure is discernible in the zero field spectrum, the system may not correspond to one describable by a spin temperature. As a test of these ideas, a series of proton dipolar spectra taken as a function of pulse angles were compared to the calculated signal intensites for a system corresponding to a dipolar ordered state in zero field. The sample was $Ba(ClO_3)_2 \cdot H_2O$ whose spectrum, as shown in Figure II.6, is a relatively simple three line pattern corresponding to the principal intramolecular coupling between the protons. Intermolecular coupling is evident in the broad lines (~7 kHz), which reduce in width with dilution with deuterium, and possibly by the presence of the 2ν and 3ν lines. The experimental spectra in Figure III.14 were obtained using the field cycle shown in Figure II.4b with pulse angles of $(\theta, \theta'=2\pi-\theta)$. The signal can be calculated for an initial state $\rho(0)=H_D$ by numerically solving Equation (III.18) averaging over all crystallite orientations. Numerical simulation, using the program PLTSIM.FOR, is generally the easist approach to calculating the signal under dc pulses. The dependence of the signal intensity for two dipolar coupled protons is shown as a function of pulse angle in Figure III.15. The signal is symmetric around a 180° pulse angle such that either the θ or $2\pi-\theta$ pulse can be applied first.

Theoretical and experimental results are compared in Figure III.16

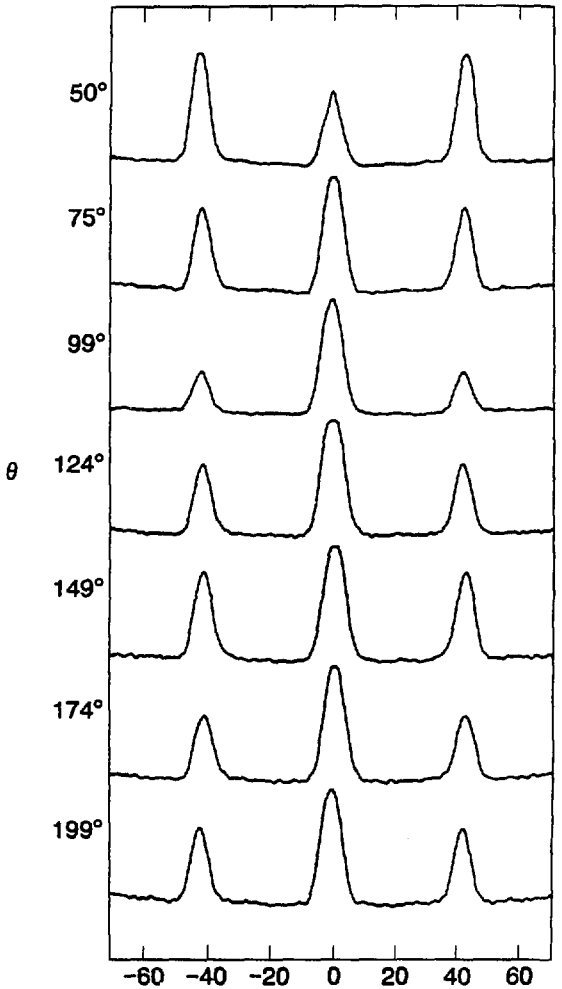

XBL 8611-6459

Figure III.14: Experimental zero field proton spectra of $Ba(ClO_3)_2 \cdot H_2O$ using the field cycle of Figure II.4b. The pulse angle on the left corresponds to the value of θ in the two pulse sequence given by $(\theta, 2\pi-\theta)$. The spectra show the predicted three line pattern and all have the same phase. The relative amplitude of the outer peak shows significant changes with pulse angle. The integrated intensity of all the spectra is identical and are not plotted to scale.

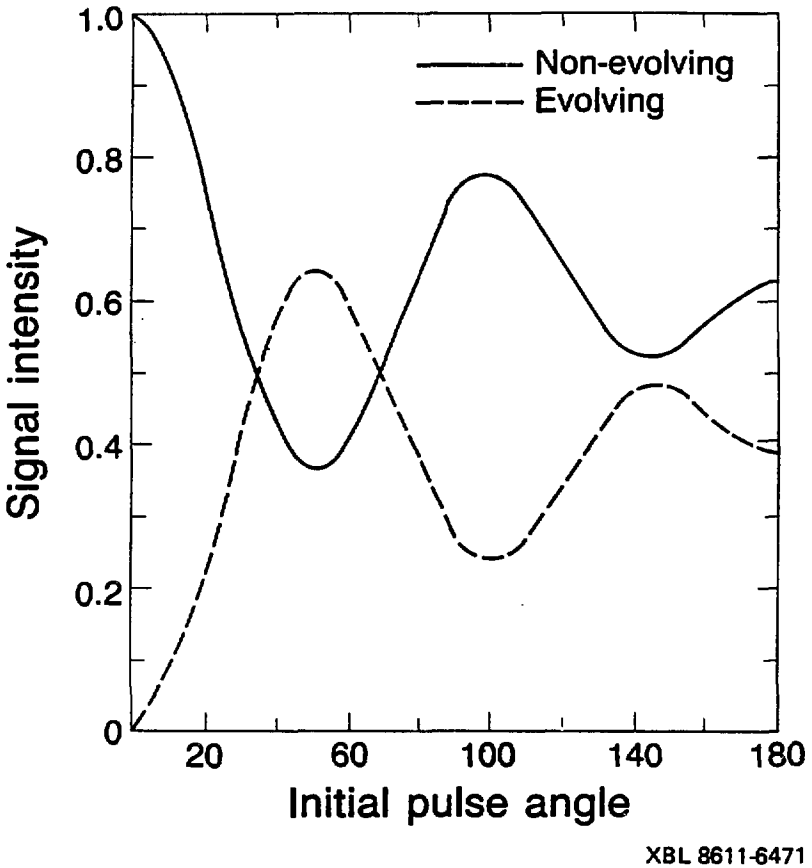

Figure III.15: Calculated signal intensity for two dipolar coupled spin I=1/2 nuclei in the field cycle of Figure II.4b with the program PLTSIM.FOR which assumes an initial condition equal to H_D. The pulse angle given corresponds to the first pulse in a $(\theta, 2\pi-\theta)$ two pulse sequence. Both the evolving signal and the nonevolving signal oscillate in amplitude and are symmetric about 180°. Maximum evolving signal is produced when $\theta=45^\circ$.

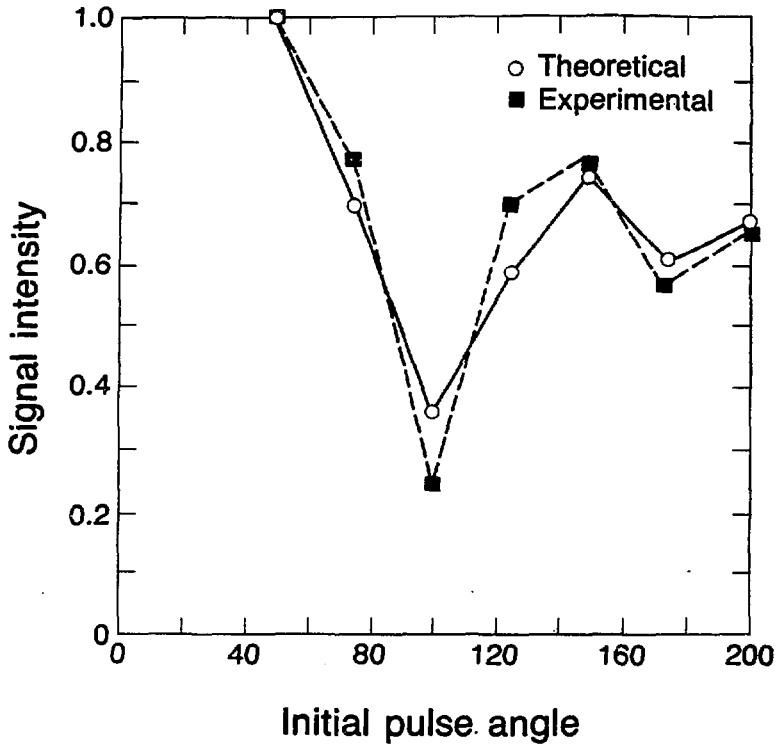

Figure III.16: Comparison of theoretical peak intensities and experimental values from the spectra of $Ba(ClO_3)_2 \cdot H_2O$ as a function of θ in $(\theta, 2\pi-\theta)$ zero field pulse sequence of Figure II.4b. The experimental intensities closely follow the theoretical values for an initial condition equal to H_D. The behavior is expected to be symmetric around the 180^o pulse, although with longer pulses, the behavior of the experimental signal begins to deviate slightly. This may be attributed to imperfections in the pulses.

by plotting the integrated intensities of the outer peaks. The behavior of the signal in the theoretical and experimental cases is very nearly identical. This is also true for the comparisons of simulations and experimental data of the coil characterization curves, presented in section B.2, in which the initial condition was also assumed to be proportional to H_D. While these experimental spectra and simulations support the idea that the demagnetized state of this particular sample is equal to H_D, no general conclusions can be reached as to what samples will or will not behave similarly when demagnetized. Barium chlorate monohydrate has often been used as a standard sample in characterization of the coils, and as such, was chosen for these experiments to test assumptions made as to the behavior of the spin system reported thusfar.

The experimental spectra shown in Figure III.14 where obtained using a homogeneous z helmholtz coil and small sample volume. All the spectra were found to have the same relative phase. Apparent artifacts, manifested as distortions in the relative phases of the peaks with pulse angle, were found to occur when weak fields or inhomogeneous pulsed fields are used.[20] Theoretically, no phase changes are predicted. Additionally in deuterium spectra, unusual phase behavior in the peaks has also been seen to occur.[18] In these cases the pulsed fields were weak as B_1-B_{loc} and may contribute to the distortions. More comments will be made on this subject in a later section.

The NQR spectra of a perdeuterated sample also demonstrates a few aspects of the field cycles. In these pulsed experiments, it is not possible to find pulses which excite evolution uniformly over the powder. Thus the signal is necessarily somewhat reduced from the previously described experiment with a sudden transition in field

(Figure II.3), as only a portion of the total spin order evolves in zero field. Figures III.17a and III.17b illustrate the results for the sudden transition field cycle, and the demagnetization and pulsed direct ^2H detection zero field experiments conducted on perdeuterated 1,4-dimethoxybenzene. As expected, the frequencies obtained in both are identical and the linewidths agree within experimental error. The assignments to two inequivalent aromatic sites (those close to and far from the methoxy groups) and the methoxy deuterons match previous results.[25] As expected, the signal-to-noise is slightly lower in the demagnetization experiment, due to the pulse excitation over the powder and possible contributions of relaxation in low fields.

The intensities differ in the experimental spectra shown in Figure III.17. For the sudden transition field cycle (Figure III.17a), the three lines of a given quadrupolar nucleus are expected to be of equal intensity as described in Chapter 2, section C.4 and essentially is found in the spectrum shown in Figure III.17a. The intensities in the pulsed experiment can be modelled by computer simulation assuming an initial state equal to that of Equation (III.15) used in Equation (III.18). A computer program, QUAD.FOR, easily incorporates different pulse angles and averages over a distribution of crystallite orientations. The intensities are independent of e^2qQ/h and η.

The signal intensity as a function of pulse angle for the three transitions of a spin I=1 quadrupolar nucleus with $\eta \neq 0$ are shown in Figure III.18. A similar figure appears in reference 18 as a result of calculating the coefficients found analytically along with a series of spectra as a function of pulse angle which roughly follow the predicted behavior. A component of the signal which does not evolve, but

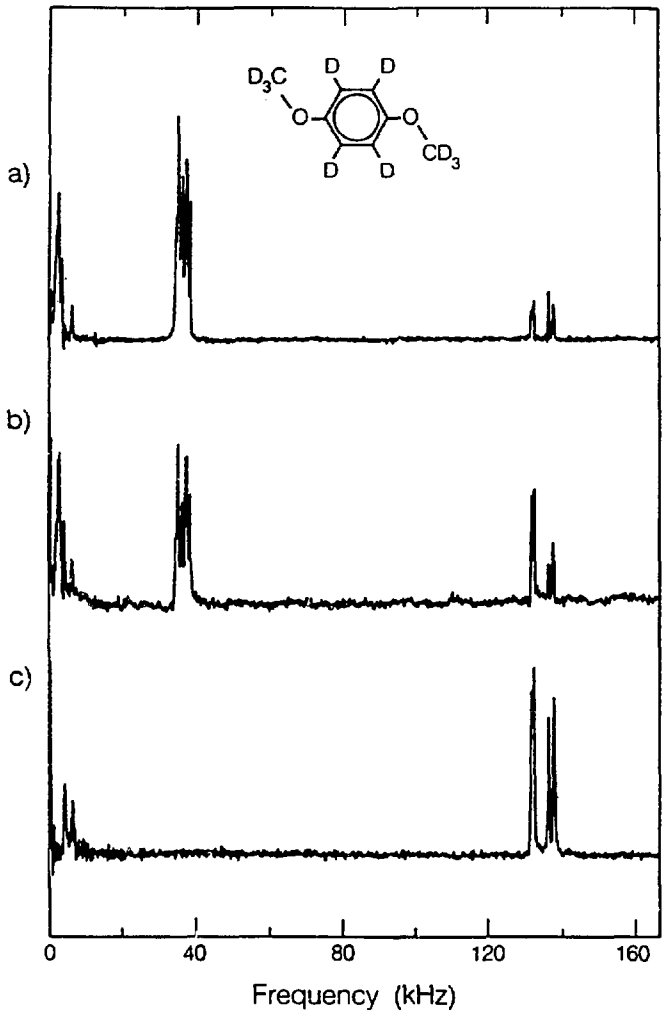

XBL 853-8831

Figure III.17: Zero field NQR spectra of 1,4-dimethoxybenzene ($CH_3OC_6H_4OCH_3$). a). Sudden transition zero field spectrum of perdeuterated dimethoxybenzene obtained using the field cycle described in Figure II.3. Peaks at frequencies corresponding to the methyl and aromatic deuterons are resolved. b). Pulsed direct detection zero field spectrum of perdeuterated dimethoxybenzene obtained using the field cycle of Figure II.4b. As the magnitude of the observed signal is dependent on the dc pulse lengths used (θ-90°), peak intensities are now scaled differently with respect to (a). Relaxation effects occurring during the different length field cycles in the sudden and pulsed experiments are manifested in the different relative methyl and aromatic signal intensities of (a) and (b). c). Indirect detection via protons of the deuterium NQR spectrum in 60-70% aromatic deuterated 1,4-dimethoxybenzene. (Note that in this sample the methyl groups were not deuterated.) Clearly resolved ν_+,ν_- and ν_o transitions are observed with no evidence of proton signal. Signal-to-noise for the aromatic deuterons is improved relative to the sudden and pulsed zero field methods.

oscillates in magnitude, appears as zero frequency signal in the spectrum. The most complete excitation over the powder occurs when this component is at a minumum, although the intensity is not divided equally among the remaining three transitions. Maximum signal is obtained for different transitions with different pulse angles but overall excitation is good for $\theta=60^{o}$ ($\theta'=2\pi-\theta$) as seen in Figure III.18. The calculated intensities are seen to match the experimental spectra (Figure III.17b) reasonably well for $\theta=90^{o}$. In spite of the altered intensities, the frequency information obtainable from these spectra is still extremely useful.

As a final comment, in previously reported deuterium experiments,[18] the NQR lines in the pulsed experiments were seen to show unusual phase behavior which is not predicted theoretically. The phase changes were found to increase with increasing pulse length (i.e. larger θ). The lines which were most strongly affected, those at higher frequencies, correspond to $e^{2}qQ/h$ values of ~150-180 kHz (or ~200-300 Gauss). The pulsed fields used were only marginally larger than this (1-2 times), if that large. Thus the pulses might be expected to act not only as rotations, and some evolution during the pulse might be expected to occur. The effects of pulsed dc fields are a function of many parameters; amplitude of the field, coil homogeneity and rise times of the field. It would seem that the apparent frequency dependence, pulse length dependence, weak fields and inhomogeneity effects indicate that the change is more likely due to experimental factors. Unfortunately, at the time of these experiments, larger pulsed fields were not available for deuterium studies. Weaker fields were seen to show a different dependence of the phase on pulse angle. Experimental results

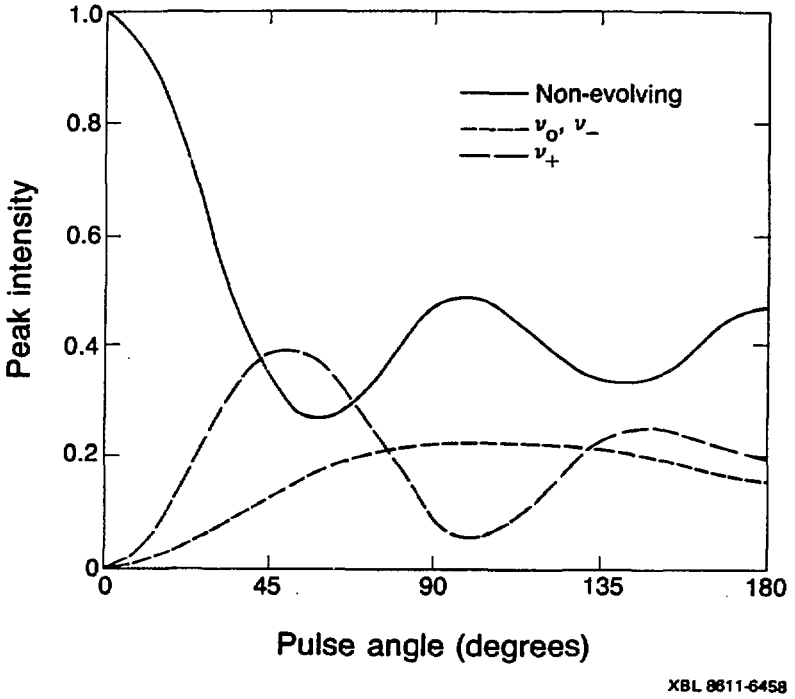

Figure III.18: Calculated intensities of the spin I=1 transitions under the field cycle of Figure II.4b with the pulse angle corresponding to θ in a $(\theta, 2\pi-\theta)$ dc pulse sequence. The intensities are not a function of e^2qQ/h and η based on an initial condition equal to the demagnetized high field populations. A large portion of the signal does not evolve. The evolving components oscillate in intensity with the ν_0 and ν_- transitions having the same angular dependence (note this does not correspond to their sum). The maximum evolving signal occurs at $\theta=60^\circ$ where the nonevolving portion is near a minimum. The signals are symmetric about 180°.

discussed earlier on dipolar coupled systems, in which the field is generally many times larger than the spin interactions, support this suggestion.

D. Indirect Detection and Selective Pulsing

In the previous section, it was shown that in a homonuclear system one can initiate evolution under the zero field Hamiltonian by simply pulsing a system which is initially in a stationary (diagonal) state in zero field. For example, this allows one to observe the NQR spectrum of a quadrupolar system. Consider a case in which the spin system consists of two isotopic species. An experiment with a sudden transition in field or pulsed dc field initiates evolution for all spin species, as long as the spin interaction with the switching field is large compared with zero field interactions. Thus any evolution of the spin system present in the detected signal produces a zero field spectrum containing both dipolar and quadrupolar frequencies. It is worth though considering pulsed experiments on completely demagnetized states[2b,26] which are better suited for indirect detection experiments as level crossings between heteronuclear spins occur during the field cycle. In this section, a time domain variation and extension of experiments developed by Hahn and others[27] is described. This method relies on the application of pulsed dc magnetic fields after demagnetization, as in the field cycle of Figure II.4b, to initiate evolution and selectively irradiate isotopic species (e.g. protons and deuterons) in zero field.

1. Introduction to Level Crossing and Selective Pulse Experiments

a. *Sensitivity Enhancement via Level Crossings.* Double resonance NQR methods have long utilized level crossings for enhanced detection of quadrupolar nuclei with small quadrupolar coupling constants. These techniques were first developed by Hahn and others[27] for use in frequency domain experiments. In this section, a description of the demagnetization behavior of a system composed of two spin species and its bearing on NQR measurements is presented. Much of the following brief overview is the same as for the frequency domain experiments and is based on review articles by Blinc[28] and Edmonds[29] where more detailed descriptions are given. Additionally, the demagnetization behavior of heteronuclear spin systems is also extensively covered in Goldman's book.[3]

The basis of the approach is that, as a natural consequence of the demagnetization of a heteronuclear I-S spin system, pairs of I and S energy levels become equal at some finite value of the field. At this level crossing field, the I and S systems can couple and transfer polarization via mutual spin flips. The transfer of polarization increases the sensitivity of the experiment by increasing the S nuclear spin polarization and by allowing for detection of the S spin evolution via the more sensitive I nuclei (i.e. double resonance). These methods are particularly applicable in NQR for nuclei which are unaccessible by direct observation due to their low interaction frequencies[29] and are difficult to study by NMR due to the broad lineshapes. While the NQR experiment allows one to use a polycrystalline sample, NMR experiments overcome the problems by using single crystals. Single crystals do provide more complete information on the quadrupolar interaction and the

orientation of the quadrupolar tensor, but are not always obtainable for all materials.

The system of interest consists of an abundant high γ spin I=1/2 nucleus such as protons (I) and a second, lower γ, spin S=1 quadrupolar nuclear species (S), such as deuterium or nitrogen, in reasonable proximity. In high field, the separation of the Zeeman levels of the protons is much greater than that of any of the quadrupolar perturbed Zeeman levels of the spin S=1 nucleus. The polarizations, as related to the difference in populations, is much greater for the I spins than for the S spins. If the differences in resonance frequencies are large relative to any coupling, then the two systems can be considered as uncoupled and may have separate spin temperatures.[3] It is assumed that a spin temperature is always well defined for the proton system but not so for the quadrupolar nuclei, unless enough time has elapsed for the system to be in equilibrium with the lattice.

If the field is decreased, the energy level separations change with the field and at some field level, B, the separation in the I Zeeman levels becomes equal with the energy level separation of one pair of the S levels. Level crossings generally do not occur in the sudden transition field cycle as the level of the field never gets low enough. The spin systems couple and via mutual spin flips come to a common spin temperature. A common spin temperature is defined only for that pair of quadrupolar levels which cross. Since the polarization of the I spins is larger, with demagnetization the I spins become quite cold. When contact is made with the S energy levels, the S system is "cooled down" with a resulting increase in the polarization. Because the protons are more abundant and tightly coupled, the I system has a larger heat

capacity and is assumed to have changed very little by a single contact with the S spins. A new spin temperature is rapidly reestablished in the I system.

The level crossing can be described by the change in the populations of the energy levels (labelled + and -).[29] The populations before (I) and after (I') a single level crossing are given by

$$\begin{aligned}(I_+ + I_-) &= (I_+' + I_-') = N_I \\ (S_+ + S_-) &= (S_+' + S_-') = N_S\end{aligned} \qquad \text{(III.19)}$$

which merely indicates that the total number of spins, N_i, of each type are conserved. Through the mutual flip-flops, energy is also conserved such that

$$S_- + I_- = S_-' + I_-' \qquad \text{(III.20)}$$

and follows similarly for the + states. Finally, since the two systems have reached a common spin temperature at the same energy level separation

$$\frac{I_-'}{I_+'} = \frac{S_-'}{S_+'} \qquad \text{(III.21)}$$

from Equation (II.4) whereas they were unequal before level crossing.

As the field is lowered further, the I levels become resonant with other pairs of S levels and with each crossing a transfer of polarization occurs. The order in which the pairs of levels cross during the demagnetization is dependent on the energy levels and their separation in the field which in turn is dependent on crystallite orientation. The result of this irreversible process[3] is an increase in the polarization of the S spins. The demagnetization of the I and S systems is reversible up until the first level crossing occurs. When

the field, B, is decreased below the level crossing value, the systems are no longer in contact. For spin S=1 nuclei, any spin-spin coupling is quenched when B approaches zero.[15]

In the NQR experiment, the spins would be irradiated in zero field with rf to induce transitions (generally to saturate the transitions) in the S system.[29] This corresponds to a heating of the S system. Remagnetizing the sample results in the level crossings again between I and S spins, but in the reverse order from before. Since the S spins have been heated, they produce a rise in the I spin temperature. By detecting a change in the I magnetization in high field as a function of irradiation frequency in zero field, the evolution of the S spins is detected indirectly. In order that the experiment succeed, the demagnetized order of the I spins can not be destroyed by the irradiation in zero field. Difficulties arise when trying to detect low frequency NQR transitions (<100 kHz), as the proton dipolar system absorbs in this region. Often in frequency domain NQR experiments, low frequency lines are obscured by the proton signal[29] which may extend from 0-50 kHz or more.

The time domain field cycle, such as that in Figure II.4b, is nearly identical to the frequency domian version except for the irradiation/evolution period in zero field. In the time domain experiment, evolution is initiated by a pulsed field and terminated after t_1 by a second pulse before remagnetizing the sample. The I spin signal, detected as a function of time in zero field, indirectly maps out the evolution of the S spins. Because of the large heat capacity of the I spins, multiple contacts between the S and I spins can be made by cycling the field to above the level crossing value.[28,29] The effect of

multiple contacts between the spin reservoirs is cumulative. The cycling of the field must be adiabatic and the number of contacts possible depends upon the T_{1D} relaxation time of the I spins.

The theory presented thus far is a very simple depiction of the actual dynamics of the situation. For a three level S spin system, the populations of separate levels are involved in more than a single level crossing. The I and S populations can be solved for from Equations (III.19-21) throughout the field cycle taking into account each subsequent change with a level crossing. Examples given by Blinc[28] and Edmonds[29] describe the theoretical increase in sensitivity and its dependence on various experimental factors such as relative numbers of I and S spins and relaxation times. These calculations are based on many assumptions as to the dynamics of the demagnetization. The rate and efficiency of the polarization transfer has great bearing on the sensitivity of the experiment. One assumption that has been made is that the transition rate through the level crossing field is slow relative to the transfer rate of polarization. If the transfer rate is given as 1/W (where W is the probability of a flip occurring), then the crossover time where the energy level separations are within the linewidths ($\Delta\omega=\omega_I-\omega_S<$linewidth) must be slow compared to the transition rate and fast compared to T_1 or a new Boltzmann populations are established.

Modelling the dynamics of the level crossing is a very complex problem. Although it can be easily calculated theoretically for individual orientations, in reality it depends upon the rate of demagnetization, the coupling of the spins, relaxation times, irradiation or evolution in zero field, and the reverse processes upon

remagnetization. The order in which the crossings occur for each crystallite may change due to the orientation dependence of the energies in the S system and requires that the level crossing effects be averaged over the powder. Additional level crossings are also possible when two spin flips occur for one "flop", e.g. at twice the energy. The probability of this occurring is low but would alter the final populations. The more likely event is the simultaneous level crossing of two pairs of S levels with one pair of I levels when there are near degeneracies of the S levels and the I levels have some width due to dipolar couplings. For example, when S=1 and n=1, then $\nu_0=\nu_-=1/2\nu_+$. For low frequency quadrupolar coupling constants, low frequency transitions or small values of η (where $\nu_+=\nu_-$), one or more pairs of levels can cross simultaneously.

It has been assumed that the relaxation times in low and zero field are long enough to allow for the polarization transfer, the irradiation/evolution period and the remagnetization step. The experiment requires that the polarization of the I spins persists over the entire field cycle, that is, that T_1 and T_{1D} of the I spins are long. The limits on the relaxation times of the S spins are not quite as stringent since the polarization and detection is through the I spins. Different limiting cases are calculated by Blinc[28] with predicted intensities for each spin I=1 NQR transition after level crossing. A few comments on the measurement of pertinent relaxation parameters. A rough measure of the T_1 in high field of the I spin system determines the overall repetition rate of the field cycle. Since the S polarization results from the level crossings, the T_1 of the S system is not as important, unless of course it is extremely short and

cross relaxation effects will not persist. The relaxation time in zero field of the demagnetized I spin order, $T_{1D}(I)$, can be measured by cycling to zero field with no irradiation or pulsing. A measure of the signal as a function of time in zero field should yield a rough estimate of the relaxation time from

$$M(t) = M_o \exp(-t/T_1) \qquad \text{(III.22)}$$

where M_o is the initial magnetization. This measurement assumes that the changes caused in the I polarization by the I-S level crossings are negligible. A rough measure of $T_{1Q}(S)$ is possible by field cycling to zero field, followed by irradiation to saturate only the I spin system. After remagnetizing, the detected signal reflects only what has occurred in the S system as transmitted to the I spins during remagnetization. A time domain version with dc pulses would consist of selectively pulsing the spins to destroy the order in the I system while leaving the S spins untouched.

b. Spin Selective DC Pulses. The selectivity of dc pulsed fields and the application to the indirect detection experiment has been hinted at previously and now is presented in more detail. In a heteronuclear system, by using a pulsed field which acts as an identity rotation for one spin species, it is possible to effectively rotate that part of the total density matrix corresponding to only one and not the other species. An identity rotation is that which leaves the state of the system unchanged after the pulse. By observing the signal as a function of pulse angle (Section III.1), it is evident that this is corresponds to a $n\times 2\pi$ pulse for all crystallite orientations.

Neglecting the heteronuclear dipolar coupling between a system of

protons and deuterons[15], the density operator for a system demagnetized from high to zero field can be written in the molecular frame as

$$\rho(0) = \rho_I + \rho_S \qquad \text{(III.23a)}$$

where

$$[\rho(0) , H_{ZF}] = 0 \qquad \text{(III.23b)}$$

and H_{ZF} is the pure dipolar Hamiltonian for protons (I) and the quadrupolar Hamiltonian for deuterons (S) in zero field. It will be necessary to evaluate the effect of applied dc pulses in the laboratory frame where the density operator ρ becomes

$$\rho_L(0) = R(\alpha\beta\gamma)^{-1}\rho(0)R(\alpha\beta\gamma) \qquad \text{(III.24)}$$

where $R(\alpha\beta\gamma)$ is the rotation operator relating the lab to the molecular axes in terms of the Euler angles α, β and γ. (Note that this is just the reverse of working in the zero field frame. Expressing operators in the laboratory frame is chosen here for convenience in calculating the effects of the pulses.) A similar expression transforms the zero field Hamiltonian into the laboratory frame:

$$H^L_{ZF} = R(\alpha\beta\gamma)^{-1}H_{ZF}R(\alpha\beta\gamma) \qquad \text{(III.25)}$$

Note that, from expanding the exponential, one finds that $R^{-1}\exp(iHt)R = \exp(iR^{-1}HRt)$. Computationally, the matrix representation of the exponentiated operator is simpler if H or $R^{-1}HR$ is diagonal, thus calculation of the left or right hand side is chosen accordingly. At time t=0, a dc pulsed magnetic field is applied for a time τ. The density operator $\rho_L(\tau)$ is written

$$\rho_L(\tau) = \exp(-iH_{dc}\tau)\rho_L(0)\exp(iH_{dc}\tau) \qquad \text{(III.26)}$$

where $H_{dc} = -[\gamma_I I_z + \gamma_S S_z]B_i$ and describes the dc pulsed field. Choosing the laboratory z axis parallel to the pulsed dc field, and using the equality, $\exp(A+B)=\exp(A)\exp(B)$ if $[A,B]=0$, to calculate the effects of the pulse separately on the I and S components of ρ, Equation (III.26) becomes

$$\begin{aligned}\rho_L(\tau) = {} & \exp(i\gamma_I I_z B_i \tau)\rho_{IL}\exp(-i\gamma_I I_z B_i \tau) \\ & + \exp(i\gamma_S S_z B_i \tau)\rho_{SL}\exp(-i\gamma_S S_z B_i \tau)\end{aligned} \qquad \text{(III.27)}$$

and pulse angles of $\theta_I=\gamma_I B_i \tau$ and $\theta_S=\gamma_S B_i \tau$ may be defined.

Since the effective pulse angle depends on the gyromagnetic ratios, and is therefore different for the protons and deuterons, it allows a selective means for their manipulation. Thus in a system of deuterons and protons one should be able to selectively excite and induce evolution of only the deuterons. In general, the effect of a pulse depends on the relative orientation of the spin system and field; however, for any particular species a 2π pulse given by $\theta=\gamma B_i \tau$ leaves the density operator unchanged for all orientations and makes selective pulses possible.

2. Experimental Results

By combining the principles of level crossings and the field cycle to zero field with pulsed dc magnetic fields, a selective indirect detection experiment is possible. Using dc pulses that are multiples of 2π for the protons in the field cycle of Figure II.4b (i.e., $\theta_S=\gamma_S B_{dc}\tau$ or $\theta_S=(\gamma_S/\gamma_I)\theta_I$ for the deuterons), the zero field spectrum of 60-70%

ring deuterated 1,4-dimethoxybenzene-d_4 ($CH_3OC_6D_4OCH_3$) shown in Figure III.17c was obtained. No signal is observed due to the protons, only the characteristic ν_+, ν_- and ν_o lines due to the two crystallographically inequivalent aromatic deuterons. The experimental results for the dimethoxybenzene samples shown in Figure III.17 allow for comparison of the signal-to-noise obtained in each of the different versions of the experiment. The length of each FID is roughly equal and the dwell time is equal for these three experiments. The pulsed direct ^2H detection (Figure III.17b) and the sudden (Figure III.17a) versions used 4 and 3 times as many signal averages, respectively, as the indirect detection version (Figure III.17c). Thus the aromatic signal-to-noise obtained via the indirect detection method is at least twice as good as in the others. Studies of partially deuterated diethylterephthalate and its perdeuterated analog provide further agreement with this result.

Arbitrary pulse lengths produce proton signal in heteronuclear systems which can obscure low frequency (<50 kHz) ^2H lines. Figure III.19 demonstrates this point in a series of indirectly detected zero field NQR spectra of diethylterephthalate-d_4 ($CH_3CD_2CO_2C_6H_4CO_2CD_2CH_3$) obtained by the method outlined above. Proton signal is clearly visible in those spectra where the $nx2\pi$ condition is not met for the protons, but is eliminated with two $nx2\pi$ dc pulses. Diethylterephthalate contains two crystallographically inequivalent methylene deuterons since the methyl-methylene bond is tilted out of the plane of the $-CO_2C_6H_4CO_2-$ moiety[30] thus producing the six line spectra for two uncoupled quadrupolar nuclei with nonzero η. The magnitude of the observed signal depends upon the demagnetization and upon the pulse lengths used, therefore the relative peak intensities are scaled differently in the

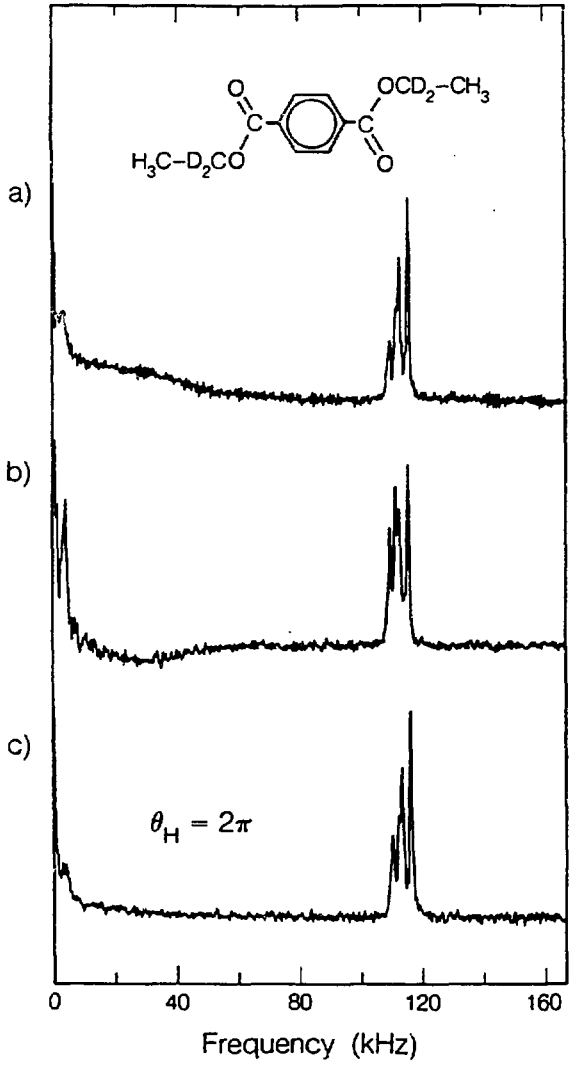

XBL 853-8829

Figure III.19: Indirect detection zero field NQR spectra of diethyl-terephthalate-d_4 ($CH_3CD_2CO_2C_6H_4CO_2CD_2CH_3$) (98% d_4). a). DC pulses used which do not satisfy the $nx2\pi$ criterion for the protons, thus signal due to both proton and deuteron evolution is observed. The proton signal appears as a broad hump below 50 kHz. b). Same as (a) except that dc pulses now used cause the proton signal to appear inverted relative to the deuteron signal. c). DC pulses equal to $nx2\pi$ allow for selective detection of only the deuterium NQR spectrum. Low frequency lines can be clearly resolved with no interfering signal from proton evolution or absorption. Three lines may be assigned to each of two crystallographically inequivalent methylene deuterons. Calculated values of $(e^2qQ)/h$ and η from the observed frequencies are: A: $(e^2qQ)/h$=153.1 kHz, η=0.051 B:$(e^2qQ)/h$=149.8 kHz, η=0.039.

spectra of Figure III.19. A further advantage of the initial selective 2π pulse on the protons is that the density operator ρ_I undergoes no t_1 dependent evolution; therefore, the dynamics of the level crossing should be sensitive only to deuterium evolution.

Although the use of selective pulses and indirect detection has been presented as a method of obtaining deuterium NQR spectra, the principles are entirely general and can be applied to any system in which there is sufficient contact between the observed and detected nuclei. As an example, the ^{14}N zero field NQR spectrum obtained from a sample of polycrystalline ammonium sulfate is shown in Figure III.20, obtained by the sequence in Figure II.4b with indirect detection by the protons. All six lines are resolved for the ν_+, ν_- and ν_o transitions of the two inequivalent ^{14}N sites and yield values of $(e^2qQ)/h$ and η in agreement with single crystal results[31] and other field cycling experiments in which the ν_o lines do not appear.[32] Under other conditions the proton signal would obscure the low frequency lines but here the use of the selective 2π pulses for the protons greatly reduces their contribution to the signal. Compensation for pulse imperfections of the dc pulsed fields should provide increased discrimination against the proton signal.

A few comments on the differences between selective excitation and decoupling should be made for clarification. In the previously described experiments, only the quadrupolar nuclei are excited and caused to evolve as $nx2\pi$ pulses are used for the protons. The initial state of the proton system in zero field is assumed to be unchanged from its equilibrium state and therefore no evolution under the homonuclear dipolar Hamiltonian occurs. The quadrupolar nuclei meanwhile evolve

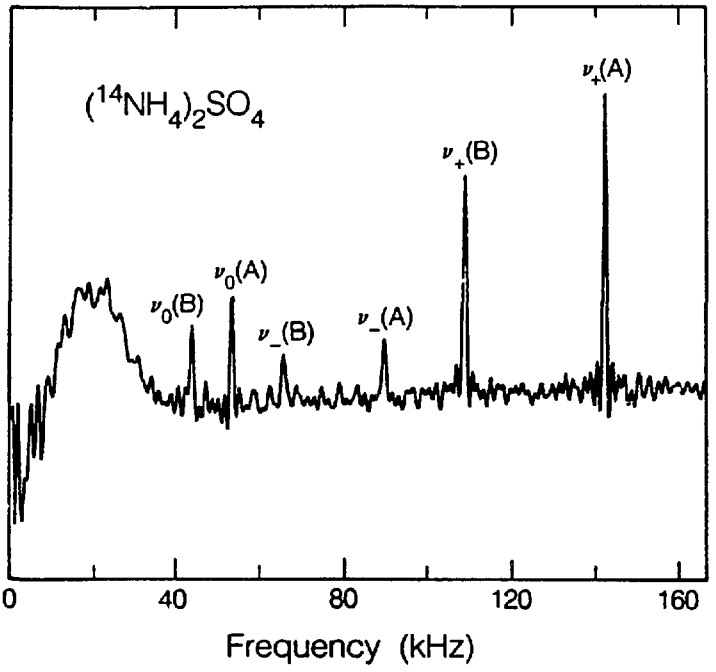

Figure III.20: Indirectly detected pulsed zero field ^{14}N NQR spectrum of $(NH_4)_2SO_4$ with selective 2π pulses for the protons. Peaks corresponding to two inequivalent sites are labelled A and B. Residual proton signal appears below 40 kHz but has been reduced enough to allow for resolution of the ^{14}N NQR lines. From the frequencies observed at room temperature, $(e^2qQ)/h$ and η can be calculated. Site A: $(e^2qQ)/h$=154.5 kHz, η=0.688, Site B: $(e^2qQ)/h$=115.9 kHz, η=0.747. (At 296.1 K, Batchelder and Ragle give values of I: $(e^2qQ)/h$=154.53 kHz, η=0.684, II: $(e^2qQ)/h$=115.71 kHz, η=0.749.)

under the quadrupolar Hamiltonian. Thus there are two separate and distinct systems which are excited independently and evolve independently in zero field. Only because the dipolar coupling between S=1 and I=1/2 spins is already quenched in zero field, does no evolution under the heteronuclear dipolar Hamiltonian occur. This is fortuitous since the NQR spectrum would be complicated by the added couplings and the proton system would be altered by contact with the deuterons.

The selectivity in the zero field experiment is an important feature in field cycling experiments. Unlike double resonance NQR experiments, the spectrum of a quadrupolar spin system can be obtained without the interference of low frequency proton signal. The time domain version of the field cycle offers the same sensitivity advantage obtainable by indirect detection without the loss of information due to proton background. Quadrupolar nuclei with small quadrupolar coupling constants are readily observed and resolution of ν_o lines for spin S=1 systems permits spectral interpretation without resorting to double transition frequencies[33] or double irradiation[34] techniques. In addition, the indirect detection experiment depends more on the relaxation times of the protons than those of the deuterons. This can be of utility when the deuteron T_1 is inconveniently long, or when T_{1Q} is inconveniently short. As long as the ^2H T_{1Q} is on the same order as the zero field time period, one can conceivably obtain the deuterium spectrum via the protons. Many double resonance NQR experiments are conducted at very low temperatures to provide the long relaxation times required for the irradiation period in zero field.[29] Irradiation in zero field can cause power broadening of the resonance lines[29] which is not a concern in the time domain experiment.

3. Isotope Selectivity with Composite Pulses

Selectivity between isotopic species in NMR is generally based on differences in Larmor frequency, $\omega_0=\gamma B_0$, or by rf amplitude $\omega_1=\gamma B$ selective pulses.[12] Variations in rf amplitude can be used to selectively invert or irradiate specific nuclear species. In NMR imaging experiments, it is often desirable to spatially select a region based on the inhomogeneities of the B_0 or B_1 field. For example, for a given nucleus and γ, the nuclear spins in a particular volume may be selectively inverted by using a field strength which varies with distance such that $\gamma B_1\tau=\pi$ for only that volume. Similarly, by applying a static field gradient, a region may be selected by the distribution of resonance frequencies. For best isolation of the spins of interest, the excitation should occur over a narrow range and many composite pulses which are narrowband in $\omega_1=\gamma B_1$ are being developed.[12] These spatially selective composite pulses can be directly adapted for spin isotope selectivity in zero field experiments.

Any pulse which is designed to be narrowband in γB_i, acts as an isotope selective pulse in zero field on the basis of the magnetogyric ratio for a constant field. The analogy between spatially selective and isotopically selective pulses is easily seen and is illustrated in Figure III.21. Previously, the selectivity by zero field pulses was based on the particular rotation angle used for a given spin species. Both species were always irradiated and the resulting pulse angle on the second spin is determined by the ratio of magnetogyric constants. This of course does not allow a choice of the pulse angle which initiates zero field evolution and may not provide optimal excitation. Nor does

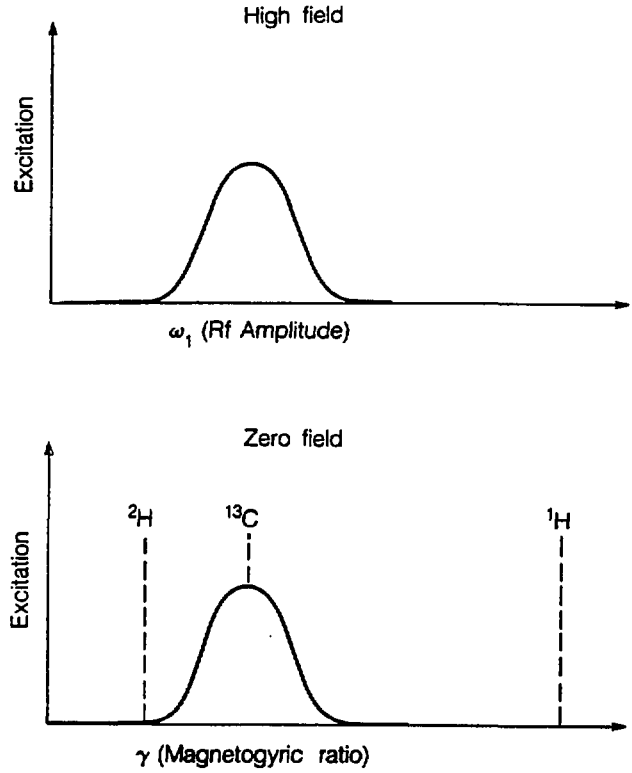

Figure III.21: Nuclear spin excitation in high field and zero field. In high field NMR experiments, spin species may be selectively irradiated on the basis of Larmor frequency $\omega_o = \gamma B_o$, or as shown at top, by irradiation which is narrowband in $\omega_1 = \gamma B_1$ (i.e. over a range of B_1 fields). In zero field, the differences in magnetogyric ratio provide a handle for selective irradiation through the relationship, $\omega_i = \gamma B_i$. Excitation of a single spin type by narrowband irradiation in zero field provides for manipulation of initial states and their subsequent evolution in zero field.

it allow much flexibility in the excitation scheme. In selective excitation experiments with dc fields, when both spin species are pulsed, the desired result for one of the spins is that it is unaffected. By using a composite pulse which is narrowband in YB_i, this result can be obtained by actually doing nothing to one isotope, that is, not irradiating the second species at all.

Before discussing experimental examples, a brief review of the features of ^1H-^{13}C spin pairs, originally presented in Chapter II.C, is covered. The appearance of the zero field spectrum for such an I-S dipolar coupled pair of spins depends upon the initial polarizations. For equilibrium polarizations of $\sim 4I_z+S_z$, the spectrum consists of seven lines. By altering the relative polarizations with rf pulses in high field before demagnetization, it has been demonstrated that lines corresponding to only certain transitions in the I-S manifold are observed.[36] Examples of these results are shown for a sample of $^{13}CHCl_3$ in a smectic liquid crystal phase, described in Chapter IV, in Figure III.22a-c.

Selective dc pulses can be used to alter the initial condition of a heteronuclear spin system in zero field prior to evolution and thereby discriminate against specific spectral frequencies. Examples of zero field selective pulses are show in Figure III.22d-f acting on an initial condition, I_z+S_z, prepared in high field by an rf pulse. Since this state is proportional to longitudinal magnetization (populations) it survives the field cycle unchanged. The resulting zero field spectrum for this initial condition is that of Figure III.22c. By applying an isotope selective pulse of 180° to either the I or S spins, transitions corresponding to an initial zero field state of $\pm(-I_z+S_z)$ are produced,

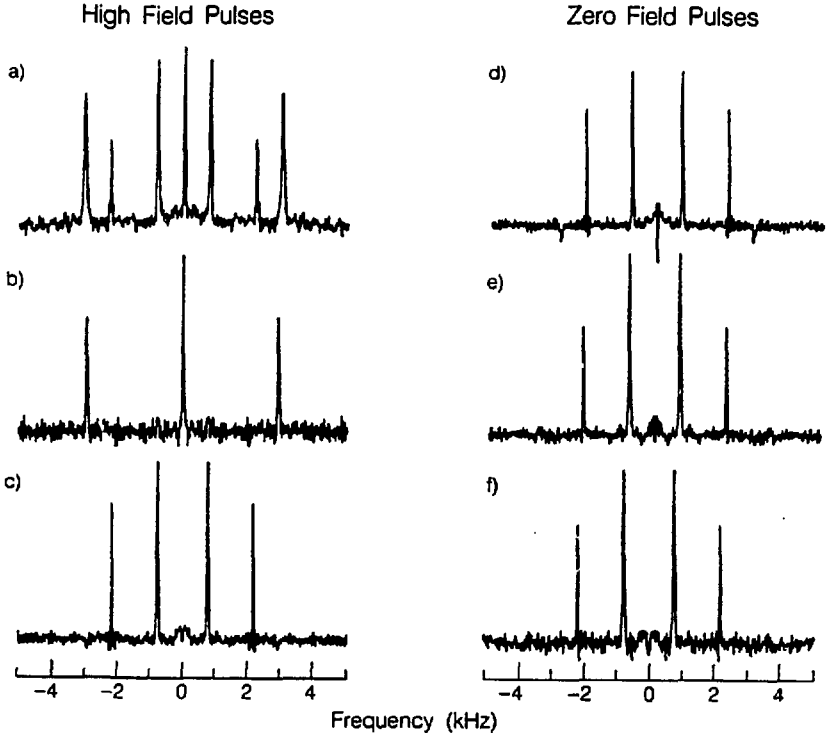

XBL 867-11638

Figure III.22: Spectra of $^{13}CHCl_3$ ($I=^1H$, $S=^{13}C$) in an unaligned smectic B liquid crystalline phase with different zero field initial conditions produced in high field and zero field. In (a) the characteristic seven line spectrum results with the initial condition equal to the equilibrium populations, $4I_z+S_z$. A change in initial condition to I_z+S_z can be produced by applying a 75^o pulse to the I spins in high field as shown in (b). Similarly the populations of one spin species can be inverted relative to the other ($-I_z+S_z$) by applying a 105^o pulse to the I spins in high field before demagnetization. Zero field analogs using composite dc pulses can also be used to selectively invert one spin species. The initial condition for (d-f) produced in high field before demagnetization is I_z+S_z. In zero field only one spin is inverted before zero field evolution with (d) a 180^o ^{13}C pulse (720^o ^1H pulse which leaves the protons unchanged), (e) a narrowband 180^o composite pulse ($180_x180_{\bar{y}}180_{\bar{x}}$) applied to the protons, and (f) a narrowband composite pulse ($180_x180_{\bar{y}}180_{\bar{x}}$) applied to the carbons. The resulting spectra all show the spectral frequencies indicative of an initial state proportional to $\pm(-I_z+S_z)$.

respectively. Because the carbon and proton magnetogyric ratios conveniently differ by a factor of ~4, the simplest selective pulse is a 720° ^{1}H pulse which is approximately a 180° ^{13}C pulse. The spectrum for $-(I_z-S_z)$ is shown in Figure III.22d. As mentioned before, not all combinations of γ_I and γ_S produce pulse angles which are useful or integer multiples. In this first example, both species are irradiated when it is advantageous to irradiate only a single spin species. Since the pulses are not without their imperfections, the desired behavior may not be obtained in a longer pulse sequence. For example, narrowband selective pulses would be ideal for saturating the I spins to determine T_{1Q} of the S spins.

Experimental results using the zero field dc analog of Shaka and Freeman's $180_x180_{\bar{y}}180_{\bar{x}}$ spatially (γB_1) selective inversion pulse[37] are presented in Figure III.22e-f. The pulses can be applied to either the carbon or proton nuclei and are seen to be more efficient at exciting only the desired transitions than the single 720° ^{1}H pulse. Unfortunately, not all useful pulse angles for zero field excitation are available in narrowband composite sequences, but the design of such pulse sequences is growing. Similar composite pulses are available to produce 90° narrowband behavior[14b] and might also be useful. The simplest composite pulses to implement are those of easily determined pulse angles such as 90°, 180°, 270° and 360°, with 90° relative phase shifts (i.e. pulse directions) in zero field.

E. Two Dimensional Zero Field Experiments

Two dimensional NMR methods involve recording the NMR signal as a

function of two time variables with subsequent transformation to produce a spectrum described by two frequency variables.[38] Applications of these experiments are generally to weakly coupled liquids, and the frequencies observed depend upon the specific excitation pulse sequence used. Common examples are those which show correlations between chemical shifts and scalar couplings,[38] between different chemical shifts[38,40] exchanging or cross relaxing dipolar coupled nuclei,[41] and multiple quantum transitions.[39b] By measuring the connectivities between spectral transitions, a determination of structure, conformation, dynamics or assignment of an otherwise intractable one dimensional spectrum is possible.

In Zero Field NMR and NQR, well-resolved, sharp line spectra are observed in polycrystalline solids. In zero field, quadrupolar frequencies label specific chemical sites while dipolar couplings should induce connectivities between zero field transitions of neighboring spins. In this section, the principles of two-dimensional NMR are applied to the detection of quadrupolar nuclei in zero applied magnetic field. The two dimensional experiments are possible through the use of pulsed field cycling methods. Through a combination of these techniques, the connectivities in the NQR transitions of a spin I = 1 nucleus are shown.

1. One Dimensional Zero Field NQR Spectra

The characteristics of a zero field NQR spectrum for a spin I=1 nucleus were described in Chapter II. Values of η and e^2qQ/h, which are descriptive of a quadrupolar system, may be calculated for a given chemical site assuming that the pair of corresponding ν_- and ν_+ lines is

distinguishable. If there are two or more inequivalent sites, the NQR spectrum will consist of a superposition of six or more lines. Therefore, resolution of the difference frequency ν_o lines at very low frequencies is essential in assigning the one dimensional spectrum.

The one dimensional zero field NQR spectrum of the methylene group of polycrystalline diethylterephthalate was shown in Figure III.19c. The spectrum was obtained using the selective indirect detection method which has been described previously. The low frequency lines are resolved and allow for calculation of quadrupole coupling constants and asymmetry parameters for the inequivalent sites as reported in Chapter II.C.4. If more sites were present, it becomes evident that overlapping lines would make assignment difficult.

2. Two Dimensional Zero Field Experiment

The correlations between the NQR frequencies can also be observed by probing the connectivities in the spin I = 1 manifold through a two dimensional version of the field cycle. The simplest form of the field cycle, in which the zero field interval is divided in half, is shown in Figure III.23. The sample is demagnetized to an intermediate field, B_{int}, which is switched off suddenly to initiate evolution. The system evolves under the quadrupolar Hamiltonian for the time t_1. Application of a short dc pulsed field transfers coherence between the energy levels of the spin 1 system. Evolution in zero field continues after the pulse for a time, t_2. Reapplication of the field and remagnetization provides for sampling of the magnetization in high field. In successive field cycles, the zero field periods are incremented independently to produce a time domain signal as a function of t_1 and t_2 which when Fourier

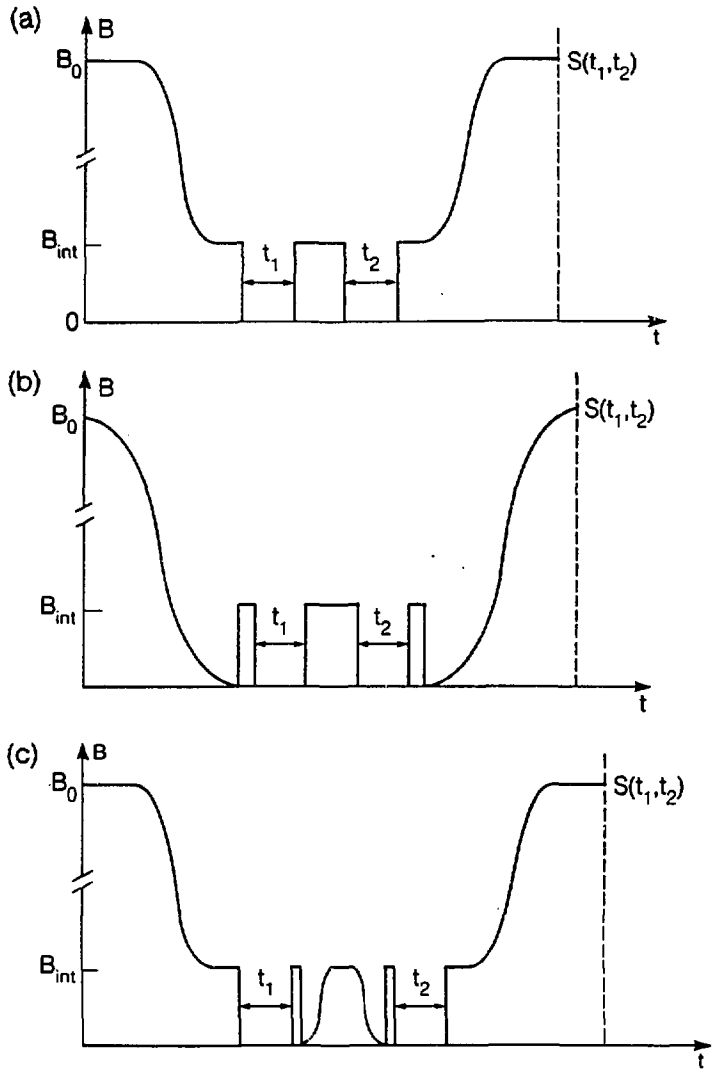

XBL 863-11048

Figure III.23: Field cycles for two dimensional zero field experiments. a). The sample is demagnetized to an intermediate field, B_{int}, which is switched off suddenly to initiate evolution in zero field. The evolution period is divided into two time periods, t_1 and t_2, by reapplication of the field. If the dc field is applied as a brief pulse, it will act as a rotation on the spin system and mix coherences. Evolution then continues for t_2 and is terminated with a sudden reapplication of the intermediate field and remagnetization to high field. The signal is sampled as a function of the independently incremented time variables. If the applied field is longer in duration, ~0.5-1 msec correlations between dipolar coupled groups of spins should develop. b). Using demagnetization to zero field, indirect detection of the zero field NQR spectrum is possible. The short pulsed dc magnetic fields are used to initiate zero field evolution for t_1, to mix coherences as in (a), and to terminate evolution after t_2. Remagnetization after the zero field period again provides for the ^1H-^2H level crossings and the detection of the signal in high field. c). The preparation of the spin system and t_1 evolution period are identical to that shown in (a). Applying a brief dc pulsed field will effectively store the magnetization, and prevent the decay of coherences under the applied field. Cycling the field slowly to an intermediate level show provide for cross relaxation between groups of spins. Evolution is reinitiated for t_2 by a second dc pulse then halted and detected in the same manner as in (a) and (b).

transformed produces the two dimensional zero field spectrum. An approach to the formal analytical calculation of the signal is presented elsewhere[18] by solving

$$S(t_1) = Tr\{RI_zR^{-1}\exp(-iH_{ZF}t_2)R\exp(-i\theta I_z)R^{-1}\exp(-iH_{ZF}t_1)$$

$$RI_zR^{-1}\exp(iH_{ZF}t_1)R\exp(i\theta I_z)R^{-1}\exp(iH_{ZF}t_2) \qquad \text{(III.28)}$$

for the field cycle of Figure III.23a and where θ is the mixing pulse. The task of calculating the signal analytically is extremely time consuming and might best be handled numerically for variable zero field pulse angles and other initial conditions.

Other initial conditions are also possible in this experiment. In actual practice, for the increase in sensitivity and potentially shorter ^1H T_1 relaxation times, the signal can be detected indirectly via the protons as described previously. The field cycle of Figure III.23b uses demagnetization to zero field followed by pulsed dc magnetic fields to initiate and terminate zero field evolution. Of course, the behavior of the spin system has the same dependence on the natural quadrupolar frequencies, as in the version with sudden transitions in the intermediate field, although now the intensities of the spectrum will also be a function of the initial and final dc pulse angles and the dynamics of the level crossings. A short dc pulsed field can be applied to mix coherences in the same manner as in Figure III.23a.

In addition to observing quadrupolar frequencies, connectivities between dipolar coupled groups of spins might be established by altering the mixing period of the experimental field cycle. Assuming a deuteron-deuteron dipolar coupling of ν_D~1 kHz, application of an intermediate

field, as in Figure III.23c, for ~1 msec ($\sim 1/\nu_D$) or longer should allow a coherence transfer between dipolar coupled spins. Thus correlations based on spatial proximity can also be developed. In cases where the coherences do not persist for longer than a few milliseconds, signal might be conserved if the evolving magnetization is stored as populations by application of a dc pulse as shown in Figure III.23c. The decay is now described by a time constant related to T_{1z} which is expected to be longer than the decay of the coherences in solids. By slowly cycling the field to an intermediate value, the energy levels of inequivalent deuterons may be brought into contact. This is similar to the signal enhancement approach via repeated level crossings used in frequency domain double resonance NQR experiments.[29]

3. Experimental Results

As an experimental verification of the applicability of these field cycles, the two-dimensional zero field spectrum of the high frequency ν_- and ν_+ lines of the same methylene sites in polycrystalline diethylterephthalate-d_4 is shown in Figure III.24. The field cycle of Figure III.23b was employed to indirectly and selectively detect only the deuterium NQR signal with all dc pulse angles equal to multiples of 2π for the protons. A mixing pulse of $3x2\pi$ radians in the laboratory z direction for the protons is approximately a 165° deuteron pulse which is close to the 180° pulse predicted from Equation (III.28) to give maximum intensity in the crosspeaks.[18] The diagonal peaks fall along the $\nu_1=\nu_2$ line and reproduce the one dimensional spectrum. Off-diagonal peaks correspond to the ν_-/ν_+ connectivities in the spin I = 1 manifold and are illustrated by the connecting lines. One connected pair of

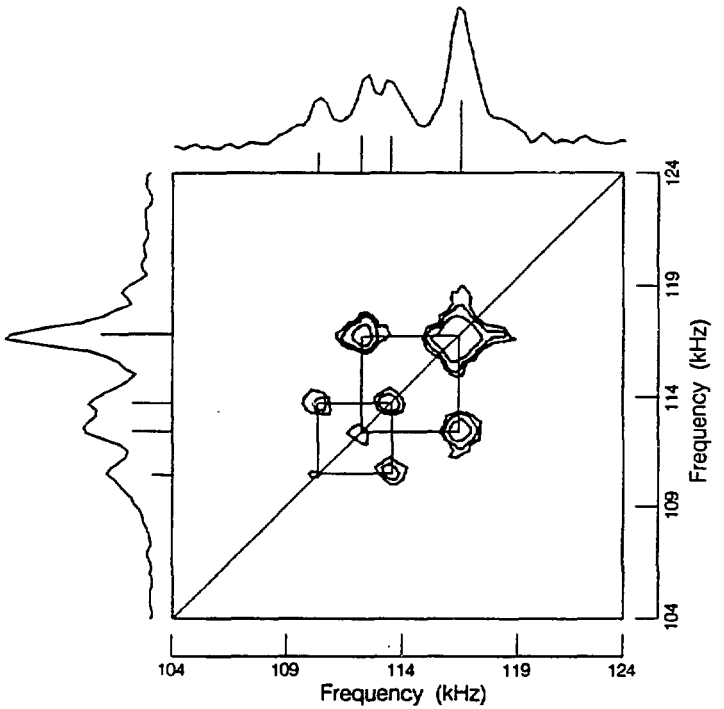

Figure III.24: Two dimensional zero field NQR spectrum of the high frquency ν_-/ν_+ transitions of polycrystalline diethylterephthalate-d_4. The spectrum was obtained through the field cycle described in Figure III.23b. By using pulses which were multiples of 2π for the protons, selective excitation of only the quadrupolar transitions is possible. The transfer of coherence between states in the spin I = 1 manifold was produced with a short dc pulsed field. Diagonal peaks along the $\nu_1 = \nu_2$ line correspond to the one dimensional spectra as shown in the projections. The peak positions of the one dimensional spectrum are indicated by the stick spectra. Cross peaks indicate correlations between the ν_+ and ν_- transition of an individual deuteron site. The connectivities are illustrated by the connecting lines.

lines belongs to one deuteron of the CD_2 group and the second pair belongs to the other inequivalent deuteron.

NQR transitions in frequency domain experiments are often assigned on the basis of weakly allowed double transition peaks,[33] double irradiation of two NQR lines[29], or by the shift in frequencies due to application of a low field[34] since the low frequency lines are often obscured or unobserved.[29] Time domain techniques have the low frequency detection capabilities, resolution and selectivity to assign transitions on the basis of ν_o lines. All of these approaches are plagued by the problem of increased complexity of the spectrum with increasing numbers of quadrupolar sites. Two dimensional zero field NMR experiments can address many of these problems by utilizing the cross-peak correlations to determine connectivities. A large variety of experimental conditions, produced with different field cycles, can be envisioned with the use of pulsed magnetic fields to manipulate the spins in zero field. The greatest increase in sensitivity and experimental expediency would result by directly detecting the zero field oscillations via an extremely sensitive detection apparatus such as a SQUID. Thus, the experiment presented here would no longer have the third time period of high field detection and as such would be two-dimensional in the truest sense.

F. References

1. M. Mehring, Principles of High Resolution NMR in Solids (Springer-Verlag, Berlin, 1983).

2. (a) R.L. Strombotne and E.L. Hahn, Phys. Rev. **133**, 1616 (1964).
   (b) S.R. Hartmann and A.G. Anderson, Phys. Rev. **128**, 2023 (1962).

3. M. Goldman, Spin Temperature and Nuclear Magnetic Resonance in Solids (Clarendon, Oxford, 1970).

4. J.M. Millar, A.M. Thayer, A. Bielecki, D.B. Zax and A. Pines, J. Chem. Phys. **83**, 934 (1985).

5. R. Kreis, D. Suter and R.R. Ernst, Chem. Phys. Lett. **118**, 120 (1985).

6. A. Bielecki, D.B. Zax, K.W. Zilm and A. Pines, Rev. Sci. Instrum. **57**, 393 (1986).

7. D.I. Hoult and R.E. Richards, J. Magn. Reson. **24**, 71 (1976).

8. E.M. Purcell, Electricity and Magnetism, vol. 2 (McGraw, New York, 1963).

9. M.H. Levitt, Prog. in Nuc. Magn. Reson. Spect. **18**, 61 (1986).

10. A.J. Shaka and J. Keeler, Prog. in Nuc. Magn. Reson. Spect., **19**, 47 (1987).

11. (a) M.H. Levitt and R. Freeman, J. Magn. Reson. **33**, 473 (1979).
    (b) R. Freeman, S.P. Kempsell and M.H. Levitt, J. Magn. Reson. **38**, 453 (1980).
    (c) M.H. Levitt and R. Freeman, J. Magn. Reson. **43**, 65 (1981).
    (d) M.H. Levitt, J. Magn. Reson. **48**, 234 (1982).
    (e) M.H. Levitt, J. Magn. Reson. **50**, 95 (1982).
    (f) A.J. Shaka, J. Keeler and R. Freeman, J. Magn. Reson. **53**, 313 (1983).
    (g) R. Tycko, Phys. Rev. Letts. **51**, 775, (1983).
    (h) J. Baum, R. Tycko and A. Pines, J. Chem. Phys. **79**, 4643 (1983).
    (i) A.J. Shaka and R. Freeman, J. Magn. Reson. **55**, 487, (1983).
    (j) R. Tycko and A. Pines, Chem. Phys. Letts. **111**, 462 (1984).
    (k) J. Baum, R. Tycko and A. Pines, Phys. Rev. A. **32**, 3435 (1985).
    (l) H.M. Cho, R. Tycko, A.Pines and J. Guckenheimer, Phys. Rev. Lett. **56**, 1905 (1986).
    (m) H.M. Cho, J. Baum and A. Pines, J. Chem. Phys.,in press (1987).

12. (a) R. Tycko and A. Pines, J. Magn. Reson. **60**, 156 (1984).
    (b) A.J. Shaka, J. Keeler, M.B. Smith and R. Freeman, J. Magn. Reson. **61**, 175 (1985).
    (c) A.J. Shaka and R. Freeman, J. Magn. Reson. **64**, 145 (1985).

(d) J. Baum, R. Tycko amd A. Pines, Chem. Phys. **105**, 7 (1986).

13. (a) W.S. Warren and A. Pines, Chem. Phys. Lett. **88**, 441 (1982).
(b) D.P. Weitekamp, in "Advances in Magnetic Resonance" (J.S. Waugh, Ed) Vol. 11, Academic Press, New York, 1983.
(c) T.M. Barbara, R. Tycko and D.P. Weitekamp, J. Magn. Reson. **62**, 54 (1985).

14. (a) M.H. Levitt, D. Suter and R.R. Ernst, J. Chem. Phys. 80, 3064 (1984).
(b) A. Bax, J. Magn. Reson. 65, 142 (1985).
(c) D.J. Siminovitch, D.P. Raleigh, E.T. Olejniczak and R.G. Griffin, J. Chem. Phys. 84, 2556.(1986).

15. (a) G.W. Leppelmeier and E.L. Hahn, Phys. Rev. **141**, 724 (1966).
(b) S. Vega, Adv. Magn. Reson. 6, 259 (1973).

16. A. Abragam, Principles of Nuclear Magnetism (Oxford, Oxford, 1963).

17. J. Jeener in "Adv. in Magn. Reson." (J.S. Waugh, Ed.) vol 3, Academic Press, New York, 1983.

18. D.B. Zax, Ph.D. Thesis, University of California, Berkeley, (1985).

19. D.B. Zax, A. Bielecki, K.W. Zilm, A. Pines and D.P. Weitekamp, J. Chem. Phys. **83**, 4877 (1985).

20. J.M. Millar, Ph.D. Thesis, University of California, Berkeley (1986).

21. A. Messiah, Quantum Mechanics (Wiley, New York).

22. G. Muha, J. Magn. Reson. **49**, 431 (1982).

23. C. Cohen-Tannoudji, B. Diu and F. Laloe, Quantum Mechanics (Wiley, New York, 1977).

24. T.P. Das and E.L. Hahn, Solid State Phys., Suppl. 1 (1958).

25. (a) A. Bielecki, J.B. Murdoch, D.P. Weitekamp, D.B. Zax, K.W. Zilm, J. Chem. Phys. **80**, 2232 (1984).
(b) T.H. Goodwin, M. Przybylska and J.M. Robertsen, Acta Crystallogr. 3, 279 (1950).

26. (a) A.G. Anderson. Phys. Rev. **115**, 863 (1959).
(b) V.S. Grechishkin, V.P. Anferov and N. Ja. Sinjavsky, Adv. Nucl. Quad. Reson. 5, 1 (1983).

27. (a) J.C. Koo, Ph.D. Thesis, University of California, Berkeley.
(b) J.C. Koo and Y.N. Hsieh, Chem. Phys. Lett. 9, 238 (1971).
(c) R.L. Strombotne and E.L. Hahn, Phys. Rev. 133, 1616 (1964).
(d) R.E. Slusher and E.L. Hahn, Phys. Rev. 166, 332 (1968).

(e) A.G. Redfield, Phys. Rev. **130**, 589 (1963).
(f) T.L. Brown, L.G. Butler, D.Y. Curtin, Y. Hiyama, I.C. Paul and R.B. Wilson, J. Am. Chem. Soc. **104**, 1172 (1982).
(g) J.W. Clymer and J.L. Ragle, J. Chem. Phys. **77**, 4366 (1982).

28. R. Blinc, Adv. Nucl. Quad. Reson. 2, 71 (1975).

29. D.T. Edmonds, Phys. Rep. **C29**, 235 (1977). and Int. Rev. Phys. Chem. **2**, 103 (1982).

30. M. Bailey, Acta Crystallogr. **2**, 120 (1949).

31. R. Blinc, M. Mali, R. Osredkar, A. Prevesnik, J. Seliger and I. Zupanic, Chem. Phys. Lett. 14, 49 (1972).

32. L.S. Batchelder and J.L. Ragle, J. Magn. Reson. **37**, 469 (1980).

33. D.T. Edmonds and A.A.L. White, J. Magn. Reson. **31**, 149 (1978).

34. (a) E.A. Keiter, Y. Hiyama and T.L. Brown, J. Mol. Struct. 111, 1 (1983).
(b) D.A. d'Avignon and T.B. Brown, J. Phys. Chem. **85**, 4073 (1981).

35. P. Mansfield and P.G. Morris, NMR Imaging in Biomedicine (Academic, New York, 1982).

36. D.B. Zax, A. Bielecki, K.W. Zilm and A. Pines, Chem. Phys. Lett. **106**, 550 (1984).

37. A.J. Shaka and R. Freeman, J. Magn. Reson. **59**, 169 (1984).

38. (a) J. Jeener, Ampere International Summer School, Basko Polje, Yugoslavia, (1971).
(b) W.P. Aue, E. Bartholdi and R.R. Ernst, J. Chem. Phys. **64**, 2229 (1976).

39. (a) L. Müller, A. Kumar and R.R. Ernst, J. Chem. Phys. **63**, 5490 (1975).
(b) W.P. Aue, J. Karhan and R.R. Ernst, J. Chem. Phys. **64**, 4226 (1976).
(c) K. Nagayama, P. Bachmann, R.R. Ernst and K. Wüthrich, Biochem. Biophys. Res. Commun. **86**, 218 (1979).

40. (a) A.A. Maudsley and R.R. Ernst, Chem. Phys. Lett. **50**, 368 (1977).
(b) G. Bodenhausen and R. Freeman, J. Magn. Reson. **28**, 471 (1977).
(c) A.A. Maudsley, L. Müller and R.R. Ernst, J. Magn. Reson. 28, 463 (1977).

41. J. Jeener, B.H. Meier, P. Bachmann and R.R. Ernst, J. Chem. Phys. **71**, 4546 (1979).

IV. ZERO FIELD NMR OF LIQUID CRYSTALS

A. Introduction

1. Liquid Crystalline Phases

Many pure organic substances exist in phases, or rather "mesophases", intermediate between the solid and liquid states. Whereas a crystal has a regular packing in a three dimensional lattice and a liquid shows no correlation between the centers of gravity of the molecules, a liquid crystalline system displays some orientational (and possibly some low dimensional positional) ordering of the elongated molecules. Local ordering is generally brought on by collective interactions between the molecules, and uniform alignment of the sample may be induced by the application of a magnetic or electric field. There are two basic categories of liquid crystals: thermotropic, in which the mesophase formation and behavior are temperature dependent, and lyotropic, in which the resulting phases are dependent on concentration. The former class of compounds is explored in the following experiments.

The study of the liquid crystalline phases, their characteristics and behavior, is an extremely extensive area of research involving many disciplines and approaches. It is inconceivable that one chapter could accomplish a complete introduction to the amount of information available. Thus several relevant texts should be mentioned which introduce the physics of liquid crystals and their study by NMR. Among these are books by de Gennes[1], Emsley and Lindon[2], Emsley[3], Gray[4],

Chandrasekhar[5], Luckhurst and Gray[6] and review articles by Diehl and Khetrapal[7], Khetrapal and Kunwar[8], and Doane[9]. An exhaustive review of many areas of liquid crystal research with extensive lists of references can be found in the Handbook by Kelker and Hatz.[10] These are only a few among many references, which can be consulted for more detailed information on the areas briefly described in the following sections, in addition to the wealth of published scientific articles.

A particular liquid crystal may display one or many phases with variations in temperature. The major classes of thermotropic liquid crystals are nematic, cholesteric and smectic each of which, especially the smectics, can have many subclasses. Each subclass is distinguished by the degree and type of order present. In describing the liquid crystalline phase, discussions will focus on a local domain of the sample. A domain is considered a region of the liquid crystal sample in which there is some short-lived coherence in the alignment of the molecules. These domains may or may not align uniformly over the entire sample in the presence of a field. This field dependent behavior is covered in Section 2, while a discussion of the phases of interest follows.

a. Nematic. These are the lowest ordering phases and always occur before the isotropic phase. Nematic phases are the most liquid-like as there is no positional order of the centers of mass of the molecules, but rather a preferred parallel alignment of the long molecular axes as shown in Figure IV.1. The average alignment can be described by an axis, **n**, called the director. There is rapid, random diffusion ($\sim 10^{-6}$ cm^2 s^{-1}) of the molecules, rapid fluctuation (10^{-8}-10^{-9} s) about the

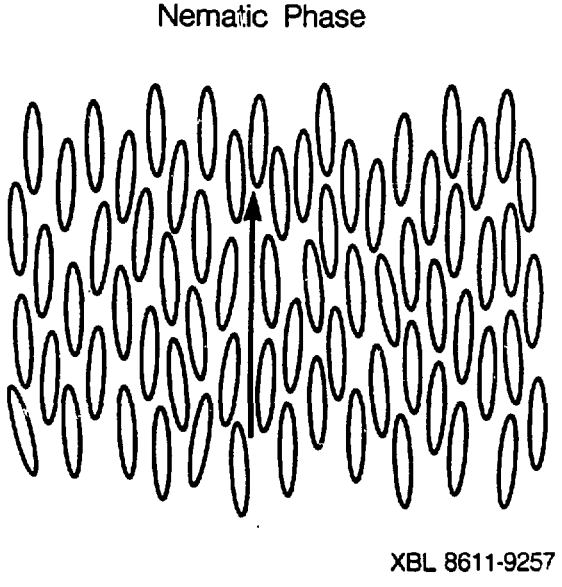

Figure IV.1: Nematic liquid crystalline phase. The elongated molecules are aligned on average with respect to the director as indicated by the arrow. There is no positional order on a local scale, only a preferred orientational order.

director, and rotation (10^{-10}-10^{-12} s) about the long molecular axes.[1] This leads to a cylindrical symmetry about **n**, where **n** and -**n** are equivalent. In most common nematics, the uniformly aligned phase is uniaxial and can be described as a monodomain with a single director axis.

b. Cholesteric. Cholesterics are potentially interesting for study by zero field NMR and are only briefly described. Cholesterics are a chiral form of the nematic phase. A cholesteric phase has a helical distortion which consists of the director axes of regions of the sample changing orientation with distance about a given axis. This changing orientation of the directors occurs regularly and continously about this axis such that a helix is swept out by the directors.[1,2] The pitch of the helix is generally many times greater (~few 1000 Å) than the molecular dimensions. Within the planes still described by the local directors, the phase has nematic properties. Such phases can be produced from either a pure optically active material, or by the addition of this material as an impurity to a non-optically active nematic phase; the helical pitch is a function of either the molecular structure of the pure compound or the relative concentrations of a mixture. In the presence of a magnetic field, cholesteric phases may have their twist axes either perpendicular (negative cholesteric) or parallel (positive cholesteric) to the field direction.

c. Smectic. These phases generally occur in a lower temperature range than the nematic. Smectic phases are the most ordered but, even among the different smectics, the type of ordering changes substantially. A feature common to all smectics, as shown in Figure

IV.2, is that the molecules form layers which are generally not positionally correlated. The layers are ~20-30 Å in thickness with a well-defined interlayer spacing and the molecules diffuse more freely within, than between, layers. The molecules within the layers may or may be translationally ordered which distinguishes some of the more common smectic phases. These are:

Smectic A: Inside the layers there is no long range order of the molecules, which orient perpendicular to the layer plane, as shown in Figure IV.3. Thus this phase is like a two dimensional liquid. The phase is uniaxial as the molecules are free to rotate about their long axes, the director axes and layer normal are nearly parallel and, **n** and **-n** are equivalent. Except for the layer structure, smectic A phases and nematic phases are nearly identical. Often smectic A samples align in an applied magnetic field.

Smectic C: Here the molecular axes are tilted with respect to the layer normal. In the presence of a field upon cooling from the nematic or smectic A phases, the molecules align with the field and the layer planes will be tilted. A random distribution of the planes in the azimuthal angle about the field direction forms a cone shaped domain. The tilt angle, ξ, is characteristic of a particular sample and is constant for a given temperature. The tilt can be attributed to the fact that the layer spacing ($d=l\cos\xi$) is less than the molecular length (l) and the molecules must therefore tip to fit within the layers.[1] Rotation about the long molecular axes might be expected to be hindered. The phase is considered biaxial in that the molecular orientation can not be described by a single uniaxial director.[9] A director axis which

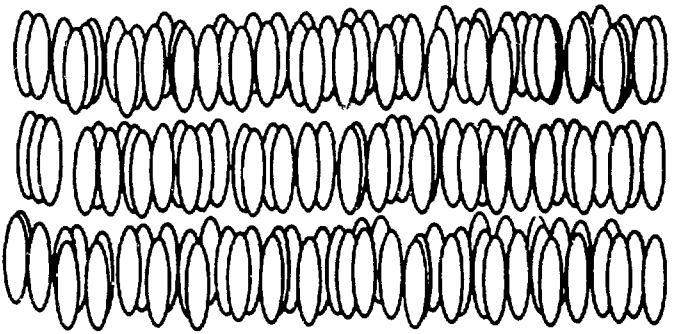

XBL 866-11149

Figure IV.2: Smectic phases are characterized by the arrangement of the liquid crystal molecules in layers which are generally not positionally correlated. The preferred direction of the molecular long axes can be either parallel or tilted with respect to the layer normal. Translational diffusion occurs freely within the layers and to a lesser extent between them. As shown here for a smectic A type phase, the molecules are randomly ordered within the layer and align perpendicular to the layer plane thus the director and layer normal are colinear.

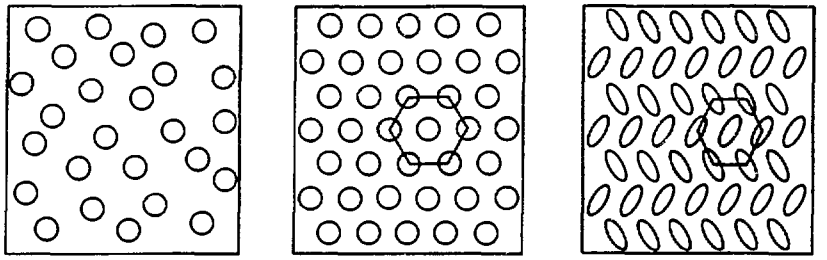

XBL 866-11157

Figure IV.3: Schematic drawing of the molecular ordering within the layer for three different smectic liquid crystalline phases in which the molecules all align perpendicular to the layer plane. The smectic A phase at left shows no positional ordering of the molecules. The molecules are free to rotate about their long axes; the area swept out by this rotation is shown by the circles. In the smectic B phase, at center, the molecules are also free to rotate about their long molecular axes although there is a hexagonal positional order within the plane. The smectic A and B phases are both uniaxial. The smectic E phase shows a molecular packing in which the molecules oscillate between one of two positions (represented by the ellipses) within the layers. There no longer is the freedom of rotation about the long molecular axes which leads to a biaxiality of the phase. The CH_2Cl_2 probe molecules are expected to reside between the liquid crystal molecules and exhibit the local symmetry.

describes the direction of the tilt is generally uniform except in certain smectic C^* phases. In the smectic C^*, formed from a mixture with a chiral component, the tilt directors follow a helical distortion.[1]

Smectic B: This is one of the smectic phases with a greater degree of order within the layers. The ordering within the layers is often considered more "solid-like" as there is a rigid periodicity in two dimensions as shown in Figure IV.3. In the smectic B phase studied, the molecules pack parallel to the layer normal in a hexagonal lattice. The molecules are free to rotate about their long axes so, in spite of the increased order, the phase is still uniaxial.

Smectic E: The smectic E phase is very similar to the B phase except that the molecules pack in an orthorhombic arrangement in the layers as shown in Figure IV.3. The molecules are also aligned parallel to the layer normal. One major difference between B and E phases is, that in the latter, the molecules can no longer freely rotate about their long axes but instead oscillate about their long axes by angles less than 180^{o}. This produces a herringbone-like pattern in the packing and is expected to produce a biaxiality of the phase.

All of the above mentioned phases can consist of a single pure compound or a mixture of two or more components. Mixtures can be formed only when the components are misicible which generally is dependent on the similarities in chemical composition and molecular symmetry. Other small organic molecules also dissolve quite readily in the liquid crystalline system which acts as an orienting solvent. When mixed with another liquid crystal or solute, the melting point and temperatures of

the phase transitions are usually depressed and not necessarily by a constant amount. Often by mixing components, one can produce a specific phase which exists over a desired temperature range (see Appendix).

2. Magnetic Field Dependent Behavior

Measurements of molecular ordering in liquid crystalline systems are often conducted in large applied magnetic or electric fields. The mode of alignment depends upon many features such as: the strength, direction and duration of the applied field, the magnetic susceptibility, concentration, dimensions and temperature of the sample.[10] Large dc fields cause the liquid crystal molecules to orient, on average, at a fixed angle with respect to the field direction. In the presence of a magnetic field, the individual molecules feel a torque and attempt to align to minimize the free energy. This is due to the anisotropic magnetic susceptibility of the molecules which determines the direction and degree of alignment in a magnetic field. The magnetic susceptibility, χ, relates the molecular diamagnetic moment, M, to the applied field B by[1]

$$M_i = \chi_{ij} B_j \qquad \text{(IV.1)}$$

where i,j=x,y,z. For uniaxial nematics, the magnetic susceptibility can be represented by a symmetric tensor with elements equal to $\chi_{\parallel}$ and $\chi_{\perp}$ relative to the long axis of the molecule. An anisotropy of the magnetic susceptibility, $\Delta\chi = \chi_{\parallel} - \chi_{\perp}$ results when these two components (which are usually negative) are unequal, and its sign is determined by their relative magnitudes. For liquid crystal systems in which there are strong molecular correlations and cooperative effects, the

contribution to the free energy of many molecules overrides thermal energies (which is not the case in a liquid) and they align. The long range order leads to a reduction in the free energy given by[2]

$$G = -\Delta\chi B^2(3\cos^2\beta-1)/6 \qquad \text{(IV.2)}$$

where β is the angle between the director and the field.

Examples of the alignment in the nematic phase for the two possibilities of $\Delta\chi>0$ and $\Delta\chi<0$ are shown in Figure IV.4. For molecules with a positive value of $\Delta\chi$, the domain directors align with the magnetic field ($\beta=0$ to minimize G in Equation (IV.2)) as shown in Figure IV.4a. In contrast, the molecules with a negative value of $\Delta\chi$ align on average perpendicular ($\beta=90^o$) to the field direction, as illustrated for a single domain in Figure IV.4b. The molecules have the same rotational and translational freedom in both cases although in the latter the domain director axis can have any direction in the plane perpendicular to the external field. Other phases such as smectics behave differently in the presence of a field. Whereas nematics readily align, an aligned smectic phase is often only produced if the temperature is reduced from an isotropic or nematic phase in the presence of the field.[3] Uniform alignment is not always obtainable as there is a dependence on factors such as the preparation and the rate of cooling of the sample. Easily aligned samples, such as nematics, are frequently used as NMR solvents, and aligned smectic phases are frequently studied by NMR analogously to single crystals as they will not reorient with rotation. Some smectics, such as A and C, may align in a magnetic field thereby leaving the experimentalist with no option of an orientation dependent study for these phases. Similarly, large enough fields have also been found to

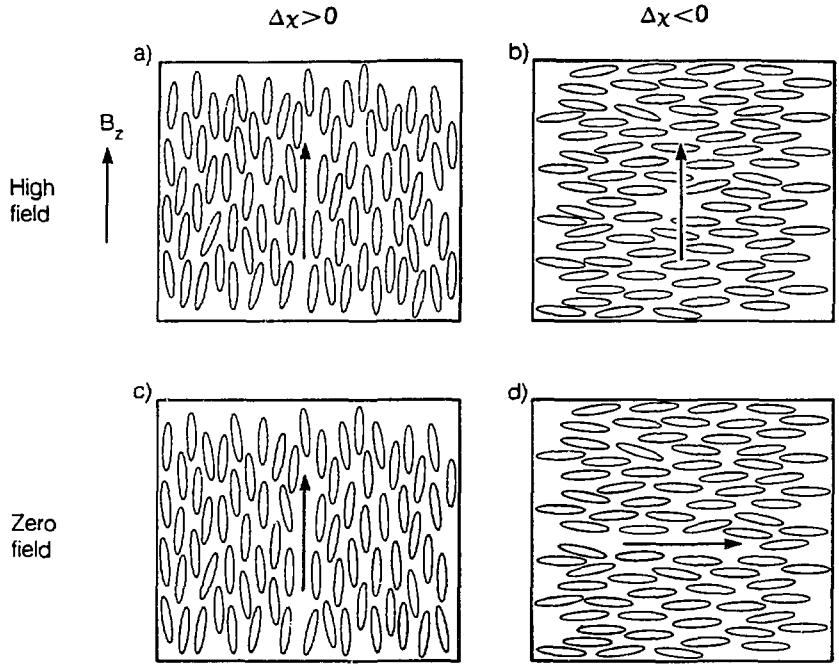

Figure IV.4: Alignment of nematic liquid crystal molecules with positive and negative magnetic susceptibility anisotropies in high and zero fields. The molecules align on average in a single direction described by a director axis. The molecules fluctuate rapidly about the director axis and rotate about their long axes. In the presence of a large field, the director axis of a domain of the system with $\Delta\chi>0$ is aligned with the field as in (a) while it is perpendicular for a system with $\Delta\chi<0$ as shown in (b). The arrows indicate the quantization axes of the spin interactions in high field. In the absence of a magnetic field, the director axes of a domain determine the quantization axes (as shown by the arrows in (c) and (d)) of the spin interactions in zero field. Note that while the molecules remain aligned in both cases, the direction of the quantization axis does not change between high and zero field in the $\Delta\chi>0$ case, while for $\Delta\chi<0$ it does.

"untwist" a cholesteric phase.[2,11]

In the absence of a magnetic field, the average orientation of the director is determined by convection and interactions with walls and surfaces of the container of the sample.[1] The degree of order, in or out of the field, is also concentration and temperature dependent. In a macroscopic sample, **n** is a function of position throughout the sample owing to these effects. In the bulk sample, order on a local scale persists over some distance known as the coherence length. This distance is generally a few microns, and in the presence of a field can be used to describe the length of the transition region between competing anchoring effects and orientation by the field.[1] The magnetic field strength dependence of the alignment on a macroscopic scale is studied by light scattering[13], optical[14] and magnetic[15] birefringence and magnetic susceptibility[16] measurements. On a molecular scale, NMR can be used to measure the ordering.[2,3,7]

In a strong enough applied field, regardless of the ordering of the liquid crystal molecules, the field direction determines the relevant NMR spin interaction frame as illustrated by the axes in Figure IV.4a and 4b. After the removal of the field, the relevant axis system is determined by the motional and symmetry properties of the liquid crystal molecules. This is illustrated for single sample domains in Figure IV.4c and 4d, and would describe the entire system as a monodomain in the former if it had been aligned in a magnetic field. In contrast, although the director axes in Figure IV.4d are all perpendicular to the original field direction (z), they are randomly distributed in the xy plane as shown in Figure IV.5 and therefore, a

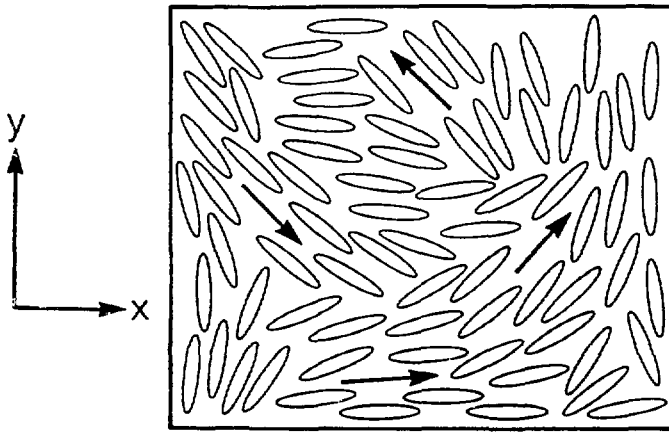

XBL 866-11150

Figure IV.5: Cross section perpendicular to the field direction for a liquid crystal sample with $\Delta\chi<0$. The separate domains are characterized by director axes, all perpendicular to the field direction, with a random distribution of director orientations in the xy plane.

single director axis does not describe the entire system. Thus between high field and zero field, or $\Delta\chi>0$ and $\Delta\chi<0$, the interaction frames which aptly describe the spin systems may differ. In the absence of a field, the orientational, motional and symmetry characteristics of the thermotropic liquid crystalline phase determine the magnitude and form of the zero field NMR Hamiltonian. Thus through the observed spin interactions in the NMR experiment, one can gain an understanding of the molecular ordering.

3. NMR of Liquid Crystals

a. Order Parameters. The next obvious question is: How does one describe the ordering of the liquid crystal molecules? The molecules are fluctuating rapidly and randomly in position and orientation yet on average are aligned in a given direction. If the molecular system can be related to the director axes, which may or may not be aligned with the laboratory/field frame, then the angular terms which relate these frames will be descriptive of the ordering of the system. In all cases that follow, the molecules are assumed to be rigid and therefore the ordering can be described by a probability function, $P(\alpha,\beta)$, of the director axis having some average orientation, given by the polar angles α and β, in the molecular frame.[2] The parameters describing the order must reflect the physical realities of the situation, to begin with they must be continuous functions of the angles and vanish in isotropic phases.

Since the interactions to be studied are generally second rank tensor interactions, an order matrix or tensor can be used to express

the director frame quantities in terms of the molecular fixed axis system.[1,2] For a nematic phase with a uniaxial director frame, this is expressed as

$$T_{ii} = \sum_{i,j}^{x,y,z} S_{ij} T_{ij} \qquad \text{(IV.3)}$$

and the elements of S are given by

$$S_{ij} = \frac{1}{2} \langle 3\cos\theta_i \cos\theta_j - \delta_{ij} \rangle \qquad \text{(IV.4)}$$

where θ is the angle between the uniaxial director frame z axis and the molecular axes i and j. In this case, the S matrix is a 3x3 cartesian matrix which is symmetric, such that $S_{ij}=S_{ji}$, and traceless, i.e. $\Sigma S_{ii}=0$. Thus there are a maximum of five independent elements. The elements of this matrix are generally called the Saupe order parameters[17] and can be related to motional constants or averages of the Wigner rotation matrix elements[7,8] (see Chapter I). The latter will become most useful in the calculations to follow and the relationships between the five S and the Wigner $D_{m,m'}$ elements are given below.[6]

$$\begin{aligned}
S_{zz} &= \langle D^2_{00} \rangle &&= \frac{1}{2}\langle 3\cos^2\beta - 1 \rangle \\
S_{xx} - S_{yy} &= \sqrt{\frac{3}{2}} (\langle D^2_{02} \rangle + \langle D^2_{0-2} \rangle) &&= \frac{3}{2}\langle \sin^2\beta\cos 2\alpha \rangle \\
S_{xy} &= \sqrt{\frac{3}{8}} (\langle D^2_{0-2} \rangle - \langle D^2_{02} \rangle) &&= \frac{3}{2}\langle \sin^2\beta\sin 2\alpha \rangle \qquad \text{(IV.5)} \\
S_{xz} &= \sqrt{\frac{3}{8}} (\langle D^2_{0-1} \rangle - \langle D^2_{01} \rangle) &&= \frac{3}{2}\langle \sin\beta\cos\beta\cos\alpha \rangle
\end{aligned}$$

$$S_{yz} = \sqrt{\frac{3}{8}} (\langle D^2_{01} \rangle + \langle D^2_{0-1} \rangle) = \frac{3}{2} \langle \sin\beta\cos\beta\sin\alpha \rangle$$

where ß and α are the angles relating the uniaxial director to the molecular frame. The order parameters range in value from 1 to -1/2. The symmetry of both the molecular system and the phase determines the number of order parameters necessary to describe the situation. Some examples of the effect of molecular symmetry operations are given below.[7]

Table IV.1: Molecular Symmetry and Required Order Parameters

Symmetry	No. of Independent S Elements	S Elements
3 fold or greater axis	1	S_{zz}
2 perpendicular planes	2	S_{zz}, $S_{xx} - S_{yy}$
1 plane	3	S_{xx}, S_{yy}, S_{xy}
none	5	S_{xx}, S_{yy}, S_{xy} S_{xz}, S_{yz}

b. Nuclear Spin Interactions in Liquid Crystals. As stated previously, the order parameters can be extracted from a measure of the second rank tensor nuclear spin interactions such as dipolar and quadrupolar couplings. Unlike isotropic liquids in which these interactions are averaged to zero, the anisotropic liquid crystalline environment merely scales the interaction and, due to fast random molecular motions, removes the intermolecular dipolar couplings thereby

producing narrow line spectra for small spin systems. The behavior of the liquid crystal system in NMR experiments can be understood if one considers the form of the Hamiltonian in an applied field which aligns the sample. For example, the dipolar Hamiltonian in the average director frame may be written in spherical tensor notation as

$$H_D = \sum_{m,m'=-2}^{2} (-1)^m T_{2,-m} A_{2,m'} \langle D^2_{m',m}(\Omega) \rangle \qquad \text{(IV.6)}$$

here $T_{2,m}$ and $A_{2,m'}$ represent director frame spin operators and principal axis system (PAS) spatial variables[18], respectively, and the $D_{m',m}(\Omega)$ ($\Omega=\alpha,\beta,\gamma$) term effects the transformation between the two frames. For two dipolar coupled spins, the internuclear vector which is the z axis of the PAS frame is taken to be coincident with the z axis of the molecular frame. If the molecular frame is not chosen as coincident with the PAS frame, for rigid molecules, there still is a fixed relative orientation of the PAS and molecular frames. Thus an additional angular term relates the order parameter of the molecular frame to the PAS frame. The brackets in Equation (IV.6) indicate a time average over the $D_{m',m}$ terms which accounts for fluctuations of the alignment of the molecular frame with respect to the director frame. Assuming that the field aligns the sample in the field direction ($\Delta\chi>0$), the director axis will be coincident with the laboratory z axis. Truncation of the spin part of the Hamiltonian by a large magnetic field leaves only the T_{20} term nonzero. Furthermore, only the $m'=0$ term of the traceless second rank tensor $A_{2,m'}$ is nonzero since the dipolar interaction is axially symmetric in the molecular/PAS frame.[18] Therefore, the effective high

field laboratory frame dipolar Hamiltonian for a proton pair is given by

$$H_D^o = T_{20}A_{20}\langle D_{00}^2(\Omega)\rangle = T_{22}A_{00}S_{zz} \qquad \text{(IV.7a)}$$

$$= -\frac{\gamma^2h^2}{4\pi^2r^3} S_{zz}(3I_{1z}I_{2z} - I_1\cdot I_2) \qquad \text{(IV.7b)}$$

where the uniaxial order parameter S_{zz} is given by

$$S_{zz} = \langle D_{00}^2(\Omega)\rangle = 1/2\langle 3\cos^2\beta - 1\rangle \qquad \text{(IV.8)}$$

and β is the instantaneous angle between the director and the proton-proton internuclear vector. Thus by measuring the dipolar coupling for a rigid proton pair, the value of S_{zz} can be determined. If the proton pair is on the liquid crystal molecule, then the order parameter corresponds to the ordering of the liquid crystal molecules.

As has become obvious, relating many interaction frames is a necessary part of the calculation. For example, descriptions of the system can easily include a few, if not more, transformations from the

PAS frame → Molecular frame → Director frame → Lab Frame

depending on the phase and the selection of frames. The number of transformations is often simplified as in the case above in which the first and second frames are chosen to be coincident as were the third and fourth. Only those transformations which reflect rapid molecular motions on the timescale of the experiment are expressed as an average. In Chapter III, high field and zero field spin operators were distinguished by subscripts. Because of the number of reference frames

required here, and their frequent coincidences, subscripts will not always be used but the relevant frames should be clear based on context. Apologies are made in advance for any confusion.

The spin system can consist of either the liquid crystal molecules themselves or a probe molecule dissolved in the liquid crystal which is constrained to the symmetry of the phase by dispersive and steric forces.[7,8,19] This aids one in studying the liquid crystalline phase via simpler spin systems (without requiring selective isotopic labelling) and greatly aids in spectral simplification and interpretation.[7,8] For example, in Figure IV.6, the high field spectrum of a fully protonated liquid crystal is shown. The broad featureless lineshape provides little information. The ordering of a rigid solute molecule (or part of the molecule) can be described by an order tensor, S, which describes the average alignment of the solute spin system molecular frame with respect to the director axis. The S parameters corresponding to the solute differ from those of the solvent, yet reflect the local symmetry and type of ordering in the phase. Unfortunately, there is no simple relationship between the two S matrices. The allowed motions of the solute reflect the anisotropic molecular tumbling in the liquid crystal medium by characteristically averaging the dipolar interaction.[1,2] The Hamiltonian of a two spin solute molecule dissolved in an aligned nematic ($\Delta\chi>0$) has the same form as that in Equation (IV.7) and the spectrum consists of two lines due to the scaled dipolar coupling. The order parameter of the solute, S, may be calculated from the observed splitting δ by $S_{zz}=4\pi^2r^3/3\gamma^2h\delta$.

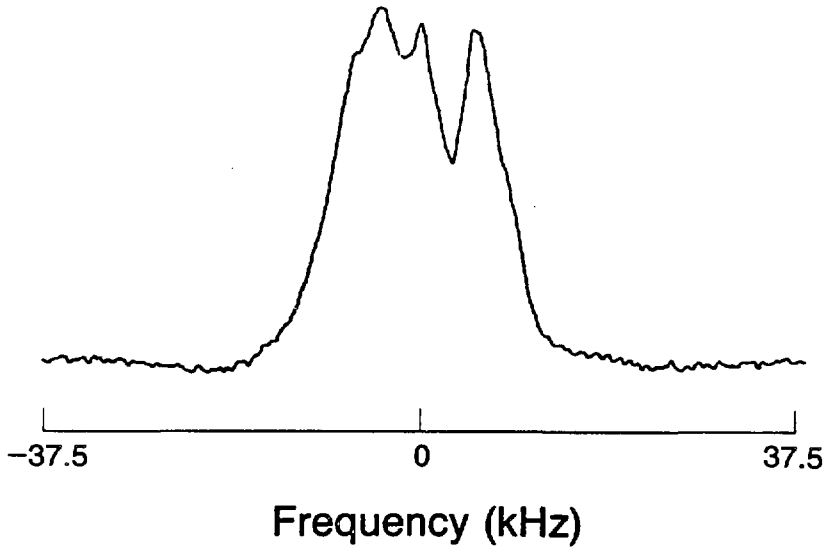

XBL 8512-12775

Figure IV.6: High field NMR spectrum (180 MHz ^{1}H) of a fully protonated nematic liquid crystal sample. Due to the large number of dipolar coupled spins, no structure is resolved in the spectrum and little information on the molecular ordering is available.

B. Nematic Phases in Zero Field Experiments

Until recently, the behavior of a liquid crystalline system in the absence of an applied magnetic field could not be studied by NMR. Field cycling time domain zero field NMR techniques now provide a means to measure both the bulk ordering and molecular order parameter without the influence of an applied field. Descriptions of the zero field NMR field cycling experiments were presented previously and require little change when applied to liquid crystal samples. The field cycling schemes used in these experiments are presented with each case as there are differing requirements for the application of dc pulsed fields.

1. Observations of the Alignment in Zero Field

Several features of liquid crystalline systems make their study by zero field NMR of interest. Because the molecules are aligned by a magnetic field, one wonders what will occur with the removal of the field. Does the bulk ordering of the sample change, as shown in Figure IV.7, and does any change occur in the local molecular ordering as characterized by the order parameter? It has been suggested that the degree of ordering may differ on a macroscopic and molecular level in spite of the small energies of the order director fluctuations.[20] The order parameter and fluctuations are important parameters in describing relaxation measurements[21], which give an indication of dynamics in liquid crystal systems, and it is thus instructive to directly measure the ordering in high and low fields.

The system chosen for study was composed of a CH_2Cl_2 probe

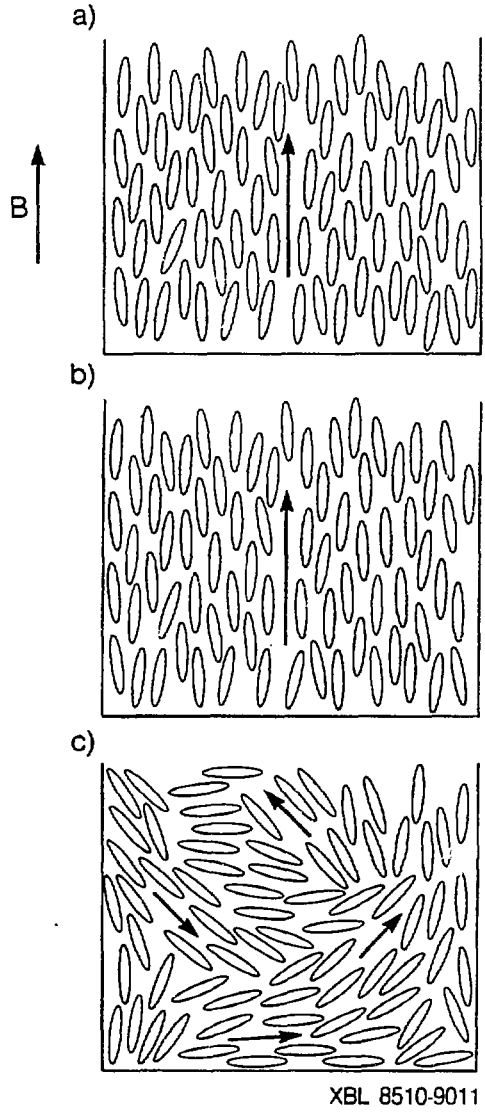

XBL 8510-9011

Figure IV.7: Ordering in nematic liquid crystals. (a) In the presence of a magnetic field, B, the average orientation of the director (shown by the arrow) is aligned along the magnetic field direction and the dipolar coupling corresponds to the truncated high field terms. (b) Order in the nematic remaining immediately after removal of the field. The sample maintains its uniform average alignment along the laboratory z axis. Due to the rotational motions and symmetry of the liquid crystals, the dipolar Hamiltonian is also truncated with respect to the z axis in the absence of a magnetic field. (c) Disordered system where the alignment of the directors is no longer in the laboratory z direction. The average orientation of the molecules on a local scale is described by the local director. The dipolar Hamiltonian of a domain is now truncated with respect to this director axis.

molecule dissolved in p-pentyl phenyl 2-chloro-4-(p-pentylbenzoyloxy)-benzoate (Eastman Kodak 11650, $\Delta\chi>0$). The high field NMR spectrum of this nematic system was obtained using a 90_x-τ-180_y-τ echo sequence[22] to reduce the effects of high field inhomogeneities where the signal intensity is measured as a function of τ. The minimum time for the incremented variable τ was selected, based on the T_2 relaxation times of the two components, to echo only the solute signal and not that of the liquid crystal itself. The resulting dipolar spectrum is shown in Figure IV.8. The alignment of the proton-proton internuclear vector with respect to the director, **n**, may be described by a single order parameter $S_{zz}=0.055 \pm 0.001$ as calculated from the observed splitting in accordance with Equation (IV.7) using a value of $r=1.771$ Å for CH_2Cl_2.

Previous work (section II.C.2) has shown that polycrystalline samples of isolated proton pairs yield a three line frequency spectrum when subjected to the sudden transition experimental sequence of Figure IV.9. The three lines are of equal intensity and occur at zero frequency and $\pm\nu_D=3\gamma^2h/8\pi^2r^3$. If this sudden transition experiment is applied to the CH_2Cl_2/11650 system, using a high field echo as above to detect only the solute signal, one obtains the one line spectrum shown in Figure IV.10. This line at zero frequency corresponds to the central line of the triplet found in the polycrystalline case and yields no dipolar information on the solute. Contained in the seemingly uninformative spectrum is, however, a great deal of information on the ordering of the nematic liquid crystal. This can be understood by remembering that the spectrum reflects the Hamiltonian of the system in zero field which is in turn determined by the liquid crystalline

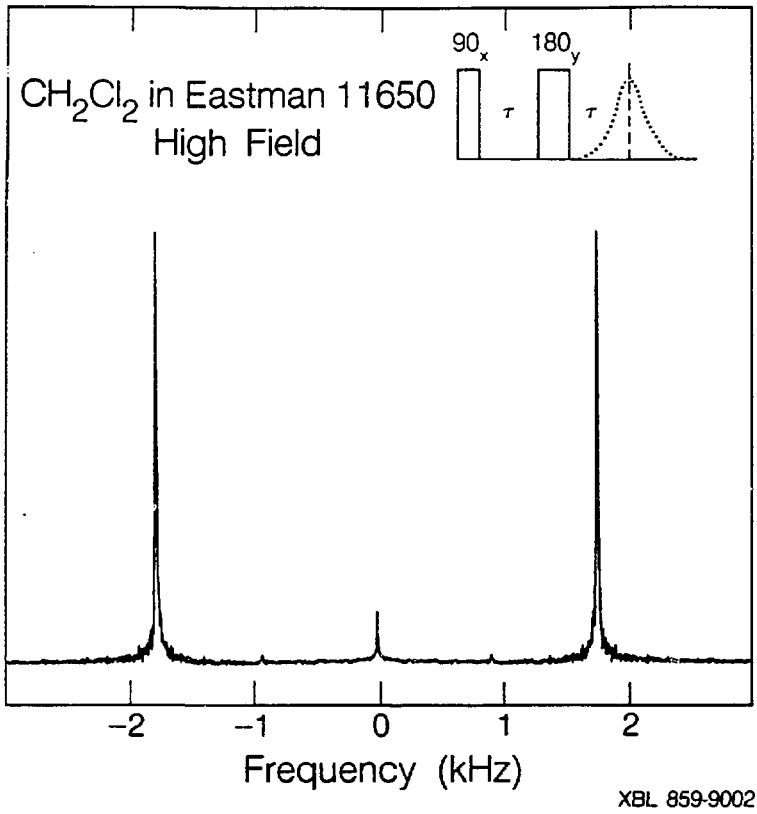

Figure IV.8: High field ^1H NMR spectrum of CH_2Cl_2 in Eastman 11650 ($\Delta\chi>0$) taken as a function of τ with the pulse sequence shown at upper right. The molecular order parameter of the solute is calculated to be $S_{zz}=0.055 \pm 0.001$ from the observed splitting.

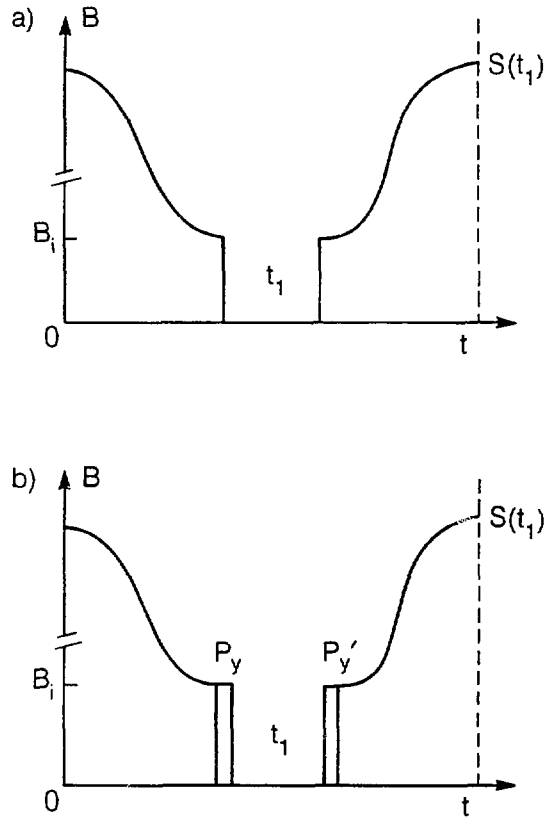

Figure IV.9: Schematics of zero field experimental field cycles. (a) This basic field cycle with a sudden transition in field has been described previously in Chapter II. (b) Sudden z/pulsed y field cycle. This field cycle is identical to (a) except for the application of pulsed dc magnetic fields (P and P') corresponding to rotation angles given by $\theta = \gamma B_{dc} t_p$. For 90°_{y} pulses the density operator at the start of the t_1 period is now proportional to I_x in the lab frame. Detection of this transverse component is completed by the final pulse and application of a field in the z direction to preserve the magnetization before remagnetization to high field.

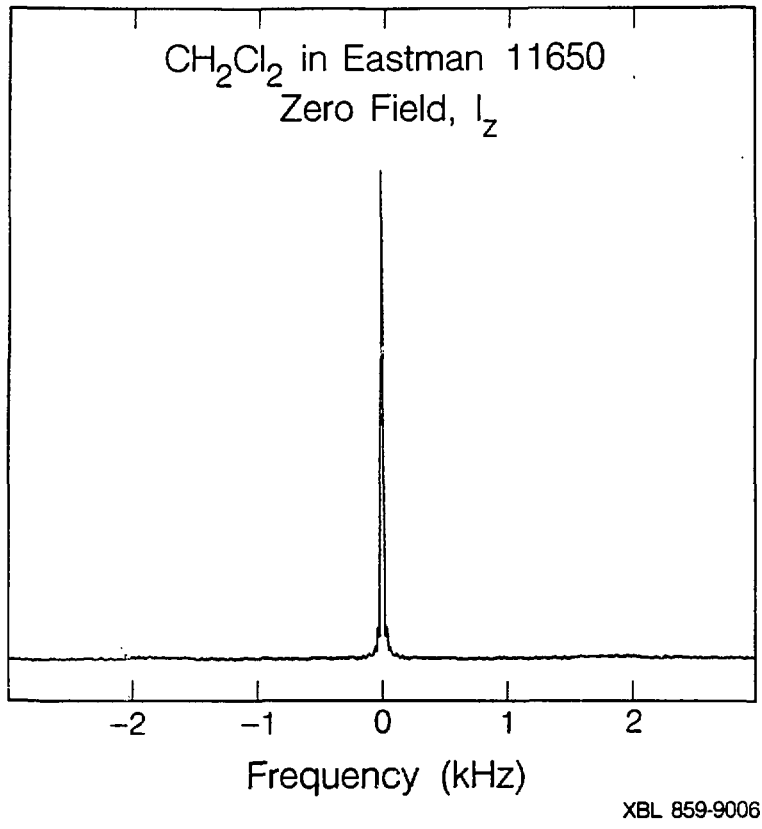

Figure IV.10: Spectrum of CH_2Cl_2 in Eastman 11650 ($\Delta\chi>0$) using the field cycle of Figure IV.9a. The single line at zero frequency indicates that no zero field evolution occurred during the time t_1. The spectrum appears as expected for an ordered nematic in which the axis of quantization is the same in high as in low field.

environment.

a. Spin Hamiltonian in Zero Field. Consider the case of a liquid crystal system which remains aligned along the original field direction ($\Delta\chi>0$) in zero field. The zero field director frame dipolar Hamiltonian for a molecule of the nematic phase, Equation (IV.6), is unchanged from that in high field and is equal to H_D^o of Equation (IV.7). This is due to motional averaging about the director oriented along the laboratory z axis as in Figure IV.7b. Rotation about the long molecular axes and the uniaxial nature of the liquid crystal require that the terms in Equation (IV.6) with m' and m not equal to zero vanish (i.e. no dependence on α and γ). In contrast to the high field case, the truncation can be accomplished solely through the spatial terms of the Hamiltonian. Again, the solute Hamiltonian has the same form as that above since the nematic environment imposes a preferred orientation and motion on the solute molecules.

The sudden transition experimental results reported above can now be interpreted. Even in the absence of an applied field, a uniformly aligned sample with **n** along the laboratory z direction, Figure IV.7, has a zero field Hamiltonian equal to the truncated laboratory frame dipolar Hamiltonian. The sudden switch-off of the intermediate field in the zero field experiment of Figure IV.9a initiates zero field evolution only if $[\rho,H_{ZF}]\neq 0$. Since $\rho(0)$ is proportional to $I_{z,L}$ before the transition, this condition is not met. Calculating the signal from

$$S(t_1) = Tr\{I_z \exp(-iH_D^o t_1) I_z \exp((iH_D^o t_1))\} = 1 \qquad \text{(IV.9)}$$

shows that no evolution occurs in zero field and the resulting spectrum

for an ordered sample in zero field is simply a line at zero frequency.

The zero field dipolar spectrum of an aligned sample should still be obtainable by the use of a pulsed dc magnetic field to change the initial condition from $\rho(0)=I_{z,L}$ to some other operator that does not commute with H_D^o. In this case, as shown in Figure IV.9b, a pulse can be used to rotate the initial magnetization to the xy plane of the laboratory frame. If the direction of the dc field is defined as the laboratory frame y axis and a 90^o pulse is applied, then the density operator after the pulse is equal to I_x. Since $[H_D^o,I_x]\neq 0$ evolution is initiated. Exact calculation of the zero field signal is quite easy as the initial state, dc pulses and zero field Hamiltonian are all referenced to a common frame for an aligned sample, and

$$S(t_1) = Tr\{I_z\exp(-i\theta' I_y)\exp(-iH_D^o t_1)\exp(-i\theta I_y)I_z \exp(i\theta I_y)\exp(iH_D^o t_1)\exp(i\theta' I_y)\} \quad \text{(IV.10)}$$

A second pulse, $\theta'=360^o-\theta$, is required to transform the evolving state back into one proportional to I_z before remagnetization. For example, rearranging terms and taking into account that $\theta=90^o$, Equation (IV.10) becomes

$$S(t_1) = Tr\{I_x\exp(-iH_D^o t_1)I_x\exp(iH_D^o t_1)\} \quad \text{(IV.11)}$$

which is identical to applying rf pulses in high field. Unlike previous calculations, this requires no transformation between frames (other than that already ascribed to the order parameter), nor is there any average taken over director orientations as only one is present in an aligned sample. This is analogous to a single crystal in zero field except that

the Hamiltonian is truncated.

A two proton spin system, in an oriented liquid crystal with $\Delta\chi>0$, is expected to yield the following normalized signal for an arbitrary dc pulse angle from Equation (IV.10) as given by

$$S(t_1) = \cos^2\theta + \sin^2\theta\cos(\tfrac{3}{2}S_{zz}\omega_D t_1) \qquad \text{(IV.12)}$$

where θ is the angle of the dc pulse and $\omega_D=2\pi\nu_D=\gamma^2\hbar/2\pi r^3$. To confirm that the sample is indeed aligned and that dipolar signal can be observed, an experiment was performed with the sequence of Figure IV.9b. Figure IV.11 presents the results of a series of these sudden z/pulsed y experiments. The angles of the dc pulses corresponding to P and P' in Figure IV.9b were determimed by the calibration procedure described previously. The spectra consist of two lines corresponding to either the zero frequency or $\pm\nu_D$ lines of the polycrystalline case. The predicted behavior for an aligned sample under different dc pulses is observed. For $\theta=90^\circ$, all the signal evolves as the local fields and magnetization are perpendicular. Calculation of the order parameter of the solute from the zero field spectrum yields, $S_{zz}=0.054 \pm 0.001$. The molecular order parameter measured from these spectra in zero field is the same as that found in high field within an experimental error based on the linewidths and small scale temperature fluctuations which may occur in the course of the experiment.

The removal of the sample to low or zero fields might be expected to show a change in the bulk alignment of the liquid crystal molecules. If the sample were to disorder, the predicted zero field spectrum would be different. For example, one case is that where the local ordering

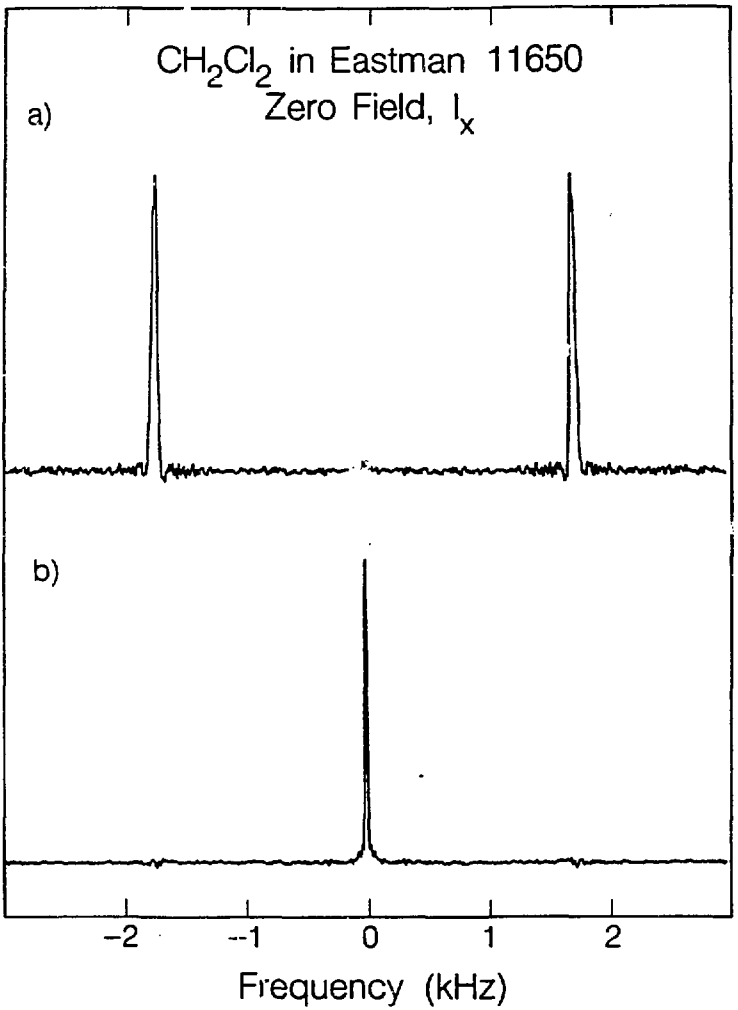
CH_2Cl_2 in Eastman 11650
Zero Field, I_x
a)
b)
−2
−1
0
1
2
Frequency (kHz)

XBL 859-9004

Figure IV.11: Spectra of the CH_2Cl_2/11650 system obtained via the sudden z/pulsed y field cycle of Figure IV.9b. DC pulses used were (a) $90^\circ_y, 270^\circ_y$ and (b) $180^\circ_y, 180^\circ_y$. The observed spectra show the dependence on pulse angle as predicted by Equation (IV.12) which was obtained assuming an ordered nematic liquid crystal in zero field. The molecular order parameter may be measured from the observed frequencies and was found to be $S_{zz}=0.054 \pm 0.001$, which is unchanged from high field within an experimental error of 2%. Linewidths of ~45 Hz may be attributed to residual fields.

within a domain remains the same, while the alignment of the local directors of these domains changes orientation as illustrated in Figure IV.7c. Assuming that the allowed motions and fluctuations within a local domain are the same as in the monodomain, then the director frame order parameter of the solute will be the same for all orientations since the director frame Hamiltonian is unchanged. The distributions of director orientations will manifest themselves as changes in the intensities of the lines in the zero field spectrum as discussed in Section II.C.2. (This is similar to a distribution of "crystallites" in which the degree of disorder may or may not lead to an isotropic distribution of director orientations.) Thus ordered and disordered nematics may be distinguished by the characteristic appearance of their zero field spectra since the relative intensities of the zero field lines will be indicative of the degree of disordering.

If the alignment is altered before reaching zero field, a sudden transition experiment would be expected to show evolving signal. In the limit of an isotropic distribution of the local directors, the normalized zero field signal for the sudden transition experiment or the sudden z/pulsed y version with both dc pulses equal to 90^{o} is given by

$$S(t_1) = 1/3[1 + 2\cos(\tfrac{3}{2}S_{zz}\omega_D t_1)] \qquad \text{(IV.13)}$$

which is the same form as that predicted for the proton pairs in a polycrystalline hydrate. Improperly prepared samples, such as those with large bubbles, result in observable zero field NMR signals due to the disruption of uniform alignment caused by surface effects and/or mechanical mixing. An example of such a spectrum showing broad peaks at

the dipolar frequencies is compared to the same material in Figure IV.12 using the sudden transition field cycle. A schematic picture of the possible disordering induced by a bubble appears in Figure IV.13. This effect was found to be exacerbated when using liquid crystal samples with very low viscosities although even here disordering was not observed in samples with no bubbles.

2. Demagnetization and Other Pulsed Experiments

Further studies were also performed to observe the effect of complete demagnetization on the liquid crystal system. The field cycle, shown in Figure IV.14a, consists of demagnetization to zero field combined with a pulsed version of the experiment. A spin temperature argument suggests that the density operator describing the initial demagnetized state in an aligned sample ($\Delta\chi>0$) should be proportional to $I_{z,L}$ since the motionally averaged dipolar and Zeeman Hamiltonians commute.[23] This predicts that the zero field signal is described by Equation (IV.12) and is confirmed experimentally since spectra produced with the same dc pulses appear identical to those in Figure IV.11. Thus the resulting state is not one characteristic of a demagnetized dipolar coupled system as described in Chapter III. If the demagnetization were to produce an initial condition other than $I_{z,L}$ then one expects an entirely different functional dependence for $S(t_1)$.

The effects of residual fields on the linewidths can be decreased, in any of the zero field experiments described, by employing a transverse dc 180° pulse to form a zero field echo. Figure IV.15 shows the results of a 180° refocussing pulse applied in the middle of the

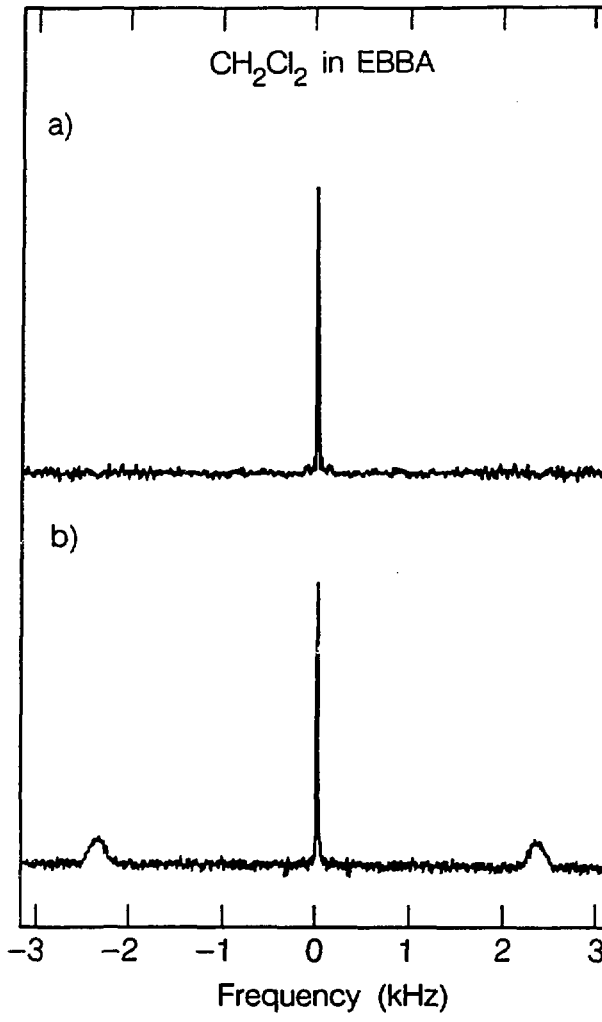

XBL 866-11155

Figure IV.12: CH_2Cl_2 in the nematic phase of EBBA with $\Delta\chi>0$. The spectrum shown in (a) results when the sudden transition field cycle of Figure IV.9a is used. The lack of dipolar signal indicates that the sample remains aligned; there is only a zero frequency signal from non-evolving magnetization. Samples in which large bubbles are present do display dipolar signals as shown in (b) which can be explained by disruption of the ordering of the liquid crystal molecules.

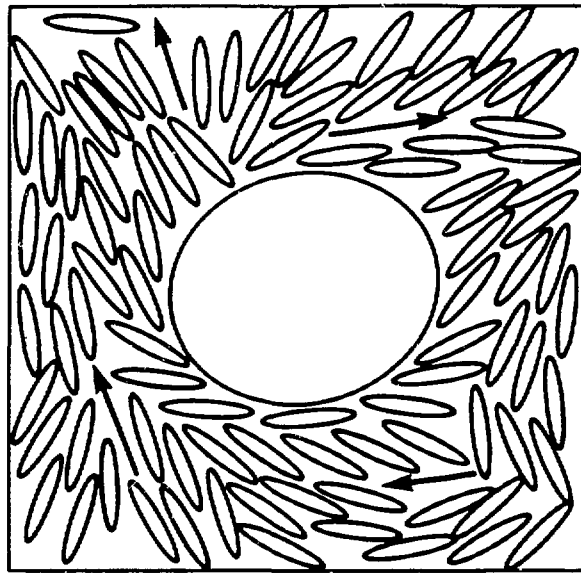

XBL 8611-4724

Figure IV.13: The uniform alignment of the sample is disrupted through the presence of a bubble in the sample. This effect may be due to either sample mixing in shuttling and/or surface effects. A possible scenario is shown above in which the director axes are anchored by a bubble and caused to point away from the z axis. This distribution of directors will alter the relative intensities of the zero field lines.

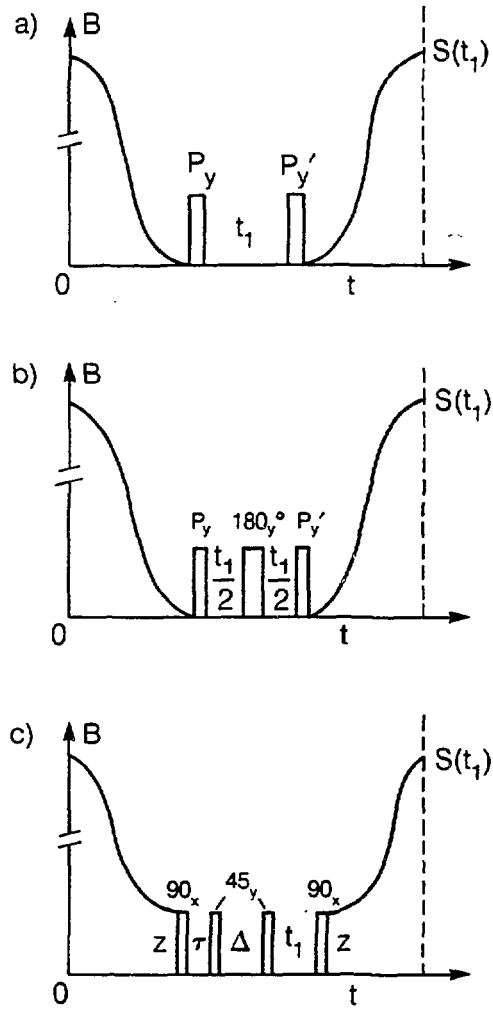
a)
B
S(t1)
Py
Py′
t1
0
t
b)
B
S(t1)
Py
180y°
Py′
t1/2
t1/2
0
t
c)
B
S(t1)
90x
45y
90x
z
τ
Δ
t1
z
0
t

XBL 859-9008

Figure IV.14: Other zero field experimental field cycles used in the study of liquid crystals. (a) After demagnetization to zero field, dc pulses are used to initiate and terminate the zero field evolution period t_1 as described in Chapter II. (b) Same field cycle as (a) except that the t_1 period is now divided in half by a 180° refocussing pulse. This pulse removes the effect of residual field inhomogeneities in the z direction. (c) Zero field dc pulse sequence for the production of dipolar order in zero field. The directions of the dc fields are shown. The sequence 90_x-τ-45_y takes the initial state of I_z to one of dipolar order in the lab frame. After the delay, Δ, the 45_y pulse transforms the state into observable transverse magnetization. Application of a 90_x pulse and the z field allows for observation of this evolution as a function of t_1 in high field.

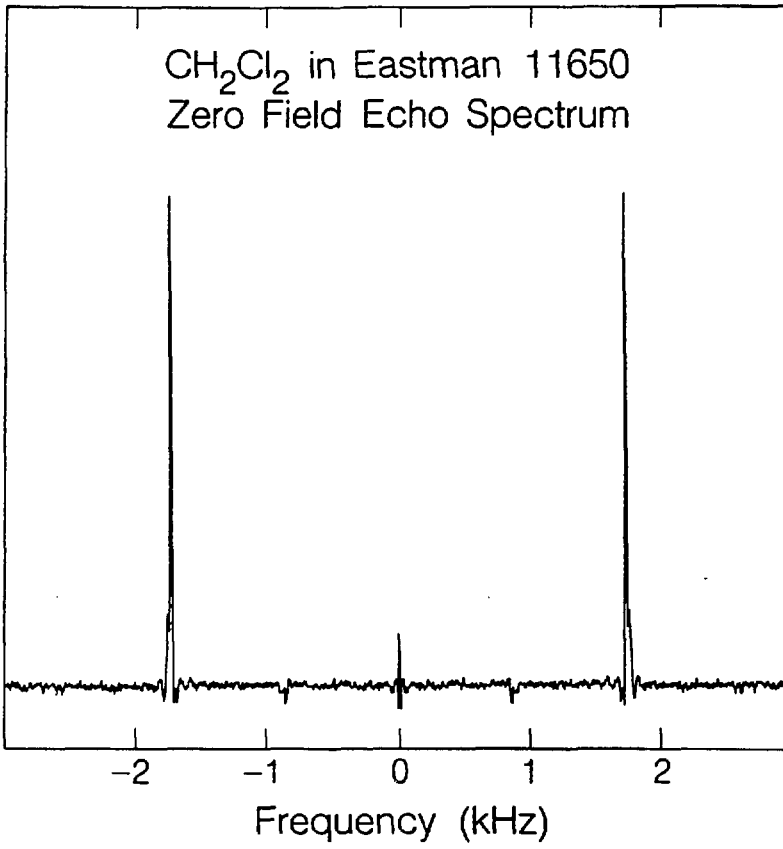

Figure IV.15: Zero field echo spectrum of CH_2Cl_2 taken using the zero field echo sequence, Figure IV.14b, which removes the effect of the linebroadening residual fields. Shown is the spectrum using the dc pulse sequence 90°_y-$t_1/2$-180°_y-$t_1/2$-270°_y, where all pulses are applied along the laboratory y axis. A linewidth of ~15 Hz is obtained. The lines at one half the dipolar frequency and zero frequency are artifacts due to pulse imperfections.

evolution period as illustrated in Figure IV.14b. After a 90^{o} y pulse on the initial state, $I_{z,L}$, the signal can be calculated from

$$S(t_1) = Tr\{I_x \exp(-iH_{ZF}t_1/2)\exp(-i\pi I_y)\exp(-iH_{ZF}t_1/2)$$
$$I_x \exp(iH_{ZF}t_1/2)\exp(i\pi I_y)\exp(iH_{ZF}t_1/2)\} \qquad (IV.14a)$$

where $H_{ZF}=H_Z + H_D^o$, and H_Z is the interaction with an inhomogeneous residual z field such that it commutes with H_D^o. The resulting signal is

$$S(t_1) = \cos(\tfrac{3}{2}S_{zz}\omega_D t_1) \qquad (IV.14b)$$

As expected, this pulsed dc field variation of the Hahn echo experiment[24] yields decreased linewidths which are measured here as ~15 Hz. This is due to reversing the sense of evolution under the residual field term without altering the evolution in t_1 under the bilinear dipolar Hamiltonian and can easily be seen by the fact that linear terms in I_z change sign with a 180^{o} pulse while the bilinear terms in H_D do not. Lines at one half the zero field frequency appear as artifacts in the echo spectrum and can be accounted for by imperfections in the dc pulses.

The initial condition for an aligned sample with $\Delta\chi>0$ is equal to $I_{z,L}$ and the zero field Hamiltonian in the laboratory frame is identical to that of the secular dipolar Hamiltonian in a high field rotating frame at resonance. With this understanding of the system, a multiple dc pulse sequence was attempted in zero field. A sequence was chosen to produce a dipolar ordered state in zero field, in the same manner as one would in high field, as such a state was not obtained by demagnetization. A zero field version of the Jeener-Broekaert sequence[25] was

performed, but unlike high field NMR techniques, separate coils were used for each orthogonal (90^{o} "phase shifted") pulse direction. Using the field cycle of Figure IV.14c, the sample was demagnetized to an intermediate field then suddenly demagnetized to zero field where the pulse sequence 90_x-τ-45_y-Δ-45_y-t_1-90_x was applied. Immediately after the final 90_x pulse the sample was remagnetized and the high field signal recorded as a function of t_1. The preparation part of the sequence (through the first 45_y) has the effect of creating a density operator given by

$$\rho = \rho_{H_D} + \rho_{DQ} \qquad \text{(IV.15)}$$

which contains both a dipolar order term and a double quantum term.[26] Here the delay Δ used in the sequence was chosen to be long enough to allow any remaining single and double quantum coherences to decay to zero. Accumulation of the high field magnetization as a function of t_1 yields the interferogram of Figure IV.16. As expected the signal arising from the created dipolar order grows in sinusoidally in t_1 (in analogy to the quadrupolar case presented in Chapter III.C). Fourier transformation of the signal produces the spectrum shown in Figure IV.16.

3. Positive and Negative Magnetic Susceptibility Anisotropies

The form of the dipolar Hamiltonian in zero field was further explored by the use of samples with positive and negative magnetic susceptibility anisotropies. As stated in section A.2 of this chapter, the quantization axes of the spin systems and director orientations in

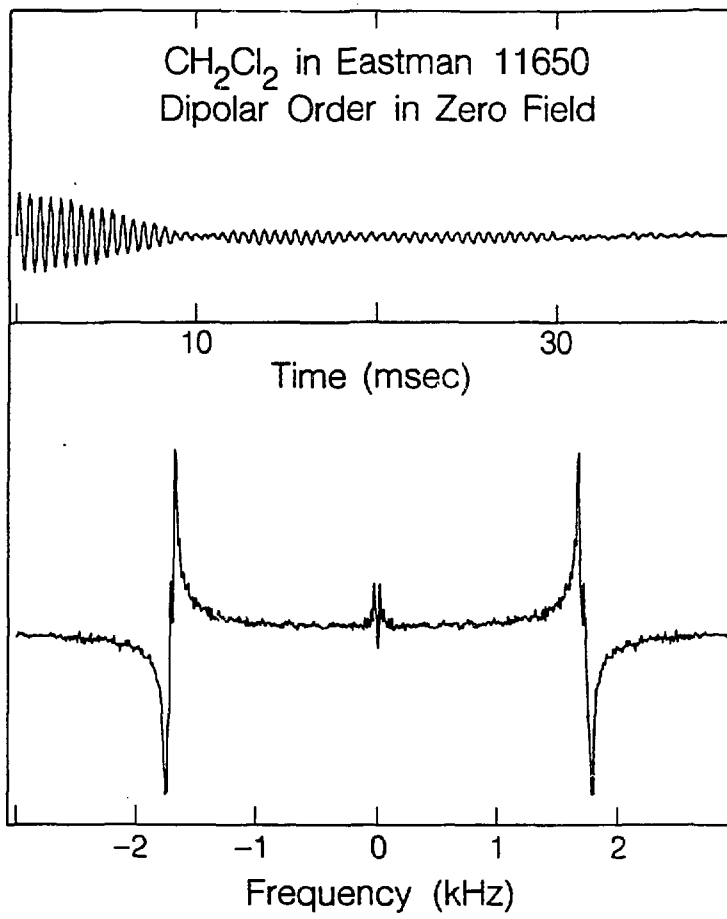
CH_2Cl_2 in Eastman 11650
Dipolar Order in Zero Field
10
30
Time (msec)
−2
−1
0
1
2
Frequency (kHz)

XBL 859-9003

Figure IV.16: Interferogram from the zero field version of the Jeener-Broekaert experiment using the pulse sequence shown in Figure IV.14c. The τ used in the preparation of dipolar order was 160 μsec and the delay δ was chosen to be 20 msec to allow for the decay of any other coherences. The sinusoidual appearance of the interferogram, $S(t_1)$, is as expected for the conversion by a 45°_{y} pulse of the dipolar order to observable single quantum coherence. Fourier transformation of the interferogram yields the dispersive zero field spectrum shown below consisting of lines centered at $\pm\nu_D$. The linewidths and splittings of the zero field lines may be attributed to dc pulse imperfections and residual fields.

high and zero fields differ with the ordering of the liquid crystalline phase. In order to observe the evolution of a spin system in zero field, the initial state of the spin system in zero field and the zero field Hamiltonian must not commute. For liquid crystals which remain aligned with the field direction, this is not the case; it was demonstrated that in such instances pulsed dc fields can be used to alter the initial condition and observe the dipolar spectrum of a solute molecule dissolved in a nematic liquid crystal. In this section, we explore the alternative possibilities of changing the zero field Hamiltonian through the use of liquid crystal systems with different magnetic susceptibilities.

The samples consisted of approximately 5 weight percent CH_2Cl_2 dissolved in EBBA (p-Ethoxybenzylidene p-butylaniline, Frinton Laboratories) with a $\Delta\chi>0$, or ZLI 1167 (EM Chemicals, a ternary mixture of propyl-, pentyl- and heptyl- bicyclohexylcarbonitriles) with a $\Delta\chi<0$. An interesting feature of these two nematics is that in binary mixtures they display an unusual temperature dependent phase behavior.[27] The apparent anisotropy in the magnetic susceptibility ranges from positive to negative with changing temperature and, at a certain transition temperature, appears to be zero.[28] High field and zero field NMR spectra of the neat phases were obtained to compare the order parameters of the solute with and without the presence of a large magnetic field. The high field dipolar spectrum of CH_2Cl_2 in EBBA appears in Figure IV.17. As with the previously discussed nematic liquid crystal sample, this system has also been found to remain aligned on the time scale of the zero field experimental field cycle and the spectrum was shown

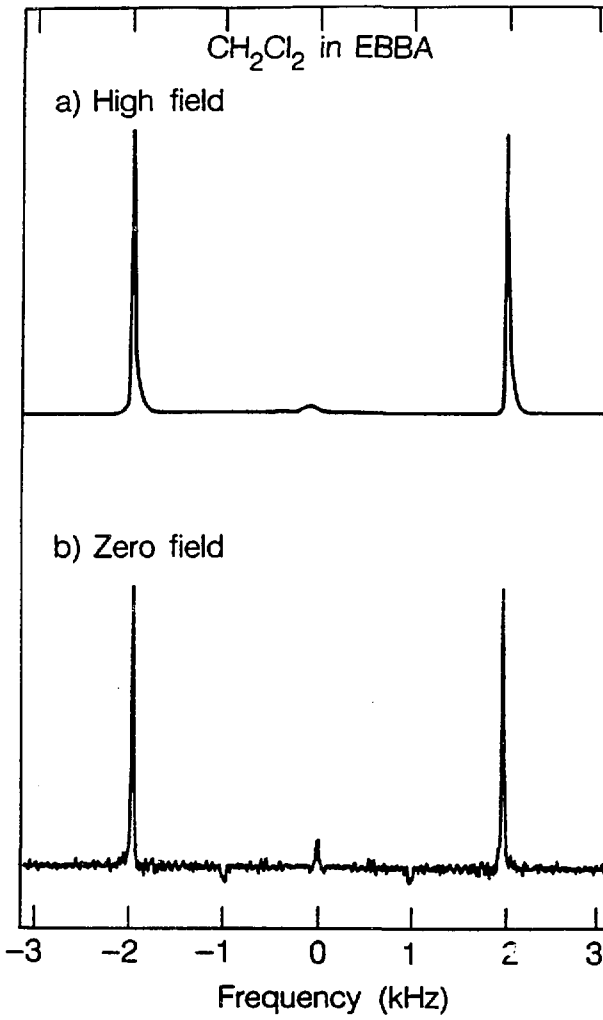

XBL 866-11154

Figure IV.17: High field and zero field spectra of 5 wgt % CH_2Cl_2 in EBBA ($\Delta\chi>0$). The high field spectrum in (a) was obtained with a 90_x-τ-90_x sequence with τ chosen to detect only the solute signal. The order parameter calculated from the observed splitting is 0.064 ± 0.001. In (b), the zero field spectrum using the field cycle of Figure IV.9b with dc pulses equal to 90 and a 180_x refocussing pulse. The order parameter measured in zero field (S_{zz} = 0.063 ± 0.001) is identical to that in high field within experimental error. The intensities and dependence of the signal on dc pulses are indicative of a sample still aligned with the original field direction.

previously in Figure IV.12. Thus in order to observe the zero field spectrum, the field cycle with 90°_{y} dc field pulses must be used to produce signal. Refocussing pulses can also be employed in the field cycles of Figure IV.9 and Figure IV.17b is the resulting zero field dipolar signal of CH_2Cl_2 in EBBA taken with a 180°_{y} echo pulse in the field cycle of Figure IV.9b. The uniaxial order parameters measured in high field (S_{zz} = 0.064 ± 0.001) and zero field (S_{zz} = 0.063 ± 0.001) are identical within experimental errors.

On the other hand, zero field evolution can be initiated by using samples with $\Delta\chi<0$ in which the axis of quantization for the nuclear spins changes on going from high to zero field. Unlike the $\Delta\chi>0$ case, no dc pulses are needed to initiate zero field evolution and the sudden transition field cycle of Figure IV.9a was used with a 180°_{z} echo pulse. The high field and zero field spectra of CH_2Cl_2 in ZLI 1167 ($\Delta\chi<0$) appear in Figure IV.18a and 18b. In this case the observed frequencies of the dipolar coupling are different in high and zero field. Due to the perpendicular alignment of the liquid crystal molecules, one would expect the zero field dipolar splittings to be twice as large as those in high field as will be discussed in the following sections.

a. Spin Hamiltonian in Zero Field. The dependence of the high or zero field NMR spectrum of a liquid crystal/solute system on field strength, the sign of $\Delta\chi$, and initial condition can easily be understood through the form of the NMR Hamiltonian. Some of the earlier discussion is repeated here. In the absence of an applied field, the liquid crystalline phase alone determines the truncation of the Hamiltonian. Only two frames of reference are needed to describe the spin inter-

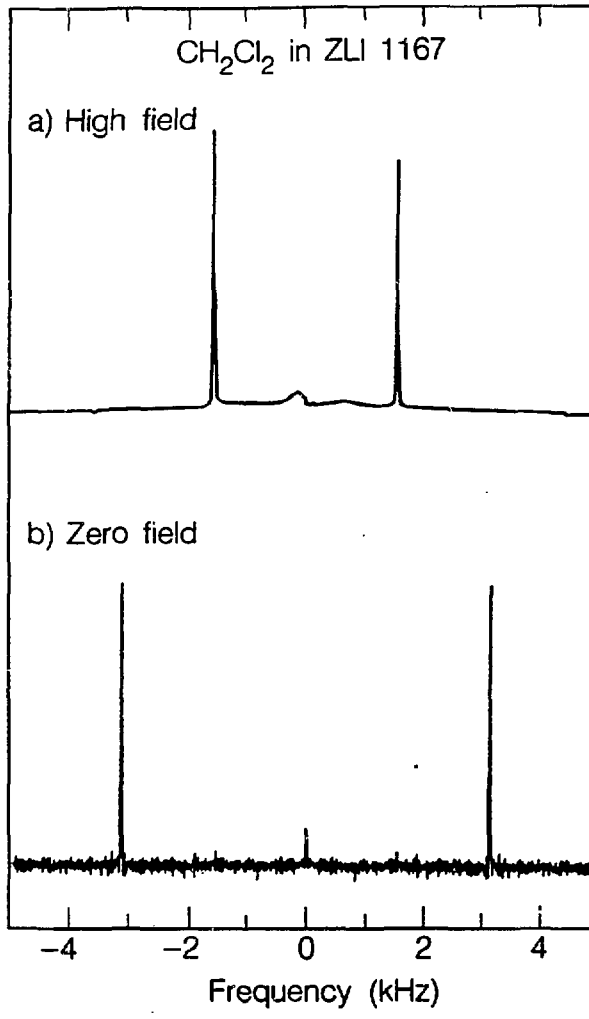

XBL 866-11161

Figure IV.18: CH_2Cl_2 (5 wgt %) in ZLI 1167 with $\Delta\chi<0$. The high field spectrum was obtained with a 90_x-τ-180_x-τ sequence with τ chosen to echo only the solute signal. The high field splitting observed in (a) is reduced by a factor of -0.5 relative to that in zero field due to the truncation of the Hamiltonian with respect to the field. The high field order parameter is calculated to be 0.100 ± 0.001. The zero field spectrum in (b) was obtained using the sudden transition field cycle of Figure IV.9a with a 180_z refocussing pulse. The order parameter is identical to that calculated in high field within experimental error with S_{zz} = 0.101 ± 0.001.

actions in zero field, the principal axis system (PAS) of the dipolar interaction and the director/zero field frame of the liquid crystal. The Hamiltonian in zero field can be written as a product of second rank spherical tensor operators as given in Equation (IV.6). Due to the axial symmetry of the two spin dipolar interaction and the uniaxial nature of either of the nematic phases, there can be no dependence on the Euler angles, γ or α, in the Hamiltonian. Therefore, with

$$D^{2}_{m'm}(\alpha\beta\gamma) = e^{-i\alpha m'} d^{2}_{m'm}(\beta)\, e^{-i\gamma m} \qquad \text{(IV.16)}$$

in Equation (IV.6) the only term which survives is that with m and m' equal to zero and the director frame Hamiltonian reduces to that given by Equations (IV.7) and (IV.8). This truncation holds regardless of the orientations of the liquid crystal molecules. That is to say, there is no dependence on the bulk alignment of the molecules as the interaction need only be considered in the local director frame. Thus for samples with $\Delta\chi>0$ or $\Delta\chi<0$ the form of the zero field Hamiltonian is identical. This similarity in zero field is apparent for CH_2Cl_2 in EBBA and ZLI 1167; the spectral splittings differ due to different order parameters, S_{zz}, but the general appearance of the spectra is the same.

Although the zero field Hamiltonians have the same form for the two phases, it may not yet be evident why dc pulses are required in the case with $\Delta\chi>0$ to initiate evolution in zero field, but not when $\Delta\chi<0$. Using any of the field cycles described thus far, the initial condition prepared in high field is proportional to $I_{z,L}$, and if this commutes with the zero field Hamiltonian evolution does not occur with the sudden transition in field as described previously. For example, if the sample

in zero field remains aligned along the original field direction, then the zero field Hamiltonian truncated with respect to the director axis has the same quantization axis as in high field and commutes with I_z. Applying a 90^o dc pulse to initiate evolution, the normalized signal as a function of t_1 is calculated according to Equations (IV.10)-(IV.12):

$$S(t_1) = Tr\{I_x \exp(-iH_D t_1) I_x \exp(iH_D t_1)\} = \cos(\tfrac{3}{2} S_{zz} \omega_D t_1) \qquad \text{(IV.17)}$$

where $\omega_D = \gamma^2 h/2\pi r^3$. This calculation does not take into account an echo pulse or residual field which can easily be incorporated as in Equation (IV.14).

When $\Delta\chi<0$ the form of the zero field Hamiltonian is truncated identically with respect to the director frame, but if the liquid crystal sample remains aligned perpendicular to the field direction, the zero field and high field frames are no longer coincident. The magnetization now precesses about the local dipolar fields in zero field after the sudden transition in field. This can be pictured as if the liquid crystal (or the averaged local field) is shifted by 90^o as a consequence of the phase rather than the magnetization by a pulsed field. In order to calculate the zero field spectrum, a transformation between the laboratory frame of the initial condition and zero field/local director frame must now be included. The normalized signal as a function of t_1 becomes identical to Equation (IV.17),

$$\begin{aligned} S(t_1) &= Tr\{RI_{z,L}R^{-1} \exp(-iH_D t_1) RI_{z,L}R^{-1} \exp(iH_D t_1)\} \\ &= \cos(\tfrac{3}{2} S_{zz} \omega_D t_1) \end{aligned} \qquad \text{(IV.18)}$$

where $R = \exp(-i\phi I_z)\exp(-i\theta I_y)$ and $\theta=90^o$ for the fixed relative

orientation of **n** and the laboratory z axis for $\Delta\chi<0$. It is clear that there is no ϕ dependence in the signal function due to the overall symmetry of the phase around z. Thus the transformation by $R(\Omega)$ with $\theta=90^{o}$ produces an initial condition, expressed in the director frame, having the form of I_x. In both cases represented in Equations (IV.17) and (IV.18), all the magnetization evolves if the alignment is uniform over the sample. The intensities in the zero field spectrum, and the dependence on the field cycle used, are again indicative of the bulk alignment of the sample.

b. Spin Hamiltonian in High Field. In a similar manner, the relative scaling factors of the high field spectra may be understood by describing the Hamiltonian in high field. The Hamiltonian can again be represented by Equation (IV.6) although now an additional transformation from the director frame to the laboratory/field frame is required and can be written as

$$H_D = \sum_{m,m',n}^{2} (-1)^m T_{2-m} A_{2n} D^2_{nm'}(\psi\theta\phi) \langle D^2_{m'm}(\alpha\beta\gamma)\rangle \qquad \text{(IV.19)}$$

where the $D^2_{nm}(\psi\theta\phi)$ term relates the director and lab frames. This angular term is not averaged over molecular motions since the fluctuations of the director with respect to the field direction are slow on the timescale of the experiment.[1,9] Since the liquid crystal and laboratory/field frames are uniaxial, only the angle θ is needed to make the transformation and $D_{00}(\theta)=1/2(3\cos^2\theta-1)$. For $\Delta\chi<0$, $\theta=90^{o}$ and the $D^2_{00}(\theta)$ term in Equation (IV.19) equals -1/2, while for $\Delta\chi>0$ the angle is zero and this term is equal to 1. The high field spectra are

then scaled by these factors of 1 or -1/2, in addition to S_{zz}, as is apparent in Figures IV.17 and IV.18, respectively. The order parameters for the $\Delta\chi<0$ case can be calculated to be $S_{zz} = 0.100 \pm 0.001$ and $S_{zz} = 0.101 \pm 0.001$ in high and zero field, respectively.

4. Summary

The molecular order parameters of nematic liquid crystal/solute mixtures have been measured in high and zero field and have been found to be the same in both cases. The resulting values do not differ by more than an experimental error which is less than a few percent. Several conclusions can be reached based on the frequencies and intensities of the zero field spectra, and the apparent dependence of the signal on the dc pulses used. Due to the short duration and relatively low fields used for the dc magnetic field pulses, only the spin states are perturbed and not the spatial ordering of the liquid crystal molecules. Experimental evidence suggests that fields of the order of 1 kG need be applied to change the alignment of the molecules in a time on the order of seconds.[9,29] Most notably, the nematic systems were not seen to disorder in low ($\lesssim$200 G) or zero fields when left in these fields for times on the order of 10-500 msec. For those samples studied, the zero field spectra are indicative of aligned systems showing no change from high field. Nematic liquid crystals may be expected to remain aligned in zero field on relatively long timescales, as thermal fluctuations would be slow in bringing about disordering[9,10], unless some perturbation such as the application of an appropriate large field causes more rapid reorientation of the sample.

It might be interesting to look for changes in the ordering of chiral phases in zero field which are "untwisted" by an applied field and steric forces cause it to retwist.[30] An attempt was made to look at cholesteric samples for which it was found that the T_1 was too short. The relaxation time is related to diffusion through the helix which is an effective relaxation mechanism.[31]

For systems with $\Delta\chi>0$, the ordering of the sample remains along the original field direction and dc pulses are necessary to produce dipolar signal in zero field. Since the alignment of the liquid crystal molecules with $\Delta\chi<0$ is perpendicular to the laboratory z axis, signal results with the sudden transition in intermediate field. High resolution spectra may be obtained with refocussing pulses and allow for more accurate determination of the order parameters. In mixtures of liquid crystal solvents with $\Delta\chi<0$ and $\Delta\chi>0$, in concentrations and at temperatures close to their phase transition region[27,28], preliminary results indicate that although these samples are very sensitive to these experimental limits, even removal of the field does not cause a change in the aligned state.

In general, demagnetization experiments on nonoriented samples are expected to produce initial conditions other than $I_{z,L}$. However, due to the unchanged ordering and molecular motions of the CH_2Cl_2/nematic systems ($\Delta\chi>0$) in the demagnetization experiment, the magnetization remains quantized along the laboratory z axis. Thus demagnetization experiments on the nematic systems produce an initial condition no different than that in experiments utilizing an intermediate field to maintain the spin order. DC pulses along various directions of the

laboratory frame may then be successfully used to produce a new spin order. Examples of such have already been shown in the composite pulse experiments and the isotope selective pulses in Sections III.A and D.

Extensions of these zero field experiments are easily envisioned to more complex systems such as smectics, discotics[32a] and lyotropics[32b] which do not order uniformly in an applied field. High field studies of such materials are hindered due to orientational disorder and thus might be productively studied in zero field. Examples incorporating the first class of materials are presented in the following section.

C. Smectic Phases in Zero Field Experiments

1. Introduction

Nematic/solute systems have been extensively studied by high field NMR techniques.[2,7,8] The alignment of the sample has a profound effect on the NMR spectra of these materials since all molecules have an equivalent average orientation with respect to the applied field. Admittedly, nematic phases are conveniently studied by such methods as the molecular motions and large fields truncate the dipolar Hamiltonian to produce discrete, narrow lines. Even in the absence of a large magnetic field, the spatial averaging in the liquid crystal retains the truncated form of the Hamiltonian. Lower temperature smectic and cholesteric phases, as well as most lyotropic liquid crystalline phases, do not possess the property of uniform alignment in a magnetic field.[3] Thus in the high field NMR spectra of such systems one find inhomogeneously broadened lines due to the random distribution of molecular

orientations with respect to the applied field. The usefulness of the zero field NMR experiment lies in the ability to obtain sharp well-resolved spectra on such disordered materials.

Smectic phases often show a complex and diverse arrangement of the molecules as discussed in Section IV.A. Some phases are uniaxial and are describable by a single order parameter while others are biaxial and require more order parameters. Biaxiality is generally attributed to the type of molecular ordering and to a partial rotational freeze-out of the molecular motions which can be observed through the angular dependence of the spectrum of an aligned sample.[9,33] The biaxial order parameters can be related to a motionally induced asymmetry in the spin interactions.[34] Biaxial smectics (primarily smectic C phases) have been studied in several cases, either optically[35], by NQR[36] or by NMR[37] methods. The latter requires oriented samples produced by sample rotation[38], ac electric fields[39] or attempting to uniformly align the phase through cooling down the sample from a higher temperature phase in the presence of a field.[40,41] Once an aligned sample is produced then, like a single crystal, it must be studied as a function of many different orientations with respect to the applied field. In most cases, the biaxiality is often a subtle effect and its observation has often been in dispute or is difficult in unaligned samples.[9,37] In this section, the high field and zero field NMR spectra of several smectic phases are presented.

2. High Field and Zero Field Spectra

The smectic phases studied were room temperature A, B and E phases

as described Section IV.A. The smectic A phase was produced using ~2 wgt % CH_2Cl_2 in 8CB (octylcyanobiphenyl, EM Chemicals). In this phase the molecules align perpendicular to the layer normal and are free to rotate about their long axes. As shown in Figure IV.3, there is no positional order to the molecules in the layer, and they diffuse rapidly throughout the layer (more rapidly than in B or E phases).[1] The smectic A sample was found to spontaneously align in an applied field. The smectic A case, due to the sample alignment, is indistinguishable from that of a nematic phase and calculation of the signal follows identically as before. Thus the high field spectrum, as shown in Figure IV.19a, consists of the doublet characteristic of a dipolar coupled pair of spins scaled by the uniaxial order parameter. In zero field using a field cycle such as Figure IV.9b with 90°_x dc pulses and a 180°_x echo pulse, the zero field spectrum of Figure IV.19b results. The order parameters for the aligned, uniaxial phase in high field and zero field are 0.077 ± 0.002 and 0.074 ± 0.001, respectively.

The molecules are arranged in more complicated intralayer structures in the B and E phases as shown in Figure IV.3. The smectic B phase has a rotational freedom of the molecules although they are arranged in a hexagonal pattern. Since in this particular B phase the molecules align parallel to the layer normal, the phase is uniaxial. In contrast, the smectic E phase has restricted rotational freedom of the molecules about the long molecular axis which is expected to lead to a biaxiality of the phase. The room temperature smectic B and E phases consist of mixtures of the same two components: 4-n-butyloxybenzylidene-4'-n-octylaniline (40.8) and 4-n-octyloxycyanobiphenyl (8OCB).

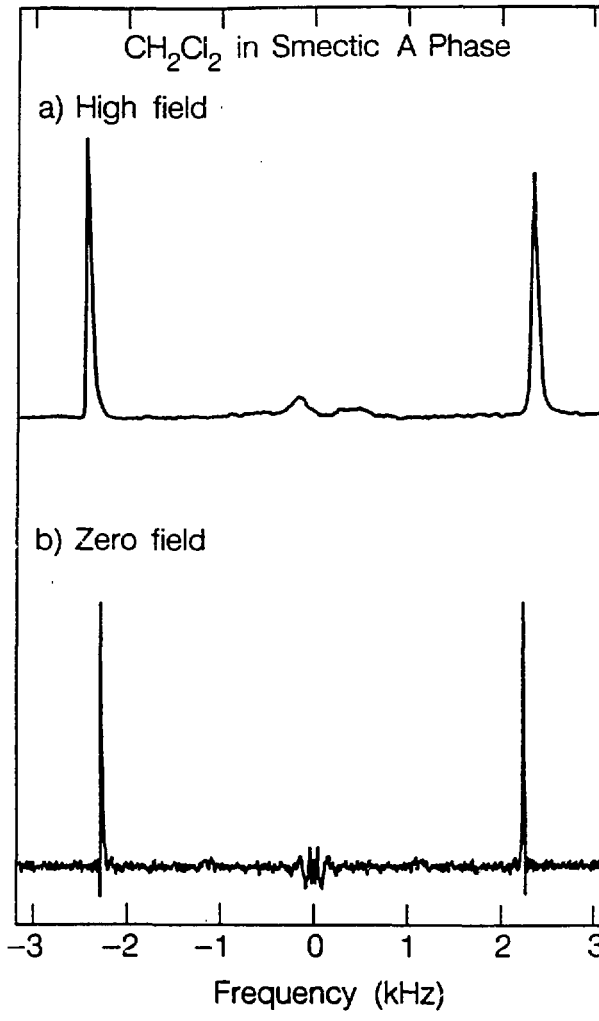

XBL 866-11162

Figure IV.19: CH_2Cl_2 (~2 wgt %) in 8CB Smectic A phase. (a) The high field spectrum was obtained with the standard echo. The order parameter was calculated to be $S_{zz} = 0.077 \pm 0.002$. The zero field spectrum in (b) was obtained using the field cycle with 90° dc pulses of Figure IV.9b and a 180_y echo pulse. The order parameter measured in zero field is $S_{zz} = 0.074 \pm 0.001$. Both high and zero field spectra are indicative of an aligned sample (indistinguishable from the aligned nematics).

The smectic B phase consists of ~5 wgt % CH_2Cl_2 in 60% 40.8 and 40% 8OCB mixture by weight. The smectic E phase consists of ~7 wgt % CH_2Cl_2 in a 50:50 mixture. The phase diagram of mixtures of these components can be found elsewhere[42]; as an example, the neat 50:50 mixture has the following phase transition temperatures

$$K \xrightarrow{15^{o}} S_E \xrightarrow{52.9^{o}} S_B \xrightarrow{83^{o}} S_A \xrightarrow{104^{o}} S_A + I \xrightarrow{107.5^{o}} I$$

Neither of these phases aligns in a magnetic field unless heated to the isotropic or nematic phase and cooled in the presence of a field. Since the zero field experiment does not require an aligned sample, the unaligned multidomain samples were used. The transition between B and E phases can also be accomplished with a change in temperature for a given sample mixture as seen above. The change in lattice structure, E being a compressed version of B, and the n-fold versus 2-fold rotation are indicative of a thermally activated motional process[40b]. The mechanisms leading to the biaxiality are just beginning to be understood with their study becoming of interest in the last 10-15 years.

Because the smectic B and E samples are not aligned in the field, a distribution of director orientations results. This produces a high field powder spectrum which is broadened by the frequency dependence on the orientational distribution. The smectic B case is described first since it is conceptually easier. Since the phase is uniaxial, the Hamiltonian in the director frame for the two spin solute system is equal to that of Equation (IV.7) since the phase is uniaxial

$$H^{dir} = T_{20}A_{20}D^2_{00}(0\beta 0) \qquad (IV.20)$$

The director frames and laboratory/field frame are no longer coincident, as for an aligned sample, and a second transformation to the laboratory frame must be included to give

$$H^{lab} = \sum A_{20}T_{2n}\langle D^2_{00}(\beta)\rangle D^2_{n0}(\psi\theta\phi) \qquad (IV.21)$$

Only the T_{20} term remains in high field and with no ϕ or ψ dependence Equation (IV.21) becomes

$$H^{lab} = A_{20}T_{20}\langle D^2_{00}(\beta)\rangle D^2_{00}(\theta) = A_{20}T_{20}S_{zz}1/2(3\cos^2\theta-1) \qquad (IV.22)$$

which represents the angular distribution in θ of the randomly oriented directors. The high field spectrum is shown in Figure IV.20a and consists of the typical powder pattern scaled by the uniaxial order parameter, S_{zz}, which can be calculated from the separation of the singularities. Since this phase is not aligned it behaves like a polycrystalline powder and dc pulses are not required to initiate evolution in zero field. Thus using the field cycle of Figure IV.9a, the predicted three line spectrum corresponding the the axially symmetric dipolar coupling of the two protons results and is shown in Figure IV.21. The linewidths are not a function of the phase but rather the effects of residual fields as is discussed in Chapter V. From the separation of the lines, the order parameter can be calculated. High field and zero field values are 0.041 ± 0.002 and 0.042 ± 0.002, respectively.

The high field powder spectrum of the smectic E phase in Figure IV.21a shows a broadened lineshape that can be attributed to the

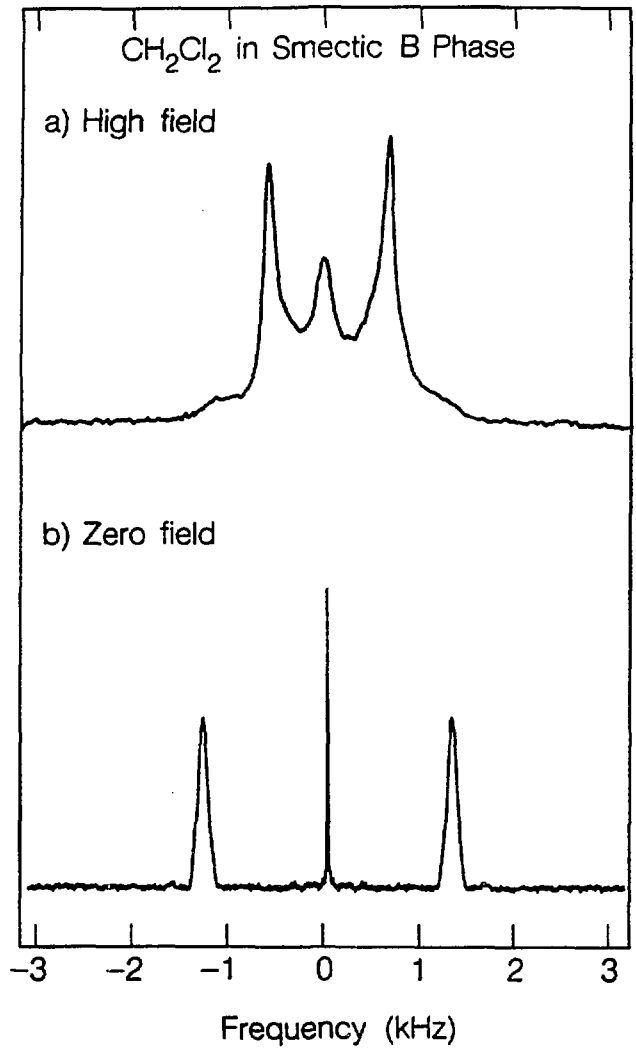

XBL 866-11153

Figure IV.20: High field and zero field spectra of CH_2Cl_2 (~5 wgt %) in an unaligned Smectic B phase. The high field spectrum of the solute (a) shows a powder spectrum scaled by the uniaxial order parameter, S_{zz} = 0.041 ± 0.002, as calculated from the separation of the singularities. The signal in the center of the spectrum is most likely liquid crystal which was not completely removed by the echo. The zero field spectrum in (b), taken with the sudden transition field cycle of Figure IV.9a (with no echo pulse), shows the expected three line spectrum of two dipolar coupled protons of an unaligned sample. The calculated order parameter is S_{zz} = 0.042 ± 0.002. The linewidths are due to residual field effects and are not a property of the phase.

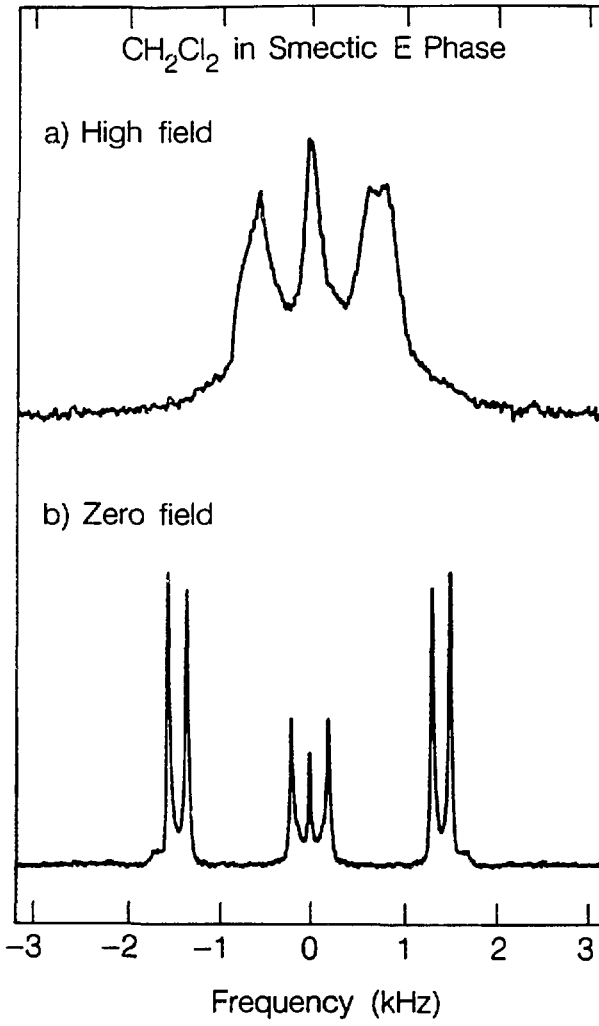

XBL 866-11152

Figure IV.21: High field and zero field spectra of CH_2Cl_2 (~5-10 wgt %) in an unaligned Smectic E phase. The high field spectrum (a) shows a broadened lineshape characteristic of a nonaxially symmetric coupling. Poor resolution makes determination of the singularities, necessary to calculate the value of η and ω_D, difficult. In (b), the zero field spectrum shows six well-resolved narrow lines due to the nonaxial symmetry of the dipolar coupling. The asymmetry induced by the biaxiality of the phase can be calculated from the spectrum.

asymmetry of the dipolar coupling induced by the biaxial phase. This is not unlike what has been seen before for the quadrupolar spectrum in a similar phase[40a]. If features of the lineshape are well enough resolved to determine their frequencies, the value of η and $S_{zz}\omega_D$ can be calculated in a manner similar to that of a spin I=1 system.[9,40a] This is often difficult in the powder spectrum, especially when η is small. The zero field spectrum is quite sensitive to the perturbations and small induced asymmetries due to the narrow lines. As shown in Figure IV.21b, an additional splitting of ~200 Hz which yields a pattern of six lines (and one at zero frequency due to residual field effects) is directly attributable to the nonaxial symmetry in the dipolar tensor. The relationship between the phase biaxiality, the asymmetry parameter and the biaxial order parameters is shown in the following calculation.

3. Expressions for the Hamiltonian

Three frames of reference, shown in Figure IV.22, are defined: the axially symmetric PAS/solute molecular frame of the dipolar interaction (z' axis is designated), the director frame (x,y,z) which describes the alignment of the liquid crystal molecules with respect to the layer normal, and the domain frame with its Z axis coincident with the layer normal and its x axis rotated by an angle of $\pm\phi$ with respect to the symmetry axis in the smectic plane. The Hamiltonian can be written in the domain frame for the second rank dipolar interaction as

$$H_D^{dom} = \sum_{m=-2}^{2}(-1)^m T_{2-m} \sum_{m'n} \sum A_{2n} \langle D^2_{m',n}(\alpha\beta\gamma) D^2_{mm'}(\phi\theta\psi) \rangle \qquad \text{(IV.23)}$$

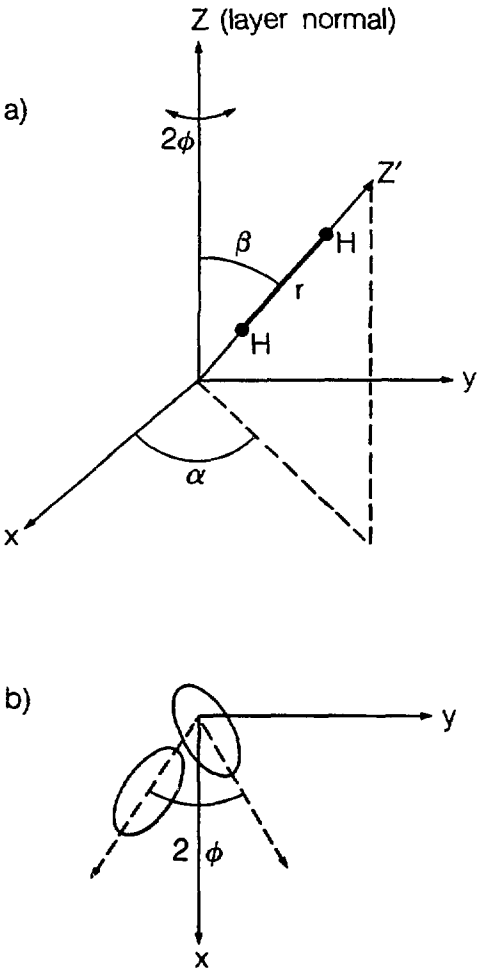

XBL 866-11159

Figure IV.22: Relationships between reference frames used in describing the Smectic E phase. (a) The z' axis of the molecular/PAS frame of the dipolar coupling (H-H internuclear vector) is related to the (xyz) frame of the liquid crystal order director by the angles α and β. The angle γ is not required due to the axial symmetry of the coupling in the PAS. The domain frame has its Z axis (layer normal) parallel to the z axis of the director frame. The molecules, as shown in cross section through the plane in (b), are aligned at an angle ϕ with respect to the symmetry axis of the liquid crystal.

where $D_{m',n}(\alpha\beta\gamma)$ transforms between the molecular frame and director frame, and $D_{mm'}(\phi\theta\psi)$ between the domain and director frames. In the PAS frame only the A_{20} spatial term is nonzero, thus n=0 and summing over m yields the nonzero terms

$$H_D^{dom} = T_{22}A_{20}\sum_{m'} \langle D^2_{m',0}(\alpha\beta 0)D^2_{-2m'}(\phi\theta 0)\rangle + T_{20}A_{20}\sum_{m'} \langle D^2_{m',0}(\alpha\beta 0)D^2_{0m'}(\phi\theta 0)\rangle + T_{2-2}A_{20}\sum_{m'} \langle D^2_{m',0}(\alpha\beta 0)D^2_{2m'}(\phi\theta 0)\rangle \quad \text{(IV.24)}$$

Substituting in for the second rank tensor operators for the spin and spatial terms[18] gives

$$H_D^{dom} = \frac{-\gamma^2 h}{2\pi r^3}\left[(3I_{z1}I_{z2} - \mathbf{I}_1\cdot\mathbf{I}_2)\sum_{m'} \langle D^2_{m',0}(\alpha\beta 0)D^2_{0m'}(\phi\theta 0)\rangle \right. \quad \text{(IV.25)}$$

$$\left. + \sqrt{\frac{3}{2}}(I_{x1}I_{x2} - I_{y1}I_{y2})\sum_{m'} \langle D^2_{m',0}(\alpha\beta 0)D^2_{2m'}(\phi\theta 0)\rangle + \langle D^2_{m',0}(\alpha\beta 0)D^2_{-2m'}(\phi\theta 0)\rangle\right]$$

Using Doane's notation[9], the expression simplifies to

$$H_D = \frac{-\gamma^2 h}{2\pi r^3}\langle S_{20}\rangle\left[(3I_{z1}I_{z2} - \mathbf{I}_1\cdot\mathbf{I}_2) + \sqrt{\frac{3}{2}}\frac{\langle S_{2-2} + S_{22}\rangle}{\langle S_{20}\rangle}(I_{x1}I_{x2} - I_{y1}I_{y2})\right]$$

$$= \frac{-\gamma^2 h}{2\pi r^3}\langle S_{20}\rangle\left[(3I_{z1}I_{z2} - \mathbf{I}_1\cdot\mathbf{I}_2) + \eta(I_{x1}I_{x2} - I_{y1}I_{y2})\right] \quad \text{(IV.26)}$$

where the terms contained in η are the biaxial order paramters and $\langle S_{20}\rangle$ is the uniaxial order parameter which scales $\omega_D = \gamma^2 h/2\pi r^3$.

The S parameters can be dealt with separately in order to express them in terms of the angles relating the different frames. Much of the following discussion can be found in Doane's review article for the spin I=1 case.[9,34] The simpler $\langle S_{20} \rangle$ term is

$$\langle S_{20} \rangle = \sum_{m'} \langle D^2_{m',0}(\alpha\beta\gamma) D^2_{0m'}(\phi\theta\psi) \rangle \qquad \text{(IV.27)}$$

At this stage there are theoretically as many as five elements with the summation over m'. Because there is a two fold symmetry axis perpendicular to the layer normal[6]

$$D^L_{mn} = (-1)^L D^L_{m-n} = (-1)^{m-n} D^L_{-m-n} \qquad \text{(IV.28)}$$

and summing over m' results in the following nonzero terms

$$\begin{aligned} \langle S_{20} \rangle &= \langle D^2_{00}(\beta) D^2_{00}(\theta) + (D^2_{-20}(\alpha\beta) + D^2_{20}(\alpha\beta)) D_{02}(\phi\theta) \rangle \\ &= \langle \tfrac{1}{2}(3\cos^2\beta - 1)\tfrac{1}{2}(3\cos^2\theta - 1) + \tfrac{3}{4}(\sin^2\beta\cos 2\alpha)(\sin^2\theta\cos 2\phi) \rangle \qquad \text{(IV.29)} \\ &= \langle S_{zz}\tfrac{1}{2}(3\cos^2\theta - 1) + (S_{xx} - S_{yy})(\tfrac{1}{2}\sin^2\theta\cos 2\phi) \rangle \end{aligned}$$

Because S_{xx}-S_{yy} is generally much less than S_{zz}, more so for a rod-like molecules, the last term can be dropped. This term describes the molecular biaxiality[9,34], i.e. fluctuations of the liquid crystal molecule about unequal molecular axes, rather than the phase biaxiality. The director, describing the alignment of the liquid crystal molecules long axes, is assumed to be along the z axis of the domain as the molecules align to a very high degree with respect to the layer normal[9], thus θ=0 for the phase and $\langle S_{20} \rangle = \langle S_{zz} \rangle$.

The $\langle S_{2-2} + S_{22} \rangle$ term can be dealt with similarly. The brackets represent an average over the molecular motions. The motions of the molecular frame with respect to the director frame ($\alpha\beta\gamma$) are assumed to be independent of the diffusion or jumps between positions in the domain which results in the biaxiality of the phase.[9,41] Asssuming that these are independent allows one to factor the terms to give

$$\langle S_{2-2} + S_{22} \rangle = \sum_{m'} \langle D^2_{m',0}(\alpha\beta 0) \rangle \langle D^2_{2m}(\phi 00) + D^2_{-2m'}(\phi 00) \rangle \qquad \text{(IV.30)}$$

The summation and substitution for the D_{1m} terms will not be shown in detail but results in nine real terms. This number can be reduced to five by considering liquid crystal phases which are apolar (i.e. the molecules can be exchanged end for end) and, as mentioned previously, there is a two fold axis perpendicular to the layer normal. The expression for η, containing the five terms of the $\langle S_{2-2} + S_{22} \rangle$ summation, can be related to the spin I=1 expression solved for by Doane[9] which for $\theta=0$ becomes

$$\eta = \frac{3\langle \sin^2\beta\cos 2\alpha \rangle \langle \cos 2\phi \rangle}{2\langle S_{20} \rangle} = \frac{3\langle \sin^2\beta\cos 2\alpha \rangle \langle \cos 2\phi \rangle}{\langle 3\cos^2\beta - 1 \rangle} \qquad \text{(IV.31)}$$

The Hamiltonian of Equation (IV.26) has energies corresponding to

$$\begin{aligned} E_1 &= -\frac{\omega_D S_{zz}}{2}(1+\eta) \\ E_2 &= -\frac{\omega_D S_{zz}}{2}(1-\eta) \\ E_3 &= \omega_D S_{zz} \end{aligned} \qquad \text{(IV.32a)}$$

for the eigenstates

$$|1\rangle = 2^{-1/2}(|\alpha\alpha\rangle + |\beta\beta\rangle)$$
$$|2\rangle = -i2^{-1/2}(|\alpha\alpha\rangle - |\beta\beta\rangle) \qquad \text{(IV.32b)}$$
$$|3\rangle = 2^{-1/2}(|\alpha\beta\rangle + |\beta\alpha\rangle)$$

expressed in the zero field eigenbasis for two dipolar coupled spin I=1/2 nuclei. The zero field signal can be calculated from

$$S_{\Omega}(t_1) = Tr\{RI_zR^{-1}\exp(-iH_Dt_1)RI_zR^{-1}\exp(iH_Dt_1)\} \qquad \text{(IV.33)}$$

where H_D is given by Equation (IV.26). Averaging over all orientations yields for the normalized signal

$$S(t_1) = \tfrac{1}{3}\{\cos(\omega_D S_{zz}\eta t_1) + \cos(\tfrac{1}{2}\omega_D S_{zz}(3-\eta)t_1) + \cos(\tfrac{1}{2}\omega_D S_{zz}(3+\eta)t_1) \qquad \text{(IV.34)}$$

In the limit of $\eta=0$, Equations (IV.26)-(IV.29) above reduce to that of the axially symmetric Smectic B case. The spectrum in Figure IV.21 appears as predicted and thus from the frequencies of the lines values of $S_{zz} = 0.045 \pm 0.001$ and $\eta = 0.208 \pm 0.001$ can be calculated. The peak seen at zero frequency is due to residual field effects explained in Chapter V.

Unfortunately, due to the dependence of η on several angular factors as given in Equation (IV.31), the problem is underdetermined by the single measurement. When $\theta=0$ in a well ordered phase, the $\langle\cos 2\phi\rangle$ term is nonzero for partially restricted rotation about the long molecular axis. This term is representative of a birotational freeze out of the rotation in a two fold potential.[33,34] The phase biaxiality is related to the fact that an axis, within the layer plane, must be

associated with the phase to describe the molecular ordering. This axis is not defined in a uniaxial phase. Due to the symmetry of the frames chosen here only the angle ϕ is required. Doane has also studied this same phase mixture using ^2H NMR experiments on oriented samples.[41] Several models are presented for the restricted motion of the liquid crystal molecules. The most likely models are those involving molecular jumps or diffusion between four positions with relative orientations ϕ, $\phi+\pi$, $-\phi$ and $-\phi+\pi$ where $\phi=22\pm0.5^{\circ}$ or on site librations with an amplitude of 2ϕ. Both motions were combined with π-flips of the liquid crystal molecules about the C_2 axis through the aromatic ring to account for the averaging seen in the quadrupolar case. The jump mechanism is feasible based on diffusion measurements[43] and the value of 22° is reasonable based on X-ray data.[44] Since S_{zz} of the ordering of the solute PAS frame is known and with $\phi=22^{\circ}$, the $\langle \sin^2\beta\cos 2\alpha \rangle$ term can be solved for from the value of η. The calculated value is found to be 0.0043, and as expected is small since it represents the molecular fluctuations about axes other then that described by S_{zz}.

4. Summary

The smectic phases discussed here were chosen to represent several aspects of the study of such phases where the differences between aligned and unaligned, and uniaxial and biaxial samples were shown. In those cases in which there is rapid n-fold rotation about the liquid crystal long molecular axis, no component perpendicular to the rotation axis is expected to survive and thus η must equal zero. The order parameter of the liquid crystal molecules is then a measure of the

degree of molecular alignment and the fluctuations of the long molecular axis. In fact, most smectic phases are biaxial due either to a molecular biaxiality which reflects the fluctuations about the short axes of the molecules, or a phase biaxiality in which there is hindered rotation of the molecules. Biaxiality has been observed directly in only a few cases through the induced asymmetry in a ^{14}N NQR spectrum or through aligned samples. In the zero field spectrum, the non-axial symmetry is readily and clearly observed.

D. Heteronuclear Spin Systems in Liquid Crystals

Heteronuclear spin systems in solids have previously been studied by zero field NMR. Inequivalent nuclear spins behave identically to homonuclear spins except that they can be manipulated independently in high and zero fields, and additional zero field transitions become allowed. In combination with liquid crystal solvents, these spin interactions can be observed in a variety of anisotropic media which often yields interesting effects in the appearance of the zero field NMR spectra. This section presents the simplest case of an I-S ($I=^{1}H$, $S=^{13}C$) spin pair in nematic and smectic liquid crystalline phases.

In order to produce dipolar signal in an aligned nematic with $\Delta\chi>0$, dc field pulses are required. This can be attributed to the symmetry of the homonuclear dipolar Hamiltonian in zero field and the initial state of magnetization prepared in high field (i.e. they commute). An alternative approach involved using nematic phases with $\Delta\chi<0$. Here the behavior of a third situation, involving heteronuclear

spin systems, is presented.

1. High Field and Zero Field Hamiltonians

A comparison of the high field and zero field Hamiltonian will begin the discussion since the differences are of the more interesting aspects of studying heteronuclear spin systems in zero field. For a ^{13}C-^{1}H pair, the high field NMR Hamiltonian in a uniaxial phase may be written as

$$H^{o}_{HF} = -\omega_I I_z - \omega_S S_z - \frac{\gamma_I \gamma_S h S_{zz}}{4\pi r^3}(2I_z S_z)(3\cos^2\theta - 1) - J I_z S_z \quad \text{(IV.35)}$$

where $S_{zz}=1/2\langle 3\cos^2\beta-1\rangle$ is the order parameter of the I-S internuclear vector relative to the liquid crystal director and scales only the anisotropic dipolar interaction. Note that the high field Hamiltonian contains only the secular terms of the dipolar and indirect couplings. The high field proton spectra of $^{13}CHCl_3$ in aligned nematic phases appear in Figure IV.23 showing the doublet patterns for which the peak separations are given by

$$\Delta\omega = 2S_{zz}\omega_D + J \qquad \text{for } \Delta\chi>0 \text{ and } \theta=0^{o}$$

$$\Delta\omega = S_{zz}\omega_D - J \qquad \text{for } \Delta\chi<0 \text{ and } \theta=90^{o}$$

where $\omega_D=\gamma_I\gamma_S h/2\pi r^3$. One can see how liquid crystals with differing magnetic susceptibility anisotropies can be used to differentiate between the contributions of J and ω_D in the spectra. Using a value of 210 Hz for J[45] and r=1.073 Å[46], the order parameters for the $\Delta\chi>0$ and $\Delta\chi<0$ cases are 0.115 ± 0.001 and 0.082 ± 0.001, respectively.

Heteronuclear spin systems in zero field have previously been discussed in Chapter II.C. In the high temperature limit, the

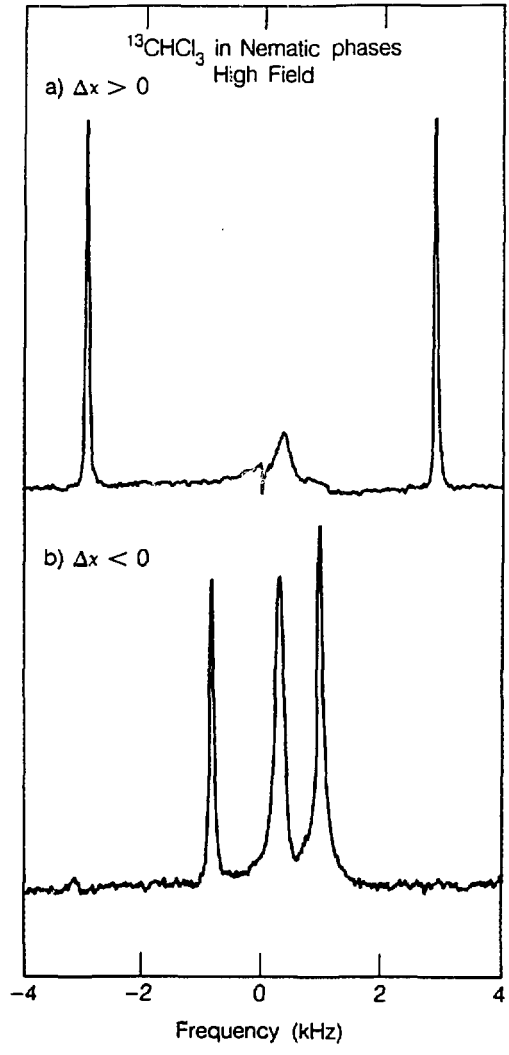

XBL 8611-9274

Figure IV.23: High field ^{1}H spectra of $^{13}CHCl_3$ in nematic liquid crystal phases. (a) $^{13}CHCl_3$ in EBBA ($\Delta\chi>0$) shows the predicted doublet pattern for a two spin system from which an order parameter of S_{zz} = 0.115 ± 0.001 is calculated. (b) $^{13}CHCl_3$ in ZLI 1167 ($\Delta\chi<0$) shows a doublet scaled by -0.5 in addition to the order parameters S_{zz} = 0.082 ± 0.001. The signal at the center of the doublet is most probably due to residual liquid crystal signal.

equilibrium initial condition produced in high field can be written as the reduced density matrix

$$\rho(0) \propto aI_{z,L} + bS_{z,L} \tag{IV.36}$$

in which the coefficients a and b represent the relative polarizations of I and S spins. As there are no Zeeman energy differences in zero field, the I and S spins are identical with respect to exchange and additional terms in the Hamiltonian become energy conserving. For the general case in zero field, the Hamiltonian is then written in the director frame as

$$H_{ZF} = -\frac{\gamma_I \gamma_S h S_{zz}}{2\pi r^3}(3I_zS_z - \mathbf{I}\cdot\mathbf{S} + \eta(I_xS_x - I_yS_y)) - J(I_zS_z + I_yS_y + I_xS_x) \tag{IV.37}$$

and follows from the same description presented previously for the homonuclear cases. The full J coupling, except anisotropic terms,[8] and dipolar coupling, including any possible asymmetry term (see Section IV.C), are now included. Truncation of the Hamiltonian by the liquid crystalline environment retains the same terms as for the homonuclear case. The energy levels and allowed transitions are illustrated in Figure IV.24, where

$$E_1 = -\frac{S_{zz}\omega_D}{2}(1+\eta) - \frac{J}{4}$$
$$E_2 = -\frac{S_{zz}\omega_D}{2}(1-\eta) - \frac{J}{4} \tag{IV.38a}$$

I-S Spin Pair, $\eta \neq 0$

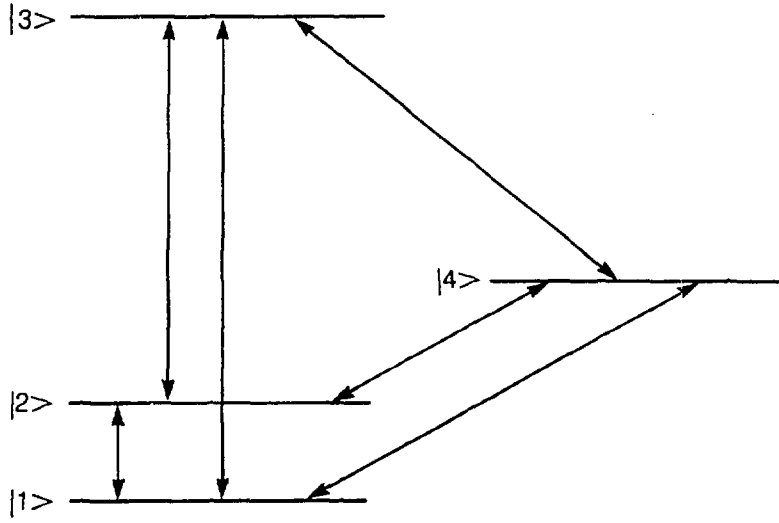

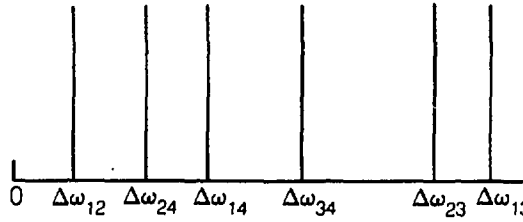

XBL 8611-9256

Figure IV.24: Zero field energy levels and allowed zero field NMR transitions for a pair of I-S spins ($I=^{1}H$, $S=^{13}C$). The most general scheme with $\eta \neq 0$ is illustrated based on the Hamiltonian, eigenstates and energies given in the text. The energies depend upon the indirect coupling constant, J, and the dipolar coupling ($\omega_D = \gamma_I \gamma_S h/2\pi r^3$) scaled by the liquid crystal unixaxial order parameter, S_{zz}. The asymmetry in the dipolar coupling ($\eta \neq 0$) removes the degeneracy of states 1 and 2 resulting in six allowed transitions. Only positive frequencies are shown as the spectrum is symmetric about zero. When $\eta = 0$, levels 1 and 2 are degenerate, thus introducing a zero frequency transition and reducing the total number to 4 as shown in Chapter II.

$$E_3 = S_{zz}\omega_D - \frac{J}{4}$$
$$E_4 = \frac{3}{4}J \qquad \text{(IV.38b)}$$

for the zero field eigenstates given previously in Equation (IV.32) including the singlet state, $|4\rangle = 2^{-1/2}(|\alpha\beta\rangle - |\beta\alpha\rangle)$. Note that transitions are now allowed between the singlet and triplet manifolds unlike the homonuclear case.

2. Zero Field Spectra

The sudden removal of the intermediate field, as in the field cycle of Figure IV.9a, initiates evolution at the dipolar frequencies if the initial condition does not commute with the zero field Hamiltonian. If the liquid crystal is aligned with the director axes along the laboratory z axis, such that the z axes in Equations (IV.36) and (IV.37) are coincident, then for a=b, the commutator is

$$[\rho(0), H_{ZF}] = 0 \qquad \text{(IV.39)}$$

and no signal will result. This is evident since if a=b then the density matrix in Equation (IV.37) is identical to a homonuclear system. If though, the coefficient a is not equal to b, as is generally true for equilibrium S=^{13}C and I=^{1}H polarizations, it can easily be shown that the commutator in Equation (IV.39) for a heteronuclear pair is not equal to zero and thus evolution will occur even in a sample aligned along the original field direction. Of course, even if a=b, evolution will also occur when, as for a polycrystalline sample, there is a distribution of director axes.

The normalized signal can be calculated for an arbitrary orientation of director frame, described by the angles θ and ϕ with respect to the laboratory z axis, from

$$S(t_1) = Tr\{RI_zR^{-1}\exp(-iH_{ZF}t)R(aI_z + bS_z)R^{-1}\exp(iH_{ZF}t)\} \quad (IV.40)$$

in which the detected operator is I_z and $R=\exp(-i\phi I_z)\exp(-i\theta I_y)$. For any single orientation of director with $\eta=0$ this reduces to

$$S_\Omega(t_1) = N\{(a+b)\cos^2\theta + (a-b)\sin^2\theta\cos(\tfrac{1}{2}S_{zz}\omega_D+J)t_1$$
$$+ (a-b)\cos^2\theta\cos(S_{zz}\omega_D-J)t_1 + (a+b)\sin^2\theta\cos(\tfrac{3}{2}S_{zz}\omega_D)t_1\} \quad (IV.41)$$

where $\omega_D=\gamma_I\gamma_S h/2\pi r^3$ and N is a normalization constant. The angular factor depends on a single value of θ for a liquid crystal sample which remains uniformly aligned in zero field. For example, nematic liquid crystals with $\Delta\chi>0$ will have $\theta=0^\circ$ and Equation (IV.41) becomes

$$S(t_1) = N\{(a+b) + (a-b)\cos(S_{zz}\omega_D-J)t_1\} \quad (IV.42)$$

Similarly, for a nematic liquid crystal with $\Delta\chi<0$ the angle of alignment with respect to the laboratory z axis is 90° and

$$S(t_1) = N\{(a-b)\cos(\tfrac{1}{2}S_{zz}\omega_D+J)t_1 + (a+b)\cos(\tfrac{3}{2}S_{zz}\omega_D)t_1\} \quad (IV.43)$$

Experimentally this means that separate transitions of the heteronuclear spin manifold will be selected by the ordering of the liquid crystal system. Spectra of $^{13}CHCl_3$ in nematic phases with $\Delta\chi>0$ and $\Delta\chi<0$ are shown in Figure IV.25 and demonstrate this effect. The order parameter

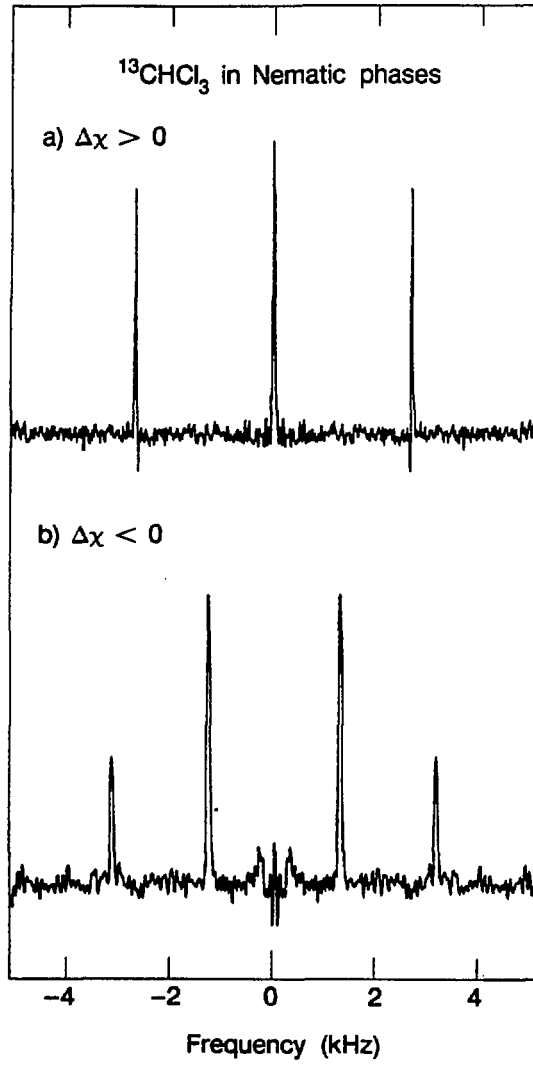

XBL 869-11693

Figure IV.25: Zero field NMR spectra of a ^{13}C-^{1}H pair in nematic liquid crystals. (a) $^{13}CHCl_3$ (6 wgt %) in EBBA, $\Delta\chi>0$. Zero field signal results after a sudden transition to zero field with lines corresponding to $\Delta\omega_{12}$ and $\Delta\omega_{34}$ of Figure IV.24 and Equation (IV.42) with $\eta=0$. The calculated value of the order parameter is $S_{zz} = 0.115 \pm 0.001$. (b) $^{13}CHCl_3$ (6 wgt %) in ZLI 1167, $\Delta\chi<0$. The spectrum shows the other possible transitions in the singlet/triplet manifold ($\Delta\omega_{14}=\Delta\omega_{24}$ and $\Delta\omega_{13}=\Delta\omega_{23}$ for $\eta=0$ in Figure IV.24). The relative intensities of the peaks in the spectrum do not match precisely with those given by Equation (IV.43) in the text for equilibrium populations and may possibly be due to relaxation or demagnetization effects. The order parameter was found to be $S_{zz} = 0.083 \pm 0.001$.

can be calculated from the spectrum using values of J=+0.210 kHz[45] and r=1.073 Å[46]. This yields values of S_{zz}=0.115 ± 0.001 ($\Delta\chi$>0) and S_{zz}=0.083 ± 0.001 ($\Delta\chi$<0) for the two nematics.

Nonaligned samples, such as smectic B (axially symmetric) and E (nonaxially symmetric), have a distribution of director orientations and describing the signal in these cases requires that Equation (IV.41) be averaged over the angle θ. An axially symmetric heteronuclear dipolar coupling (η=0) produces the spectrum shown in Figure IV.26 and the signal is given by the normalized expression below

$$S(t_1) = N\{(a+b) + 2(a-b)\cos(\tfrac{1}{2}S_{zz}\omega_D+J)t_1 + (a-b)\cos(S_{zz}\omega_D-J)t_1 + 2(a+b)\cos(\tfrac{3}{2}S_{zz}\omega_D)t_1\} \qquad (IV.44)$$

Due to the symmetry effects of the liquid crystalline phase, the Hamiltonian may be nonaxially symmetric (η≠0) as defined previously for the Smectic E phase. This asymmetry lifts the degeneracy of the two lowest energy levels and increases the number of peaks in the spectrum such that

$$S(t_1) = N\{(a+b)\cos(S_{zz}\omega_D\eta)t_1 + (a-b)\cos(\tfrac{1}{2}S_{zz}\omega_D(1-\eta)+J)t_1 + (a-b)\cos(\tfrac{1}{2}S_{zz}\omega_D(1+\eta)+J)t_1 + (a-b)\cos(S_{zz}\omega_D-J)t_1 + (a+b)\cos(\tfrac{1}{2}S_{zz}\omega_D(3-\eta))t_1 + (a+b)\cos(\tfrac{1}{2}S_{zz}\omega_D(3+\eta))t_1\} \qquad (IV.45)$$

The spectrum of a nonaxially symmetric dipolar coupled pair is shown in Figure IV.27. This spectrum illustrates the most general form of the heteronuclear dipolar Hamiltonian for two spins as all possible transitions in the singlet/triplet manifold are present. An interesting

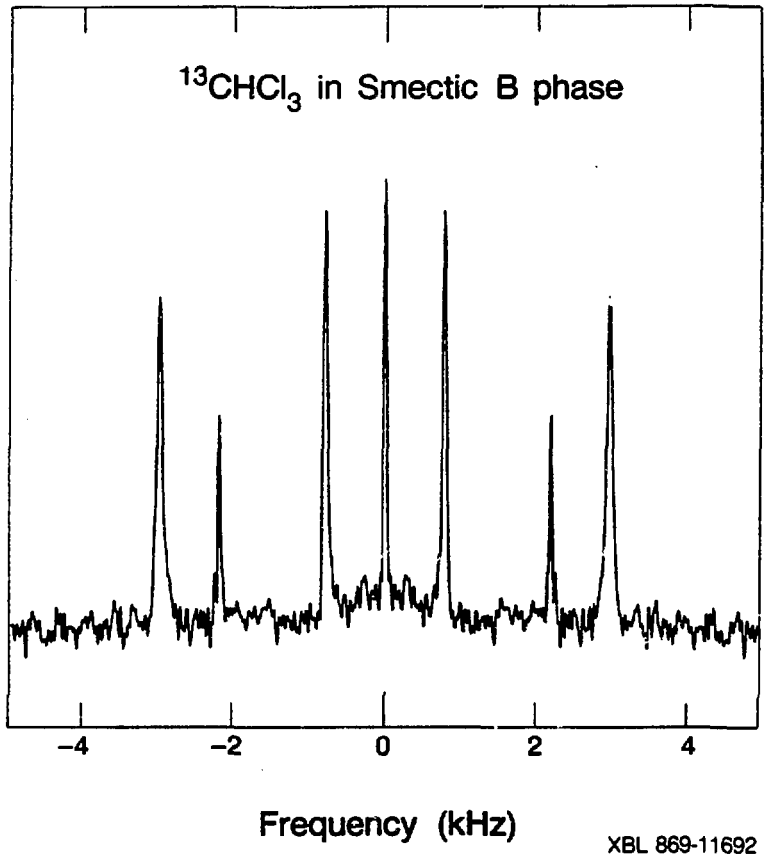

Figure IV.26: $^{13}CHCl_3$ in an unaligned Smectic B phase liquid crystal. The seven peaks correspond to the transitions with n=0 of $\Delta\omega_{12}$, $\pm\Delta\omega_{13}=\Delta\omega_{23}$, $\pm\Delta\omega_{34}$ and $\pm\Delta\omega_{14}=\Delta\omega_{24}$ between the triplet and singlet energy levels. In order to account for the positions of the peaks in the experimental spectrum the sign of S_{zz} must be negative in Equation (IV.44). The calculated value of S_{zz} is found to be -0.080 ± 0.001.

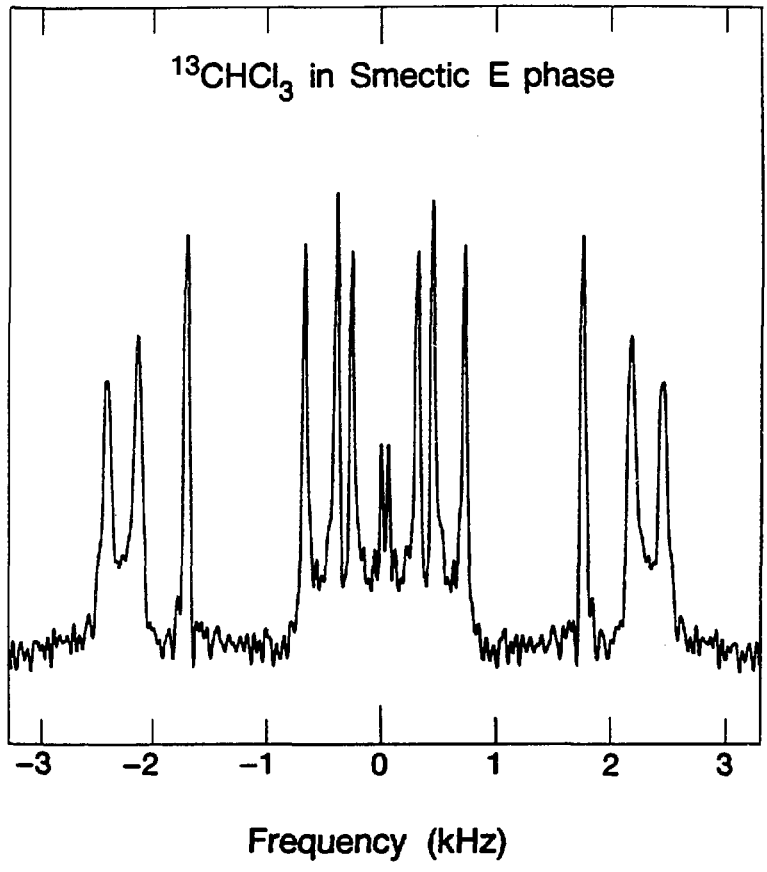

XBL 869-11691

Figure IV.27: $^{13}CHCl_3$ in Smectic E phase liquid crystal with a nonaxially symmetric dipolar coupling ($\eta \neq 0$). The twelve peaks in the spectrum correspond to all possible allowed transitions in the singlet/triplet manifold for two heteronuclear spins. The slight linebroadening and artifacts at low frequencies are most likely caused by small residual fields. The uniaxial order parameter was found to have a negative value of $S_{zz} = -0.062 \pm 0.001$ and an asymmetry parameter of $\eta = 0.186 \pm 0.002$.

result arises when calculating the order parameter for the Smectic B and E cases. In order to account for the frequencies in the spectrum, the sign of S must be negative for the proper relationship of the dipolar and J coupling terms, which are written with the same sign of the Hamiltonian, and J being positive.[47] The order parameters for the smectic phases are then S_{zz}=-0.080 ± 0.001 and S_{zz}=-0.062 ± 0.001 for smectic B and E, respectively, with an asymmetry parameter of η=0.186 ± 0.002 in the latter. The relative change in sign of the S_{zz} parameter between nematics and smectics may be indicative of the different average alignment of the solute molecules being trapped among different parts of the liquid crystal molecules.[48]

E. Appendix: Liquid Crystal Samples and Experimental Details

1. Experimental Aspects

a. Sample preparation. Sample preparation is also mentioned briefly in the Appendix of Chapter II. Samples were made homogeneous by thoroughly heating and mixing the liquid crystal solvent/solute mixture above its clearing point (isotropic phase) using a carefully regulated hot water bath as extremely high temperatures can decompose the liquid crystals. The precision in determining the clearing points is only good to within a few degrees. Ascertaining the phase is probably the most difficult aspect of sample preparation. Clearing points are only useful for determining the nematic to isotropic transition and the liquid-like nematic phase is often easily recognizable at room temperature. Other phases are not easily identifiable by sight and one can not assume from

one known transition temperature that the others will be depressed by the same amount. Therefore, the liquid crystal samples chosen were those which had the desired phase over a reasonably broad and accessible temperature range to allow for the addition of a solute.

b. Field Cycling. The pneumatic shuttling system employed for translation of the sample and the electronics for producing the zero field have been described in Chapter II. Minimum air pressures were used to reduce the physical shock of shuttling the sample. The possibility of complete disordering and subsequent reordering in the time of the field cycle is ruled out by the behavior demonstrated under pulsed dc fields. The samples were generally found to be extremely stable under field cycling conditions. Some samples which were found to be less stable are those consisting of mixtures of two liquid crystal components where upon shuttling the sample separated or changed phase. This may be due to problems with miscibility or using mixtures near a phase transition.

The most serious experimental problems involved temperature fluctuations over the course of the experiment. These were generally small ($<\pm 2^{o}$) but can affect either the liquid crystal phase or alter the value of the order parameter. Samples such as nematics were more sensitive than the smectics to these effects. Thermal fluctuations can result in linebroadening and/or a shift in the spectral splitting in subsequent spectral acquistions. Other experimental aspects such as concentration or field gradients/inhomogeneities will also broaden the lines.[7,8] Eddy currents, produced by the switching coils, result in time varying magnet fields and require that long delays be included in

the field cycle to allow for their decay.

c. Experiments to detect disordering. Several attempts were made to detect a change in the alignment of the sample in low or zero fields. The field cycle consisted of the usual sudden transition or demagnetization cycle with an extension of the time spent in either the intermediate field or zero field. Initiating evolution after this time interval would be expected to show any changes in the system. The limits on the time allowed were determined by the relaxation time in low or zero fields (~ few 100 msec) and the stability of the electronics. On this timescale, no changes were seen to occur.

d. Relaxation times. The proton relaxation times of the solute molecules in most nematics and smectics were generally on the order of a few seconds in high field and 100 msec or more in low fields. An example shown in Figure IV.28 illustrates the magnitude of the solute signal as a function of time in zero field from which a rough estimate of the zero field T_1 is gained. The relaxation times of the liquid crystal molecules is generally so short in high or zero field that only the evolving solute magnetization is detected. Several experiments were conducted on selectively deuterated or protonated liquid crystals but no zero field signal was ever observed. The solvent and solute signals can be separated in high field by waiting a delay on the order of a few 100 μsec between initial echo pulses. When working in a more homogeneous magnet to obtain the high field spectra, a delay on the order of milliseconds is required. Thus using the high field echo may be unnecessary, as only the solute signal is observed to oscillate, except its use removes the large background solvent signal.

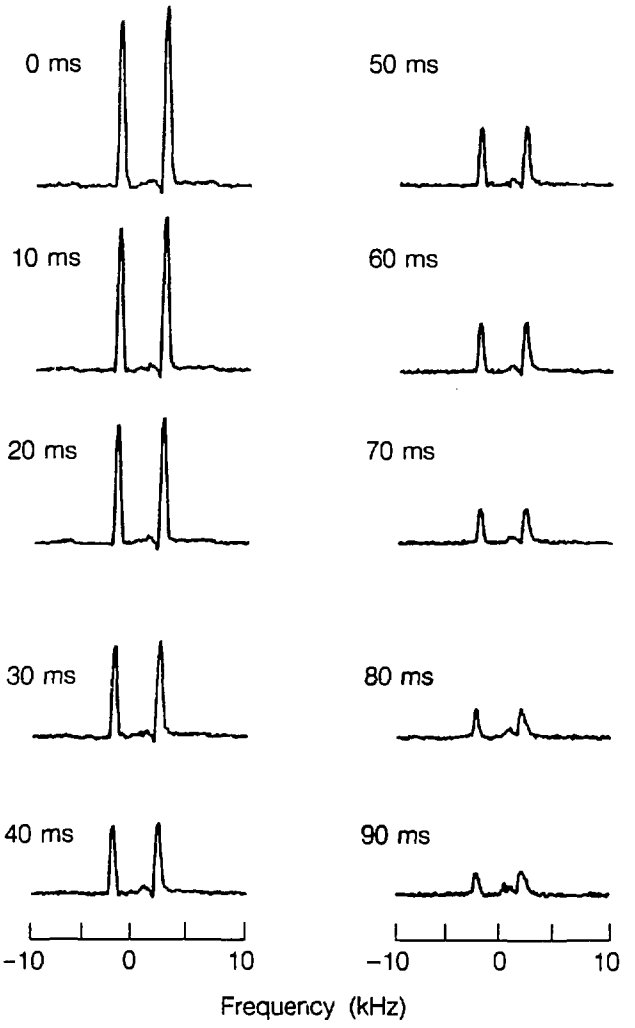

XBL 8611-9558

Figure IV.28: High field spectra of CH_2Cl_2 in Eastman 11650 as a function of time in zero field. The sample is shuttled to zero field using of the field cycle of Figure IV.14a with no dc pulses to initiate evolution in the aligned sample. The sample is allowed to remain in zero field for a given amount of time before being remagnetized to high field where the high field spectrum or signal amplitude is measured. As shown in this figure, the amplitude of the signal decays and from such the zero field T_1 can be calculated. No change in the system ordering is observed with demagnetization to zero field and immediate remagnetization as is the case for t_1=0 milliseconds.

2. Samples

a. Solutes. Dichloromethane and ^{13}C-chloroform were chosen as simple convenient two spin systems.[49] Both solutes readily dissolve in the liquid crystals and, in moderately low weight percents (~5 %), produce sufficient signal without altering the phase ranges by more than a few tens of degrees. CH_2Cl_2 and $CHCl_3$ have previously been studied by NMR in liquid crystal solvents.[10] Although the order parameters are not large, indicating a small degree of alignment, these solute molecules were still sensitive probes of the phases. Other solutes with simple spin systems might be found which align to a higher degree.

b. Liquid Crystals. Compounds which show liquid crystalline phases generally consist of long organic molecules with one or more rings in the structure. This ring structure helps to introduce the diamagnetic susceptibility; samples with $\Delta\chi>0$ generally have aromatic structures, while samples with $\Delta\chi<0$ generally have cyclohexane rings. The following section includes some details about the liquid crystals used. Temperatures are reported in degrees C. The notation is as follows: K=crystalline, S=smectic, N=nematic, and I=isotropic.

1. 11650: p-pentylphenyl-2-chloro-4-(p-pentylbenzoyloxy) benzoate
   (Kodak) MW 493.0 $\Delta\chi>0$ $K\rightarrow39^{o}\rightarrow N\rightarrow122^{o}\rightarrow I$
   Stable solute/nematic mixture at room temperature with a broad range. Fairly viscous and stable under shuttling.
2. EBBA: p-Ethoxybenzylidene p-butylaniline (Frinton)
   MW 281.4 $\Delta\chi>0$ $K\rightarrow35^{o}\rightarrow N\rightarrow78^{o}\rightarrow I$

Reasonably stable nematic at room temperature with most solutes. Some sample separation may occur with shuttling.

3. ZLI2141: mixture of cyanobiphenyls and cyanotriphenyls. (EM Chemicals) Low viscosity liquid crystal with nematic phase. Used to see if disordering occurred.

4. ZLI1167: Mixture of propyl, pentyl and heptyl bicyclohexylcarbonitriles (EM Chemicals) $\Delta\chi<0$

$n=3$ $K\rightarrow58^{o}\rightarrow N\rightarrow80^{o}\rightarrow I$ $n=5$ $K\rightarrow62^{o}\rightarrow N\rightarrow82^{o}\rightarrow I$ $n=7$ $K\rightarrow71^{o}\rightarrow N\rightarrow83^{o}\rightarrow I$

No data on mixture. Stable nematic phase with all solutes.

5. ZLI1537: ethylbicyclohexylcarbonitrile (EM Chemicals)

$\Delta\chi<0$ $K\rightarrow29^{o}\rightarrow S_{A}\rightarrow46^{o}\rightarrow N\rightarrow48^{o}\rightarrow I$

Similar behavior to 4 with narrow phase ranges.

6. ZLI1538: butylbicyclohexylcarbonitrile (EM Chemicals)

$\Delta\chi<0$ $K\rightarrow28^{o}\rightarrow S_{A}\rightarrow54^{o}\rightarrow N\rightarrow79^{o}\rightarrow I$

Similar to 4 and 5. Useful smectic A range. Aligns in field

7. MBBA: N-(p-methoxybenzylidene)-p-butylaniline

$\Delta\chi>0$ MW 267.4 $K\rightarrow20^{o}\rightarrow N\rightarrow47^{o}\rightarrow I$

MBMBA: p-methoxybenzal-p-methylbutylaniline

$K\rightarrow22^{o}\rightarrow N\rightarrow24.5^{o}\rightarrow I$

The latter is chiral and in small weight percents (<12%) with MBBA forms a chiral phase with the helix axis perpendicular to the field. Very narrow temperature range and with solute/isotropic transition is near room temperature. Short relaxations times of solute.

8. HOAB: 4-4'-bis-(heptyloxy)azoxybenzene

$K\rightarrow74^{o}\rightarrow S_{C}\rightarrow93^{o}\rightarrow N\rightarrow122^{o}\rightarrow I$

Frequently studied smectic C phase. Predicted biaxiality.

9. ZLI3488: Ferroelectric RT smectic C* Mixture

Composition unknown, obtained via H. Zimmermann from Merck Darmstadt $K \rightarrow <30^{o} \rightarrow S_{C*} \rightarrow 61^{o} \rightarrow S_{A} \rightarrow 66^{o} \rightarrow Ch \rightarrow 85^{o} \rightarrow I$

Aligns in magnetic field, no observable biaxiality.

10. 40.8: 4-n-butyloxybenzylidene-4'-n-octylaniline (Frinton)

MW 365.6 $K \rightarrow 32^{o} \rightarrow S_{B} \rightarrow 48^{o} \rightarrow S_{A} \rightarrow 60^{o} \rightarrow N \rightarrow 76^{o} \rightarrow I$

See 11. Unstable neat smectic B phase.

11. 8OCB: 4-n-octyloxycyanobiphenyl (EM Chemicals/BDH)

MW 307 $K \rightarrow 54^{o} \rightarrow S_{A} \rightarrow 67^{o} \rightarrow N \rightarrow 80^{o} \rightarrow I$

Used in combination with 10, these liquid crystals show room temperature A, B and E phases. Reasonably stable phases if mixtures not near phase transition except for A which separates due to low miscibility.

12. 8CB: octylcyanobiphenyl (EM Chemicals, K24)

$\Delta\chi>0$ $K \rightarrow 21.5^{o} \rightarrow S_{A} \rightarrow 33.5^{o} \rightarrow N \rightarrow 40.5^{o} \rightarrow I$

Similar to 11 in structure. Narrow but useable and stable smectic A phase with solute. Aligns in a field.

Results using all the compounds listed were not reported in this chapter. This is generally due to the fact that the behavior of the nematics with $\Delta\chi>0$ or $\Delta\chi<0$ was identical in terms of alignment, demagnetization, solutes, similar order parameters, etc. A principal application of liquid crystals with $\Delta\chi<0$ and $\Delta\chi>0$ comes about when it is desirable to spin the sample for higher resolution. Depending on whether the field is produced by a superconducting magnet (B_z along

spinning axis) or an electromagnet (B_z perpendicular to spinning axis), it is useful to use one or the other sample where spinning would otherwise cause the sample to reorient about the spinner axis. In the mixtures of $\Delta\chi>0$ and $\Delta\chi<0$ (primarily 2 and 4), it is very difficult to prepare the exact concentration to produce the phase transition at room temperature. Temperature regulation is the most direct approach for observing the transition, but even so T_c occurs over a very narrow ~1-2° range. Chiral systems, such as 7 and 9, and Smectic C phases, such as 8, are interesting systems to study as there is predicted to be a biaxiality to such phases and a non-uniform alignment with respect to an applied field direction.

F. References

1. P.G. de Gennes, The Physics of Liquid Crystals (Clarendon, Oxford, 1974).

2. J.W. Emsley and J.C. Lindon, NMR Spectroscopy Using Liquid Crystal Solvents (Pergamon, Oxford, 1975).

3. J.W. Emsley, ed. Nuclear Magnetic Resonance of Liquid Crystals NATO ASI Series (D. Reidel, Dordrecht, 1985).

4. G.W. Gray, Molecular Structure and the Properties of Liquid Crystals (Academic, New York, 1962).

5. S. Chandrasekhar, Liquid Crystals (Cambridge, Cambridge, 1977).

6. G.R. Luckhurst and G.W. Gray, Molecular Physics of Liquid Crystals (Academic, New York, 1979).

7. P. Diehl and C.L. Khetrapal, NMR Basic Principles and Progress, Vol.1 (Springer-Verlag, Berlin, 1969).

8. (a) C.L. Khetrapal and A.C. Kunwar, in Adv. in Magn. Reson. **9** (J.S. Waugh, ed., Academic, New York, 1977).
   (b) C.L. Khetrapal, A.C. Kunwar, A.S. Tracey and P. Diehl, NMR Basic Principles and Progress, Vol.9 (Springer-Verlag, Berlin, 1975).

9. J.W. Doane in Magnetic Resonance of Phase Transitions (Academic, New York, 1979) and references therein.

10. H. Kelker and R. Hatz, Handbook of Liquid Crystals (Verlag Chemie, Weinheim, 1980).

11. J.W Doane, Chapter 17, p. 421 in Reference 3.

12. G. Meier, E. Sackmann and J.G. Grabmaier, Applications of Liquid Crystals (Sp. inger-Verlag, Berlin, 1975).

13. I. Haller and J.D. Litster, Phys. Rev. Lett. **25**, 1550 (1970) and Mol. Cryst. Liq. Cryst. **12**, 277 (1977).

14. (a) E.G. Hanson and Y.R. Shen, Mol. Cryst. Liq. Cryst. **36**, 193 (1976).
   (b) H. de Jeu and P. Bordewijk, J. Chem. Phys. **68**, 109 (1978).

15. T.W. Stinson and J.D. Litster, Phys. Rev. Lett. **25**, 503 (1970).

16. (a) J.C. Paul, W.D. Phillips, L.R. Melby and M. Panar, J. Chem. Phys. **43**, 3442 (1965).
   (b) H. Gasparoux, B. Regaya and J. Prost, C.R. Acad. Sci. B, **272**,

1168 (1971).

17. A. Saupe, Z. Natur. A19, 161 (1964).
A. Saupe, Z. Natur. A20, 572 (1965).

18. J.G. Snijder, C.A. de Lange and E.E. Burnell, Isr. J. Chem. 23, 269 (1983).

19. A.Saupe and G. Englert, Phys. Rev. Lett. 11, 462 (1963).

20. M. Warner, Mol. Phys. 52, 677 (1984).

21. P.R. Luyten, J. Bulthuis, W.M.M.J. Bovee and L. Plomp, J. Chem. Phys. 78, 1712 (1983).

22. A. Kumar, J. Magn. Reson. 30, 227 (1978).

23. M. Goldman, Spin Temperature and Nuclear Magnetic Resonance in Solids (Oxford, London, 1970).

24. E.L. Hahn, Phys. Rev. 80, 580 (1950).

25. (a) J. Jeener and P. Brokaert, Phys. Rev. A 157, 232 (1969).
(b) J. Jeener, H. Eisendrath and R. van Steenwinkel, Phys. Rev. A 478, 133 (1974).

26. S. Vega, J. Chem. Phys. 68, 5518 (1978).

27. C.L. Khetrapal and A.C. Kunwar, Mol. Cryst. Liq. Cryst. 72, 13 (1981) and Chem. Phys. Lett. 82, 170 (1982).

28. (a) P. Diehl and J. Jokisaari, Chem. Phys. Lett. 87, 494 (1982).
(b) C.L. Khetrapal and A.C. Kunwar, Isr. J. Chem. 23, 299 (1983).
(c) C.L. Khetrapal, H.J. Yeh and A. Saupe, Mol. Cryst. Liq. Cryst. 92, 243 (1984).
(d) J. Jokisaari and Y. Hiltunen, Chem. Phys. Lett. 115, 441 (1985).
(e) B.M. Fung, J. Amer. Chem. Soc. 105, 5713 (1983).

29. R.A. Wise, A. Olah and J.W. Doane, J. de Phys. C136, 117 (1975).

30. G. Moro, U. Segre and P.L. Nordio, Chapter 9, p. 207 in Reference 3.

31. Z. Luz, D. Goldfarb and H. Zimmermann, Chapter 14, in Reference 3.

32. For example, Chapter 20-23 in Reference 3.

33. J.W. Doane, Chapter 18, p. 431 in Reference 3.

34. J.W. Doane, Chapter 19, p. 441 in Reference 3.

35. (a) T.R. Taylor, J.L. Fergason and S.L. Arora, Phys. Rev. Lett. 24, 359 (1970).

(b) J. Doucet and A.M. Levelut, J. Phys. (Paris) **38**, 1163 (1977).
(c) W.H. de Jeu and J.A. de Poorter, Phys. Lett. **61A**, 114 (1977).
(d) J. Doucet, A.M. Levelut, M. Lambert, L. Liebert and L. Strzelecki, J. Phys. (Paris) Colloq. **C1 36**, 13 (1975).
(e) A.J. Leadbetter, R.M. Richardson and J.C. Frost, J. Phys. (Paris) Colloq. **C3 40**, 125 (1977).

36. J. Seliger, R. Osredkar, V. Zagar and R. Blinc, Phys. Rev. Lett. **38**, 411 (1977).

37. (a) Z. Luz and S. Meiboom, J. Chem. Phys. **59**, 275 (1973).
(b) Z. Luz, R.C. Hewitt and S. Meiboom, J. Chem. Phys. **61**, 1758 (1974).
(c) D.J. Photinos, P.J. Bos and J.W. Doane, Phys. Rev. A **20**, 2203 (1979).

38. (a) P.J. Collings, D.J. Photinos. P.J. Bos, P. Ukleja and J.W. Doane, Phys. Rev. Lett. **42**, 996 (1979).
(b) D.J. Photinos and J.W. Doane, Mol. Cryst. Liq. Cryst. **76**, 159 (1981).
(c) D.J. Photinos, P.J. Bos, J.W. Doane and M.E. Neubert, Phys. Rev. A **23**, 3346 (1981).

39. P.J. Bos, J. Pirs, P. Ukleja, M.E. Neubert and J.W. Doane, Mol. Cryst. Liq. Cryst. **40**, 59 (1977).

40. (a) T. Barbara and B.P. Dailey, Mol. Cryst. Liq. Cryst. **87**, 239 (1982).
(b) R.Y. Dong, H. Schmiedel, N.A.P. Vaz, Z. Yaniv, M.E. Neubert and J.W. Doane, Mol. Cryst. Liq. Cryst. **98**, 411 (1983).

41. N.A. Vaz, M.J. Vaz and J.W. Doane, Phys. Rev. A **30**, 1008 (1984).

42. P.E. Cladis, Mol. Cryst. Liq. Cryst. **67**, 177 (1981).

43. (a) G.J. Kruger, Phys. Reports **82**, 231 (1982).
(b) R.M. Richardson, A.J. Leadbetter, C.J. Carlile and W.S. Howels, Mol. Phys. **35**, 1697 (1978).

44. (a) A. de Vries, Mol. Cryst. Liq. Cryst. **63**, 215 (1981).
(b) A.J. Leadbetter, M.A. Mazid and K.M.A. Malik, Mol. Cryst. Liq. Cryst. **61**, 39 (1980).

45. (a) P.K. Bhattacharyya and B.P. Dailey, J. Magn. Reson. **12**, 36 (1973).
(b) J.R. Everett, J. Chem. Soc. Perkins Trans. II, **7**, 1151 (1984).

46. S.N. Ghosh, R. Trambarulo and W. Gordy, J. Chem. Phys. **31**, 1471 (1959).

47. (a) J.M. Courtieu, C.L. Mayne and D.M. Grant, J. Chem. Phys. **66**, 2669, (1977).

(b) I. Morishima, A. Mizuno and T. Yonezawa, J. Amer. Chem. Soc. **93**, 1520 (1971).
(c) D. Gill, M.P. Klein and G. Kotowycz, J. Amer. Chem. Soc. **90**, 6870, (1968).
(d) B.M. Fung, M.J. Gerace and L.S. Gerace, J. Phys. Chem. **74**, 83 (1970).

V. NONAXIALLY SYMMETRIC DIPOLAR COUPLINGS

A. Introduction

NMR is an excellent tool for the study of motion in condensed matter since one observes a time average over the motion resulting in an average chemical shift, quadrupolar interaction, or dipolar coupling. Small amplitude motions can result in an asymmetry in the dipolar coupling, although such motions typically do not result in easily observable changes in the high field NMR powder spectrum. Zero field NMR should be sensitive to small amplitude motions which will result in splittings or extra lines in the frequency spectrum. In the previous chapter, an asymmetry in the dipolar coupling was found as a result of the biaxiality and restricted motions in a liquid crystalline phase. In this chapter, two further examples of motionally induced asymmetries in dipolar coupled systems are presented. The first case is a study of the libration of the water molecules in a polycrystalline hydrate by proton and deuterium zero field experiments. The second involves the effects of proton jumps in a hydrogen bonded carboxylic acid dimer. As a concluding section, the relationship between the induced asymmetry and the effects of residual fields in the zero field NMR experiment is presented.

B. Librational Motions in a Polycrystalline Hydrate

1. Molecular Motions and Tensor Averaging

a. Dipolar tensor. The characteristic motion of the water

molecules in a typical hydrate are rapid 180° flips about their C_2 axes[1] and librations about three axes.[2,3] To a good approximation the librational modes correspond to rotations about the x, y, and z axes[3] of the molecular coordinate system shown in Figure V.1 and are commonly referred to as rocking, waving and twisting, respectively. The influence of the motion on the proton zero field spectrum is treated by calculation of its effect on the dipolar Hamiltonian, H_D. The rapid 180° degree flips have no effect since they merely exchange the two protons. Waving has no effect since it leaves the orientation of the internuclear vector r unchanged. The dipolar Hamiltonian is therefore motionally averaged by only two of the librational modes. The resulting motionally averaged Hamiltonian, H_D', is given in the molecular frame by

$$\begin{aligned} H_D' &= \langle R_z(\theta_z)R_x(\theta_x)H_D R_x(\theta_x)^{-1}R_z(\theta_z)^{-1} \rangle \\ &= \mathbf{I}_1 \cdot \langle R_z(\theta_z)R_x(\theta_x)\mathbf{D}R_x(\theta_x)^{-1}R_z(\theta_z)^{-1}\rangle \cdot \mathbf{I}_2 \qquad (V.1) \\ &\equiv \mathbf{I}_1 \cdot \mathbf{D}' \cdot \mathbf{I}_2 \end{aligned}$$

where θ_x and θ_z are the librational angles about the x and z axes respectively, and the brackets signify a time average over the librational motion. To second order in the angles θ_i characterizing the libration, we can write the motionally averaged tensor, $\mathbf{D}'$, in angular frequency units as[2,4]

$$\mathbf{D}' = d \begin{bmatrix} 1-3\langle\theta_z^2\rangle & 0 & 0 \\ 0 & -2+3\langle\theta_z^2\rangle+3\langle\theta_x^2\rangle & 0 \\ 0 & 0 & 1-3\langle\theta_x^2\rangle \end{bmatrix} \qquad (V.2)$$

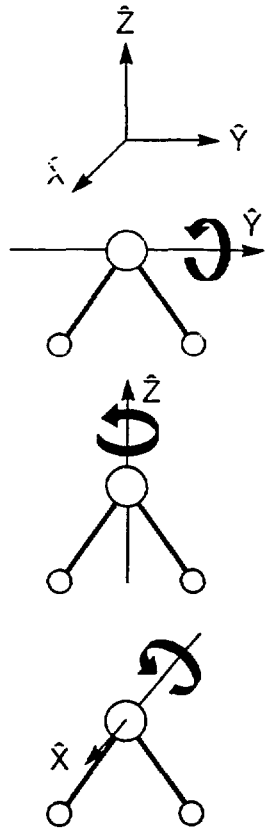

XBL 859-12121

Figure V.1: The three librational modes of the water molecules in barium chlorate monohydrate. In this molecular coordinate, system the H_2O molecule lies in the plane of the paper with its C_2 axis parallel to the z axis. From top to bottom these modes are referred to as waving, twisting and rocking. Waving does not produce a reorientation of the internuclear vector, thus only twisting and rocking have an averaging effect on the dipolar tensor.

where $d=\gamma^2h/2\pi r^3$. Application of the rotations in the reverse order of Equation (V.1) produces the same expression for **D'** to this order of approximation. An unequal intensity in the amplitudes of the two librational modes produces a nonaxially symmetric average dipolar tensor. This is made more clear by defining $\Delta = D'_{22}$ and $\eta = (D'_{11} - D'_{33})/D'_{22}$ and rewriting Equation (V.2) as

$$D' = \begin{bmatrix} -\Delta(1-\eta)/2 & 0 & 0 \\ 0 & \Delta & 0 \\ 0 & 0 & -\Delta(1+\eta)/2 \end{bmatrix} \qquad (V.3)$$

Calculation of the sudden transition experiment zero field spectrum for this case proceeds in a manner analagous to that described previously. The eigenvalues for the Hamiltonian in Equation (V.1) can be solved for using Equation (V.3). The normalized high field signal expected for a powder sample is given by

$$S(t_1) = \cos\{\tfrac{\Delta}{4}(3+\eta)t_1\} + \cos\{\tfrac{\Delta}{4}(3-\eta)t_1\} + \cos\{\tfrac{\Delta}{2}\eta t\} \qquad (V.4)$$

where t_1 is the evolution time in zero field. The proton zero field spectrum of a static water molecule, $\eta=0$ in Equation (V.4) above, would consist of lines at zero frequency and at $\pm\nu_d=3\gamma^2h/8\pi^2r^3$, where r is the internuclear distance of the two protons. The effect of the motion is to split the lines of the static spectrum by an amount proportional to the asymmetry of the dipolar tensor. These motionally produced splittings or additional lines in the zero field spectrum are in sharp contrast with the shoulders on broad powder patterns which occur in the high field case.

b. Quadrupolar Tensor. The zero field spectrum of a motionally averaged spin I=1 nucleus follows from a treatment similar to that above. Explicit expressions for the dependence of the quadrupole coupling constants and asymmetry parameter on the librational amplitudes have been calculated.[2,4] Both the quadrupole coupling constant and asymmetry parameter depend on all three librational modes as well as the exchange frequency characterizing the 180° flips. In barium chlorate at room temperature, however, the flip frequency is sufficiently high that one need only consider an average over the two orientations.[1] The 180° flips average the static quadrupole tensor, which has its principal axis along the O-D bond, to one with its principal component either along the C_2 axis or perpendicular to the molecular plane of the water molecule.[5] The asymmetry parameter is also affected, its value near unity is a consequence of the motion.[6] One notes however that librational amplitudes are a function of the reduced mass of the molecule, hence the amplitudes and NQR frequencies will differ slightly in HDO and D_2O.

2. Zero Field Experiments

a. Proton zero field spectra. The proton zero field spectrum of isotopic abundance barium chlorate has been presented before in Chapter II. Intermolecular dipolar couplings produce linewidths of approximately 7 kHz thus obscuring the splitting due to the motion. The effect of isotopic dilution by deuterium on the linewidth of the proton zero field spectrum is shown for a series of dilution levels in Figure V.2. An increase in the amount of structure in the spectrum is seen as the level of protonation decreases. The spectrum from a 10% protonated sample, Figure V.3, shows all three lines predicted by Equation (V.4)

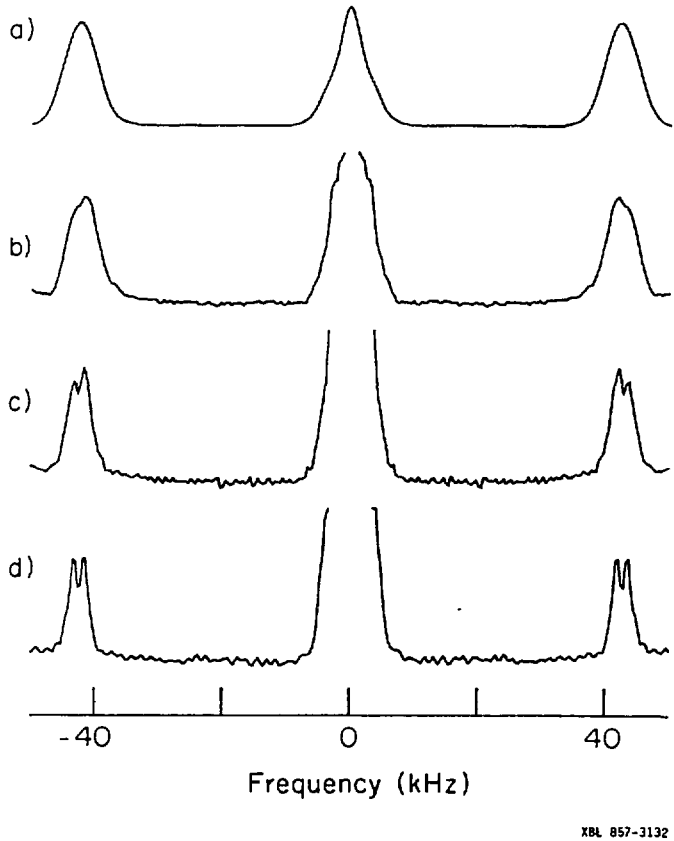

Figure V.2: Proton zero field spectra of barium chlorate monohydrate as a function of isotopic dilution by deuterium: (a) isotopic abundance, (b) 60% protons, (c) 31% protons, (d) 10% protons. Structure due to the asymmetric dipolar tensor of dilute water molecules is observed as the intermolecular contribution to the linewidth is reduced. Unpaired protons in the dilute samples contribute to the line centered at zero frequency.

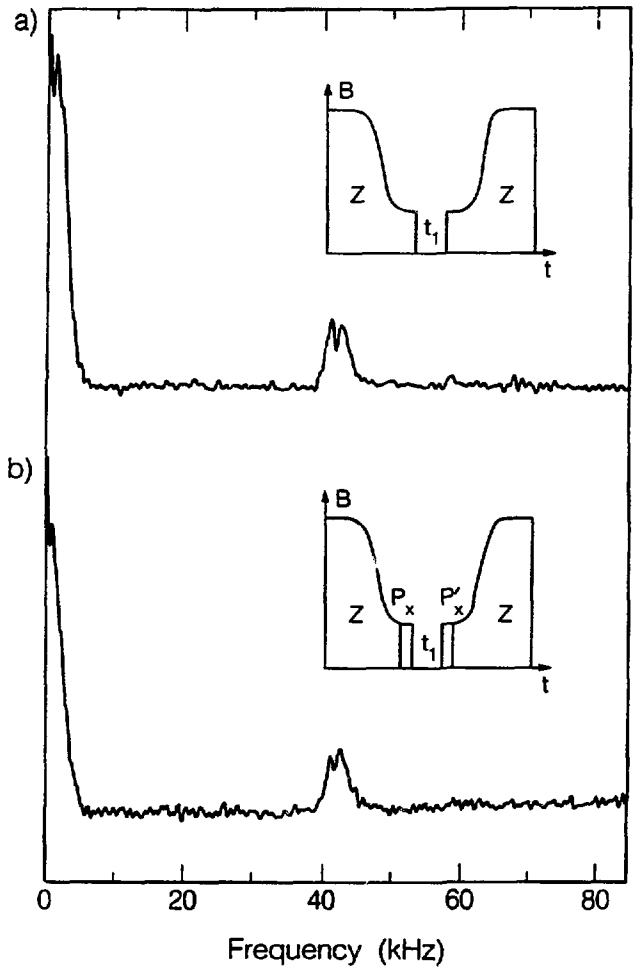

XBL 859-12123

Figure V.3: a). Proton zero field spectrum of 90% deuterated $Ba(ClO_3)_2 \cdot H_2O$ obtained with the field cycle shown at the inset. Here only the positive frequency portion of the spectrum is displayed. All three lines characteristic of the motionally averaged non-axially symmetric dipolar tensor are resolved, appearing at 1.37, 41.8 and 43.4 kHz with linewidths of approximately 2 kHz, considerably narrower than that obtained with the fully protonated material. b). Zero field spectrum from the field cycle with 90^{o} dc pulses shown in the inset. This experiment employed a dc field of 0.010 Tesla oriented orthogonal to B_o. The spectrum is essentially identical with that of the sudden experiment.

for the asymmetric dipolar tensor. A value of $\eta=0.047 \pm 0.004$ can be calculated from the observed splitting.

By combining Equations (V.2) through (V.4) one can use the experimental splittings and a value of r=1.52 angstroms, obtained from neutron diffraction measurements[7], to calculate $\langle\theta_x^2\rangle=0.044$ and $\langle\theta_z^2\rangle=0.070$ (radians^2). Ideally for the zero field calculations one would like to use the value r' given by $r'=\langle 1/r^3\rangle^{-1/3}$ where the brackets signify averaging over the librational and vibrational modes. In the absence of this information the neutron diffraction data seems reasonable, however, as Pedersen's[8] calculations have found the internuclear distances, r_e, varying from 1.52 to 1.55 A and that $\langle 1/r^3\rangle=0.98(1/r_e^3)$ which is a rather negligible difference. A detailed treatment of this subject is beyond the scope of this chapter, however it is clear that corrections due to differences[9] in $\langle 1/r^3\rangle$, $1/r_e^3$, and $\langle 1/r\rangle^3$ will have little effect on the calculated $\langle\theta_i^2\rangle$'s.

A second experiment was performed to determine if the observed splittings could be due to residual magnetic fields present during the zero field evolution period. The field cycle is shown in the inset of Figure V.3b. In this experiment a 90^o dc pulse was given immediately after the sudden switch-off of the intermediate field and a second was applied after the t_1 period. This sequence, being identical with the sudden experiment in every other detail, has the effect of simply changing the relative orientation of the stray field with the initial condition of the magnetization. The spectrum obtained with this sequence, Figure V.3b, is essentially identical with that of the sudden experiment. Results of computer simulations of the effects of stray fields[24] indicate that residual fields >1 gauss are required to produce

splittings comparable to those seen in Figure V.3. Experimental measurements typically place an upper limit of 0.025 gauss on the magnitude of the stray field and thus this is not considered to be an effect in the splitting.

b. Deuterium spectrum. Although the rapid C_2 flips do not manifest themselves in the proton spectrum, they are readily observable via their effect on the deuterium quadrupolar spectrum.[2,5,6] The deuterium zero field NQR spectrum of a 50% deuterated sample of barium chlorate was obtained at room temperature using the indirect detection method which is described in detail in Chapter III to selectively observe only the ^2H signal. Since room temperature deuterium low field T_1's are of the order of milliseconds, an indirect detection method is necessary to observe those deuterons in the HDO molecules. In the spectrum, shown in Figure V.4, the ν_+, ν_-, and ν_o lines are all clearly resolved and from their frequencies one calculates e^2qQ/h =122.7 kHz and η=0.960 which is in good agreement with earlier work.[2] Combining the zero field proton and deuterium data with the quadrupole coupling constants of the static molecule found by Chiba,[2] one can calculate $\langle\theta_y^2\rangle$ for the H_2O molecule. In brief this is done by 1) calculating $\langle\theta_x^2\rangle_{HDO}$ and $\langle\theta_z^2\rangle_{HDO}$ using the formulas in reference 8 to correct for the reduced masses, 2) using these expressions to calculate $\langle\theta_y^2\rangle$ from the zero field HDO data, and 3) calculating $\langle\theta_y^2\rangle_{H2O}$ by the reverse procedure in step 1. Using the explicit expressions for the field gradient tensor averaged by libration and the C_2 flipping, one obtains $\langle\theta_y{}^2\rangle$=0.123(radians^2). The librations have a relatively minor effect on the quadrupole spectrum, the value of η near unity is primarily a consequence of the C_2 flips.[6] An advantage of the dipolar measurements is that the static dipole

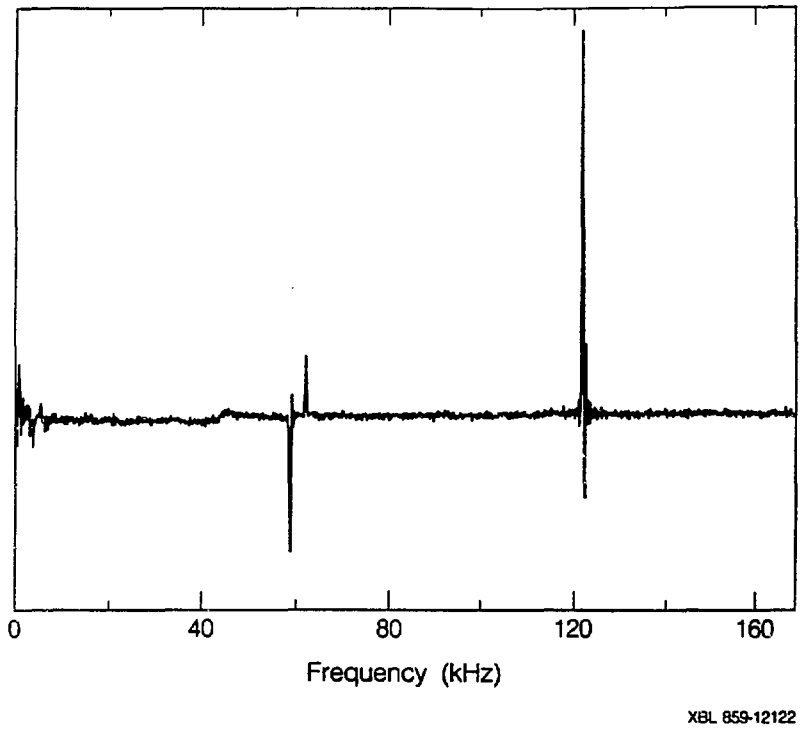

Figure V.4: Indirect detection zero field deuterium NQR spectrum of 50% deuterated barium chlorate monohydrate. All three lines expected are resolved from which one calculates e^2qQ/h=122.7 kHz and η=0.96 in reasonable agreement with single crystal results of the perdeuterated material where values of e^2qQ/h=121.5 kHz and η=0.976 ± 0.007 were obtained. The intensities and phases of the peaks are a complicated function of the level crossing dynamics, initial zero field state and dc pulse angles, and are therefore not easily calculated. The bump at approximately 40 kHz is due to residual proton signal and its small relative size gives an indication of the selectivity of the indirect experiment for the deuterons.

interaction is inherently axially symmetric and any asymmetry is observed the direct result of motion.

3. Discussion

The non-axially symmetric dipolar tensor produced by libration is readily observable via the proton zero field spectrum. The agreement between the results of the two versions of the zero field experiment, as well as the results of computer simulations, rule out the possibility of splittings due to residual fields. Results for the mean square amplitudes of the librational modes are in fair agreement with earlier data,[2,8] especially when one considers that the exact librational modes might differ slightly from the inertial rotations assumed.[3] The zero field NQR results for HDO demonstrate the high resolution of the experiment and the precision with which it can measure the asymmetry parameter. The parameters relating to the motion are underdetermined with a single NQR experiment since the quadrupolar frequencies are a function of the three librational modes, the rate of the 180^{o} flips, as well as the values of $(e^2qQ/h)_o$ and η_o, the parameters of the static molecule. The room temperature deuterium NQR measurements of a hydrate are usually inaccessible to frequency domain techniques because of their relatively short T_1's and low quadrupolar frequencies. In general the ^2H and ^1H results provide complementary information on the motional characteristics of the system since they possess unique principal axis systems and hence are affected differently by the different motions which occur in a system. The zero field measurements have the significant advantage of being made with a powder sample whereas the earlier measurements required a single crystal.[2] This aspect should

allow study of subtle motions in systems inaccessible to single crystal measurements including amorphous and polycrystalline materials. In addition, temperature dependent studies can be compared to computer simulations to understand the dynamics of the system.[10]

C. Proton Jumps in a Carboxylic Acid Dimer

1. Introduction

A second example of a motionally induced asymmetry is found in the dipolar coupling between the carboxylic acid protons in a hydrogen bonded dimer. In p-toluic acid (methyl benzoic acid), like many carboxylic acids, the molecules form dimers in the solid state.[11] X-ray[11] and NMR[12] data have shown that the protons are in a state of dynamic disorder at room temperature. The motion of the protons between two sites relative to the oxygen atoms is expected to lead to an asymmetry in their dipolar coupling. This motion has been previously studied via single crystals where the asymmetry was observed[12] and should be directly observable in the zero field NMR spectrum. NQR studies of the ^{17}O atoms in the carboxylic acid sites have corraborated the fact that the protons jump back and forth between sites rather than the -COOH moieties undergoing 180° flips.[13]

2. Motionally Averaged Dipolar Tensor

This case can be considered to be identical to that of the twisting libration in the water molecule. Choosing a molecular axis system such that the internuclear vector of the protons in the dimer, as illustrated in Figure V.5, lies in the xy plane of the molecule and that

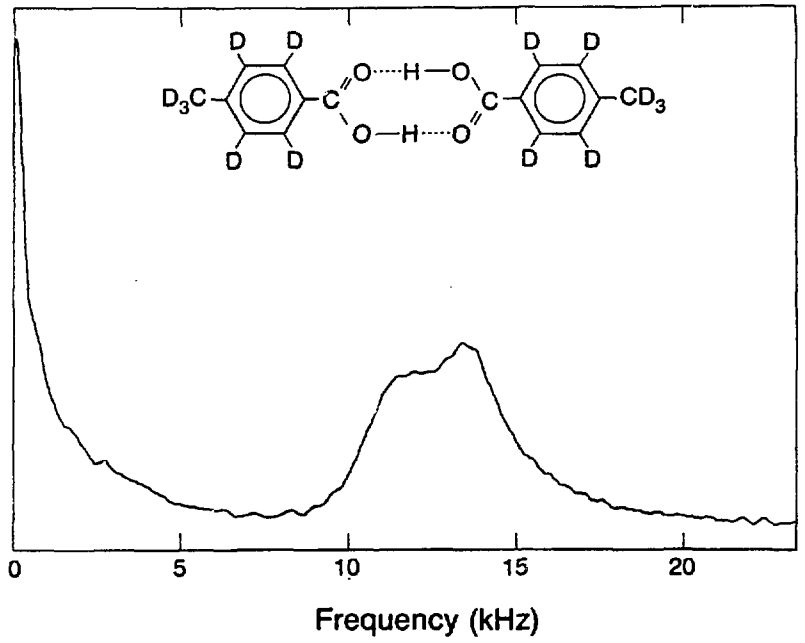

XBL 8511-11499

Figure V.5: Zero field proton spectrum of p-toluic acid, 98% deuterated at all positions except the carboxylic acid protons as shown at top. The protons of the dimer jump between equivalent positions on the two carboxylic acid oxygens. The shoulder of the high frequency dipolar peak suggests the presence of a motionally induced asymmetry in the dipolar coupling. The large peak at zero frequency is due to unpaired protons.

the jumping protons cause the internuclear vector to change positions symmetrically by an angle ϕ about the y axis. (This corresponds to a twist about the z axis out of the plane.)

The average tensor can be calculated as the sum of the dipolar tensors at either of the two positions

$$\bar{D} = x_1 D_1' + x_2 D_2' = x_1 R_z(\phi) D_1 R_z^{-1}(\phi) + x_2 R_z(-\phi) D_2 R_z^{-1}(-\phi) \qquad (V.5)$$

where D_1 and D_2 are the two tensors differing in orientation in the molecular frame by $\pm\phi$ and, x_1 and x_2 are the mole fractions or populations of each site. The internuclear vector for the two positions is assumed equal based on crystallographic data for a closely related nondisordered carboxylic acid dimer.[14] Thus D_1 and D_2 are equal and assuming equal populations of the two sites as expected at room temperature due to the low energy barrier[12], the matrix form of Equation (V.5) becomes

$$\bar{D} = d\begin{bmatrix} 1-3\sin^2\phi & 0 & 0 \\ 0 & 1-3\cos^2\phi & 0 \\ 0 & 0 & 1 \end{bmatrix} \qquad (V.6)$$

where $d=\gamma^2 h/2\pi r^3$.

3. Zero Field Spectrum

For the static case, the spectrum is expected to be the usual three line spectrum. The eigenvalues for the Hamiltonian can be derived from the averaged tensor in Equation (V.6) and the zero field spectrum will also be given by an expression similar to that of Equation (V.4). The zero field spectrum is shown in Figure V.5. From the value calculated by Meier et al.[12] for a jump angle of $\phi=18.6^\circ \pm 2^\circ$ and a

value of r=2.33 ± 0.005 Å, peaks are expected at 13.0, 11.52 and 1.48 kHz. The spectrum does not clearly show resolved splittings but the features in the high frequency peak suggest an asymmetry and appear at approximately the correct frequencies. The low frequency peak is not resolved due to the large zero frequency peak due to residual uncoupled protons.

D. Quenching of Residual Fields by Nonaxially Symmetry Dipolar Couplings

1. Introduction

This discussion was motivated by the observation that in recent zero field NMR experiments, the spectra due to axially symmetric dipolar couplings were broadened by residual fields, whereas those due to nonaxially symmetric couplings were not. It is well known that dipolar couplings involving integer spins can be quenched.[15] This quenching effect has been seen to increase with the increasing asymmetry of the quadrupolar interaction and is reduced in the presence of a magnetic (local dipolar or applied) field.[15,16] The study of NQR lineshapes in the presence of a modulating field has long been of interest as a means of assigning NQR transitions and for determining asymmetry parameters.[17,18] Additionally, analytic expressions for the Zeeman effect on the energy levels of a spin I=1 nucleus have also been reported.[17] In this section, an analogous case of the quenching effect of residual fields with the onset of the asymmetry in the homonuclear dipolar coupling between two spin I=1/2 nuclei (a pseudo spin I=1 case) in zero field NMR is discussed.

2. Zero Field NMR Theory with Residual Field Effects

a. The Hamiltonian. Generally the dipolar Hamiltonian is treated as axially symmetric ($\eta=0$) in the principal axis system of the interaction. However, through motional or symmetry effects, the resulting Hamiltonian in a molecule fixed frame may become nonaxially symmetric ($\eta\neq0$). With this in mind, the zero field dipolar Hamiltonian for two homonuclear dipolar coupled spin I=1/2 nuclei, with the z axis chosen to be along the internuclear vector, can be written

$$H_D = -\frac{\gamma^2\hbar}{2\pi r^3}\left[3I_{z1}I_{z2} - \mathbf{I}_1\cdot\mathbf{I}_2 + \eta(I_{1x}I_{2x} - I_{1y}I_{2y})\right] \qquad (V.7)$$

The Hamiltonian has no angular dependence in the laboratory frame and is identical for every crystallite in a powder sample. The energies for the triplet manifold of two dipolar coupled spin I=1/2 nuclei are

$$\begin{aligned} E_1 &= E_2 = \frac{-\omega_D}{2} \\ E_3 &= \omega_D \end{aligned} \qquad \eta = 0$$

$$\begin{aligned} E_1 &= \frac{-\omega_D}{2}(1+\eta) \\ E_2 &= \frac{-\omega_D}{2}(1-\eta) \\ E_3 &= \omega_D \end{aligned} \qquad \eta \neq 0 \qquad (V.8)$$

where $\omega_D=\gamma^2\hbar/2\pi r^3$. The eigenstates and energy levels for this system, written in the zero field basis set, are illustrated in Figure V.6. The additional η dependent term is seen to lift the degeneracy of two of the levels when $\eta\neq0$. The dipolar coupled system is entirely analogous to

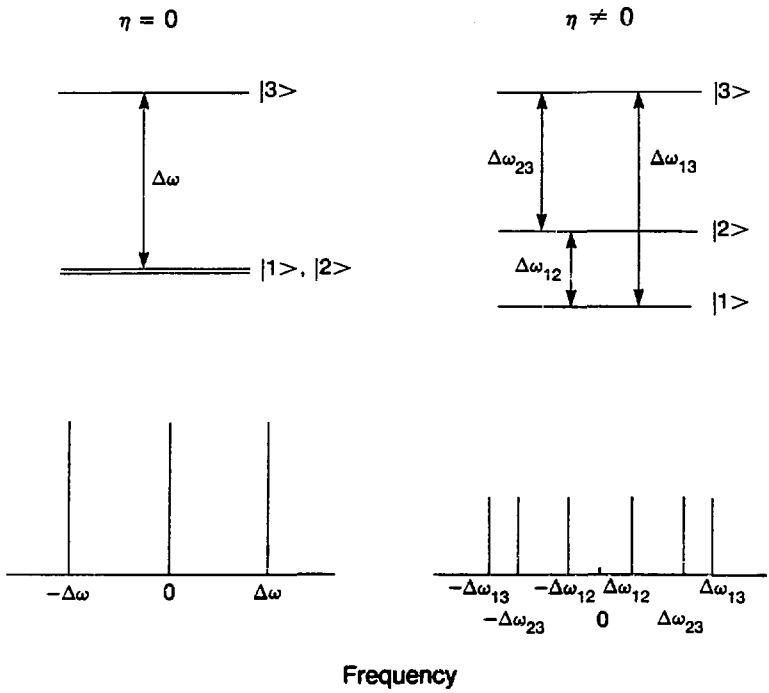

Figure V.6: Unperturbed triplet manifold energy levels, eigenstates and predicted spectral transitions of the zero field homonuclear dipolar Hamiltonian with $\eta=0$ and $\eta\neq0$. The eigenstates are written in terms of the zero field basis set for two spin I=1/2 nuclei and for both cases are given as $|1\rangle = 2^{-1/2}(|\alpha\alpha\rangle+|\beta\beta\rangle)$, $|2\rangle = -i2^{-1/2}(|\alpha\alpha\rangle-|\beta\beta\rangle)$ and $|3\rangle = 2^{-1/2}(|\alpha\beta\rangle+|\beta\alpha\rangle)$. The zero field energy levels are independent of orientation as can be seen from their respective energies E_1, E_2 and E_3 given in the text. The η term of the Hamiltonian lifts the degeneracy of the two lowest energy levels. The lines which appear in the zero field spectrum are of equal intensity in the absence of a perturbation. The zero frequency line in the $\eta=0$ cases arises from nonevolving magnetization corresponding to the degenerate energy levels.

the quadrupolar spin I=1 case. The similarity has been noticed for the S=1 EPR case where expressions for the lineshapes in the presence of a spin-spin coupling and a field have been calculated.[19] Due to this similarity, the effects of coupling to a local dipolar field (a nonresonant I=1/2 spin) or a residual field (due to incomplete cancellation in the zero field region) should be similar to that found previously for quadrupolar spins.[15]

b. Perturbation by Residual Fields. A rough estimate of the effect of a small residual DC field on the dipolar Hamiltonian is made first by perturbation theory. These calculations have been presented before for $\eta \neq 0$,[20] and are repeated here for comparison to the $\eta=0$ case. The magnitude of Zeeman interactions with the residual field, B_{res}, is assumed to be much smaller than the dipolar interaction. The zero field Hamiltonian now contains an extra term:

$$H_{ZF} = -\frac{\gamma^2 h}{2\pi r^3}\left[3I_{z1}I_{z2} - \mathbf{I}_1\cdot\mathbf{I}_2 + \eta(I_{x1}I_{x2} - I_{y1}I_{y2})\right] + \gamma B_{res}\left[(\sin\theta\cos\phi(I_{x1} + I_{x2}) + \sin\theta\sin\phi(I_{y1} + I_{y2}) + \cos\theta(I_{z1} + I_{z2})\right] \qquad (V.9)$$

The angular terms relate the residual field, assumed to be in the lab z direction, to the molecular frame. If $\eta \neq 0$, one can easily show that the perturbation does nothing to first order as the matrix elements of I_x, I_y and I_z are zero.[15,16,21] To second order in the perturbation the resulting energy levels for $\eta \neq 0$ are

$$E_1 = -\frac{\omega_D}{2}(1+\eta) - \frac{D_z^2}{\omega_D \eta} - \frac{2D_x^2}{\omega_D(3+\eta)}$$

$$E_2 = -\frac{\omega_D}{2}(1-\eta) + \frac{D_z^2}{\omega_D \eta} - \frac{2D_y^2}{\omega_D(3-\eta)} \qquad (V.10)$$

$$E_3 = \omega_D + \frac{2D_y^2}{\omega_D(3-\eta)} + \frac{2D_x^2}{\omega_D(3+\eta)}$$

where the D terms contain the orientation dependence of the residual field in the molecular frame: $D_x=\gamma B_{res}\sin\theta\cos\phi$, $D_y=\gamma B_{res}\sin\theta\sin\phi$ and $D_z=\gamma B_{res}\cos\theta$. The perturbation is seen to shift the energy levels quadratically in second order and the low frequency transition ($E_1 - E_2$) is affected most strongly. The shift in energy levels is different for each crystallite orientation due to the angular dependence in the D terms and results in a linebroadening effect when averaged over all orientations. From these expressions, it is evident that as η increases the shift in energy levels decreases.

When $\eta=0$, due to the degeneracy of two of the zero field energy levels, degenerate perturbation theory must be used to describe the situation. In this case, the degeneracy is lifted to first order linearly in the residual field. To second order the resulting energy levels for $\eta=0$ are

$$E_1 = -\frac{\omega_D}{2} - D_z - \frac{1/2(D_x^2 + D_y^2)}{3/2\omega_D + D_z}$$

$$E_2 = -\frac{\omega_D}{2} + D_z - \frac{1/2(D_x^2 + D_y^2)}{3/2\omega_D - D_z} \qquad (V.11)$$

$$E_3 = \omega_D + \frac{1/2(D_x^2 + D_y^2)}{3/2\omega_D + D_z} + \frac{1/2(D_x^2 + D_y^2)}{3/2\omega_D - D_z}$$

The effective perturbation is larger for $\eta=0$ as it is a first order

effect. The spectrum in either case will involve a distribution of Equations (V.10) and (V.11) over all relative orientations of B_{res}.

c. Numerical Simulations. The effect of the residual fields can be illustrated through numerical simulations. The residual field is chosen to be along the laboratory z axis as this is generally the largest component present in practice. Of course the actual direction of the residual field has no effect on the form of the zero field Hamiltonian. The simulations calculate the shift in energy levels for each relative orientation of the field direction in the molecular frame. The normalized signal, $S(t_1)$, is then calculated as a sum over all orientations from

$$S(t_1) = Tr\{RI_zR^{-1}\exp(-iH_{ZF}t_1)RI_zR^{-1}\exp(iH_{ZF}t_1)\} \qquad (V.12)$$

where $R = \exp(-i\phi I_z)\exp(-i\theta I_y)$ is the transformation between the lab and zero field frames. The appearance of the spectrum depends most strongly on the relative orientations of the initial condition and the residual field and, of course, the relative magnitudes of the zero field interaction and the residual field.

The simulated spectra, produced with the program RESID.FOR, for a given residual field and increasing η values appear in Figure V.7. For $\eta=0$, the linebroadening of the high frequency line is significantly greater than for an individual line with $\eta\neq0$. The low frequency peak is most strongly affected as predicted from the perturbation theory calculations and the component at zero frequency results from the fact that the residual field and initial magnetization are colinear, thus a component remains along the z axis and does not evolve. As expected

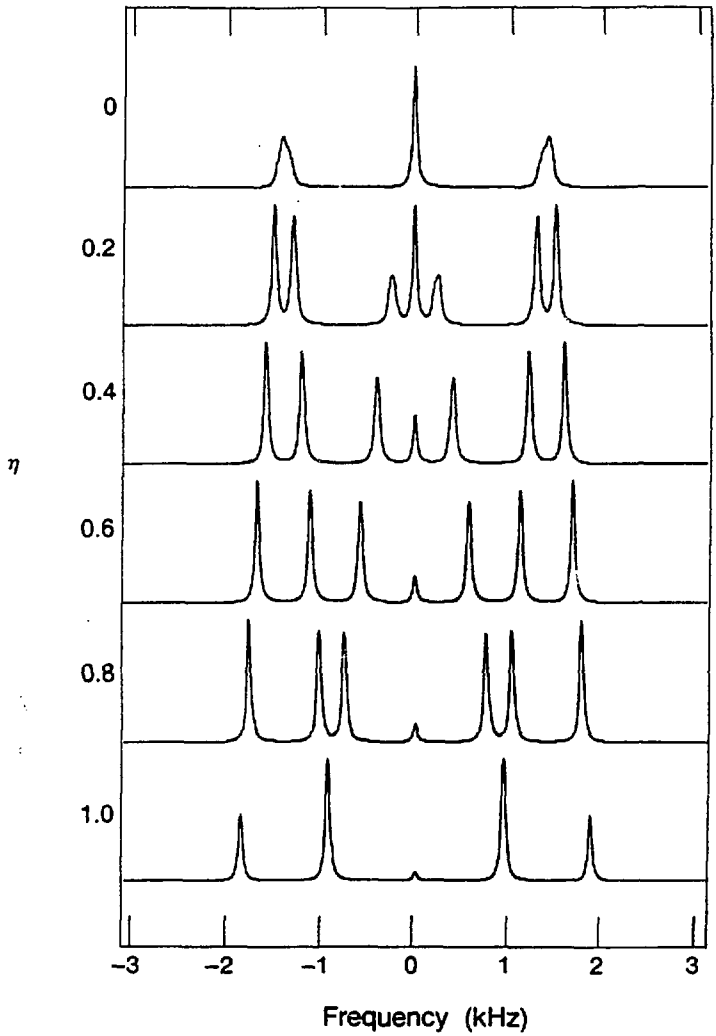

XBL 868-11678

Figure V.7: Numerical simulations of zero field NMR spectra of two homonuclear dipolar coupled spin I=1/2 nuclei with a residual field of 0.025 G in the laboratory z direction and increasing values of η. The first spectrum with η=0 shows substantial broadening of the high frequency lines. The zero frequency peak corresponds to nonevolving magnetization proportional to $I_{z,lab}$ and is not strongly affected by the field. With a nonzero value of η, the low frequency lines are most affected by the residual field showing broadening and a decrease in intensity. In addition, a peak appears at zero frequency which should not occur when $\eta \neq 0$. This peak is a component of the magnetization which does not evolve but rather remains along the residual field. The effect of the residual field decreases noticeably as individual lines broaden very little (although are altered in intensity) with larger values of η. (Note that the spectra are not plotted to scale as the integrated intensity is in fact constant.)

this peak increases in size with increasing levels of the residual field. In the limit of a residual z field which is greater than the local interactions, a large proportion of the magnetization will remain locked along the field direction although interesting low field NMR phenomena result with the sudden transition in intermediate field.[22]

3. Experimental Results

The quenching effect has been experimentally observed in two liquid crystal systems. The zero field NMR spectra of these systems, consisting of a CH_2Cl_2 probe molecule in Smectic B and Smectic E phases, have been presented in Chapter IV. Both are disordered powder-like phases, the former with axial symmetry and the latter a biaxial phase thereby inducing an asymmetry in the dipolar coupling tensor. The spectra display inherently narrow lines due to the lack of intermolecular dipolar couplings. Typically a residual field of approximately 0.025 G results from shimming the zero field region with a Gaussmeter. The liquid crystal samples, with very small dipolar frequencies and narrow lines, have made it necesary to improve upon this. The zero field NMR spectra taken under identical experimental conditions are compared with computer simulations in Figure V.8. The spectrum of the axially symmetric dipolar interaction shows the effect of a residual field in the broadening of the outer lines and narrow zero frequency peak. In the case of a nonzero η in the biaxial phase, the effect of the residual field is reduced although the decreased intensity of the low frequency lines and the peak at zero frequency are clear evidence of its presence.

The effects of residual fields can be removed from the zero field

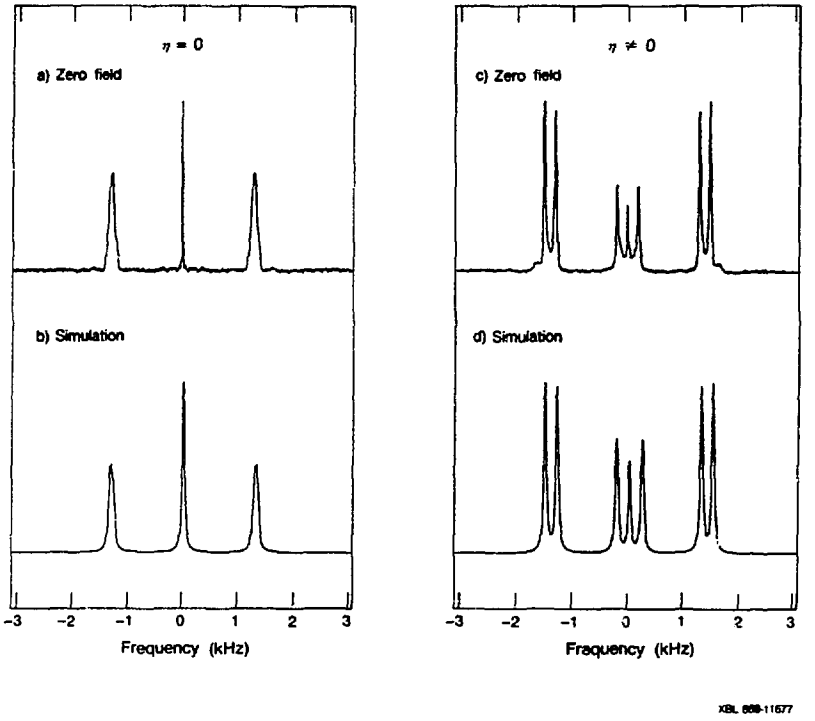

Figure V.8: Experimental spectra of CH_2Cl_2 in Smectic B (axially symmetric, η=0) and E (nonaxially symmetric, $\eta \neq 0$) phases and computer simulations of the effect of a residual field. For η=0, the high frequency lines in (a) are broadened considerably relative to the line at zero frequency. The simulation below in (b) was produced with a residual z field of 0.0175 G and is broadened slightly with a Lorentzian function. In (c) the linewidths with $\eta \neq 0$ are quite narrower than in the former case. The simulation shown in (d) uses the same residual field as (b) and shows the expected broadening of the low frequency lines, the altered intensities and zero frequency peak.

spectrum by using a dc pulsed field as a refocussing echo pulse in analogy to a high field Hahn echo.[23] For samples such as aligned nematic liquid crystals, a 180^{o} pulse applied in the middle of the zero field t_1 interval will refocus the magnetization and remove the linebroadening. For powder samples with $\eta=0$, the normalized signal after a dc pulse in the laboratory x direction can be calculated from

$$S(t_1) = Tr\{RI_zR^{-1}\exp(-iH_{ZF}t_1/2)R\exp(-i\pi I_x)R^{-1}\exp(-iH_{ZF}t_1/2)$$

$$RI_zR^{-1}\exp(iH_{ZF}t_1/2)R\exp(i\pi I_x)R^{-1}\exp(iH_{ZF}t_1/2)\} \qquad (V.13)$$

which for the normalized signal averaged over all molecular orientations is

$$S(t_1) = 1/15(5 + 4\cos 3/2(S_{zz}\omega_D t_1/2) + 6\cos 3/2(S_{zz}\omega_D t_1)) \qquad (V.14)$$

where S_{zz} is the liquid crystalline order parameter which scales the dipolar interaction. The analytic expression shows that not all the signal is refocussed and will show no effect of the residual field. A certain component evolves for only half the t_1 period and is then broadened by the residual field to half the width of the original line. The experimental spectrum of the Smectic B phase with a 180^{o}_{x} dc pulse is shown in Figure V.9. The high frequency lines are narrowed appreciably and the half frequency broad lines are evident.

4. Conclusions

The residual field quenching by dipolar coupled spin I=1/2 nuclei

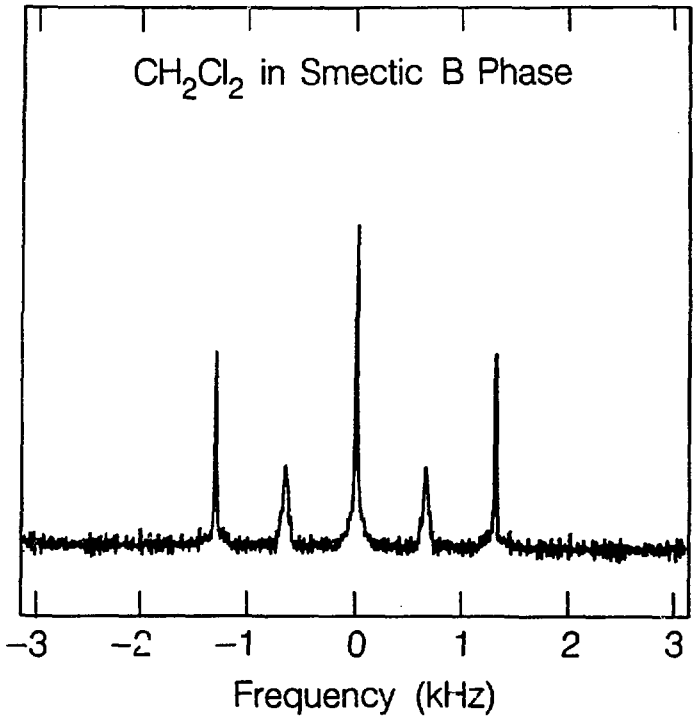

XBL 866-11160

Figure V.9: Experimental spectrum of CH_2Cl_2 in Smectic B phase after the application of a 180° dc refocussing pulse in the laboratory x direction in the middle of the zero field period. The signal appears as predicted in the text with a portion of the magnetization refocussed into narrow lines at the higher dipolar frequencies. At half this frequency, magnetization which evolves under the residual field for only one half the zero field period produces a broadened line.

has been shown experimentally and is in agreement with predictions made from perturbation theory and numerical simulations. This effect is analogous to that seen for integer spin systems in NQR experiments (1). The simulations assume a residual field in the laboratory z direction but can easily incorporate any field direction. As stated above, altering the direction of the residual field will not affect the zero field Hamiltonian when averaged over a powder distribution, but altering the relative orientations of the initial condition and residual field will affect the appearance of the spectrum.[24] Through pulsed dc field experiments which remove the effects of very small residual fields, high resolution spectra of disordered materials are obtained.

E. References

1. A.J. Silvidi, J.W. McGrath and D.F. Holcomb, J. Chem. Phys. **41**, 105 (1964).

2. T. Chiba, J. Chem. Phys. **39**, 947 (1963).

3. A. Eriksson, M.A. Hussein, B. Berglund, J. Tegenfeldt and J. Lindgren, J. Mol. Struct. **52**, 95 (1979).

4. T.P. Das and E.L. Hahn in Solid State Physics, Suppl. 1 (F. Seitz and D. Turnbull, Eds, Academic, New York, 1958).

5. G. Soda and T. Chiba, J. Chem. Phys. **50**, 439 (1969).

6. R.G. Barnes in Adv. Magn. Reson., vol 1 (Heyden, New York, 1974).

7. S. Sikka, S.N. Momin, H. Rajogopal and R. Chidambaram, J. Chem. Phys. **48**, 1883 (1968).

8. B. Pedersen, J. Chem. Phys. **41**, 122 (1964).

9. P. Diehl and C.L. Khetrapal, NMR Basic Principles and Progress, Vol 1 (Springer-Verlag, New York, 1969) pgs 14-5.

10. P. Jonsen, M. Luzar, A.Pines and M. Mehring, J. Chem. Phys. **85**, 4873 (1986).

11. (a) L. Leiserwitz, Acta Crystallogr. B **32**, 775 (1976).
    (b) M.G. Takwale and L.M. Pant, Acta Crystallogr B **27**, 1152 (1971).

12. B.H. Meier, F. Graf and R.R. Ernst, J. Chem. Phys. **76**, 767 (1982).

13. A. Gough, M.M. Haq and J.A.S. Smith, Chem. Phys. Lett. **117**, 389 (1985).

14. V. Benghiat and L. Leiserwitz, J. Chem. Soc. Perkins Trans. **2**, 1779 (1972).

15. G.W. Leppelmeier and E.L. Hahn, Phys. Rev. **141**, 724 (1966).

16. S. Vega, Adv. Magn. Reson. **6**, 259 (1973).

17. G.M. Muha, J. Magn. Reson. **49**, 431 (1982) and references therein.

18. S. Pissanetsky, J. Chem. Phys. **59**, 4197 (1973).

19. (a) R.B. Creel, E.D. Von Meerwall and R.G. Barnes, Chem. Phys. Lett. **49**, 501 (1977).
    (b) P. Kottis and R. Lefebvre, J. Chem. Phys. **39**, 393 (1963).

20. P.A. Casabella and P.J. Bray, J. Chem. Phys. **28**, 1182 (1958) and J. Chem. Phys. **29**, 1105 (1958).

21. D.T. Edmonds, Phys. Reps. **29**, 233 (1977).

22. (a) A.G. Anderson, Phys. Rev. **115**, 863 (1959) and **125**, 1517 (1962).
(b) S. Clough, A.J. Horsewill, P.J. McDonald and F.O. Zelaya, Phys. Rev. Lett. **55**, 1794 (1985).
(c) A. Bielecki and A. Pines, submitted to Chem. Phys. (1987).

23. E.L. Hahn, Phys. Rev. **80**, 580 (1950).

24. D.B. Zax, Ph.D. Thesis, University of California, Berkeley, (1985).

VI. COMPUTER PROGRAMS

Five computer programs which were written in the course of this work are included in this chapter. Fortran and executable versions are stored on magnetic tape. Comments are included in the programs to aid in their interpretation.

1. INHOM: Computes the effect of a single dc magnetic field pulse on a zero field state proportional to the dipolar Hamiltonian. The effects of pulsed magnetic field inhomogeneity, to a linear or quadratic approximation of the change in pulse angle over the sample, can also be included. Single crystal orientations or averages over a powder can be calculated over a wide range of pulse angles.

2. PLTSIM: Calculates the zero field NMR spectrum for two dipolar coupled spin I=1/2 nuclei assuming an initial state equal to H_D. The signal is calculated for the demagnetization field cycle using two dc magnetic field pulses. An output file for plotting is produced.

3. DEMAG: Predicts the final demagnetized state in zero field for a single spin I=1 nucleus as a function of initial crystal orientation, e^2qQ/h and η values. The output indicates numerically whether one, two, or more level crossings occur during the demagnetization. A matrix of these level crossing values, produced as a function of crystal orientation angles θ and ϕ, can be displayed visually on the Lexidata using a program written by D.B. Zax.

4. QUAD: Calculates the zero field NQR spectrum for a single spin I=1 nucleus under two dc magnetic field pulses applied in zero field. The initial condition is that found by program DEMAG and corresponds to the high field populations being carried over to zero field. An output file for plotting is produced.

5. RESID: Computes the perturbation of a small residual z field on the spectrum of two dipolar coupled spin I=1/2 nuclei, with or without a non-zero asymmetry parameter. The initial condition is assumed to be $I_{z,L}$ as for the sudden transition field cycle.

```
c
c       program to calculate signal intensities
c       for two dipolar coupled spins after a single adlf
c       pulse in zf. Initial state = H(D).  Single crystal
c       orientations are weighted by sin(th) and summed.
c       Signal in arbitrary units, scale with no. divisions.
c       DC coil inhomogeneities are also considered
c       to a linear or quadratic approximation.
c
c       this program is INHOM: incremented calculations of
c       pulses and orientations.    amt    9/3/84
c
        complex*16 m(3,3),n(3,3),rm(3),rn(3),st
        complex*16 w(3),x,y,z,s,ra(3),rb(3)
        double precision p(3),r(3,3),g(3),th,dd,ai
        double precision aa,t,ac,tc,ar,pi,del,div,as
        dimension f(3)
c
        fct(b,l) = -(b**l)
c
        type*,'this program will calculate the zero field
     @  intensities'
        type*,'as a fct. of a single zf pulse for a
     @  homonuclear '
        type*,'dipolar coupled pair of proton spins demag.
     @  to zf.'
        type*,'enter initial pulse angle in degrees.'
        accept*,aa
        type*,'enter increment in pulse length and no. of
     @  repetitions'
        accept*,ai,nn
        type*,'enter coil inhomogeneity (% field) and no.
     @  of divisions'
        accept*,del,div
        type*, 'enter functional dependence of inhomogeneity'
        type*, '(0=none, 1=linear, 2=quadratic)'
        accept*, ft
        ft=ft-1
        type*,'enter initial angle of cryst. orient. in degs.'
        accept*,t
        type*,'enter increment in orientation angle and no.
     @  of repetitions'
        accept*,ti,mm
c
        pi=4.0*atan(1.0)
        del=del/100
        aa=(aa*(pi/180.0))
        t=(t*(pi/180.0))
        ac=(ai*(pi/180.0))
        tc=(ti*(pi/180.0))
        p(1)=-1
        p(2)=2
        p(3)=-1
c
```

```
c       Set up functional dependence of field over coil
c
        if (ft) 10,20,30
10      l=1
        go to 40
20      l=1
        go to 40
30      l=2
c
c       calculate zero field signal for nn increments of
c       dc pulse, and mm increments of theta
c
40      do 800 ii=1,nn+1
        st=0.0
        ar=0.0
        ar=aa+(ac*(ii-1))
        do 600 kk=1,mm+1
        th=t+(tc*(kk-1))
c
c       rotation matrices to be calculated with value
c       of (th) calculated above
c
        r(1,1)=0.5*(1+dcos(th))
        r(1,2)=(2**-.5)*dsin(th)
        r(1,3)=0.5*(1-dcos(th))
        r(2,1)=-(2**-.5)*dsin(th)
        r(2,2)=dcos(th)
        r(2,3)=(2**-.5)*dsin(th)
        r(3,1)=r(1,3)
        r(3,2)=-r(1,2)
        r(3,3)=r(1,1)
c
c       calculation of unitary transforms and multipli-
c       cation by initial density matrix
c
c       now to take into account the inhomogeneity
c
        s=0.0
        do 500 JJ=0,div
        b=JJ/div
        as=ar+ar*del*(fct(b,l))
c
c
        do 110 i=1,3
110     f(i)=(2-i)*(as)
        do 111 i=1,3
        x=cexp(cmplx(0.0,f(i)))
        do 111 J=1,3
        m(i,J)=x*r(i,J)
111     n(i,J)=(conjg(x))*r(i,J)
        do 140 J=1,3
        do 130 i=1,3
        y=0.0
        z=0.0
```

```
      do 120 k=1,3
      y=y+r(k,i)*m(k,J)
120   z=z+r(k,i)*n(k,J)
      rm(i)=y
130   rn(i)=z
      do 135 i=1,3
      m(i,J)=p(i)*rm(i)
135   n(i,J)=rn(i)
140   continue
c
c     now to use subroutines to calculate the final
c     matrices to give the intensities and frequencies
c
      call matml(n,m,rb)
c
      do 400 i=1,3
      w(i)=p(i)*n(i,i)
      s=s+w(i)
400   continue
500   continue
c
c     weighting of single crystal orientations after
c     incrementing the angle (th) to produce powder 'sum'.
c     Note, if only single orientation is counted,
c     then all are weighted the same.
c
      if (ti.eq.0 .and. mm.eq.0) then
        wgt=1
      else if (th .eq. 0) then
        wgt=0.1*sin(ti)
      else
        wgt=sin(th)
      end if
      st=st+s*wgt
600   continue
c
c
c     output for plotting
c
700   print*,ar*(180/pi),real(st/(mm+1))
800   continue

      stop
      end
c
c     subroutines
c
      subroutine matml(a,b,ra)
c     matrix multiplier   a=a*b
      complex*16 a(3,3),b(3,3),ra(3),s
      do 14 i=1,3
      do 12 J=1,3
      s=0.0
      do 11 k=1,3
```

```
11      s=s+a(i,k)*b(k,j)
12      ra(j)=s
        do 13 j=1,3
13      a(i,j)=ra(j)
14      continue
        return
        end
```

```
c       program to calculate zero field intensities
c       and frequencies for two dipolar coupled spins
c       under adlf w/pulses in zf.  Crystal orientations
c       are weighted by sin(th) and summed.
c
c       this program is PLTSIM: incremeneted calculations of
c       pulses and orientations with the option of producing
c       a spec file for plotting.     amt 9/2/84
c
        character*15,fname
        complex ru(3),rv(3),m(3,3),n(3,3),rm(3),rn(3),at,
        complex bt,st,c(3,3),d(3,3),a,w(3),u,v,x,y,z,a,b,
        complex s,ra(3),rb(3)
        dimension e(3),p(3),r(3,3),f(3),g(3),tn(3),
        dimension npt(3),freq(3)
        real nt
        type*,'this program will calculate the zero'
        type*,'field intensities and frequencies for'
        type*,'a homonuclear dipolar coupled pair of'
        type*,'proton spins.'
        type*,'enter internuclear distance in angstroms'
        accept*,h
        type*,'enter initial pulse angles alpha, beta (degs).'
        type*,'where alpha is the first pulse in zfield.'
        accept*,aa,bb
        type*,'enter alpha and beta increments and no. of
     @  repetitions'
        accept*,ai,bi,nn
        type*,'enter initial angle of crystal orientation.'
        accept*,t
        type*,'enter increment in orientation angle and no.
     @  of repetitions'
        accept*,ti,mm
        pi=4.0*atan(1.0)
        dd=(6.0067e-20)/((h*1e-8)**3)
        aa=(aa*(pi/180))
        bb=(bb*(pi/180))
        t=(t*(pi/180))
        bc=(bi*(pi/180))
        ac=(ai*(pi/180))
        tc=(ti*(pi/180))
        p(1)=-1*(dd/1000)
        p(2)=2*(dd/1000)
        p(3)=-1*(dd/1000)
c
c       more information for output format
c
        type*,'output to spec file? if yes,type 0.'
        accept*,ll
        if (ll.ne.0) go to 1
        type*,'what bandwidth will you be plotting?(in khz)?'
        accept*,bw
c
c       calculate zf signal for nn increments of beta,
```

```
c       end of alpha, and mm increments of theta
c
1       do 900 ii=1,nn+1
        at=0.0
        bt=0.0
        st=0.0
        do 700 kk=1,mm+1
        br=0.0
        ar=0.0
        br=bb+(bc*(ii-1))
        ar=aa+(ac*(ii-1))
        th=t+(tc*(kk-1))
c
c       rotation matrices to be calculated with value
c       of (th) calculated above
c
        r(1,1)=0.5*(1+cos(th))
        r(1,2)=(2**-.5)*sin(th)
        r(1,3)=0.5*(1-cos(th))
        r(2,1)=-(2**-.5)*sin(th)
        r(2,2)=cos(th)
        r(2,3)=(2**-.5)*sin(th)
        r(3,1)=r(1,3)
        r(3,2)=-r(1,2)
        r(3,3)=r(1,1)
c
c       calculation of unitary transforms and multipli-
c       cation by initial density matrix
c
c       matrices for second angle calculated first
c
        do 10 i=1,3
10      e(i)=(2-i)*-br
        do 11 i=1,3
        a=cexp(cmplx(0.0,e(i)))
        do 11 j=1,3
        c(i,j)=a*r(i,j)
11      d(i,j)=(conjg(a))*r(i,j)
        do 40 j=1,3
        do 30 i=1,3
        v=0.0
        u=0.0
        do 20 k=1,3
        v=v+r(k,i)*c(k,j)
20      u=u+r(k,i)*d(k,j)
        rv(i)=v
30      ru(i)=u
        do 35 i=1,3
        c(i,j)=r(i)*rv(i)
35      d(i,j)=ru(i)
40      continue
c
c       for first zero field pulse angle
c
```

```
      do 110 i=1,3
110   f(i)=(2-i)*(ar)
      do 111 i=1,3
      x=cexp(cmplx(0.0,f(i)))
      do 111 j=1,3
      m(i,j)=x*r(i,j)
111   n(i,j)=(conjg(x))*r(i,j)
      do 140 j=1,3
      do 130 i=1,3
      y=0.0
      z=0.0
      do 120 k=1,3
      y=y+r(k,i)*m(k,j)
120   z=z+r(k,i)*n(k,j)
      rm(i)=y
130   rn(i)=z
      do 135 i=1,3
      m(i,j)=p(i)*rm(i)
135   n(i,j)=rn(i)
140   continue
c
c     now to use subroutines to calculate the final
c     matrices to give the intensities and frequencies
c
      call matml(d,c,ra)
      call matml(n,m,rb)
c
c     calculation of final intensities and frequencies
c
      a=0.0
      b=0.0
      s=0.0
      do 400 i=1,3
      do 300 j=1,3
      w(j)=d(i,j)*n(j,i)
      g(j)=p(i)-p(j)
      if (g(j).eq.0) b=b+w(j)
      if (g(j).lt.0) a=a+w(j)
      if (g(j).gt.0) s=s+w(j)
300   continue
400   continue
c
c     weight single crystal orientations and sum to
c     get powder 'sum'
c
550   if (th .eq. 0) then
         wgt=0.1*sin(tc)
      else
         wgt=sin(th)
      end if
      at=at+a*wgt
      bt=bt+b*wgt
      st=st+s*wgt
700   continue
```

```
c
c       output to file
c
        norm=at+bt+st
        if (ll.eq.0) go to 800
710     print*,'for alpha and beta pulses of:'
        print*,ar*(180/pi),br*(180/pi)
        print*,'initial orientation, inc., reps.'
        print*,t*(360/pi),ti,nn
        print 730
730     format (/,1x,'intensities',14x,'frequencies(khz)',/)
        print 750,at/norm,p(1)-p(2)
        print 750,bt/norm,p(1)-p(3)
        print 750,st/norm,p(2)-p(3)
750     format ((f10.3,f10.3),5x,f10.3)
        go to 900
c
c       creation of spec file for plotting
c
800     freq(1)=p(1)-p(2)
        freq(3)=p(2)-p(3)
        freq(2)=p(1)-p(3)
        tn(1)=at/norm
        tn(2)=bt/norm
        tn(3)=st/norm
        type*,'spec file name (spec*.da):'
        accept810,fname
810     format(a)
        open(unit=3,name=fname,status='new')
        hzpt=(bw*1000)/1024
        ipts=3
        write (3,840) ipts
840     format(i3)
        write (3,850) hzpt
850     format(f10.3)
        do 870 i=1,3
        npt(i)=512+jnint(1000*freq(i)/hzpt)
        write (3,860) npt(i),tn(i)
860     format(i5,f10.3)
870     continue
        print 875
875     format(//)
        print*,'the spec file:'
        print 880, fname
880     format (1x,a15)
        print*,'has a bandwidth of:'
        print*,bw,'khz,for the following exptl. info.'
        go to 710
900     continue
        stop
        end
c
c       subroutines
c
```

```
      subroutine matml(a,b,ra)
c     matrix multiplier    a=a*b
      complex a(3,3),b(3,3),ra(3),s
      do 14 i=1,3
      do 12 J=1,3
      s=0.0
      do 11 k=1,3
11    s=s+a(i,k)*b(k,J)
12    ra(J)=s
      do 13 J=1,3
13    a(i,J)=ra(J)
14    continue
      return
      end
```

```
      program DEMAG
c     a program to calculate the demagnetized
c     state of a spin one nucleus
c     amt  6/11/86
c
      complex ize(3,3),iex(3,3),iyy(3,3),c(3,3),f(3,3)
      complex zz(3,3),zzz(3,3),isq(3,3),r(3,3),s(3,3)
      complex q(3,3),x(3,3),y(3,3),z(3,3),ox(3,3),oy(3,3)
      complex oz(3,3),ozz(3,3),ozzz(3,3),u(3,3)
      dimension st(3),pop(3),htemp(3),ipts(100,100),ixf(3)
      common nst,a,eta,th,ph
      nst=3
      type*,'Input value of e2qQ/h and eta.'
      accept*,quad,eta
      type*,'Input no. of repetitions in theta and phi.'
      accept*,nreps
      type*,'Input initial field value (gauss).'
      accept*,ho
      pi=4.0*atan(1.0)
      a=quad*(0.25)
      gamma=6.45e-1
      tc=2.0/float(nreps-1)
      pc=180.0/float(nreps-1)
c
c
c     Setting up the quadrupolar hamiltonian
c
      aa=3.0*a
      bb=-1.0*a
      cc=eta*a
c
c     Setting up the initial matrices
c
      do 10 i=1,nst
      do 10 J=1,nst
      f(i,J)=cmplx(0.0,0.0)
      c(i,J)=cmplx(0.0,0.0)
      isq(i,J)=cmplx(0.0,0.0)
      ize(i,J)=cmplx(0.0,0.0)
      iex(i,J)=cmplx(0.0,0.0)
10    iyy(i,J)=cmplx(0.0,0.0)
      iyy(1,3)=cmplx(1.0,0.0)
      iyy(3,1)=cmplx(1.0,0.0)
      ize(1,2)=cmplx(0.0,-1.0)
      ize(2,1)=cmplx(0.0,1.0)
      iex(2,3)=cmplx(1.0,0.0)
      iex(3,2)=cmplx(1.0,0.0)
      do 11 i=1,3
      isq(i,i)=cmplx(-2.0,0.0)
      isq(i,i)=a*isq(i,i)
11    continue
c
c     Now finish the hamiltonian by multiplying
```

```
c       and adding the matrices
c
        call matml(ize,ize,nst,aa,c)
        call matadd(f,c,nst)
        call matadd(f,isq,nst)
        call matml(iex,iex,nst,cc,c)
        call matadd(f,c,nst)
        call matml(iyy,iyy,nst,-cc,c)
        call matadd(f,c,nst)
c
c       Looping over theta and phi values
c       note that each theta and phi combination represented
c
        print*,nreps
        do 600 iii=1,nreps
        tang=-1.0 + tc*float(iii-1)
        th=acos(tang)
        do 500 JJJ=1,nreps
        ph=(0.0 + pc*float(JJJ-1))*(pi/180)
        ihold=0.0
c
c       Calculate the level crossings before the next step
c
        abit=10.0
        h=500.0
        hinc=1.0
        call levelx(h,hinc,500,lxf)
        count=-1
        do 20 ii=1,nst
        if (lxf(ii)) 14,14,15
14      go to 20
15      count=count+1
        kk=count+2
        htemp(kk)=lxf(ii) + abit
20      continue
        if (count) 26,27,28
26      hc=0.0
        in=-1
        go to 100
27      hc=htemp(2)
        in=0
        go to 100
28      in=1
        if ((htemp(2)-htemp(3)).le.0.0) then
            hn=htemp(3)
            hb=htemp(2)
        else
            hn=htemp(2)
            hb=htemp(3)
        end if
        go to 100

c
c       Now diagonalize the hamiltonian and store populations
```

```
c
100     call zterm(ho,iex,iyy,ize,r)
        call matadd(r,f,nst)
        call heisen(r,u,nst)
        call order(r,u,nst)
        do 12 ii=1,nst
12      eop(ii)=r(i,i)
        if (in) 50,60,70
c
c       No level crossing
c
50      ihold=273
        go to 400
c
c       One level crossing
c
60      call zterm(hc,iex,iyy,ize,r)
        call matadd(r,f,nst)
        call heisen(r,x,nst)
        call order(r,x,nst)
c       find overlap u and x
        call matraml(u,x,nst,ox)
        call overlap(ox,nst,ihold)
        ha=hc-2.0*abit
        call zterm(ha,iex,iyy,ize,r)
        call matadd(r,f,nst)
        call heisen(r,y,nst)
        call order(r,y,nst)
c       find overlap x and y
        call matraml(x,y,nst,oy)
        call overlap(oy,nst,ihold)
        go to 400
c
c       Two level crossings
c
70      call zterm(hn,iex,iyy,ize,r)
        call matadd(r,f,nst)
        call heisen(r,x,nst)
        call order(r,x,nst)
c       find overlap u and x
        call matraml(u,x,nst,ox)
        call overlap(ox,nst,ihold)
        ha=hn-2.0*abit
        call zterm(ha,iex,iyy,ize,r)
        call matadd(r,f,nst)
        call heisen(r,y,nst)
        call order(r,y,nst)
c       find overlap x and y
        call matraml(x,y,nst,oy)
        call overlap(oy,nst,ihold)
        call zterm(hb,iex,iyy,ize,r)
        call matadd(r,f,nst)
        call heisen(r,z,nst)
        call order(r,z,nst)
```

```
c       find overlap w and z
        call matraml(w,z,nst,oz)
        call overlap(oz,nst,ihold)
        hc=hb-2.0*abit
        call zterm(hc,iex,iyy,ize,r)
        call matadd(r,f,nst)
        call heisen(r,zz,nst)
        call order(r,zz,nst)
c       find overlap z and zz
        call matraml(z,zz,nst,ozz)
        call overlap(ozz,nst,ihold)

c       produce final density matrix for zero field program
c       the numbers produced were used to plot a two
c       dimensional map on the lexidata, each color
c       represented the presence or absence of a level
c       crossing and which levels cross

400     if (ihold.eq.273) then
            pt=1
        else if (ihold.eq.266) then
                pt=2
        else if (ihold.eq.161) then
                pt=3
        else if (ihold.eq.84) then
                pt=4
        end if
        ipts(i,J)=pt
        print*,ipts(i,J)
500     continue
600     continue
        stop
900     end
c
c       Subroutines
c
        subroutine zterm(ho,iex,iyy,ize,r)
c
c       sets up field terms of hamiltonian
c
        complex r(3,3),iex(3,3),iyy(3,3),ize(3,3)
        complex xt(3,3),yt(3,3),zt(3,3)
        common nst,a,eta,th,ph
        gamma=6.45e-1
        do 10 i=1,nst
        do 10 J=1,nst
10      r(i,J)=(0.0,0.0)
        wo=gamma*ho
        dx=wo*sin(th)*cos(ph)
        dy=wo*sin(th)*sin(ph)
        dz=wo*cos(th)
        do 11 i=1,nst
        do 11 J=1,nst
        r(i,J)=dx*iex(i,J)+dy*iyy(i,J)+dz*ize(i,J)
```

```
11      continue
        return
        end
c
        subroutine matml(a,b,n,x,d)
c
c       a matrix multiplier   c=a*b
c
        complex a(n,n),b(n,n),d(n,n),rv(64),s
        do 14 i=1,n
        do 12 J=1,n
        s=0.0
        do 11 k=1,n
11      s=s+a(i,k)*b(k,J)
12      rv(J)=s
        do 13 J=1,n
13      d(i,J)=x*rv(J)
14      continue
        return
        end
c
c
        subroutine matadd(a,b,n)
c
c       adds two nxn complex matrices     a=a+b
c
        complex a(n,n),b(n,n)
        do 10 i=1,n
        do 10 J=1,n
10      a(i,J)=a(i,J) + b(i,J)
        return
        end
c
c
        subroutine order(r,u,n)
c
c       orders the eigenstates by energy as heigen does not
c       always return them in the same order
c
        complex r(n,n),u(n,n),t(3,3)
        dimension e(3)
        do 10 i=1,n
        e(i)=real(r(i,i))
10      continue
        do 11 ii=1,n
        if (e(1).gt.e(2) .and. e(1).gt.e(3)) then
            t(ii,1)=u(ii,1)
            if (e(3).gt.e(2)) then
                t(ii,2)=u(ii,3)
                t(ii,3)=u(ii,2)
            else
                t(ii,2)=u(ii,2)
                t(ii,3)=u(ii,3)
            end if
```

```
      else if (e(2).gt.e(1) .and. e(2).gt.e(3)) then
               t(ii,1)=u(ii,2)
               if (e(1).gt.e(3)) then
                   t(ii,2)=u(ii,1)
                   t(ii,3)=u(ii,3)
               else
                   t(ii,2)=u(ii,3)
                   t(ii,3)=u(ii,1)
               end if
      else if (e(3).gt.e(2) .and. e(3).gt.e(1)) then
               t(ii,1)=u(ii,3)
               if (e(1).gt.e(2)) then
                   t(ii,2)=u(ii,1)
                   t(ii,3)=u(ii,2)
               else
                   t(ii,2)=u(ii,2)
                   t(ii,3)=u(ii,1)
               end if
      end if
11    continue
      do 12 i=1,n
      do 12 J=1,n
      u(i,J)=t(i,J)
12    continue
      return
      end
c
c
      subroutine matraml(a,b,n,o)
c
c     a matrix multiplier      o=a-adJoint*b
c
      complex a(n,n),b(n,n),cv(64),s,o(n,n)
      do 14 J=1,n
      do 12 i=1,n
      s=0.0
      do 11 k=1,n
11    s=s+conJg(a(k,i))*b(k,J)
12    cv(i)=s
      do 13 i=1,n
13    o(i,J)=cv(i)
14    continue
      return
      end

c
      subroutine overlap(a,n,ihold)
c
c     looks for max overlap of eigenstates and assigns
c     final state after level crossing
c
      complex a(n,n)
      real max
      dimension iJ(3)
```

```
      indx(ii,JJ,kk)=ii + 8*JJ +64*kk
      ii=1
      JJ=2
      kk=4
      ihold=0.0
      ihold=indx(ii,JJ,kk)
      do 10 J=1,n
      iJ(1)=ii
      iJ(2)=JJ
      iJ(3)=kk
      if (real(a(1,J)).ge.real(a(2,J))) then
          max=real(a(1,J))
          aa=1
          bb=J

      else
          max=real(a(2,J))
          aa=2
          bb=J
      end if
      if (real(a(3,J)).gt.max) then
          aa=3
          bb=J
      end if
      if (aa.ne.bb) then
          temp=iJ(aa)
          iJ(aa)=iJ(bb)
          iJ(bb)=temp
          ihold=indx(iJ(1),iJ(2),iJ(3))
      end if
10    continue
      return
      end
c
      subroutine prin(a,n)
c
      complex a(n,n)
      do 10 i=1,n
      print*,(a(i,J),J=1,n)
10    continue
      return
      end
c
      subroutine levelx(h,hinc,n,lxf)
c
c     a program to calculate the level crossing field
c     of the spin 1 eigenstates from analytic solutions
c     of the energies
c
      dimension e(3),v(3),lxf(3)
      common nst,a,eta,th,ph
      gamma=(6.45e-1)
      pi=4.0*atan(1.0)
      ea=(1.0+eta)*a
```

```
      eb=(1.0-eta)*a
      ec=-2.0*a
      x=0.0
      y=0.0
      z=0.0
      ix=0.0
      iy=0.0
      iz=0.0
      lxf(1)=0.0
      lxf(2)=0.0
      lxf(3)=0.0
      do 100 i=1,n+1
      v(1)=0.0
      v(2)=0.0
      v(3)=0.0
      hh=h - hinc*(i-1)
      d=gamma*hh
      p=-(d**2 + (a**2)*(3.0 + eta**2))
      aa=a*(d**2)*(((cos(th))**2)+cos(2*th)+eta*
     @ ((sin(th))**2)*(cos(2*ph)))
      ab=ea*eb*ec
      aa=aa+ab
      c=(aa/2.0)*(((3.0/abs(p))**3)**.5)
      beta=acos(c)
      do 10 J=1,3
      k=J-1
      ctr=cos((beta+float(k)*2.0*pi)/3.0)
      cnt=((4.0*abs(p))/3.0)**.5
      e(J)=ctr*cnt
10    continue
      v(1)=abs(e(1)-e(2))
      v(2)=abs(e(1)-e(3))
      v(3)=abs(e(2)-e(3))
      if (v(1).le.1.0) then
          x=x+hh
          ix=ix+1
      end if
      if (v(2).le.1.0) then
          y=y+hh
          iy=iy+1
      end if
      if (v(3).le.1.0) then
          z=z+hh
          iz=iz+1
      end if
100   continue
      if (ix.ne.0.0) lxf(1)=x/(ix)
      if (iy.ne.0.0) lxf(2)=y/(iy)
      if (iz.ne.0.0) lxf(3)=z/(iz)
      return
      end
```

```
c       program to calculate zero field intensities
c       and frequencies for a single spin 1 nucleus
c       under adlf w/pulses in zf.  Initial condition
c       corresponds to HF pops. Single crystal orientations
c       are weighted in phi by sin(th) dependence
c
c       this program is QUAD: incremeneted calculations of
c       pulses and orientations with the option of producing
c       a spec file for plotting.     amt 10/86
c
        character*15,fname
        complex ru(3),rv(3),m(3,3),n(3,3),rm(3),rn(3),at,bt,
        complex st,c(3,3),d(3,3),a,w(3),u,v,x,y,z,a,b,s,
        complex ra(3),rb(3),tha,thb,ephi,r(3,3),ths,thz,zt,
        complex zz,t(3,3),cv(3),cb(3)
        dimension e(3),p(3),f(3),s(3),en(3),tens(4),nt(4),
     @  freq(4)
        double precision qq,eta
        type*,'this program will calculate the zero'
        type*,'field intensities and frequencies for'
        type*,'a single spin 1 nucleus.'
        type*,'enter e2qQ/h (kHz) and eta'
        accept*,qq,eta
        type*,'enter initial pulse angles alpha and beta
     @  in degs.'
        type*,'where alpha is the first pulse in zfield.'
        accept*,aa,bb
        type*,'enter alpha and beta increments and no. of
     @  repetitions'
        accept*,ai,bi,nn
        type*,'enter increments in theta and phi (equator)'
        accept*,tt,incp
c
c       Setting up all those handy little numbers for later
c
        pi=4.0*atan(1.0)
        qq=qq*.25
        aa=(aa*(pi/180.0))
        bb=(bb*(pi/180.0))
        bc=(bi*(pi/180.0))
        ac=(ai*(pi/180.0))
c
c       The quadrupolar energies and populations
c       in zf eigenstates
c
        en(1)=qq*(1+eta)
        en(2)=-2*qq
        en(3)=qq*(1-eta)
        p(1)=1
        p(2)=-1
        p(3)=0
c
c       more information for output format
c
```

```
      type*,'output to spec file? if yes,type 0.'
      accept*,xxx
      if (xxx.ne.0) go to 1
      type*,'what bandwidth will you be plotting?(0-? khz)'
      accept*,bw
c
c     calculate zf signal for nn increments of beta,
c     and of alpha, and tt increments of theta
c
1     ar=0.0
      br=0.0
      do 900 ii=1,nn+1
      ar=aa+(ac*(ii-1))
      br=bb+(bc*(ii-1))
      tha=0.0
      thb=0.0
      ths=0.0
      thz=0.0
c
c     Looping over theta
c
      if (tt .ne. 1) tinc=2.0/(tt-1.0)
      do 701 ll=1,tt
      at=0.0
      bt=0.0
      st=0.0
      zt=0.0
      c1 = -1.0 + tinc*float(ll-1)
      theta=acos(c1)
      ipp=jnint(float(incp)*abs(sin(theta)))
      if (ipp .eq. 0) ipp=1
      pinc=2*pi/ipp
c
c     Looping here for phi dependence
c
      do 700 kk=1,ipp
      phi=pinc*float(kk-1)
      ephi=cexp(cmplx(0.0,phi))
c
c     rotation matrices to be calculated with value
c     of (theta) and (phi) calculated above
c
      r(1,1)=.5*(1+cos(theta))*conjg(ephi)
      r(1,2)=(2**-.5)*sin(theta)
      r(1,3)=.5*(1-cos(theta))*(ephi)
      r(2,1)=-(2**-.5)*sin(theta)*conjg(ephi)
      r(2,2)=cos(theta)
      r(2,3)=(2**-.5)*sin(theta)*(ephi)
      r(3,1)=conjg(r(1,3))
      r(3,2)=-(r(1,2))
      r(3,3)=conjg(r(1,1))
c
c     Unitary transform between basis sets
c
```

```
      t(1,1)=(2**-.5)
      t(1,2)=0.0
      t(1,3)=(2**-.5)
      t(2,1)=0.0
      t(2,2)=1.0
      t(2,3)=0.0
      t(3,1)=(2**-.5)
      t(3,2)=0.0
      t(3,3)=-(2**-.5)
c
c     calculation of transformed pulses
c
c     matrices for second angle beta calculated first
c
      do 10 i=1,3
10    e(i)=(2-i)*-br
      do 11 i=1,3
      a=cexp(cmplx(0.0,e(i)))
      do 11 j=1,3
      c(i,j)=a*r(i,j)
11    d(i,j)=(conjg(a))*r(i,j)
      do 40 j=1,3
      do 30 i=1,3
      v=0.0
      u=0.0
      do 20 k=1,3
      v=v+conjg(r(k,i))*c(k,j)
20    u=u+conjg(r(k,i))*d(k,j)
      rv(i)=v
30    ru(i)=u
      do 35 i=1,3
      c(i,j)=rv(i)
35    d(i,j)=ru(i)
40    continue
      call uamu(t,c,cv)
      call uamu(t,d,cb)
c
c     for first zero field pulse angle
c
      do 110 i=1,3
110   f(i)=(2-i)*(ar)
      do 111 i=1,3
      x=cexp(cmplx(0.0,f(i)))
      do 111 j=1,3
      m(i,j)=x*r(i,j)
111   n(i,j)=(conjg(x))*r(i,j)
      do 140 j=1,3
      do 130 i=1,3
      y=0.0
      z=0.0
      do 120 k=1,3
      y=y+conjg(r(k,i))*m(k,j)
120   z=z+conjg(r(k,i))*n(k,j)
      rm(i)=y
```

```
130     rn(i)=z
        do 135 i=1,3
        m(i,J)=rm(i)
135     n(i,J)=rn(i)
140     continue
        call uamu(t,m,cv)
        call uamu(t,n,cb)
c
c       now to use subroutines to calculate the final
c       matrices to give the intensities and frequencies
c
        do 200 i=1,3
        do 180 J=1,3
        c(i,J)=p(i)*c(i,J)
        m(i,J)=p(i)*m(i,J)
180     continue
200     continue
        call matml(d,c,ra)
        call matml(n,m,rb)
c
c       calculation of final intensities and frequencies
c       for a given theta and phi
c
        a=0.0
        b=0.0
        s=0.0
        zz=0.0
        do 400 i=1,3
        do 300 J=1,3
        w(J)=d(i,J)*n(J,i)
        g(J)=abs(en(i)-en(J))
        if (abs(g(J)-0.0).le.1d-4) zz=zz+w(J)
        if (abs(g(J)-(2*eta*qq)).le.1d-4) a=a+w(J)
        if (abs(g(J)-((3-eta)*qq)).le.1d-4) b=b+w(J)
        if (abs(g(J)-((3+eta)*qq)).le.1d-4) s=s+w(J)
300     continue
400     continue
c
c
c       Sum over phi values first and weight by dphi
c
        at=at+a*pinc
        bt=bt+b*pinc
        st=st+s*pinc
        zt=zt+zz*pinc
700     continue
c
c       Now to sum over theta
c
        tha=tha+at
        thb=thb+bt
        ths=ths+st
        thz=thz+zt
701     continue
```

```
c
c       output to file
c
        rnorm = thz+tha+thb+ths
        dnorm=2*rnorm
        if (xxx.eq.0) go to 800
710     print*,'For a spin 1 nucleus with e2qQ/h and eta:'
        print*,4*qq,eta
        print*,'for alpha and beta pulses of:'
        print*,ar*(180/pi),br*(180/pi)
        print 730
730     format (/,1x,'intensities',40x,'frequencies(khz)',/)
        print 750,real(thz)/rnorm,qq*0.0
        print 750,real(tha)/rnorm,2*eta*qq
        print 750,real(thb)/rnorm,(3-eta)*qq
        print 750,real(ths)/rnorm,(3+eta)*qq
750     format (f20.5,5x,f20.3)
        go to 900
c
c       creation of spec file for plotting
c
800     type*,'spec file name (spec*.da):'
        accept810,fname
810     format(a)
        open(unit=3,name=fname,status='new')
        ipts=4
        freq(1)=0.0
        freq(2)=2*eta*qq*1000
        freq(3)=(3-eta)*qq*1000
        freq(4)=(3+eta)*qq*1000
        tens(2)=real(tha)/rnorm
        tens(3)=real(thb)/rnorm
        tens(4)=real(ths)/rnorm
        tens(1)=real(thz)/rnorm
        hzpt=(bw*1000)/512
        write (3,840) ipts
840     format(i3)
        write (3,850) hzpt
850     format(f10.3)
        do 870 i=1,4
        nt(i)=1+jnint(freq(i)/hzpt)
        write (3,860) nt(i),tens(i)
860     format(i5,f10.3)
870     continue
        print 875
875     format(//)
        print*,'the spec file:'
        print 880, fname
880     format (1x,a15)
        print*,'has a bandwidth of:'
        print*,bw,'khz,for the following exptl. info.'
        go to 710
900     continue
        stop
```

```
      end
c
c     subroutines
c
      subroutine prin(a)
      complex a(3,3)
      do 12 i=1,3
      do 11 J=1,3
11    print*, a(i,J)
12    continue
      return
      end
c
      subroutine uamu(u,b,v)
c
c     unitary transform b=u-adJoint*b*u
c
      complex u(3,3),b(3,3),v(64)
      call matraml(u,b,v)
      call matml(b,u,v)
      return
      end
c
      subroutine matraml(a,b,cv)
c
c     matrix multiplier b=a-adJoint*b
c
      complex a(3,3),b(3,3),cv(64),s
      do 14 J=1,3
      do 12 i=1,3
      s=0.0
      do 11 k=1,3
11    s=s+conJg(a(k,i))*b(k,J)
12    cv(i)=s
      do 13 i=1,3
13    b(i,J)=cv(i)
14    continue
      return
      end
c
      subroutine matml(a,b,ra)
c     matrix multiplier   a=a*b
      complex a(3,3),b(3,3),ra(3),s
      do 14 i=1,3
      do 12 J=1,3
      s=0.0
      do 11 k=1,3
11    s=s+a(i,k)*b(k,J)
12    ra(J)=s
      do 13 J=1,3
13    a(i,J)=ra(J)
14    continue
      return
      end
```

```
c       program to calculate the effects of a
c       residual field (z) in zero field on
c       a non-axially symmetric dipolar tensor
c
c       Program RESID    AMT  6/29/86
c
c       equal increments of dcos(theta) and increments in
c       phi determined by sin(theta) weighted by d(phi).
c       Total intensity normalized to 2 units.  Warning:
c       this program may not work when the residual field
c       interaction approaches the splittings due to eta.
c       Also, the eigenvalues and eigenvectors returned
c       from heisen are sorted by energy level.  This may
c       not hold for all cases.
c
        complex u(3,3), a(3,3), h(3,3), f, e(3), w
        dimension peak(2,1024)
        common nst,n
        nst = 3
        n = 3
        type*, ' Input residual field strength in Gauss.'
        accept*, res
        resk = res * 4200.0
        type*, ' Input dipolar coupling scaled by S (kHz),
     @  and eta.'
        accept*, dd, eta
c       note that dd is 1/3*spectral frequency
        ddd = dd*1000.0
        pi = 4.0*atan(1.0)
        type*, ' Input no. of increments in theta, and phi
     @  (at equator).'
        accept*, tt, incp
        ip = incp/360
        type*, ' Input full bandwidth in kilohertz.'
        accept*, bdw
        hzpt = bdw*1000.0/1024.0
        type*, ' Output to file for plotting? (0=no,1=yes)'
        accept*, iplot
        if (iplot .ne. 1) go to 5
        type*,  ' Input number of spec file for plotting.'
        accept*, ifl
5       print*, ' Field, Coupling, Eta, Theta Inc., Phi Inc.,
     @  Bndwth'
        print*, res, dd, eta, tt, incp, bdw
        if (iplot .eq. 1) print*, 'Spec file no. ' ,ifl
c
c       The following matrix a(n,n) is I(z,lab) and also
c       the form of the residual field.
c
        if (tt .ne. 1) tinc = 2.0/(tt-1.0)
        do 700 ii = 1, tt
        c1 = -1.0 + tinc*float(ii-1)
        theta = acos(c1)
        ipp = jnint(ip*360*abs(sin(theta)))
```

```
      if (ipp .eq. 0) ipp = 1
      pinc = 2*pi/ipp
      do 600 JJ = 1, ipp
      phi = pinc*float(JJ-1)
c
      xxx = sin(theta)*cos(phi)
      yyy = sin(theta)*sin(phi)
      zzz = cos(theta)
      a(1,1) = cmplx(0.0,0.0)
      a(1,2) = yyy*cmplx(1.0,0.0)
      a(1,3) = xxx*cmplx(1.0,0.0)
      a(2,1) = a(1,2)
      a(2,2) = a(1,1)
      a(2,3) = zzz*cmplx(0.0,1.0)
      a(3,1) = a(1,3)
      a(3,2) = conjg(a(2,3))
      a(3,3) = a(1,1)
c
c
c     Set up initial Hamiltonian
c
c     The matrix h(n,n) is the initial state includins the
c     dipolar terms and the residual field.
c
      do 11 i = 1,3
      do 10 J = 1,3
      h(i,J) = cmplx(0.0,0.0)
      u(i,J) = cmplx(0.0,0.0)
10    continue
11    continue
      h(1,1) = ddd*cmplx(2.0,0.0)
      h(1,2) = a(1,2)*resk
      h(1,3) = a(1,3)*resk
      h(2,1) = a(2,1)*resk
      h(2,2) = ddd*cmplx(-(1-eta),0.0)
      h(2,3) = a(2,3)*resk
      h(3,1) = a(3,1)*resk
      h(3,2) = a(3,2)*resk
      h(3,3) = ddd*cmplx(-(1+eta),0.0)
c
c     Now diagonalize this matrix
c
      call heigen(h,u,nst)
      if (eta .eq. 0) go to 15
      call sort(h,u)

15    do 50 i=1,nst
50    e(i) = h(i,i)
c
c     Now find the I(z,lab) in the zero field basis
c
      call uamu(u,a,n,v)
c
c     Now find ij and ji elements for intensities and
```

```
c       scale by angular powder terms and find energies
c       Save this information in an array for plotting
c
        w = 0.0
        do 300 i = 1, nst
        do 200 j = 1, nst
        w = a(i,j)*a(j,i)
        if (real(w) .lt. 1e-6) go to 200
        f = e(i) - e(j)
        ipnt = 512 + jnint(real(f)/hzpt)
        peak(1,ipnt) = ipnt
        peak(2,ipnt) = real(w)*pinc + peak(2,ipnt)
200     continue
300     continue
c
c
600     continue
700     continue
c
c       Output to plotting file
c
        k = 0.0
        summ = 0.0
        print*, ' Point Number and Intensities!'
        do 701 iii=1,1024
        if (peak(2,iii) .ne. 0.0) print*, peak(1,iii),
     @  peak(2,iii)
        summ = summ + peak(2,iii)
        if (peak(2,iii) .ne. 0.0) k = k + 1
701     continue
c
        if (iplot .eq. 0.0) go to 900
        call defile('spec',ifl,0)
        write(1,705) k
705     format(i6)
        write(1,710) hzpt
710     format(e14.6)
        do 800 i = 1,1024
        if (peak(2,i) .eq. 0.0) go to 800
        write(1,750) jifix(peak(1,i)),
     @  peak(2,i)/(summ/2)
750     format(i6, e14.6)
800     continue
        close (unit=01)
c
900     stop
        end
c
c       subroutines
c
        subroutine sort(a,b)
c
c       sorts the hamiltonian and eigenvectors
c       based on magnitude of eigenvalues
```

```
c
      complex a(3,3), b(3,3), awork(3,3), bwork(3,3)
      dimension s(3), t(2)
c
      do 15 i=1,3
15    s(i) = real(a(i,i))
      rmax1 = amax1(s(1),s(2),s(3))
      if (rmax1 .eq. s(1)) then
         iflag = -1
      else if (rmax1 .eq. s(2)) then
         iflag = 0
      else if (rmax1 .eq. s(3)) then
         iflag = 1
      end if
c
      if (iflag) 100,200,300
100   go to 400
200   do 220 i=1,3
      awork(i,1) = a(i,2)
      awork(i,2) = a(i,1)
      awork(i,3) = a(i,3)
      bwork(i,1) = b(i,2)
      bwork(i,2) = b(i,1)
220   bwork(i,3) = b(i,3)
      do 230 i=1,3
      a(1,i) = awork(2,i)
      a(2,i) = awork(1,i)
      a(3,i) = awork(3,i)
      b(1,i) = bwork(2,i)
      b(2,i) = bwork(1,i)
230   b(3,i) = bwork(3,i)
      go to 400
300   do 320 j=1,3
      awork(j,1) = a(j,3)
      awork(j,2) = a(j,2)
      awork(j,3) = a(j,1)
      bwork(j,1) = b(j,3)
      bwork(j,2) = b(j,2)
320   bwork(j,3) = b(j,1)
      do 330 j=1,3
      a(1,j) = awork(3,j)
      a(2,j) = awork(2,j)
      a(3,j) = awork(1,j)
      b(1,j) = bwork(3,j)
      b(2,j) = bwork(2,j)
330   b(3,j) = bwork(1,j)
400   do 415 i=1,2
415   t(i) = real(a(i+1,i+1))
      rmax2 = amax1(t(1),t(2))
      if (rmax2 .eq. t(1)) go to 600
      do 520 k=1,3
      awork(k,1) = a(k,1)
      awork(k,2) = a(k,3)
      awork(k,3) = a(k,2)
```

```
      bwork(k,1) = b(k,1)
      bwork(k,2) = b(k,3)
520   bwork(k,3) = b(k,2)
      do 530 k=i,3
      a(1,k) = awork(1,k)
      a(2,k) = awork(3,k)
      a(3,k) = awork(2,k)
      b(1,k) = bwork(1,k)
      b(2,k) = bwork(3,k)
530   b(3,k) = bwork(2,k)
600   return
      end
```